

On the Zeros of Flexible Systems

by

Siddharth Rath

A dissertation submitted in partial fulfillment
of the requirements for the degree of
Doctor of Philosophy
(Mechanical Engineering)
in the University of Michigan
2024

Doctoral Committee:

Professor Shorya Awtar, Chair
Professor Dennis Bernstein
Associate Professor Michael Cullinan, University of Texas at Austin
Dr. Samir Nayfeh, Top Flight Technologies
Professor Chinedum Okwudire

Siddharth Rath

rathsid@umich.edu

ORCID iD: 0000-0002-9488-418X

© Siddharth Rath 2024

Dedication

I dedicate this thesis to the almighty who is the source of all the hardwork, perseverance and resilience that has gone into the making this thesis a reality. I seek his blessings for whatever comes next in my life.

Acknowledgements

I would like to wholeheartedly thank my advisor, Professor Shorya Awtar for his infinite patience and steadfast support. He has guided me all along my doctoral journey with writing high quality journal papers, dealing with rejections and becoming better a researcher and engineer.

I would like to thank my committee members Professor Dennis Bernstein, Professor Chinedum Okwudire, Professor Michael Cullinan, and Dr. Samit Nayfeh for agreeing to be on my thesis committee and providing me the much needed suggestions, criticism and help along the way.

I would like to acknowledge Leqing Cui for providing me the mathematical tools and helping me frame the research in Chapter 2 of my thesis. I would like to thank Rahul Ramamoorthy for helping me complete the rigorous mathematical proofs in Chapter 3. I would like to thank Arunav Maheshwari and Moeen Radgolchin for helping me brainstorm and carry out the mathematical derivations in Chapter 4, 5 and 6.

Finally, I would also like to thank my friends Revanth Damerla, Nishant Jalgoankar, Johann Chacko Mathew, Swathi Muthyala, Brinda Gokul, and Pavan Kumar Vaddi who have always provided me with their invaluable counsel and support at times of need. I would like to thank my family, especially mother, Manisha Rath for her unconditional love and unwavering faith in me.

Table of Contents

Dedication	ii
Acknowledgements	iii
List of Tables	vii
List of Figures	ix
Abstract	xii
Chapter 1 Introduction and Background	1
1.1 Flexible System Dynamics and Zeros	1
1.2 Limitations of Non-minimum Phase Zeros	5
1.3 Literature Review	14
1.3.1 Physical Interpretation of Zeros	16
1.3.2 Analytical Investigation of Zeros of General Multi-DoF Flexible Systems	19
1.4 Problem Statement	32
1.5 Organization of the Thesis	33
1.6 Research Contributions	35
Chapter 2 On the Zeros of Undamped Three-DoF Flexible Systems	37
2.1 Introduction and Motivation	38
2.2 Literature Review	40
2.3 Zero Dynamics and Modal Decomposition	44
2.4 Two DoF Flexible LTI System	47
2.5 Three DoF Flexible LTI System ¹	49

2.6 Conclusion.....	57
Chapter 3 On the Zeros of Two and Three DoF Damped Flexible Systems	59
3.1 Introduction and Background.....	59
3.2 Zero Dynamics and Modal Decomposition	65
3.3 Multi-DoF Damped Flexible System	67
3.4 Two DoF Damped Flexible LTI Systems	70
3.4.1 Sufficient and Necessary Condition for eliminating CNMP Zeros.....	77
3.4.2 Sufficient and Necessary Conditions for Eliminating RNMP zeros	79
3.4.3 Sufficient and Necessary Conditions for Eliminating all NMP zeros.....	80
3.5 Three-DoF Damped Flexible LTI Systems.....	81
3.5.1 Sufficient Condition for eliminating CNMP Zeros	168
3.5.2 Sufficient and Necessary Conditions for Eliminating all NMP zeros.....	172
3.6 Case Study of Three-DoF Flexible System.....	179
3.7 Conclusion.....	187
Chapter 4 Non-minimum Phase Zeros of Multi-DoF Undamped Flexible Systems	189
4.1 Introduction and Motivation.....	189
4.2 Parity of Number of Zeros on the Real and Imaginary axis.....	195
4.2.1 Parity of number of zeros between $j\omega_f$ and $j\omega_{f+1}$	198
4.2.2 Parity of number of zeros between $j\omega_n$ and $j\infty$	199
4.2.3 Parity of number of zeros between 0 and ∞ on the real axis	202
4.2.4 Parity of number of zeros between 0 and $j\omega_1$ on the imaginary axis.....	204
4.3 Multi-DoF Undamped Flexible Systems.....	206
4.3.1 A Sufficient Condition to eliminate only CNMP zeros.....	207
4.3.2 A Sufficient Condition for the elimination of all NMP zeros	211
4.4 Case Study: Four DoF Undamped Flexible System.....	217

4.5 Conclusion.....	223
Chapter 5 Non-minimum Phase Zeros of Multi-DoF Damped Flexible Systems	226
5.1 Introduction and Background.....	226
5.2 Proportional Damping and Modal Decomposition	231
5.3 Necessary and Sufficient Condition for the elimination of NMP Zeros	236
5.4 Case Study: Four-DoF Flexible System.....	255
5.5 Conclusion.....	261
Chapter 6 Improving the Step Response Performance of Flexible Systems in the Presence of Real Non-minimum Phase Zeros	263
6.1 Introduction and Background.....	263
6.2 Proportional Viscous Damping Strategy.....	267
6.3 Three-link manipulator: Case Study	273
6.4 Conclusion.....	283
Chapter 7 Conclusion and Future Work	284
7.1 Conclusion.....	298
7.2 Future Work	300
Bibliography	303

List of Tables

Table 3-1 Combination of modal residue signs	83
Table 3-2 Range of χ and ζ_v for which Condition (I) of Eq.(3-32) is satisfied.	88
Table 3-3 Range of χ and ζ_v for which Condition (IIA) of Eq.(3-35) is satisfied	89
Table 3- 4 Range of χ and ζ_v for which Conditions (IIB, IIC) of Eq.(3-35) is satisfied. The sign of b is irrelevant in these cases as the sign of a and c cannot be satisfied simultaneously	90
Table 3-5 Range of χ and ζ_v for which Condition (IID) of Eq.(3-35) is satisfied	90
Table 3-6 Range of χ and ζ_v for which Condition (IIIA) of Eq.(3-35) is satisfied.....	91
Table 3-7 Range of χ and ζ_v for which Condition (IIIB) of Eq.(3-35) is satisfied.....	91
Table 3-8 Range of χ and ζ_v for which Condition (IIIC) of Eq.(3-35) is satisfied.....	92
Table 3-9 Range of χ and ζ_v for which Condition (IIID) of Eq.(3-35) is satisfied.....	92
Table 3-10 Facts used to eliminate different scenarios for meeting points of the zero locus of $G_3(s)$ on the positive real axis that are not possible for case (a)	100
Table 3-11 Facts used to eliminate different scenarios for meeting points of the zero locus of $G_3(s)$ on the positive real axis that are not possible for case (b)	106
Table 3-12 Facts used to eliminate different scenarios for meeting points of the zero locus of $G_3(s)$ on the positive real axis that are not possible for case (c)	111
Table 3-13 Facts used to eliminate different scenarios for meeting points of the zero locus of $G_3(s)$ on the positive real axis that are not possible for case f)	119
Table 3-14 Range of χ and ζ_v for which Condition (IIA) of Eq.(3-35) is satisfied	120
Table 3-15 Range of χ and ζ_v for which Condition (IIB) and (IIC) of Eq.(3-35) is satisfied....	120
Table 3-16 Range of χ and ζ_v for which Condition (IID) of Eq.(3-35) is satisfied	121
Table 3-17 Range of χ and ζ_v for which Condition (IIIA) of Eq.(3-35) is satisfied.....	121
Table 3-18 Range of χ and ζ_v for which Condition (IIIB) of Eq.(3-35) is satisfied	122

Table 3-19 Range of χ and ζ_v for which Condition (IIIC) of Eq.(3-35) is satisfied	123
Table 3-20 Range of χ and ζ_v for which Condition (IIID) of Eq.(3-35) is satisfied	123
Table 3- 21 Facts used to eliminate different scenarios for meeting points of the zero locus of $G_3(s)$ on the positive real axis that are not possible for case (g)	129
Table 3- 22 Facts used to eliminate different scenarios for meeting points of the zero locus of $G_3(s)$ on the positive real axis that are not possible for case (h)	134
Table 3- 23 Facts used to eliminate different scenarios for meeting points of the zero locus of $G_3(s)$ on the positive real axis that are not possible for case (i)	139
Table 3-24 Range of χ and ζ_v for which Condition (IIA) of Eq.(3-35) is satisfied	140
Table 3-25 Range of χ and ζ_v for which Condition (IIB) and (IIC) of Eq.(3-35) is satisfied....	140
Table 3-26 Range of χ and ζ_v for which Condition (IID) of Eq.(3-35) is satisfied	140
Table 3-27 Range of χ and ζ_v for which Condition (IIIA) of Eq.(3-35) is satisfied	141
Table 3-28 Range of χ and ζ_v for which Condition (IIIB) of Eq.(3-35) is satisfied	141
Table 3-29 Range of χ and ζ_v for which Condition (IIIC) of Eq.(3-35) is satisfied	142
Table 3-30 Range of χ and ζ_v for which Condition (IIID) of Eq.(3-35) is satisfied	142
Table 3-31 Facts used to eliminate different scenarios for meeting points of the zero locus of $G_3(s)$ on the positive real axis that are not possible for case (j)	147
Table 3-32 Facts used to eliminate different scenarios for meeting points of the zero locus of $G_3(s)$ on the positive real axis that are not possible for case (k)	152
Table 3-33 Facts used to eliminate different scenarios for meeting points of the zero locus of $G_3(s)$ on the positive real axis that are not possible for case (n)	160
Table 3-34 Range of χ and ζ_v for which Condition (IIA,IIIA) of Eq.(3-35) is satisfied	164
Table 4-1 Modal residue sign sequence for transfer functions.....	220
Table 5-1: Intersection of the hyperbola and envelope curve with the x and y axis.....	240
Table 5-2 Zeros of the transfer functions of the proportionally damped four DoF flexible system	259
Table 6-1 Step response characteristics during successive design steps.....	281

List of Figures

Fig 1-1 Root locus for two different relative positions of open loop poles (cross) and zeros (circle) (a) Zero-pole alternation (b) No zero-pole alternation	3
Fig 1-2 (a) Location of poles and zero in the s -plane (b) Step response of lightly and heavily damped flexible system.....	7
Fig 1-3 Tradeoff between settling time and undershoot in the presence of CNMP zeros	9
Fig 1-4 Feedback control using single-input (F) and single-output (q).....	10
Fig 1-5 Graphical illustration of the Poisson sensitivity integral in the presence of NMP zeros ..	12
Fig 1-6 Different types of zeros in the s -plane	15
Fig 1-7 Physical interpretation of MMP zeros.....	16
Fig 1-8 Example of a flexible system that satisfies Hoagg's sufficient condition.....	21
Fig 1-9 Example of a multi-directional flexible system	22
Fig 1-10 Flexible system demonstrating physical equivalence between Lin's sufficient condition and actuator-sensor collocation.....	27
Fig 1-11 An example to demonstrate that all modal residue signs being the same does not necessarily satisfy Lin's sufficient condition.....	29
Fig 1-12 Venn diagram of sufficient conditions for the absence of CNMP and RNMP zeros.....	33
Fig 2-1 Types of zeros in a LTI system	38
Fig 2-2 Zero locus of two-DoF flexible system.....	48
Fig 2-3 Zero loci of $G(s)$	53
Fig 3-1 Sign of $\sin(\theta)$ when the zero $(x+jy)$ lies in various regions of the s -plane	69
Fig 3-2 Zero Loci of $G_2(s)$ for different ranges of χ as κ varies from $-\infty$ to 0. Zeros and poles of $T_2(s)$ provide the starting and ending locations, respectively, of these zero loci.....	76
Fig 3-3 Scenarios for the meeting points on the real axis by the zero locus of $G_3(s)$	97
Fig 3-4 Flowchart showing the entire process of characterization of zeros for case (a)	101

Fig 3-5 Zero Loci of $G_3(s)$ for different ranges of κ , χ and ζ_v as α_v varies from $-\infty$ to 0 (green curve) and 0 to $+\infty$ (red curve). The parameter ranges of κ , χ and ζ_v are given below each sub figure.....	167
Fig 3-6 Three-DoF undamped flexible system.....	179
Fig 3-7 Three-DoF damped flexible system.....	180
Fig 3-8 Bode plots of: a) Undamped vs. damped system with tuned damping to eliminate NMP zeros, b) Damped system with tuned damping and sensor vector to place the zero on the imaginary axis.....	186
Fig 3-9 Robust elimination of NMP zeros under variation in sensor vector.....	187
Fig 4-1 Imaginary and real axis divided into four distinct segments.....	197
Fig 4-2 Distribution of zeros w.r.t the poles when $r = 0$ and number of modal residue sign change = 1 (a) Zero is in Segment 2 as MMP (b) Zero is in Segment 3 as RNMP (c) Zero is in Segment 4 as MMP.....	216
Fig 4-3 Four-doF collinear lumped parameter undamped flexible LTI system.....	217
Fig 4-4 Modal frequencies of the Four DoF undamped flexible system as a function of Δk	219
Fig 4-5 Zeros of transfer functions as a function of Δk (from $\Delta k = -100$ to $\Delta k = 500$).....	222
Fig 4-6 Damping strategy that preserves the MP behavior of multi-DoF undamped flexible systems.....	225
Fig 5-1 Flowchart of design strategies to eliminate NMP zeros.....	229
Fig 5-2 Pink shaded regions in the first quadrant of the Cartesian plane that satisfy Eq. (5-20)	252
Fig 5-3 Undamped four-DoF flexible system.....	255
Fig 5-4 Position of the zeros of the undamped flexible system with respect to the envelope curve for different c_K	259
Fig 5-5 Dashpot placement in proportionally damped four-DoF flexible system.....	261
Fig 6-1 Effect of the proportional viscous damping strategy i.e. $c_M = 0$ and $c_K > 0$ on the real zeros of flexible systems.....	273
Fig 6-2 Schematic view of a three-link manipulator.....	273
Fig 6-3 Step response of the system for various $\text{Re}(p_1)$	275
Fig 6-4 Step response of the system for various $\text{Im}(p_1)$	276

Fig 6-5 Step response of the system in the presence of feedback controller and proportional damping for various damping constants	278
Fig 6-6 Final step response of the system vs. feedback controller best performance.....	280
Fig 6-7 Pole-zero map of the system during the proposed design strategy	281
Fig 6-8 Control block diagram of the proposed design strategy.....	282
Fig 7-1 Flexure bearing based motion system	285
Fig 7-2 Frequency response function of the transfer function: $x_1(s)/F_{x4}(s)$	286
Fig 7-3 Mode shapes for 210 Hz and 220 Hz when $\varepsilon_{\text{actuator}} > 0$ and $\varepsilon_{\text{sensor}} > 0$ (only showing m_1 and m_4)	289
Fig 7-4 Mode shapes for 210 Hz and 220 Hz when $\varepsilon_{\text{actuator}} > 0$ and $\varepsilon_{\text{sensor}} < 0$ (only showing m_1 and m_4)	291
Fig 7-5 Frequency response function of the transfer function: $x_1(s)/F_{x4}(s)$ for $\varepsilon_{\text{sensor}} < 0$	293

Abstract

The objective of this thesis is to investigate the genesis of zeros in the single-input single-output (SISO) transfer function of flexible linear time invariant (LTI) systems, and provide necessary and sufficient conditions to specifically guarantee the absence of non-minimum phase zeros. Flexible system dynamics plays a vital role in several motion and vibration control applications such as space structures, rotorcraft blades, hard-disk drives, flexure mechanisms, flexible manipulators, and motion systems with transmission compliance. These applications often require feedback and feedforward controls to achieve desirable dynamic performance, which generally includes high speed, low settling time, effective disturbance rejection, low sensitivity to modeling uncertainties, and stability robustness.

Zeros in the transfer function, defined by the actuated load input and sensed displacement output of a flexible system, have a significant impact on its dynamic performance. Non-minimum phase zeros (i.e. zeros in the right half s-plane), in particular, lead to significant tradeoffs among the competing dynamic performance requirements. Therefore, there is a need for physical design strategies that are informed by mathematical conditions to guarantee the absence of non-minimum phase zeros. Comprehensive and precise mathematical conditions do not currently exist in the literature. A well-known mathematical condition states that when all the modal residue signs of an undamped flexible LTI system are the same, the zeros of that system are guaranteed to be minimum phase. However, the same sign of all modal residues is a sufficient condition and not a necessary one. In other words, this condition is overly restrictive – there are many systems that *do not* satisfy this condition but still exhibit no non-minimum phase zeros. Furthermore, it may not always be possible to achieve the same sign of all modal residues given various practical constraints on the distribution of mass and stiffness and

location of actuators and sensors. Apart from mass-stiffness distribution and actuator-sensor placement, one can also explore the use of viscous damping to change the position of zeros. Viscous damping is generally found to be beneficial for the poles of the flexible system because it moves them to the left-hand side of the s -plane leading to smaller overshoot and residual vibration. However, the effect of viscous damping on the zeros has not been adequately investigated in the existing literature and therefore, there does not exist any physical design strategy where viscous damping is used in a deterministic manner to guarantee the absence of non-minimum phase zeros in the transfer functions of flexible LTI systems. In order to fill these various technical gaps, this thesis makes three key contributions: (i) create a mathematical and graphical framework to explore the necessary and sufficient conditions for the occurrence of different types of zeros in the transfer function of flexible LTI systems, with and without viscous damping; (ii) derive the necessary and/or sufficient conditions to guarantee the absence of non-minimum phase zeros for various flexible LTI systems with and without viscous damping; and, (iii) implement design strategies informed by the above mathematical conditions to demonstrate the absence of non-minimum phase zeros with and without viscous damping.

The necessary and sufficient conditions for the absence of non-minimum phase zeros are derived for undamped and viscous damped, two and three degrees of freedom (DoF) flexible LTI systems by constructing a comprehensive set of zero loci that cover all possible distribution of the zeros with respect to the poles for all possible values of system parameters, which include modal residues, modal frequencies, and modal damping ratios. However, as the number of DoFs increase, the parameter space rapidly expands, making this zero loci based framework tedious and complicated. In order to overcome this issue and prove that there exist other sequences of modal residue signs apart from ‘same sign of all modal residues’ that guarantee the absence of NMP zeros, the parity (i.e. odd/even) of the number of zeros with respect to the poles in the system transfer function is investigated. This investigation leads to a non-unique sufficient condition for the absence of non-minimum phase zeros in terms of the system parameters that is applicable to undamped flexible LTI system with any arbitrary number of

DoFs (or modes). Furthermore, the zero dynamics of a multi-DoF proportionally viscous damped flexible LTI system is investigated using a change of variable method that reduces its large parameter space to a few composite parameters. This leads to a sufficient condition for the absence of non-minimum phase zeros using proportional viscous damping in multi-DoF flexible LTI systems.

The efficacy of the sufficient conditions derived for undamped and viscous damped flexible systems with any arbitrary number of DoFs (modes) is theoretically demonstrated in multiple case studies by making informed design choices of physical parameters such as actuator-sensor placement, mass-stiffness distribution and viscous damping strategy that satisfy these sufficient conditions for different flexible systems. For undamped flexible systems, a step-by-step physical design strategy is provided to choose mass-stiffness distribution and actuator-sensor placement that lead to the required sequence of modal residue signs (not necessarily ‘same sign of all modal residues’) that guarantee the absence of NMP zeros. For proportionally viscous damped flexible systems, keeping the mass-stiffness distribution and actuator-sensor placement unchanged, a step-by-step design strategy is provided to choose only the viscous damping values to guarantee the absence of NMP zeros. Furthermore, in certain cases where proportional viscous damping cannot guarantee the absence of NMP zeros, a step-by-step design strategy is provided to use proportional viscous damping to move all these NMP zeros further away from the imaginary axis, thereby mitigating their effect on the dynamic performance of the flexible systems. These various case studies demonstrate the practical utility (from a physical system design standpoint) of the mathematical results derived in this thesis.

Chapter 1 Introduction and Background

1.1 Flexible System Dynamics and Zeros

A flexible system is a dynamic system that consists of inertia and compliance elements. A spring mass system is an ideal example of a flexible system in the mechanical domain where the mass is the inertia element and the spring is the compliance element. Similarly, an inductor capacitor (LC) circuit is an example of a flexible system in the electrical domain where the inductor is the inertia element and capacitor is the compliance element. Flexible systems may or may not include an energy dissipating element such as a viscous damper (dashpot) in the mechanical domain or a resistor in the electrical domain. In this thesis, we will be studying linear time invariant (LTI) flexible system dynamics. The equations of motion of such flexible system dynamics is given by:

$$\begin{aligned} [\mathbf{M}]_{n \times n} \ddot{w} + [\mathbf{C}]_{n \times n} \dot{w} + [\mathbf{K}]_{n \times n} w &= [\mathbf{B}]_{n \times 1} F \\ q &= [\mathbf{D}]_{1 \times n} w \end{aligned} \quad (1-1)$$
$$\Rightarrow \frac{q(s)}{F(s)} = [\mathbf{D}]_{1 \times n} \left([\mathbf{M}]s^2 + [\mathbf{C}]s + [\mathbf{K}] \right)_{n \times n}^{-1} [\mathbf{B}]_{n \times 1}$$

where, $[\mathbf{M}]$, $[\mathbf{C}]$, and $[\mathbf{K}]$ denote the mass (inertia element), damping (energy dissipating element), and stiffness (compliant element) matrices, respectively; F denotes the force acting on the system through an input vector $[\mathbf{B}]$; and, q is the measured displacement and is a linear combination, captured by sensor vector $[\mathbf{D}]$, of the individual DoF displacements denoted by w . n denotes the degrees of freedom (DOFs) or the number of flexible modes of the system. The dynamics of a LTI single-input single-output (SISO) flexible system can be expressed in terms of its transfer function,

defined by the actuated load input, F and sensed displacement output, q as shown in Eq.(1-1). To understand the genesis of poles and zeros in the system dynamics, the transfer function in Eq.(1-1) can be re-written in terms of a numerator and denominator polynomial as shown below.

$$\frac{q(s)}{F(s)} = \frac{b_m s^m + \dots + b_1 s + b_0}{a_{2n} s^{2n} + \dots + a_1 s + a_0} \quad (1-2)$$

The coefficients in the numerator and denominator of the transfer function i.e. a_n to a_0 and b_m to b_0 are real and depend on the physical parameters $[\mathbf{M}]$, $[\mathbf{C}]$, $[\mathbf{K}]$, $[\mathbf{B}]$, and $[\mathbf{D}]$. Since, the flexible system under investigation is a physical system (and therefore causal), the relative degree of the transfer function i.e. $(2n - m)$ is positive. The transfer function is characterized by poles and zeros which are the roots of the denominator and the numerator of the transfer function, respectively. The flexible systems under investigation in this thesis are assumed to be stable. Mathematically, this means that all the poles of the transfer function of the flexible system lie on the closed left-hand side (LHS) of the imaginary axis in the s -plane (this also includes the imaginary axis).

Several machines used in motion and vibration control application exhibit flexible system dynamics such as spacecrafts [1, 2], hard disks [3, 4], rotorcraft blades [5], flexure mechanisms [6, 7], and motion systems with transmission compliance [8], among others. In all these applications, the machines are expected to fulfill some or all of the following dynamic requirements simultaneously: low settling time, low undershoot & overshoot in step response, high rejection of disturbances (from actuator and environment) and noise (from sensor), high stability robustness under parametric variations, and excellent trajectory tracking. The ability of a flexible system to achieve all these dynamic requirements simultaneously, via feedback and/or feedforward controls, depends on the position of the poles and zeros of its transfer function in the s -plane. This can be shown via the following example. Consider the case of two flexible systems (whose open-loop poles and zeros in the s -plane are shown in Fig 1-1a and Fig 1-1b) that are operating under the

same closed-loop control where the controller is a simple lead compensator. The root loci (or the trajectories of the closed-loop poles) of the two flexible systems under closed-loop control are shown in Fig 1-1a and Fig 1-1b. Based on the rules of root locus, the trajectory of the closed-loop poles start from the open-loop poles for small values of controller gains and approach the open-loop zeros for large controller gains.

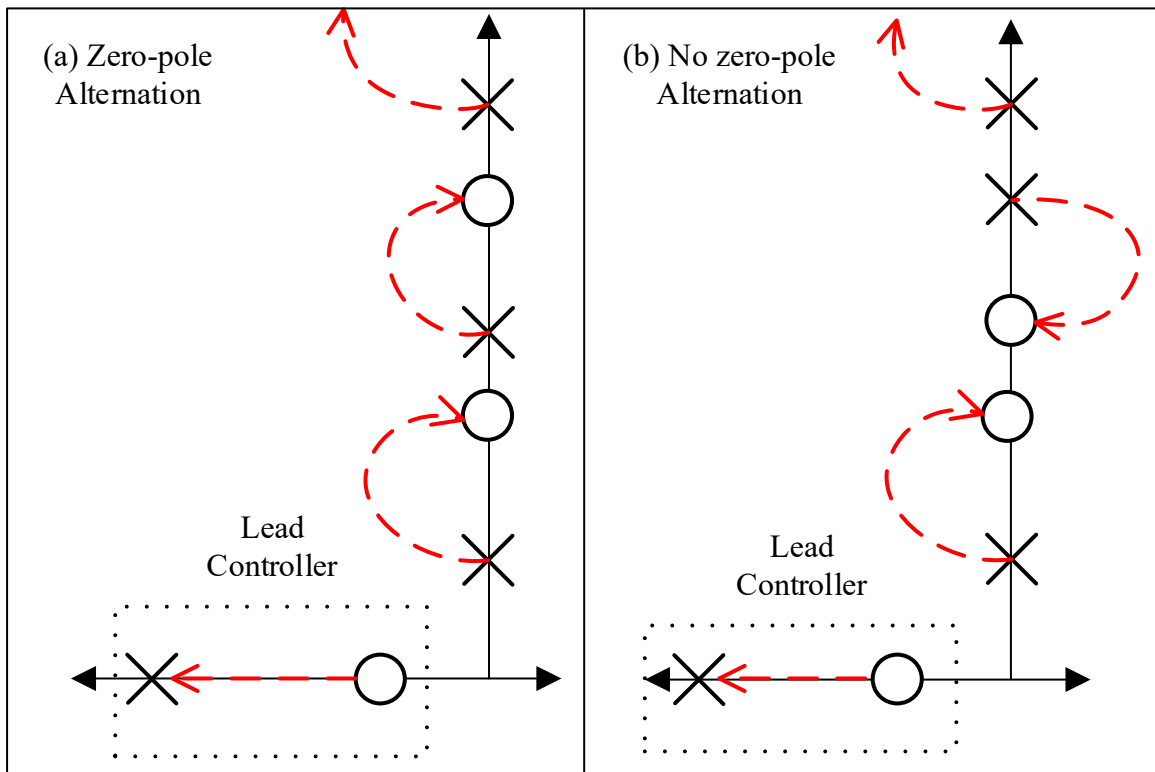


Fig 1-1 Root locus for two different relative positions of open loop poles (cross) and zeros (circle) (a) Zero-pole alternation (b) No zero-pole alternation

Fig 1-1a illustrates a sequence of open-loop zeros and poles on the imaginary axis, referred to as zero-pole alternation. In zero-pole alternation, every pole is preceded by a zero on the imaginary axis except the first pole which correspond to the 'rigid body mode'. For this sequence of open-loop poles and zeros on the imaginary axis, the closed-loop system is always stable for any value of controller gain since the root locus lies strictly on the left-hand side (LHS) of the imaginary

axis. Therefore, one can choose the closed-loop controller gain (associated with the lead compensator) to achieve a good tradeoff between competing dynamic performance requirements such as disturbance rejection and noise rejection, without worrying about stability. In contrast, Fig 1-1b illustrates the case when zero-pole alternation is not observed. In this case, the closed-loop system cannot be made stable for any value of closed-loop controller gain since a portion of the root locus always lies on the right-hand side (RHS) of the imaginary axis. In reality, any flexible system is lightly damped and therefore, the the open-loop poles lie slightly to the LHS of the imaginary axis. Therefore, the closed-loop system (root locus is given by Fig 1-1b) can be stable for very small values of closed-loop controller gain. This negatively impacts the closed-loop system's ability to achieve a good tradeoff between competing dynamic performance requirements. For example, small closed-loop controller gain will lead to good noise rejection but poor disturbance rejection. This example demonstrates that the position of poles and zeros of a flexible system in the s -plane can significantly impact its ability to simultaneously achieve different dynamic performance requirements.

Note that for the sequence of open-loop poles and zeros illustrated by Fig 1-1b, one can still use feedforward control strategies to invert the open-loop dynamics in order to achieve better dynamic performance [9, 10] if an accurate model of the open-loop dynamics is readily available. Oftentimes, a combination of feedback and feedforward control strategy [11, 12] is used to satisfy the key dynamic requirements, wherein the feedforward portion of the control strategy provides high speed and good trajectory tracking performance by inverting the flexible system dynamics and the feedback portion of the control strategy provides stability robustness against parametric variation and good disturbance rejection capabilities. However, if the open-loop zero lies strictly on the right-hand side (RHS) of the imaginary axis then irrespective of the control strategy

(feedback / feedforward / their combination), it becomes even more challenging (as compared to other positions of open-loop zeros in the s -plane such as the one shown in Fig 1-1b) to simultaneously achieve all key dynamic performance requirements. The zeros that lie strictly on the RHS of the imaginary axis are referred to as non-minimum phase (NMP) zeros. The presence of these zeros lead to significant tradeoffs between the competing dynamic performance requirements [13-15].

1.2 Limitations of Non-minimum Phase Zeros

A zero that has a positive real component is a non-minimum phase (NMP) zero. There are two types of NMP zeros: real NMP (RNMP) zero whose imaginary component is zero and complex NMP (CNMP) zero whose imaginary component is non-zero. The latter always occur in complex conjugate pairs. The detrimental effects of NMP zeros are evident in the time domain as well as the frequency domain. We will use simple feedback and feedforward control strategies in this section to demonstrate the detrimental effects of NMP zeros.

In the time domain, the presence of atleast one RNMP zero in the transfer function guarantees the occurrence of undershoot in the step response of the flexible system [13]. Furthermore, the presence of RNMP zeros introduces a tradeoff between undershoot and settling time in the step response [16]. This tradeoff between settling time and undershoot is algebraically expressed by:

$$\frac{1-\beta}{e^{xt_s}-1} \leq y_{us} \quad (1-3)$$

where $\beta (< 1)$ is the settling window, t_s is the settling time for the given settling window β , $x (> 0)$ is the RNMP zero, $y_{us} (> 0)$ is the undershoot in the step response as shown in Fig 1-2b. Eq.(1-3) demonstrates that for a fixed value of RNMP zero (x) and settling window (β), if one tries to reduce the settling time (t_s), the LHS of Eq.(1-3), will increase. Since the LHS of Eq.(1-3) defines the

lower limit of the undershoot (y_{us}), a higher value of this LHS will eventually lead to a larger undershoot (y_{us}). Conversely, it also demonstrates that smaller undershoot is achieved at the expense of larger settling time. This tradeoff between undershoot and settling time in the presence of RNMP zeros was independently proven by other researchers [17, 18] as well who demonstrated that fast settling time and small undershoot, which are of practical relevance in several motion control applications, are conflicting requirements in the presence of RNMP zeros.

The tradeoff between settling time and undershoot is demonstrated via an illustrative example of a flexible system with one pair of complex conjugate poles and one RNMP zero in the s -plane in Fig 1-2a. As expected, the presence of the RNMP zero leads an initial undershoot in the step response in time domain. Furthermore, in the beginning, this flexible system is characterized by lightly damped poles. Therefore, its step response exhibits a large undershoot ($y_{us,ld}$), a large overshoot, slow settling time ($t_{\beta,ld}$). In order to achieve faster settling time and smaller overshoot, a simple feedforward control strategy can be implemented that cancels the two lightly damped poles with two controller zeros at the same location as the poles, and add two heavily damped controller poles. The net effect is that the poles of the flexible system are moved further away from the imaginary axis (assuming perfect or close to perfect pole-zero cancellation). However, the position of the RNMP zero remains the same because cancelation of the RNMP zero requires a controller pole in the RHS of the s -plane which will lead to an unstable system.

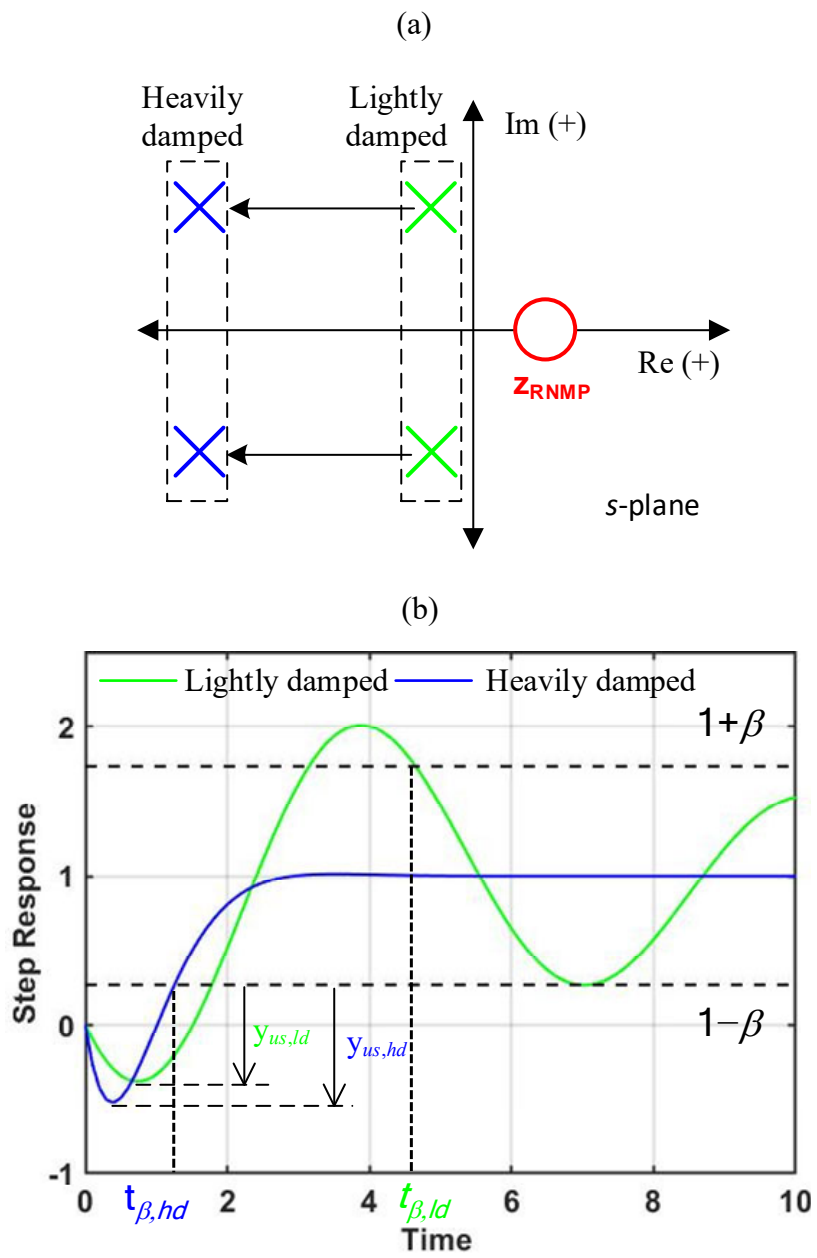


Fig 1-2 (a) Location of poles and zero in the s -plane (b) Step response of lightly and heavily damped flexible system

The heavily damped flexible system now demonstrates faster settling time, $t_{\beta,hd}$ and almost no overshoot in its step response as shown in Fig 1-2b. However, because the position of the RNMP zero remained constant the undershoot of the heavily damped system becomes greater as compared

to its lightly damped counterpart i.e. $y_{us,ld} < y_{us,hd}$. This demonstrates the tradeoff between settling time and undershoot in the presence of a simple feedforward control strategy. In the presence of this control strategy, faster settling time and smaller undershoot can indeed be achieved simultaneously but only via the absence of the RNMP zero or by moving it further away from the imaginary axis.

RNMP zeros are not the only zeros that exhibit undershoot. Certain positions of CNMP zeros in the RHS of the s -plane can also lead to an undershoot in the step response. Numerical simulations of simple flexible systems [19] have shown that when a pair of CNMP zeros is far away from the positive real axis, the step response does not exhibit any undershoot. However, as the CNMP zero pair gets closer to the positive real axis, the step response starts to exhibit undershoot. Therefore, one can conjecture that when the CNMP zero pair lies sufficiently close to the positive real axis, it can impose a tradeoff between settling time and undershoot. However, unlike the case for RNMP zero, there is currently no mathematical expression in the existing literature that captures this tradeoff. In order to demonstrate the conjecture that the presence of CNMP zeros can impose a tradeoff between settling time and undershoot, consider a simple numerical example shown below where the CNMP zero pair is chosen close enough to the positive real axis for the step response to exhibit an undershoot.

$$G_1(s) = \frac{s^2 - s + 1.25}{0.06064s^4 + 0.1455s^3 + 1.161s^2 + 1.106s + 1.25} \quad (1-4)$$

$$G_2(s) = \frac{s^2 - s + 1.25}{0.002155s^4 + 0.05172s^3 + 0.4332s^2 + 1.216s + 1.25}$$

Both $G_1(s)$ and $G_2(s)$ have one pair of CNMP zero at the same location i.e. $0.5 \pm 1j$. However, the poles of $G_2(s)$ i.e. $-2 \pm 1j$ and $-10 \pm 4j$ are further away from the imaginary axis and well damped as compared to the poles of $G_1(s)$ i.e. $-0.5 \pm 1j$ and $-0.7 \pm 4j$. Therefore, $G_2(s)$ represents

a flexible system with faster dynamics and smaller settling time as compared to $G_1(s)$. This is evident in the figure below where $t_{\beta,1} > t_{\beta,2}$. However, due to the presence of a CNMP zero pair close to the positive real axis, the smaller settling time is obtained at the cost of higher undershoot i.e. $y_{us,1} < y_{us,2}$.

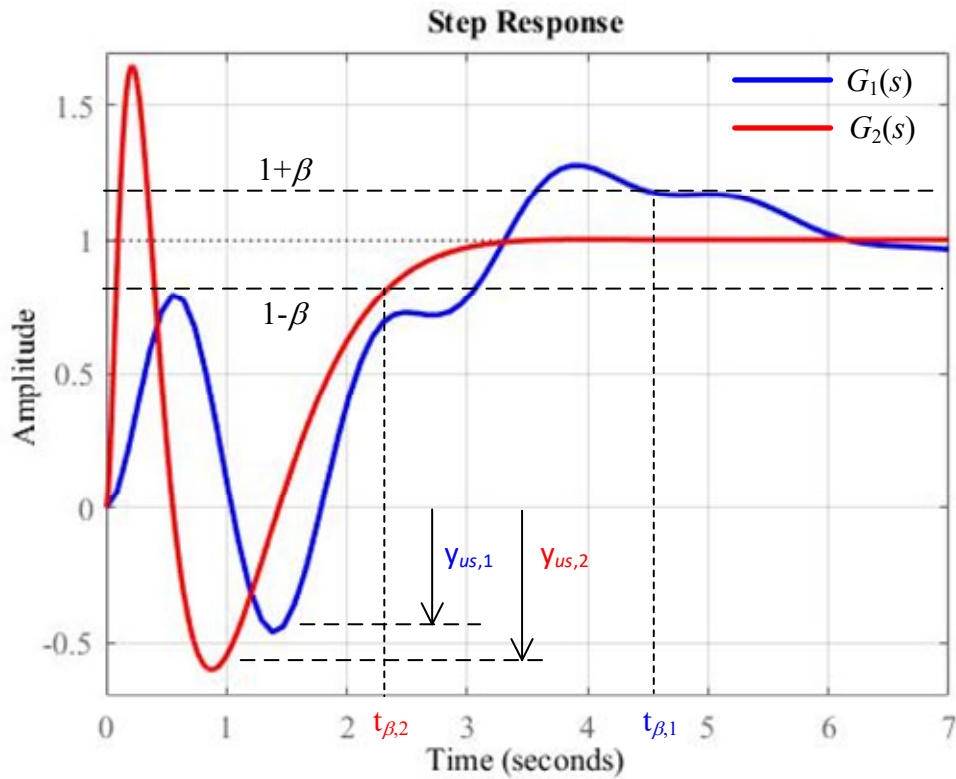


Fig 1-3 Tradeoff between settling time and undershoot in the presence of CNMP zeros

Note that a simple feedforward control strategy (similar to the one used in Fig 1-2a) can be used to transform the transfer function $G_1(s)$ into $G_2(s)$. This feedforward control strategy can only change the location of the poles. The location of the CNMP zero pair will remain unchanged. Therefore, in the presence of a simple feedforward control strategy (similar to the one used in Fig 1-2a), faster settling time and smaller undershoot can be simultaneously achieved only via the elimination of the CNMP zero pair or moving it further away from the positive real axis (based on

the above conjecture supported by the numerical examples in [19]) or moving it further away from the imaginary axis (similar to RNMP zeros).

So far we have discussed the detrimental effects of RNMP and CNMP zeros in the time domain. The step response demonstrates undershoot in the presence of RNMP zeros. However, the step response may or may not demonstrate undershoot in the presence of CNMP zeros depending on their location in the RHS of the s -plane. Now we will discuss the detrimental effect of NMP zeros in the frequency domain. In the frequency domain, performance tradeoff is imposed in the presence of both CNMP and RNMP zeros, irrespective of their location in the RHS of the s -plane.

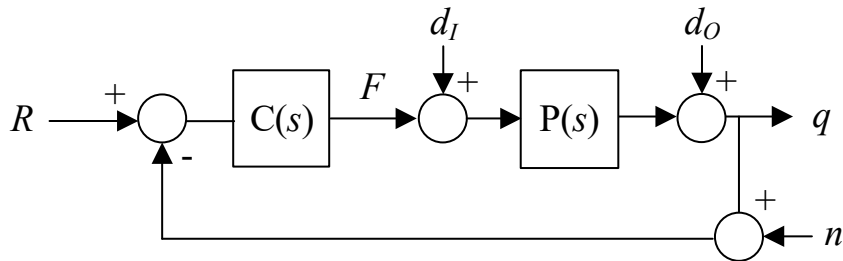


Fig 1-4 Feedback control using single-input (F) and single-output (q)

To understand the detrimental effect of NMP zeros in the frequency domain, consider the feedback control strategy shown in Fig 1-4 where only a single sensor is used to measure the displacement q , and this measurement is fed back to the controller $C(s)$, which actuates the plant, $P(s)$ via force, F . This control strategy is referred to as single-input single-output (SISO) feedback control. In the frequency domain, disturbance rejection and low sensitivity to modeling uncertainties dictate the low frequency performance specification. Noise rejection, robustness against unmodelled dynamics as well as actuator saturation dictate the high frequency bandwidth limitation. For the SISO control strategy, the bode gain-phase relationship implies a tradeoff between the low frequency performance specification and the high frequency bandwidth limitation. Specifically, the rate of gain decrease near crossover frequency should not be greater

than -20 dB/decade in order to achieve nominal stability and reasonable phase margin that guarantee stability robustness. However, the presence of NMP zero in the open loop transfer function $q(s)/F(s)$ contributes additional phase lag, therefore worsening the design tradeoff between high gain at low frequencies and low gain at high frequencies. This implies that the gain crossover frequency must lie well below the frequency where the NMP zero contributes to the additional phase lag. Since the gain crossover frequency is closely related to closed-loop bandwidth, the presence of NMP zero limits the achievable closed-loop bandwidth.

Another way to understand the limitation imposed by NMP zeros is through the Poisson sensitivity integral (defined only in the presence of NMP zeros) which mathematically demonstrates the tradeoff between disturbance rejection at low frequencies, noise rejection at high frequencies and stability robustness of the closed-loop system in the presence of an NMP zero [18].

$$\text{Poisson Sensitivity Integral: } \int_0^{\infty} \log|S(j\omega)| W(\mathbf{z}_{NMP}, \omega) d\omega = 0$$

$$\text{where } \mathbf{z}_{NMP} = x + jy, W(\mathbf{z}_{NMP}, \omega) = \frac{x}{x^2 + (y - \omega)^2} + \frac{x}{x^2 + (y + \omega)^2} \quad (1-5)$$

$$S(j\omega) = \frac{q(s)}{d_o(s)} = \frac{1}{1 + P(s)C(s)}$$

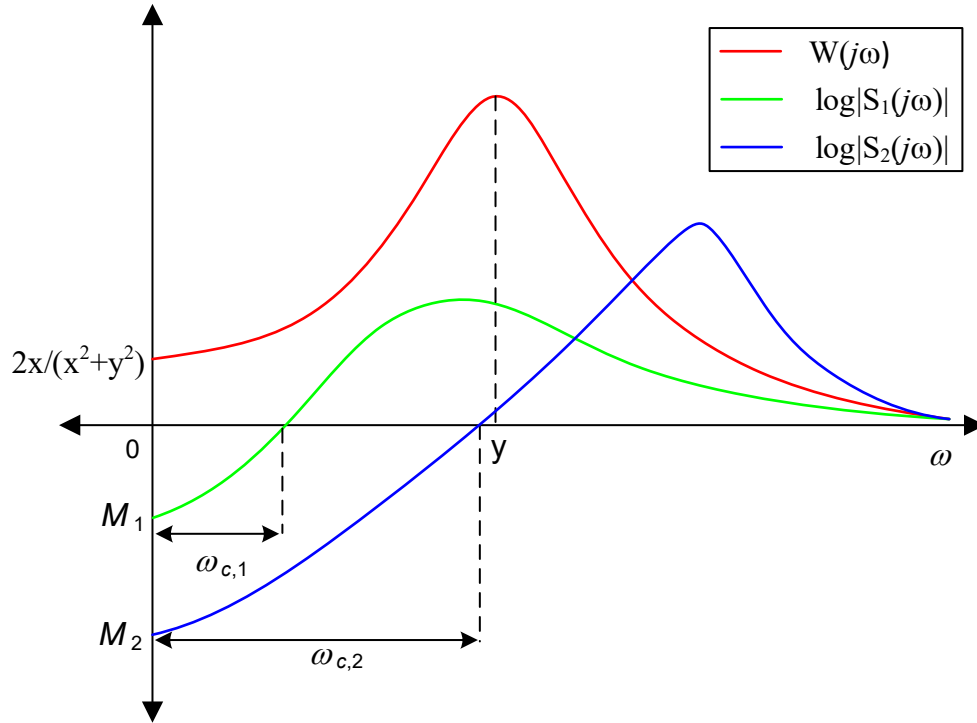


Fig 1-5 Graphical illustration of the Poisson sensitivity integral in the presence of NMP zeros

$S(j\omega)$ is the sensitivity function of the closed-loop system (shown in Fig 1-4) which is illustrated in Fig 1-5 by a representative curve, $\log|S_1(j\omega)|$. In order to achieve good disturbance rejection over a large frequency range, M_1 and $\omega_{c,1}$ should be as large as possible. Furthermore, in order to achieve good noise rejection, $\log|S_1(j\omega)|$ should tend to 0 at high frequencies. Now, in the presence of an NMP zero, the Poisson sensitivity integral must be satisfied. This means that the weighted area under the $\log|S_1(j\omega)|$ must be equal to zero. Therefore, the weighted negative area under $\log|S_1(j\omega)|$ (for $\omega < \omega_{c,1}$) should be balanced by its weighted positive area (for $\omega > \omega_{c,1}$). The weightage function, $W(j\omega)$ is small when $\omega \ll y$ (location of NMP zero), achieves its maxima at y and then rapidly goes to zero at high frequencies. If one tries to achieve good disturbance rejection over a wider range of frequency i.e. $\omega_{c,1} < \omega_{c,2}$, the negative area under $\log|S_2(j\omega)|$ (for $\omega < \omega_{c,2}$) increases which must be balanced by the positive area under $\log|S_2(j\omega)|$ (for $\omega > \omega_{c,2}$). As the frequency

range gets closer to the location of the NMP zero i.e. $\omega_{c,2} \approx \gamma$, it leads to a larger peak in this positive area in $\log|S_2(j\omega)|$ as compared $\log|S_1(j\omega)|$. The peak of the sensitivity function is a measure of the stability robustness of the closed loop system. Larger peak suggests low stability robustness and higher likelihood of instability in the presence of modeling uncertainties, unmodelled dynamics and parametric variations. $\omega_{c,1}$ and $\omega_{c,2}$ are a measure of the closed-loop bandwidth of the system. Therefore, as the closed-loop bandwidth gets closer to the location of the NMP zero, the stability robustness of the closed-loop system gets poorer. Therefore, NMP zeros that lie within the desired closed-loop bandwidth impose non-trivial and significant performance tradeoff in the frequency domain. Unlike the design tradeoff imposed by the Bode waterbed effect, the Poisson sensitivity integral ensures a peak in the sensitivity function due to the presence of NMP zeros even without the assumption of additional bandwidth constraints imposed by effects such as actuator saturation. This follows from the weightage function, $W(j\omega)$ in the Poisson sensitivity integral, which implies that the weighted length of the $j\omega$ axis is finite.

Simple feedback and feedforward control strategies were used in this section to highlight the dynamic performance challenges imposed by the presence of NMP zeros. Various other advanced control strategies have been reported in the literature to alleviate these challenges with limited success. The various control strategies reported in the literature can be broadly classified into: approximate model inversion, direct model inversion with preview, and optimal control among others. Approximate model inversion strategies either cancel the magnitude or the phase error across all frequencies but not both, leading to poor transient behavior of the system [20, 21]. Several variations of these control strategies have been reported in the literature that provide incremental improvements [22, 23]. Direct model inversion strategies provide better transient response by optimally choosing the control input that minimizes the error between the desired and

output trajectory [24, 25]. However, these strategies require apriori knowledge of the desired trajectory which may not be suitable for applications where trajectory anticipation is not available. On the other hand, certain optimal control strategies [26, 27] generate control inputs that minimize the settling time subject to the undershoot constraint. If NMP zeros could be eliminated in flexible systems or if RNMP zeros of flexible systems could be moved further away from the imaginary axis via suitable physical system design e.g. mass-stiffness distribution, actuator-sensor placement, and viscous damping strategy, these control strategies will lead to the minimum settling time subject to even smaller undershoot constraint.

Therefore, there is a need for a broader mechatronic design strategy that combines physical system and control system design to achieve better dynamic performance. The objective of the physical system design would be to either eliminate NMP zeros or at least move them outside the desired closed-loop bandwidth so that existing control strategies can be more effectively implemented on the flexible system. *Therefore, in this thesis, we will primarily investigate the impact of physical system design i.e. change in mass-stiffness distribution, actuator-sensor placement, and viscous damping strategies on the genesis of NMP zeros and formulate design strategies in terms of physical parameters to guarantee their absence.*

1.3 Literature Review

There are six different types of zeros that can occur in the transfer function of a flexible system. These zeros are graphically shown in the s -plane in Fig 1-6. The mathematical definitions of these zeros are provided below. Let the zero be denoted by $z = x+jy$, where x and y represent the coordinates of the zero in the Cartesian plane.

1. Marginally minimum phase (MMP) zero lies purely on the imaginary axis i.e. $x = 0, y \neq 0$.

2. Complex minimum phase (CMP) zero lies strictly on the left hand side of the imaginary axis i.e. $x < 0, y \neq 0$.
3. Complex non-minimum phase (CNMP) zero lies strictly on the right hand side of the imaginary axis i.e. $x > 0, y \neq 0$.
4. Real minimum phase (RMP) zero lies strictly on the negative real axis i.e. $x < 0, y = 0$.
5. Real non-minimum phase (RNMP) zero lies strictly on the positive real axis i.e. $x > 0, y = 0$.
6. Zero at the origin. It has no real and imaginary component i.e. $x = 0, y = 0$.

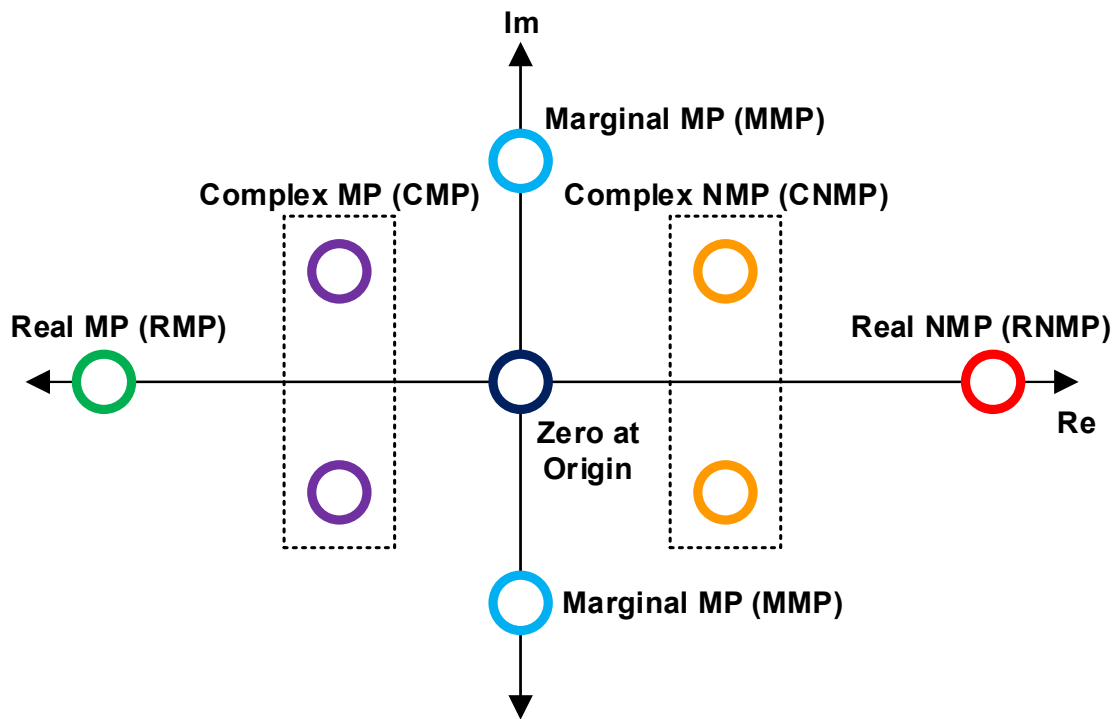


Fig 1-6 Different types of zeros in the s -plane

Having defined the different types of zeros, we will now discuss the existing literature on these zeros especially NMP zeros i.e. CNMP and RNMP zeros. The existing literature on the zeros of flexible LTI systems can be broadly divided into two categories:

1. Physical Interpretation of Zeros

2. Analytical Investigation of Zeros in General Multi-DoF Flexible Systems

1.3.1 Physical Interpretation of Zeros

A physical explanation for the origin of MMP zeros in flexible systems was attempted by Miu [28] and later by Straete [29] and Calafiore [30]. They claimed that the MMP zeros of flexible systems are the resonant frequencies of the substructures constrained by the actuator and sensor.

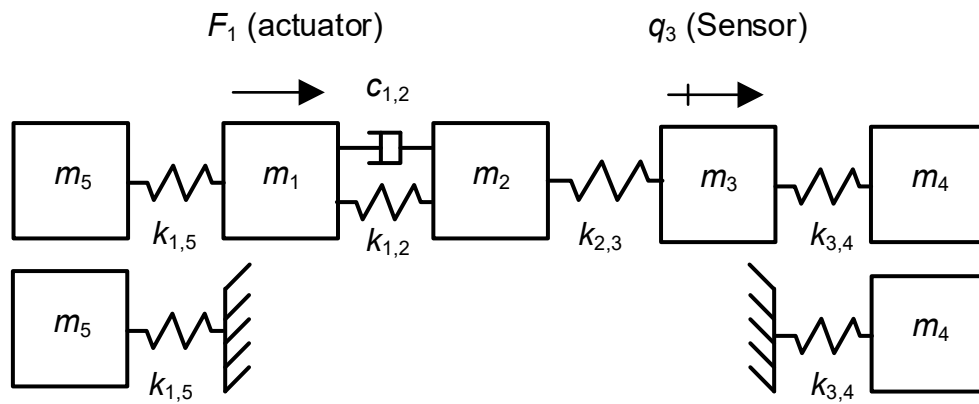


Fig 1-7 Physical interpretation of MMP zeros

In order to demonstrate this physical insight, consider the flexible system shown in Fig 1-7. The transfer function $q_3(s)/F_1(s)$ exhibits two pairs of MMP zeros. In order to predict these MMP zero pairs, first artificially constrain the masses where the actuator and sensor are located and then find the remaining substructures i.e. the substructures that are not confined between the actuator and sensor position. According to Miu, the resonant frequencies of these remaining substructures are the MMP zeros of the transfer function: $q_3(s)/F_1(s)$. In order to physically understand why this happens, consider the following reasoning: when the mass at the actuator location is excited at the MMP zero frequency of the flexible system, there is no output displacement observed in the mass at the sensor location (as per the definition of transfer function zeros). Therefore, the energy being provided by the actuator must be getting localized elsewhere in the system. This localization of

the energy happens in the remaining substructures when the actuator excitation frequency matches their resonant frequency. In Fig 1-7, there are two remaining substructures, one to the left of m_1 and another to the right of m_3 . The resonant frequencies (eigenvalues) of these substructures are $\omega_1 = \sqrt{k_{1,5}/m_5}$ and $\omega_2 = \sqrt{k_{3,4}/m_4}$. Therefore, ω_1 and ω_2 are also the MMP zeros of the transfer function $q_3(s)/F_1(s)$. Miu claimed that the same argument also holds in the presence of viscous damping. If the remaining substructure consists of viscous dampers, then its poles no longer lie purely on the imaginary axis but on its LHS. Therefore, underdamped poles of the remaining substructures are the CMP zeros of the flexible system and critically or overdamped poles of the remaining substructures are the RMP zeros of the flexible system. This physical insight is useful in identifying the remaining substructures and choosing their mass, stiffness and viscous damping properties to place the MMP zeros (or CMP/RMP zeros in the presence of viscous damping) at the desirable position in the s -plane. Since the poles of the remaining substructures either lie on the imaginary axis (for undamped remaining substructures) or on the LHS of the imaginary axis (for damped remaining substructures), Miu's work can only explain the genesis of MMP, CMP and RMP zeros but not CNMP and RNMP zeros.

Miu [28] provides a physical explanation for the genesis of RNMP zeros in the transverse vibration of beams. He argues that the presence of RNMP zeros is attributed to the dynamic coupling that exists between shear forces and bending moments or equivalently, between linear and rotary inertia. This physical argument is useful in explaining the absence of RNMP zeros in dynamic systems characterized by a single type of force and inertia because there is no scope for any dynamic coupling between different forces and inertias. Examples include the longitudinal vibration of bars which is characterized by axial force and linear inertia; and the torsional vibration of bars which is characterized by shear force and rotary inertia. However, in cases where multiple

forces and inertias exist, Miu does not provide any general mathematical description of this so called “dynamic coupling” between the different forces or inertias that lead to RNMP zeros, thereby limiting the usefulness and applicability of his work. In other words, Miu’s work cannot be used to choose physical parameters to guarantee the absence of RNMP zeros in transverse vibration of beams.

Spector [31] suggested that RNMP zeros are a result of the propagation delay caused by finite speed of waves traveling from the actuator to the sensor. This physical explanation was based on the observation that both RNMP zeros and propagation delay cause phase loss in the open-loop frequency response function (FRF) of the flexible system. However, this equivalence between RNMP zeros and propagation delay is flawed on the account that RNMP zeros contribute +20 dB/decade increase in magnitude of the FRF at frequencies higher than the zero frequency but the propagation delay does not contribute anything to the magnitude. In fact, the combination of increase in magnitude and phase loss in the FRF makes the presence of RNMP zeros more detrimental than the propagation delay in the dynamics of flexible systems. Therefore, the genesis of RNMP zeros cannot be attributed to propagation delay. Based on the discussion so far, the physical meaning of RNMP zeros still remains an open question.

Similarly, there is no conclusive physical meaning for CNMP zeros as well. Recent investigation in the dynamics of flexure mechanisms revealed that CNMP zeros and mode localization occur together for the same values of physical parameters [19]. It has been observed that these two phenomena concurrently occur in flexible systems that exhibit closely spaced modes arising from their periodic structure as well as small parametric asymmetry. It is well-known that mode localization is responsible for localized vibration in large space structures and turbine blades which leads to their premature failure [32-34]. So far the correlation between CNMP zeros and

mode localization appears circumstantial and based on observing the dynamics of a flexure mechanism. A detailed investigation is needed to gain a deeper understanding between the physical ties between CNMP zeros and mode localization.

1.3.2 Analytical Investigation of Zeros of General Multi-DoF Flexible Systems

There does not exist any conclusive physical meaning for the presence of RNMP or CNMP zeros that can be used to guarantee their absence in any flexible system. However, there do exist some mathematically derived sufficient conditions for the absence of these zeros that can be applied to a broad range of flexible systems. First, we will discuss Hoagg's sufficient condition for the absence of only RNMP zeros [35]. This condition is composed of two subconditions given below, both of which must be satisfied to guarantee the absence of RNMP zeros:

1. $[\mathbf{B}]$ and $[\mathbf{D}]$ should have only one non-zero element; remaining all elements must be zero.
2. $[\mathbf{M}]$, $[\mathbf{C}]$, and $[\mathbf{K}]$ must be M -matrices.

Consider the equation below where the transfer function $q(s)/F(s)$ has been written in terms of the mass ($[\mathbf{M}]$), viscous damping ($[\mathbf{C}]$), stiffness matrices ($[\mathbf{K}]$), actuator ($[\mathbf{B}]$) and sensor vectors ($[\mathbf{D}]$). $[\mathbf{e}_i]_{1 \times n}$ is a column vector where only the i^{th} element is non-zero and $[\mathbf{e}_j]_{n \times 1}$ is a row vector where only the j^{th} element is non zero. The first condition is satisfied by choosing $[\mathbf{D}] = [\mathbf{e}_i]_{1 \times n}$ and $[\mathbf{B}] = [\mathbf{e}_j]_{n \times 1}$. If a matrix $[\mathbf{A}]$ is an M -matrix, then $[\mathbf{A}]^{-1}$ is elementwise positive i.e. all elements of $[\mathbf{A}]^{-1}$ are positive. Therefore, if $[\mathbf{M}]$, $[\mathbf{C}]$, $[\mathbf{K}]$ are M -matrices, then the transfer function $q(s)/F(s)$ cannot be zero for any value of $s = z$ where z lies strictly on the positive real axis or at the origin. This is mathematically shown in the equation below.

$$\frac{q(s)}{F(s)} = [\mathbf{D}]_{1 \times n} \left([\mathbf{M}]s^2 + [\mathbf{C}]s + [\mathbf{K}] \right)_{n \times n}^{-1} [\mathbf{B}]_{n \times 1}$$

$$\text{Let } z > 0, [\mathbf{D}] = [\mathbf{e}_i], [\mathbf{B}] = [\mathbf{e}_j] \quad (1-6)$$

Let $[\mathbf{M}]$, $[\mathbf{C}]$, and $[\mathbf{K}]$ be M -matrices

$$\Rightarrow \frac{q(z)}{F(z)} = [\mathbf{e}_i]_{1 \times n} \left([\mathbf{M}]z^2 + [\mathbf{C}]z + [\mathbf{K}] \right)_{n \times n}^{-1} [\mathbf{e}_j]_{n \times 1} > 0$$

Hence, the flexible systems that satisfy Hoagg's sufficient condition cannot exhibit RNMP zeros or zeros at the origin. As a simple rule, if $[\mathbf{M}]$, $[\mathbf{C}]$ and $[\mathbf{K}]$ display the following property on visual inspection then they are M -matrices: All off diagonal elements must be non-positive AND all diagonal elements must be positive AND the sum of each and every row must be non-negative. This property is a sufficient condition (not a necessary condition) for a matrix to be an M -matrix.

Hoagg's sufficient condition for the absence of RNMP zeros is completely mathematical in nature and therefore, it is not straightforward to see what kind of flexible systems will satisfy this condition. However, Hoagg [35] mathematically shows that there exists a class of flexible systems, which he refers to as 'collinear lumped parameter' flexible systems, that satisfy his above-stated sufficient condition. Hoagg has mathematically shown that a 'collinear lumped parameter' flexible system must satisfy the following three physical conditions:

1. The force is only applied on one mass and the displacement of only one mass is measured.
2. Any two masses can only be connected via springs and/or viscous dampers.
3. When a unidirectional force is applied on one mass, all the masses (if they move) must move along the same direction along which the force was applied. In other words, unidirectional force must lead to unidirectional motion of all masses.

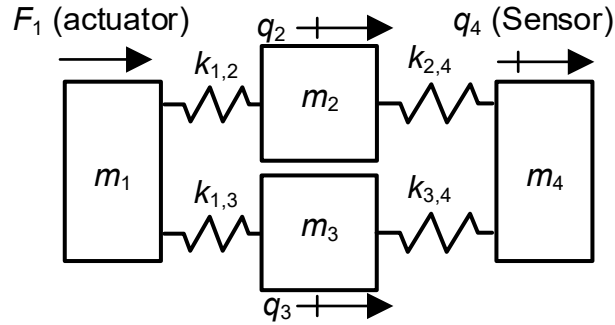


Fig 1-8 Example of a flexible system that satisfies Hoagg’s sufficient condition

It can be seen that the flexible system shown in Fig 1-8 satisfies all three physical conditions. Force is only applied at mass m_1 and displacement is only measured at mass m_4 , all the masses are connected only via springs and they are allowed to move in the same direction along which the force is applied (achievable via the appropriate bearing). Since, the above-stated three physical conditions are satisfied, the $[\mathbf{M}]$, $[\mathbf{K}]$, $[\mathbf{B}]$, and $[\mathbf{D}]$ of this flexible system satisfy Hoagg’s sufficient condition and therefore, there will be no RNMP zeros in the transfer function: $q_4(s)/F_1(s)$. Note that the set of these three physical conditions is only a sufficient (and not necessary) condition to satisfy Hoagg’s sufficient condition. There can be other examples of flexible systems that do not satisfy these three physical conditions but its $[\mathbf{M}]$, $[\mathbf{C}]$, $[\mathbf{K}]$, $[\mathbf{B}]$, and $[\mathbf{D}]$ parameters can still satisfy Hoagg’s sufficient condition.

Hoagg’s sufficient condition is the only reported sufficient condition in the existing literature for the absence of only RNMP zeros. Even though it can be applied to a wide range of flexible systems, there are still other flexible systems that do not satisfy this sufficient condition and yet do not exhibit RNMP zeros. That means that there should be other sufficient conditions as well. We will discuss the example of one such flexible system to motivate the need to find newer sufficient conditions for the absence of RNMP zeros.

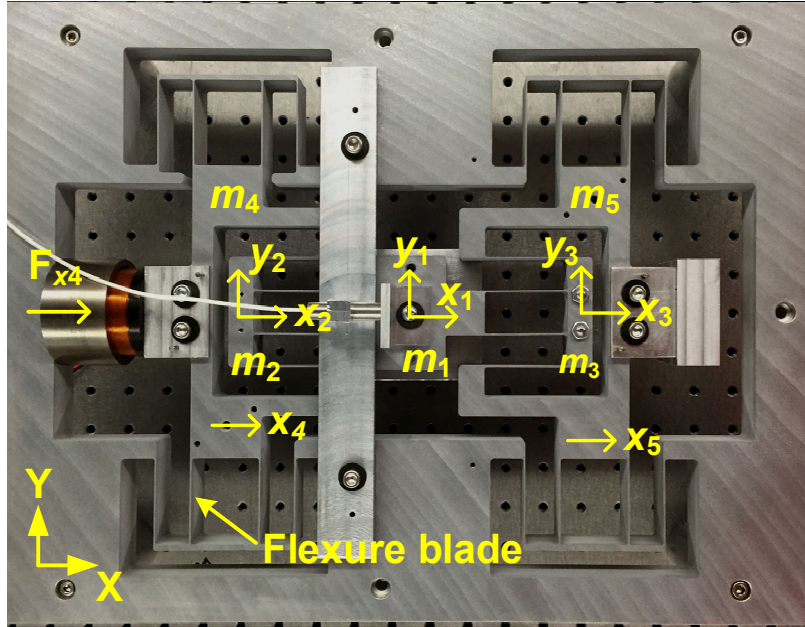


Fig 1-9 Example of a multi-directional flexible system

Fig 1-9 shows a flexure bearing based motion system where the flexure blades act as springs connecting multiple masses; X direction force is applied at mass m_4 i.e. F_{x4} and the X direction displacement of mass m_1 is measured i.e. x_1 . This flexible system is an example of a multidirectional system because the masses m_1 , m_2 , and m_3 can move in both X and Y direction. However, when m_1 is not statically displaced in the Y direction, then an X direction force applied at m_4 only leads to X direction displacement of all the masses. Therefore, in this nominal configuration, this flexible system satisfies all three physical conditions of Hoagg's 'collinear lumped parameter' flexible system and as a result, does not exhibit RNMP zeros. However, if the mass m_1 is statically displaced in the Y direction then an X direction force applied at m_4 leads to X and Y direction displacement of m_1 , m_2 , and m_3 [36]. This occurs due to the fact that the static displacement of m_1 in the Y direction leads to the static deformation of the beams which kinematically relates the X and Y direction motions of the individual masses m_1 , m_2 and m_3 due to beam arc length conservation. Hence, a unidirectional application of force along the X direction

now excites the masses m_1 , m_2 and m_3 in both the X and Y directions simultaneously. Therefore, in its non-nominal configuration the flexible system does not satisfy the physical conditions that are sufficient for its $[\mathbf{M}]$ and $[\mathbf{K}]$ matrices to be M -matrices. On visual inspection of its $[\mathbf{M}]$ and $[\mathbf{K}]$ matrices in [36], it can be easily concluded that the $[\mathbf{M}]$ and $[\mathbf{K}]$ matrices are indeed not M -matrices. In this particular system (for non-nominal operating point) even though Hoagg's sufficient condition is not satisfied, it has been theoretically [36] and experimentally [37] verified that the transfer function between x_1 and F_{x4} does not exhibit RNMP zeros. This motivates the need for new sufficient conditions that guarantee the absence of RNMP zeros in flexible systems that do not satisfy Hoagg's sufficient condition.

Chandrasekhar [38] built on Hoagg's results and showed that when the three physical conditions provided by Hoagg are satisfied (therefor, no RNMP zeros), additionally if the flexible system is also 'serially connected' then its transfer function will not exhibit CNMP zeros as well. There exists one and only one path of connection (made up of springs, masses and viscous dampers) between any two masses in a 'serially connected' flexible system, as shown in Fig 1-7. As previously discussed, the flexible system illustrated in Fig 1-8 does not exhibit RNMP zeros because it satisfies Hoagg's sufficient condition but it is not serially connected, therefore it can exhibit CNMP zeros. The flexible system shown in Fig 1-8 is an example of 'non-serially connected collinear lumped parameter' flexible system which can only exhibit CNMP zeros. Certain other flexure based motion systems with closely spaced modes [37, 39], catilevered beam [40], flexible manipulator [41] and motion system with transmission compliance [42] have been shown to exhibit only CNMP zeros in their transfer functions. However, there is no reported sufficient condition in the existing literature that can be used to guarantee the absence of CNMP

zeros in all these different flexible systems. This motivates the need for new sufficient conditions that can guarantee the absence of CNMP zeros in a broad range of flexible systems.

So far, we have discussed Hoagg’s sufficient condition for the absence of only RNMP zeros as well as its limitations and the lack of any sufficient condition for the absence of only CNMP zeros. Now we will discuss sufficient conditions for the absence of all NMP zeros i.e. RNMP and CNMP zeros, the relationships between these sufficient conditions and their limitations, thereby motivating the need for newer sufficient conditions.

Martin [43] and Gevarter [44] investigated the transfer function of a general multi-DoF undamped flexible system by modally decomposing it into second order modes where each mode is characterized by two system parameters – modal residue (α_i) and modal frequency (ω_i) as shown below. n is the Degrees of freedom (DoF) of the flexible system.

$$\frac{q(s)}{F(s)} = \frac{b_{2m}s^{2m} + \dots + b_1s^2 + b_0}{a_{2n}s^{2n} + \dots + a_1s^2 + a_0} = \sum_{i=1}^n \frac{\alpha_i}{s^2 + \omega_i^2} \quad (1-7)$$

They showed that when all the modal residues have the same sign, all the zeros of the flexible system are guaranteed to be MMP. Furthermore, Martin also showed that these MMP zeros are interlaced with the poles on the imaginary axis where every pole except the first one (referred to as the pole of the ‘rigid body mode’) is preceded by a zero. This interlacing property of the zeros and poles is referred to as zero-pole alternation (see Fig 1-1a) because the zeros and poles (except the pole of the ‘rigid body mode’) alternate on the imaginary axis. This distribution of the zeros with respect to the poles is robust to variations in the system parameters caused by modelling uncertainties and/or unmodelled dynamics as long all the modal residue signs remain the same [45, 46]. The modal residue (α_i) corresponding to a particular mode is the product of the elements of its eigenvector at the actuator and sensor position. Therefore, one of the easiest ways to satisfy this

condition is to place the actuator and sensor at the same location. This physical arrangement of the actuator and sensor is referred to as actuator-sensor collocation.

If multiple sensors are allowed as opposed to a single sensor, then different researchers have proposed different linear combinations of outputs from these multiple sensors in order to achieve the same sign for all modal residues [47-56]. Even when multiple sensors are used, the system still remains SISO and the sensor vector $[\mathbf{D}]$ is still a column vector because the outputs from all the sensors are linearly combined to form one composite output. The linear combination is chosen in such a way that all the modal residues corresponding to the transfer function between this composite output and the applied force have the same sign. This technique, referred to as sensor blending, has been shown to guarantee the absence of NMP zeros in multi-DoF undamped flexible systems with non-collocated actuator-sensor configurations in the presence of multiple sensors and a single actuator. However, in doing so, it only makes use of one sufficient condition i.e. all modal residue signs are the same which can overly restrict the actuator-sensor placement even in the non-collocated configuration. If there were other sequences of modal residue signs that could guarantee the absence of NMP zeros then they could be used together with sensor blending to provide many more choices of actuator-sensor placements. This motivates the need for new sufficient conditions for the absence of NMP zeros when all modal residue signs are not the same.

Williams [57] extended the result that the same sign of all modal residues guarantees the absence of all NMP zeros to classical viscous damped multi-DoF flexible systems. A viscous damped flexible system is classical if its $[\mathbf{M}]$, $[\mathbf{C}]$ and $[\mathbf{K}]$ matrices satisfy $[\mathbf{C}] [\mathbf{M}]^{-1} [\mathbf{K}] = [\mathbf{K}] [\mathbf{M}]^{-1} [\mathbf{C}]$. The assumption of classical damping [58, 59] allowed Williams to modally decompose the transfer function into second order modes. Unlike the undamped flexible system, each second order mode of the classically damped flexible system is characterized by three system parameters

– modal residue (α_i), modal frequency (ω_i), and modal damping ratio (ζ_i), as shown below. However, William derived this result only for underdamped flexible systems i.e. $\zeta < 1$. It is not clear so far whether the result provided by Williams holds for critically and overdamped flexible systems i.e. $\zeta \geq 1$.

$$\frac{q(s)}{F(s)} = \frac{b_m s^m + \dots + b_1 s + b_0}{a_{2n} s^{2n} + \dots + a_1 s + a_0} = \sum_{i=1}^n \frac{\alpha_i}{s^2 + 2\zeta_i \omega_i s + \omega_i^2} \quad (1-8)$$

Lin [60] provided a sufficient condition which states that if the actuator vector ($[\mathbf{B}]$) and the sensor vector ($[\mathbf{D}]$) are proportional to each other, then the absence of all NMP zeros is guaranteed. Unlike William's result which was only applicable to classical viscous damped systems, Lin's sufficient condition holds for any viscous damping matrix, $[\mathbf{C}]$. This sufficient condition is mathematically expressed below.

$$[\mathbf{B}]_{n \times 1} = p [\mathbf{D}]_{1 \times n}^T \text{ where } p \text{ is a scalar proportionality constant} \quad (1-9)$$

Physical actuator-sensor collocation for a SISO system means that $[\mathbf{D}] = [\mathbf{e}_i]_{1 \times n}$ is a column vector where only the i^{th} element is non-zero and $[\mathbf{B}] = [\mathbf{e}_i]_{n \times 1}$ is a row vector where only the i^{th} element is non-zero. Therefore, it is easy to see that physical collocation implies that Lin's sufficient condition is satisfied. Our conjecture in this thesis is that if Lin's sufficient condition is satisfied then it implies physical collocation. This means that for any actuator vector, $[\mathbf{B}]$ and sensor vector, $[\mathbf{D}]$ that satisfy Lin's sufficient condition, one can always construct a physical system with these vectors where the actuator and sensor are physically collocated. This conjecture has not been proven in this thesis (or in the existing literature to the best of the author's knowledge) but it is supported by the following example.

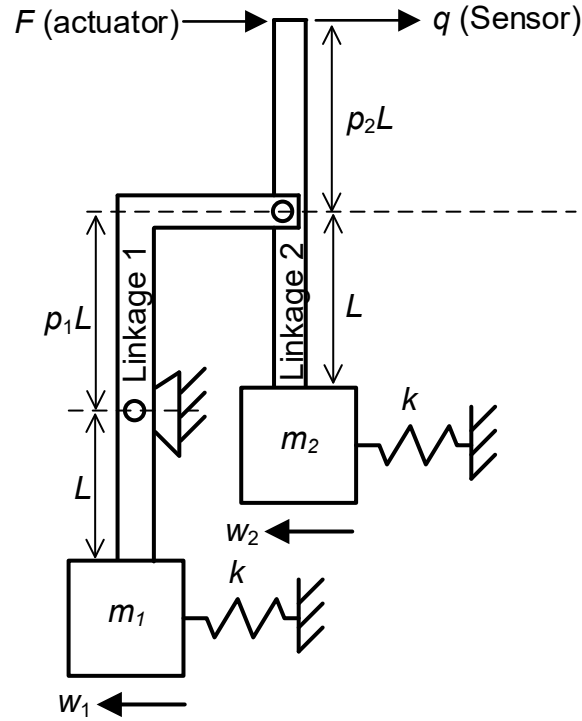


Fig 1-10 Flexible system demonstrating physical equivalence between Lin’s sufficient condition and actuator-sensor collocation

Let $[\mathbf{B}] = [p_1 (1 + p_2) \ p_2]^T$ and $[\mathbf{D}] = [p_1 (1 + p_2) \ p_2]$ where p_1 and p_2 are some scalar. Clearly, $[\mathbf{B}]$ and $[\mathbf{D}]$ satisfy Lin’s sufficiency condition in Eq. (1-9). Now the task is to construct a flexible system with collocated actuator-sensor placement whose equations of motion lead to the above-stated $[\mathbf{B}]$ and $[\mathbf{D}]$. In order to complete this task, we choose masses i.e. m_1 and m_2 and two massless links i.e. Linkage 1 and Linkage 2 and connect them as shown in Fig 1-10. In Fig 1-10, Linkage 1 is rigidly connected to mass m_1 and connected to the ground via a pivot. Linkage 2 is connected to Linkage 1 via a pivot and it is connected rigidly to mass m_2 . The location of the pivots with respect to the masses have been chosen to achieve the above-stated $[\mathbf{B}]$ and $[\mathbf{D}]$. Eq.(1-10) is the equations of motion for the flexible system shown in Fig 1-10.

$$\begin{bmatrix} m_1 & 0 \\ 0 & m_2 \end{bmatrix} \begin{bmatrix} \ddot{w}_1 \\ \ddot{w}_2 \end{bmatrix} + \begin{bmatrix} k & 0 \\ 0 & k \end{bmatrix} \begin{bmatrix} w_1 \\ w_2 \end{bmatrix} = \begin{bmatrix} p_1(1+p_2) \\ p_2 \end{bmatrix} F \quad (1-10)$$

$$q = \begin{bmatrix} p_1(1+p_2) & p_2 \end{bmatrix} \begin{bmatrix} w_1 \\ w_2 \end{bmatrix}$$

Eq.(1-10) shows that the above-stated $[\mathbf{B}]$ and $[\mathbf{D}]$ have been achieved in the equations of motion. Note that the flexible system in Fig 1-10 is just one non-unique system with collocated actuator-sensor placement that was constructed to achieve the above-stated $[\mathbf{B}]$ and $[\mathbf{D}]$. Other instances of flexible systems (with collocated actuator-sensor placement) are also possible that lead to the above-stated $[\mathbf{B}]$ and $[\mathbf{D}]$. The key point here is the demonstration of the conjecture that for any given $[\mathbf{B}]$ and $[\mathbf{D}]$ that satisfy Lin's sufficient condition, we can always construct a flexible system with collocated actuator-sensor placement, thereby implying that Lin's sufficient condition and actuator-sensor collocation are equivalent.

Now, we will mathematically show that if Lin's sufficient condition is satisfied then Williams sufficient condition is also satisfied. Let $[\Psi]$ be the matrix whose columns are the eigenvectors of the flexible system. Then, under the assumption of classical viscous damping, the modal residue (α_i) can be expressed in terms of the eigenvector matrix $[\Psi]$, actuator vector $[\mathbf{B}]$, and sensor vector $[\mathbf{D}]$ as shown below:

$$\frac{q(s)}{F(s)} = \sum_{i=1}^n \frac{\alpha_i}{s^2 + 2\zeta_i\omega_i s + \omega_i^2} \text{ where } \alpha_i = ([\mathbf{D}][\boldsymbol{\psi}]_i)([\boldsymbol{\psi}]^T[\mathbf{B}])_i$$

$$\text{Lin's sufficiency condition } \Rightarrow [\mathbf{B}] = p[\mathbf{D}]^T$$

$$\Rightarrow \alpha_i = p([\mathbf{D}][\boldsymbol{\psi}]_i)([\boldsymbol{\psi}]^T[\mathbf{D}]^T)_i \tag{1-11}$$

$$\Rightarrow \alpha_i = p([\mathbf{D}][\boldsymbol{\psi}]_i)([\mathbf{D}][\boldsymbol{\psi}]_i)^T$$

$$\text{Let } ([\mathbf{D}][\boldsymbol{\psi}]_i) = a_i$$

$$\Rightarrow \alpha_i = pa_i^2 > 0$$

The above equation proves that if Lin's sufficient condition is satisfied then all modal residue signs are the same. However, all modal residue signs being the same does not necessarily mean that Lin's sufficient condition is satisfied, as demonstrated by the following example.

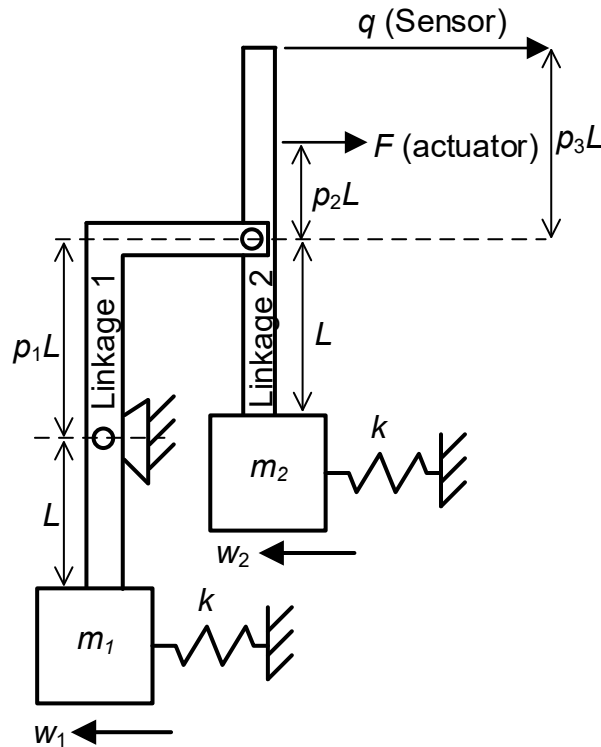


Fig 1-11 An example to demonstrate that all modal residue signs being the same does not necessarily satisfy Lin's sufficient condition

Consider the flexible system shown in Fig 1-11, where the actuator and sensor are physically non-collocated. In fact, the actuator vector $[\mathbf{B}]$ and sensor vector $[\mathbf{D}]$ do not satisfy Lin's sufficient condition, as is evident from the equations of motion below.

$$\begin{bmatrix} m_1 & 0 \\ 0 & m_2 \end{bmatrix} \begin{bmatrix} \ddot{w}_1 \\ \ddot{w}_2 \end{bmatrix} + \begin{bmatrix} k & 0 \\ 0 & k \end{bmatrix} \begin{bmatrix} w_1 \\ w_2 \end{bmatrix} = \begin{bmatrix} p_1(1+p_2) \\ p_2 \end{bmatrix} F \quad (1-12)$$

$$q = \begin{bmatrix} p_1(1+p_3) & p_3 \end{bmatrix} \begin{bmatrix} w_1 \\ w_2 \end{bmatrix}$$

The matrix of eigenvector for this flexible system i.e $[\Psi]$ is a 2 x 2 unity matrix. Therefore, the modal residues for this flexible system are given by:

$$\alpha_1 = ([\mathbf{D}][\Psi])_1 ([\Psi]^T [\mathbf{B}])_1 = (p_1(1+p_3))(p_1(1+p_2)) > 0$$

$$\alpha_2 = ([\mathbf{D}][\Psi])_2 ([\Psi]^T [\mathbf{B}])_2 = (p_3)(p_2) > 0 \quad (1-13)$$

The above equation demonstrates that even though Lin's sufficient condition is not satisfied, all the modal residue signs are still the same. Based on the arguments presented in the above paragraphs, the relationship between actuator-sensor collocation, Lin's sufficient condition, and same sign of all modal residues (given by Martin for undamped [43] and Williams for viscous damped [57]) is summarized in Eq.(1-14). It shows that 'same sign of all modal residues' is a broader and richer sufficient condition as compared to Lin's sufficient condition and actuator-sensor collocation.

$$\text{Actuator - Sensor Collocation} \Leftrightarrow \{[\mathbf{B}] = p[\mathbf{D}]^T\} \Rightarrow \text{Same Sign of all modal residues} \quad (1-14)$$

$$\Rightarrow \text{Absence of all NMP zeros}$$

Having discussed the sufficient conditions for the absence of NMP zeros from the existing literature, the following is the summary of the technical gaps that are identified:

1. Hoagg's sufficient condition is the only reported sufficient condition for the absence of only RNMP zeros in viscous damped and undamped flexible systems with any arbitrary number of DoFs (or modes). However, certain flexure based motion systems [36, 37] do not satisfy Hoagg's sufficient condition and yet do not exhibit RNMP zeros. This motivates the need to find new sufficient conditions for the absence of RNMP zeros that can be applied to flexible systems that do not satisfy Hoagg's sufficient condition.

2. There is no known sufficient condition for the absence of only CNMP zeros in viscous damped and undamped flexible systems with any arbitrary number of DoFs (modes). However, there are several flexible systems that can only exhibit CNMP zeros such as 'non serially connected collinear lumped parameter' flexible systems [35] because they already satisfy Hoagg's sufficient condition. This motivates the need to find new sufficient conditions for the absence of only CNMP zeros.

3. There is no known sufficient condition that makes use of viscous damping to guarantee the absence of NMP zeros. For a fixed actuator-sensor placement and mass-stiffness distribution, viscous damping has been used extensively to push the poles of flexible systems to the LHS of the imaginary axis thereby leading to smaller overshoot and residual vibrations [61-63]. Given the beneficial effect of viscous damping on the poles of flexible systems, this motivates the need to find sufficient conditions that use viscous damping to also guarantee the absence of NMP zeros for a given actuator-sensor location and mass-stiffness distribution.

4. The same sign of all modal residues is the only known sufficient condition for the absence of all NMP zeros i.e. CNMP and RNMP zeros. If a single actuator and sensor are used, then the only known technique in the existing literature to achieve the same sign of all modal residues is actuator-sensor collocation. If multiple sensors and a single actuator are used, then the concept of sensor

blending can be used to achieve the same sign of all modal residues even for non-collocated actuator-sensor configuration. Even then, the availability of just one sufficient condition restricts the design space in terms of mass-stiffness distribution as well as actuator-sensor location. Furthermore, it may not always be possible to achieve the same sign for all modal residues if a single actuator and a single sensor is being used and there are practical constraints on the location of actuators and sensors [36, 37, 39, 41]. For example, in certain parallel kinematic flexure mechanism based XY motion stages used for nanopositioning [36, 37, 39], the actuator and sensor cannot be placed at the same location. Light weight robotic arms and manipulators used in space applications [41, 64, 65] also employ non-collocated actuator-sensor configuration in order to conserve weight and cost as well as control the end effector position precisely. Therefore, there is a need to characterize the zeros of multi-DoF flexible systems when all the modal residue signs are not the same so that new sufficient conditions for the absence of NMP zeros can be conceived.

1.4 Problem Statement

Based on the above mentioned technical gaps, the problem addressed in this thesis is stated as follows. *“Formulate mathematical framework(s) for general flexible LTI SISO systems to derive the sufficient condition(s) for the absence of CNMP and RNMP zeros, with and without viscous damping, when all modal residue signs are not the same.”*

Solving this problem statement leads to several novel sufficient conditions for the absence of CNMP and RNMP zeros in viscous damped and undamped multi-DoF flexible LTI systems with any arbitrary number of DoFs (modes). These novel sufficient conditions are referred to as ‘Rath’s sufficient conditions’ in Fig 1-12. Fig 1-12 shows how the novel sufficient conditions derived in this thesis compare and contrast against already existing sufficient conditions in the literature (italicized in Fig 1-12).

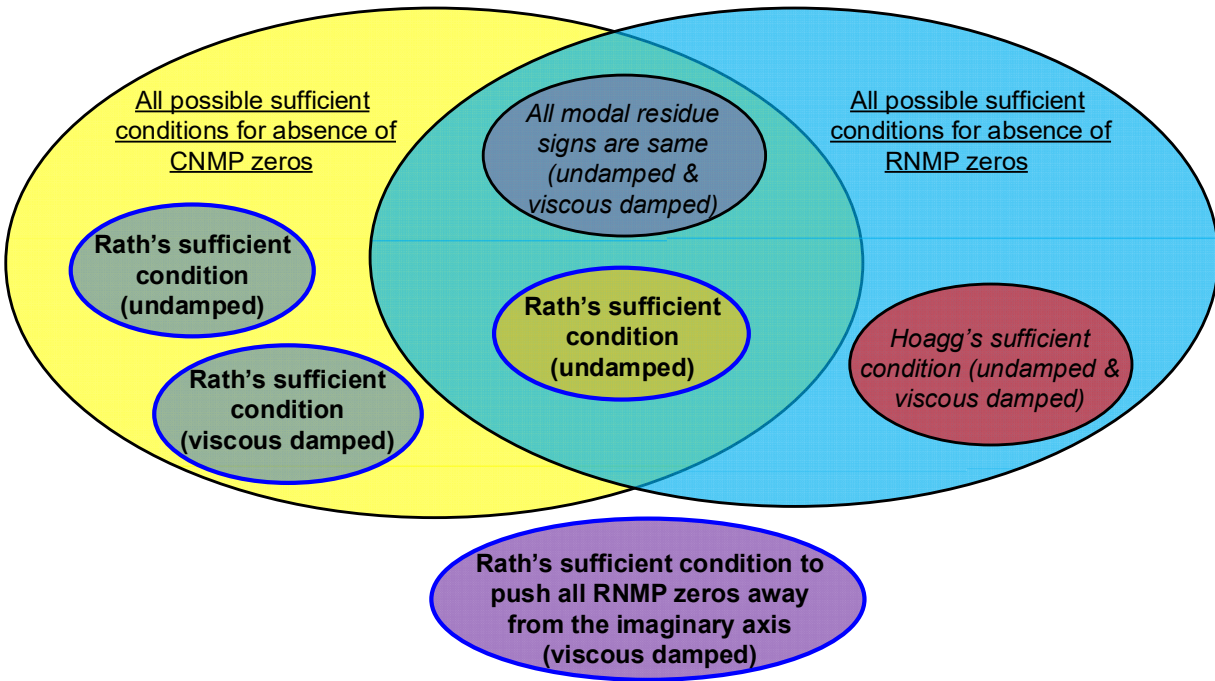


Fig 1-12 Venn diagram of sufficient conditions for the absence of CNMP and RNMP zeros

1.5 Organization of the Thesis

In order to solve the problem statement, the work in this thesis is organized into five research tasks as shown below. The organization of the chapters is based on these tasks:

Task 1 (Chapter 2): Conduct a systematic investigation based on modal theory and zero loci to explain the genesis and existence of different types of zeros in the transfer function of a three-DoF undamped flexible LTI system. Provide the necessary and sufficient conditions for the absence of non-minimum phase zeros in terms of the system parameters – modal residues and modal frequencies. This is achieved by constructing a comprehensive set of zero loci that cover all possible distribution of the zeros with respect to the poles for any value of system parameters. Based on these zero loci, the necessary and sufficient conditions for the absence of non-minimum phase zeros are derived in terms of the system parameters.

Task 2 (Chapter 3): Extend the investigation in Chapter 2 to study the genesis and existence of different types of zeros in the transfer function of two and three-DoF viscous damped flexible LTI systems under the assumption of classical viscous damping. A flexible system is classical viscous damped if its mass matrix ($[\mathbf{M}]$), viscous damping matrix ($[\mathbf{C}]$) and stiffness matrix ($[\mathbf{K}]$) satisfy the following condition: $[\mathbf{C}] [\mathbf{M}]^{-1} [\mathbf{K}] = [\mathbf{K}] [\mathbf{M}]^{-1} [\mathbf{C}]$. Provide the necessary and sufficient conditions for the absence of non-minimum phase zeros in terms of the system parameters which now also includes modal damping ratio. However, as the number of DoFs (modes) increase, the parameter space rapidly expands, making this investigation tedious and complicated for higher DoF flexible LTI systems.

Task 3 (Chapter 4): In order to study the zeros of multi-DoF undamped flexible LTI systems with any arbitrary number of DoFs (modes), the parity (odd/even) of the number of zeros with respect to the poles is investigated. This investigation leads to a non-unique sufficient condition for the absence of only CNMP zeros in terms of the sequence of modal residue signs. Under the assumption that the sufficient condition for the absence of only CNMP zeros is satisfied, an additional mathematical condition is derived to guarantee the absence of RNMP zeros as well. The sufficient condition for the absence of only CNMP zeros and the additional mathematical condition for the absence of RNMP zeros together form a sufficient condition for the absence of all NMP zeros. A case study is used to provide a step-by-step design strategy to choose mass-stiffness distribution and actuator-sensor location to achieve the required sequence of modal residue signs (not necessarily ‘all modal residue signs are same’) that satisfies the sufficient condition for the absence of CNMP zeros. However, there still remains a need for a design strategy that makes use of viscous damping to guarantee the absence of non-minimum phase zeros in multi-DoF damped flexible LTI systems.

Task 4 (Chapter 5): Conduct a systematic investigation of the zero dynamics of proportionally viscous damped multi-DoF flexible LTI system with any arbitrary number of DoFs (modes) using a change of variable methodology to reduce its large parameter space to a few composite parameters. A flexible system is proportional viscous damped if its mass matrix ($[\mathbf{M}]$), viscous damping matrix ($[\mathbf{C}]$) and stiffness matrix ($[\mathbf{K}]$) satisfy the following: $[\mathbf{C}] = c_M[\mathbf{M}] + c_K[\mathbf{K}]$ where c_M and c_K are proportional damping coefficients. This investigation shows that proportional viscous damping cannot guarantee the absence of RNMP zeros but it leads to the necessary and sufficient condition for the absence of only CNMP zeros in proportional viscous damped flexible systems. A case study is used to provide a step-by-step design strategy that makes use of proportional viscous damping to guarantee the absence of CNMP zeros for a given actuator-sensor location and mass-stiffness distribution.

Task 5 (Chapter 6): Derive a proportional viscous damping strategy that pushes all RNMP zeros further away from the imaginary axis. A case study is used to demonstrate that this simultaneously leads to fast settling time and small undershoot which were otherwise conflicting requirements due to the tradeoff imposed by RNMP zeros.

1.6 Research Contributions

The contributions of this thesis are summarized below:

1. Create mathematical framework(s) to explore the necessary and/or sufficient conditions for the occurrence of different types of zeros in the transfer function of multi-DoF flexible LTI systems with and without damping.
2. Derive some necessary and/or sufficient conditions for the absence of non-minimum phase zeros from the transfer functions of multi-DoF flexible LTI systems.

3. Create design strategies informed by the above mentioned mathematical conditions to demonstrate via various case studies the absence of non-minimum phase zeros or pushing the non-minimum phase zeros further away from the imaginary axis.

Chapter 2 On the Zeros of Undamped Three-DoF Flexible Systems

This chapter presents an investigation of zeros in the SISO dynamics of an undamped three-DoF LTI flexible system. Of particular interest are non-minimum phase zeros, which severely impact closed-loop performance. This study uses modal decomposition and zero loci to reveal all types of zeros – marginal minimum phase (MMP), real minimum phase (RMP), real non-minimum phase (RNMP), complex minimum phase (CMP) and complex non-minimum phase (CNMP) – that can exist in the system under various parametric conditions. It is shown that if CNMP zeros occur in the dynamics of an undamped LTI flexible system, they will always occur in a quartet of CMP-CNMP zeros. Consequently, the simplest undamped LTI flexible system that can exhibit CNMP zeros in its dynamics is a three-DoF system. Motivated by practical examples of flexible systems that exhibit CNMP zeros, the undamped three-DoF system considered in this chapter comprises of one rigid-body mode and two flexible modes. For this system, the following conclusions are mathematically established: (1) This system exhibits all possible types of zeros. (2) The precise conditions on modal frequencies and modal residues associated with every possible zero provide a mathematical formulation of the necessary and sufficient conditions for the existence of each type of zero. (3) Alternating signs of modal residues is a necessary condition for the presence of CNMP zeros in the dynamics of this system. Conversely, avoiding alternating signs of modal residues is a sufficient condition to guarantee the absence of CNMP zeros in this system.

2.1 Introduction and Motivation

The dynamics of flexible systems is of interest in a wide range of motion and vibration control applications including space structures [1, 2, 66], dexterous manipulation [67-71], locomotion [72, 73], hard-disk drives [3, 4, 74], and flexure mechanisms [6, 75, 76], among others. These applications typically require a combination of range, speed, settling time, noise and disturbance rejection, control robustness, motion accuracy, etc. – performance specifications that are met by careful choice of sensors, actuators, and associated electronics, as well as design of various control strategies [77-79]. Yet the presence of resonant peaks along with ill-behaved zero dynamics such as non-minimum phase behavior [36, 37, 41, 43, 80] severely limits the performance that can be achieved through feedback and feedforward control strategies [14, 15, 81, 82].

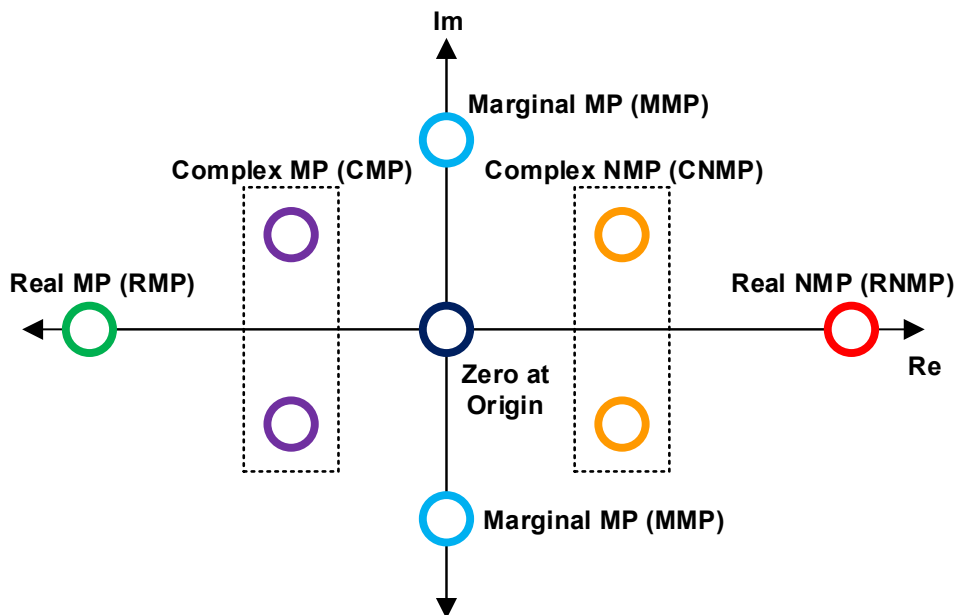


Fig 2-1 Types of zeros in a LTI system

Fig 2-1 shows the various types of zeros that can appear in the SISO dynamics of a LTI system – marginal minimum phase (MMP) that lie on the imaginary axis, real minimum phase (RMP),

real non-minimum phase (RNMP), complex minimum phase (CMP) and complex non-minimum phase (CNMP). These zeros are dictated by the physical design of the LTI system, including the location of sensor and actuator, and cannot be altered by output or state feedback. Given the critical role that zeros play (particularly NMP zeros) in control performance, an intimate knowledge of the existence of the various types of zeros and their dependence on the various system parameters is of interest.

Section 2.2 of this chapter provides a review of the extensive literature on system zeros, but the existing results fail to present an analysis of systems that include all possible types of zeros. Furthermore, an interpretation of the genesis of zeros (particularly CNMP zeros) based on physical parameters and design is still lacking. In our previous work, we mathematically predicted [36] and experimentally demonstrated [37] the existence of CNMP zeros under certain combinations of physical parameters and operating conditions in flexure mechanisms. However, this was a system-specific investigation and did not provide a more fundamental understanding into the origin of these zeros.

To achieve such an understanding, we employ modal decomposition [83] to study zeros in the SISO dynamics of an undamped three-DoF LTI flexible system in this chapter. This system comprises of one rigid-body mode and two flexible modes. The genesis of different types of zeros and their transition from one type to another is shown to depend on mathematical conditions that involve the modal frequencies and residues of the flexible system. Since these modal parameters (i.e. frequencies and residues) can be expressed in terms of physical parameters of the system (e.g. stiffness and mass), the mathematical framework presented here offers a direct connection between the zeros and the physical parameters of the system. The mathematical framework and associated results of this chapter can therefore be used to derive key physical insights into the zero dynamics

of any flexible system that can be approximated by the undamped three-DoF LTI flexible system investigated here.

2.2 Literature Review

There is a significant body of research literature on the zero dynamics of flexible systems. Existing frequency domain studies may be broadly classified into three groups: (1) studies that focus on fundamental system types irrespective of the type of zeros, (2) studies that focus on gaining physical meaning into various types of zeros, and (3) studies that focus on specific types of zeros (e.g. CNMP) irrespective of the system type.

Studying the zeros of LTI systems using fundamental system types is based on the idea of modal decomposition [83]. Since a single mode cannot lead to any zeros, the simplest flexible system type to study zeros is a system with two modes or DoFs. A simpler variation of this two-DoF system is one where the first mode has zero natural frequency (i.e. is a rigid-body mode). In the literature, Miu [84] used such a two-DoF model for a torsional system and studied the variation of zeros due to the variation of sensor location. Rankers [85] studied the interaction between the rigid body mode and the flexible mode on a frequency response plot. It was demonstrated that the variation of zeros arises due to the variation of modal residues (magnitude and signs) associated with these two modes. Colingh [86] studied a motion stage with flexible guidance and showed the mapping between sensor/actuator locations and various types of zeros. Using a two-DoF flexible system model, this work demonstrated marginally minimum phase (MMP), real minimum phase (RMP) zeros, and real non-minimum phase (RNMP) zeros, but did not capture complex non-minimum phase (CNMP) zeros.

Studying the zeros of systems with a single flexible beam has also been an active area of research. Spector and Flashner [31, 87] studied a non-collocated pinned-free beam model and identified the migration of zeros on the real and imaginary axes due to variation in the sensor location. Wie [[88] studied the pole-zero patterns in flexible structures including beams, membranes and triangular trusses. Lee and Speyer [89] used a Bernoulli-Euler beam model and studied the migration of zeros in various input-output transfer functions. In addition, Aphale [90] studied the zeros of a cantilever beam with the impact of a feed-through term and Vakil [91] studied the location of zeros for a single flexible beam under the variation of different physical parameters. In all of this work, the migration of zeros is restricted to the real and imaginary axes, i.e. zeros are MMP, RMP, or RNMP, but not CMP or CNMP.

There are also studies that focus on zeros of systems that extend beyond a two-DoF model. Tohyama and Lyon [92, 93] used a system with two modes and a constant remainder to study the transfer function in room acoustics. By varying the remainder, they identified marginally minimum phase (MMP) zeros and complex non-minimum phase (CNMP) zeros. These studies however, only investigate variation of the remainder without investigating the influence of changing the two modal residues or frequencies. As a result, RMP and RNMP zeros are not captured in this work. Duffour and Woodhouse [94] studied the transfer function of linearized systems with frictional contact. In their investigation, analytical and graphical locus techniques were used to examine cases with only two modes, with two modes with a constant remainder, and with three modes. While MMP zeros and CNMP zeros are reported in this work, RNMP zeros were not captured due to inadequate spanning of the parameter space. Martin [43] proposed modal decomposition to identify MMP, RNMP, RMP and CNMP zeros by studying a numerical model with three modes, but he did not draw any broader conclusions from his numerical results. He concluded that for the

situation of sensor and actuator collocation, the zeros are MMP, wherein zeros are alternately located between the system poles. He also argued that such a system is robust against modeling uncertainties and unmodeled high frequency dynamics when operated in closed loop.

The second group of studies on zeros focuses on gaining physical meaning into various types of zeros. Miu [28] studied the MMP zeros in serially connected spring mass systems. He concluded that for this simple class of systems, MMP zeros indicate the natural frequencies of several sub-systems defined by the actuator and sensor locations. Chandrasekar [38] showed that all zeros in such serially connected spring-mass systems are MMP zeros. Straete [29] used the approach of bond graphs to study all types of zeros and reached the physical insight that zeros are related to subsystems where energy is “trapped”. In addition, Calafiore’s [30] analysis also characterized how sub-systems are related to zeros. Nevertheless, in all of this work, a sub-system-based physical insight is applicable only in simple classes of systems, namely serially connected spring-mass systems. For a general flexible system, sub-systems and any associated physical insights are difficult to identify. Examples include Coelingh’s model [86] and the multi-axis flexure mechanism [36, 37] that exhibits dynamic coupling between the modes in different axes.

The third group of studies focuses on specific types of zeros irrespective of the system type. In particular, CNMP zeros have been reported in flexible systems [36, 37, 41], [40, 42, 95] but there remains very little physical understanding of these zeros. Cannon and Schmitz [41] identified RNMP and CNMP zeros numerically in the transfer function of a pinned-free beam. Loix et al. [40] studied a four-DoF spring-mass model with spring stiffness variation. They numerically identified the existence of CNMP zeros and the corresponding zero locus. They also provided an experimental observation of CNMP zeros in a cantilever beam set-up but did not present a mathematical formulation for these zeros. Hoagg [35] investigated a three DoF spring-mass-

damper model that also captured CNMP zeros. However, they assumed an unusually large damping ratio ($\zeta > 1.3$) to create the CNMP zeros. Awatar [42] predicted and experimentally measured CNMP zeros in the non-collocated transfer function of a multiple spring-mass servo system. Electromagnetic modeling showed that these zeros arose due to a coupling between the DC motor and the tachometer in this servo system. In our recent work, CNMP zeros have been modeled [36] and measured [37] in a lightly damped flexure mechanism-based motion stage.

In all of these studies, the advantage of focusing on specific systems is that it allows one to validate the existence of certain types of zeros (particularly RNMP and CNMP) via models and experiments. Furthermore, the relationship between physical parameters and the location/existence of zeros can be demonstrated. Yet, all of these existing studies are system-specific and do not provide a deeper understanding into the existence of zeros for flexible systems in general.

Thus, the gap in the existing literature on zeros may be summarized via two key points. First, while zeros of flexible systems have been studied using the technique of modal decomposition by varying modal parameters, the existing results are incomplete in terms of capturing all possible types of zeros in a single, general flexible system. Second, there remains a lack of physical understanding of the conditions for which certain zeros (especially RNMP and CNMP) appear or change from one type to another.

This chapter addresses this gap by identifying the simplest LTI system – an undamped three-DoF flexible system – that exhibits all types of zeros. A mathematical framework based on modal decomposition is used to relate system zeros to modal parameters. Specifically, for a three-DoF flexible system with one rigid-body mode, the precise conditions on modal parameters (frequencies and residues) are derived for every possible zero type. This leads to a comprehensive set of necessary and sufficient conditions on modal parameters for the existence of each type of

zero. Since modal parameters can be ultimately correlated to physical parameters of the system (e.g. stiffness and mass), the mathematical framework presented here can be used to not only gain physical insights into the origin of zero dynamics but also influence them through the appropriate choice of physical parameters.

The rest of this chapter is organized as follows. *Section 2.3* captures zero dynamics via modal decomposition and presents key results that help narrow down the scope of this investigation to a three-DoF system. *Section 2.5* provides an explicit mathematical and graphical correlation between the modal frequencies and the modal residues of a three-DoF flexible system (with one rigid-body mode) and the associated zeros. This leads to several important mathematical observations and physical insights. *Section 2.6* concludes the chapter with a summary of the conclusions and design insights obtained in this work and a brief discussion on the subsequent course of this research.

2.3 Zero Dynamics and Modal Decomposition

The input-output dynamics of a LTI SISO system given by transfer function $G(s)$ can be expressed as the sum of the contributions of its decomposed modes.

$$G(s) = \frac{b_m s^m + \dots + b_1 s + b_0}{a_n s^n + \dots + a_1 s + a_0} = \sum_{i=1}^n \frac{\alpha_i}{s + p_i} \quad (2-1)$$

Assumption 1: The LTI SISO flexible system investigated in this chapter is assumed such that all the decomposed modes are second order, and that there are no first order modes. Additionally, it is assumed that these second order modes are all oscillatory in nature (i.e. the poles associated with each mode lie on the imaginary axis and not on the real axis). This is a reasonable assumption for many continuous structural and discrete spring-mass systems.

Assumption 2: Next, it is assumed that the flexible system is undamped. This assumption is reasonable for flexible systems such as flexure mechanisms that are monolithic with no rolling or sliding joints [6, 75, 76], for space structures [1, 2, 66], and for machines that operate in vacuum [96], where damping is negligible.

Assumption 3: If force is assumed to be the input and displacement is selected as the output of such a LTI SISO flexible system, then the input-output transfer function $G(s)$ from Eq.(2-1) can be restated as follows:

$$G(s) = \frac{N(s)}{D(s)} = \frac{b_m s^{2m} + \dots + b_1 s^2 + b_0}{a_n s^{2n} + \dots + a_1 s^2 + a_0} = \sum_{i=1}^n \frac{\alpha_i}{s^2 + \omega_i^2} \quad (2-2)$$

Here the total number of second order modes is n , which is also the DoF of the system per the nomenclature of this chapter, and ω_i is the natural frequency of the i^{th} mode. Additionally, it is assumed that $G(s)$ represents a physical system (as opposed to a mathematical system), and is strictly proper (i.e. $m < n$). In other words, the number of zero pairs is less than the number of modes in the system.

From Eq. (2), it may be seen that the variation of modal residues (α_i) leads to the variation of the numerator coefficients (b_i), and thus, the variation of the zeros of $G(s)$. There are some key results that can be readily derived for a LTI SISO flexible system defined by the above assumptions.

Result 1: For an undamped LTI flexible system whose SISO dynamics is given by Eq.(2), if a pair of complex non-minimum phase (CNMP) zeros occurs, it will always occur in a quartet along with a pair of complex minimum phase (CMP) zeros.

Proof: Transfer function $G(s)$ can be expressed in terms of its numerator $N(s)$ and denominator $D(s)$, as follows:

$$G(s) = \sum_{i=1}^n \frac{\alpha_i}{s^2 + \omega_i^2} = \frac{\sum_{i=1}^n \left[\alpha_i \prod_{j \neq i} (s^2 + \omega_j^2) \right]}{\prod_i (s^2 + \omega_i^2)} = \frac{N(s)}{D(s)} \quad (2-3)$$

As a consequence of the assumptions made above, it is evident that $N(s)$ and $D(s)$ are even functions (i.e. $N(s) = N(-s)$ and $D(s) = D(-s)$).

Therefore, if $a \pm ib$ (where $a > 0$) are CNMP zeros of $G(s)$ (i.e. $N(a \pm ib) = 0$), and $N(a \pm ib) = N(-(a \pm ib))$ because $N(s)$ is an even function, then it follows that $N(-a \pm ib) = 0$. In other words, $-a \pm ib$ are also zeros of $G(s)$. Since $a > 0$ these two zeros constitute a CMP zero pair. Thus, zeros that are neither on the imaginary axis nor on the real axes of the s -plane, always appear as a CMP-CNMP quartet ($\pm a \pm ib$).

Result 2: An undamped LTI flexible system must have a minimum of three modes (i.e. three-DoF) to exhibit a CMP-CNMP zero quartet in its SISO dynamics.

Proof: According to Result 1, CMP-CNMP zeros always appear as a quartet. This means that for such a quartet to appear, the numerator $N(s)$ in Eq.(2-3) should be at least a 4th order polynomial in s . Further, because the physical system is strictly proper, the denominator $D(s)$ should at least be a 6th order polynomial in s . Since all the decomposed modes of $G(s)$ are second order, it follows that the system should consist of at least three such modes to exhibit a CMP-CNMP zero quartet.

Based on these results, since a three-DoF undamped LTI flexible system is the simplest system that exhibits CMP-CNMP zeros, we choose this system for the intended investigation that captures all the zero types. As discussed in *Section 2.2*, two-DoF undamped LTI flexible systems have been extensively studied [30-32] but exhibit only MMP, RMP and RNMP zeros.

2.4 Two DoF Flexible LTI System

A two-DoF undamped LTI flexible system that follows Assumption 1 through 3 can be expressed as:

$$G(s) = \frac{\alpha_u}{s^2 + \omega_u^2} + \frac{\alpha_v}{s^2 + \omega_v^2} \quad (2-4)$$

Note that Coelingh [86] studied a special case of the undamped two-DoF flexible system with one rigid body mode and one flexible mode. The zeros of $G(s)$ are the roots of its numerator which can be expressed as follows:

$$G(s) = \frac{\alpha_v \left[\frac{\alpha_u}{\alpha_v} (s^2 + \omega_v^2) + (s^2 + \omega_u^2) \right]}{(s^2 + \omega_u^2)(s^2 + \omega_v^2)} \quad (2-5)$$

The zeros of $G(s)$ are studied by varying the ratio of its modal residues (α_u/α_v) from $-\infty$ to $+\infty$. In order to do this, we define a mathematical transfer function, $T(s) = (s^2 + \omega_v^2) / (s^2 + \omega_u^2)$ and plot the root locus of $T(s)$ as a function of (α_u/α_v). The root locus of $T(s)$ gives the zero locus of $G(s)$. Note that the zeros of undamped flexible systems are symmetric about the real and imaginary axis. Therefore, for the sake of brevity, only the first quadrant of the s -plane is shown in the figure below to capture the zero locus of $G(s)$ (root locus of $T(s)$). It must be kept in mind that when the zero locus shows a MMP zero on the positive imaginary axis, there is a symmetric MMP zero on the negative imaginary axis. Similarly, when the zero locus shows an RNMP zero on the positive real axis, there is a symmetric RMP zero on the negative real axis.

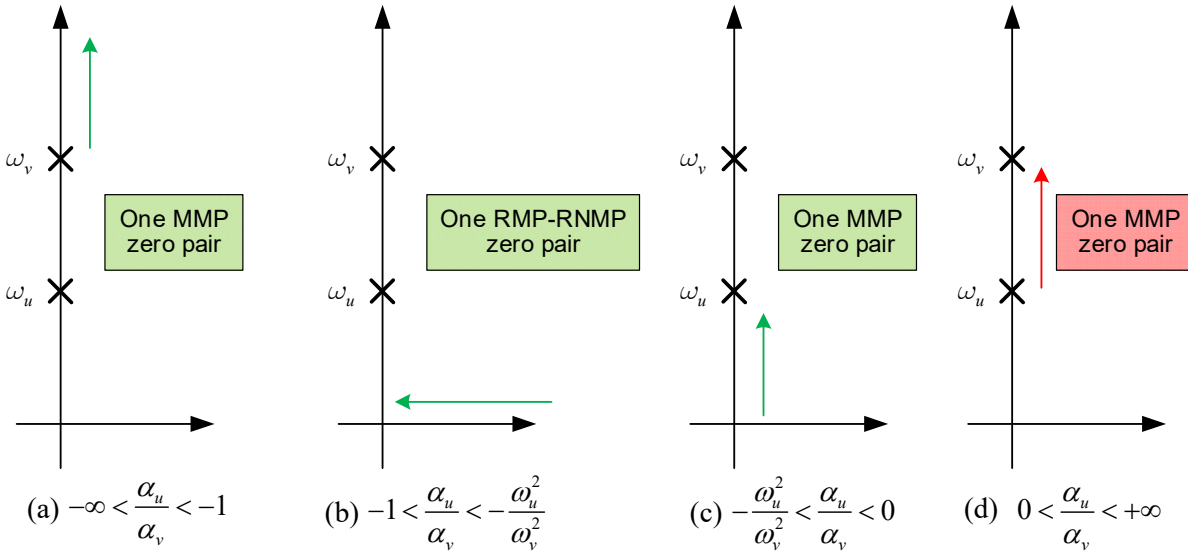


Fig 2-2 Zero locus of two-DoF flexible system

Part (a) to Part (c) in Fig 2-2 are the negative (complementary) root locus of $T(s)$ because $(\alpha_u/\alpha_v) < 0$. Part (d) in Fig 2-2 is the positive root locus of $T(s)$ because $(\alpha_u/\alpha_v) > 0$. The following inferences can be drawn based on the zero locus of $G(s)$ in Fig 2-2.

1. When all modal residue signs are the same i.e. $(\alpha_u/\alpha_v) > 0$, Fig 2-2d shows that the zeros are always MMP.
2. When all modal residue signs are not the same i.e. $(\alpha_u/\alpha_v) < 0$, Fig 2-2a – c show that the zero is either MMP or RNMP.
3. As (α_u/α_v) is increased from $-\infty$, the MMP zero moves along the imaginary axis towards $+\infty$ as shown in Fig 2-2a.
4. Beyond a critical value of (α_u/α_v) , the MMP zero transitions into a RNMP zero. This critical value of (α_u/α_v) can be obtained by equating the coefficient of s^2 in the numerator of $G(s)$ to 0. This leads to $(\alpha_u/\alpha_v) = -1$.

5. As (α_u/α_v) is increased from -1, the RNMP zero moves along the positive real axis towards the origin as shown in Fig 2-2b.
6. Beyond a critical value of (α_u/α_v) , the RNMP zero transitions back to a MMP zero. This critical values of (α_u/α_v) can be obtained by equating the coefficient of s^0 in the numerator of $G(s)$ to 0. This leads to $(\alpha_u/\alpha_v) = -\omega_u^2/\omega_v^2$.

2.5 Three DoF Flexible LTI System¹

A three-DoF undamped LTI flexible system that follows Assumptions 1 through 3 can be expressed as:

$$G(s) = \frac{\alpha_R}{s^2 + \omega_R^2} + \frac{\alpha_u}{s^2 + \omega_u^2} + \frac{\alpha_v}{s^2 + \omega_v^2} \quad (2-6)$$

where $\omega_R < \omega_u < \omega_v$. Here we make one more assumption – that the first mode is much lower in frequency compared to the subsequent two modes. While a general three-DoF system can be considered, this assumption offers some practical advantages. In previous modeling [36] and experimental [37] work, we have shown that CNMP zeros appear in systems that have a low-frequency mode and at least two higher frequency closely-spaced modes. This provides the motivation to investigate a slightly simpler system by setting ω_R to zero in Eq.(2-6). This additional assumption also helps simplify the mathematical and graphical analysis of the zero locus in this section, which allows for better physical interpretation of the results.

Yet, the three-DoF model that stems from this assumption can still be used to explain the dynamics of flexible systems that are characterized by a low-frequency rigid body mode and a couple of relatively high-frequency flexible modes. In such instances, the low-frequency flexible

¹ This work was done in collaboration with Leqing Cui (M.E. Ph.D. 2017) at the University of Michigan

mode is approximated as a pure rigid body mode to study its interaction with the two higher frequency modes that give rise to the CMP-CNMP zero quartet trapped between them.

Assuming the first mode to be a rigid-body mode, the three-DoF flexible system of Eq.(2-6) reduces to:

$$G(s) = \frac{\alpha_R}{s^2} + \frac{\alpha_u}{s^2 + \omega_u^2} + \frac{\alpha_v}{s^2 + \omega_v^2} \quad (2-7)$$

Furthermore, α_R can be set to be +1, without any loss in generality. This helps reduce the number of parameters that need to be carried through the subsequent mathematical steps. The system transfer function from Eq.(2-7) may be further expressed as:

$$G(s) = \frac{\alpha_v s^2 [(1 + \alpha_u / \alpha_v) s^2 + (\alpha_u \omega_v^2 / \alpha_v + \omega_u^2)] + [(s^2 + \omega_u^2)(s^2 + \omega_v^2)]}{s^2 (s^2 + \omega_u^2)(s^2 + \omega_v^2)}$$

Next, if we define:

$$\kappa \triangleq \frac{\alpha_u}{\alpha_v} \quad \text{and} \quad \eta \triangleq \frac{\omega_u}{\omega_v}$$

Then $G(s)$ may be expressed as:

$$G(s) = \frac{N(s)}{D(s)} = \frac{(\alpha_v A(s) + B(s))}{D(s)} \quad (2-8)$$

$$\text{where } A(s) \triangleq (1 + \kappa)s^4 + \omega_v^2(\kappa + \eta^2)s^2, \quad B(s) \triangleq (s^2 + \omega_u^2)(s^2 + \omega_v^2)$$

Now, we create a transfer function $T(s) = A(s)/B(s)$, which has no physical meaning and simply serves as a mathematical tool, as described next. First, the poles of $T(s)$ are the poles associated with the modes u and v . Second, $T(s)$ has two pairs of zeros. One pair is fixed at the origin and the other pair changes position based purely on the ratio α_u/α_v . For a given α_u/α_v ratio, ω_u , and ω_v , if α_v is varied, then the root locus of $T(s)$ with unity feedback is obtained. But note that the root-locus of $T(s)$ is also the zero-locus of $G(s)$. Moreover, if the sign of α_v is flipped, then the complementary

root locus is obtained. Thus, $T(s)$ serves as an intermediate mathematical tool to obtain the zero-locus of $G(s)$ for various modal parameters.

The root-loci of $T(s)$, which correspond to the full zero-loci of $G(s)$, are shown in Fig 2-3 for four different value ranges of α_u/α_v . For ease of illustration, only the first quadrant is shown in each case. As noted above, the value ranges of α_u/α_v determine the location range of the second zero pair of $T(s)$ (shown in blue) as follows:

(a) $\frac{\alpha_u}{\alpha_v} > 0$: 2nd zero pair of $T(s)$ lies between ω_u and ω_v

(b) $-\frac{\omega_u^2}{\omega_v^2} < \frac{\alpha_u}{\alpha_v} < 0$: 2nd zero pair of $T(s)$ lies b/w origin and ω_u

(c) $-1 < \frac{\alpha_u}{\alpha_v} < -\frac{\omega_u^2}{\omega_v^2}$: 2nd zero pair of $T(s)$ lies on the real axis

(d) $\frac{\alpha_u}{\alpha_v} < -1$: 2nd zero pair of $T(s)$ lies between ω_v and infinity

The top panel of Fig 2-3 shows the zero-loci of $G(s)$ for positive α_v (varying from 0 to ∞) and the bottom panel shows the zero-loci of $G(s)$ for negative α_v (varying from $-\infty$ to 0). A key observation here is that CNMP zeros arise in instances (b), (c), and (d) of the top panel, where the zero-locus branches break-away from the imaginary axis and subsequently re-join at the real or imaginary axes, as α_v increases. To find the α_v value at these break-away and re-join points, one simply needs to find the repeated roots of s^2 in $N(s)$, where

$$\begin{aligned} N(s) &= \alpha_v A(s) + B(s) \\ &= \{1 + \alpha_v(1 + \kappa)\}s^4 + \{\alpha_v(\kappa + \eta^2) + (1 + \eta^2)\}\omega_v^2 s^2 + \omega_u^2 \omega_v^2 \end{aligned}$$

To find the repeated roots, one can set the discriminant of the above quadratic expression in s^2 to 0,

$$[\{\alpha_v(\kappa + \eta^2) + (1 + \eta^2)\}\omega_v^2]^2 - 4(\omega_u^2\omega_v^2)\{1 + \alpha_v(1 + \kappa)\} = 0$$

$$\Rightarrow \alpha_v = \frac{-(\kappa - \eta^2)(1 - \eta^2) \pm |(1 - \eta^2)|\sqrt{-4\kappa\eta^2}}{(\kappa + \eta^2)^2}$$

Here, the smaller value of α_v corresponds to the break-away point and the larger value corresponds to the re-join point:

$$\text{Break-away: } \Rightarrow \alpha_v = \frac{-(\kappa - \eta^2)(1 - \eta^2) - |(1 - \eta^2)|\sqrt{-4\kappa\eta^2}}{(\kappa + \eta^2)^2} \quad (2-9)$$

$$\text{Re-join: } \Rightarrow \alpha_v = \frac{-(\kappa - \eta^2)(1 - \eta^2) + |(1 - \eta^2)|\sqrt{-4\kappa\eta^2}}{(\kappa + \eta^2)^2}$$

Another key observation in Fig 2-3 is that a pair of MMP zeros can approach infinity and then transition over to a RMP-RNMP pair, as seen in instance (d) of the top panel and instances (a), (b), and (c) of the bottom panel. The value of α_v for which this transition happens can be determined by finding the condition when $N(s)$ has only one pair of roots.

$$N(s) = \alpha_v A(s) + B(s)$$

$$= \{1 + \alpha_v(1 + \kappa)\}s^4 + \{\alpha_v(\kappa + \eta^2) + (1 + \eta^2)\}\omega_v^2 s^2 + \omega_u^2 \omega_v^2$$

This condition corresponds to setting the coefficient of s^4 in the above expression to zero.

$$\{1 + \alpha_v(1 + \kappa)\} = 0 \quad \Rightarrow \quad \alpha_v = -\frac{1}{1 + \kappa} \quad (2-10)$$

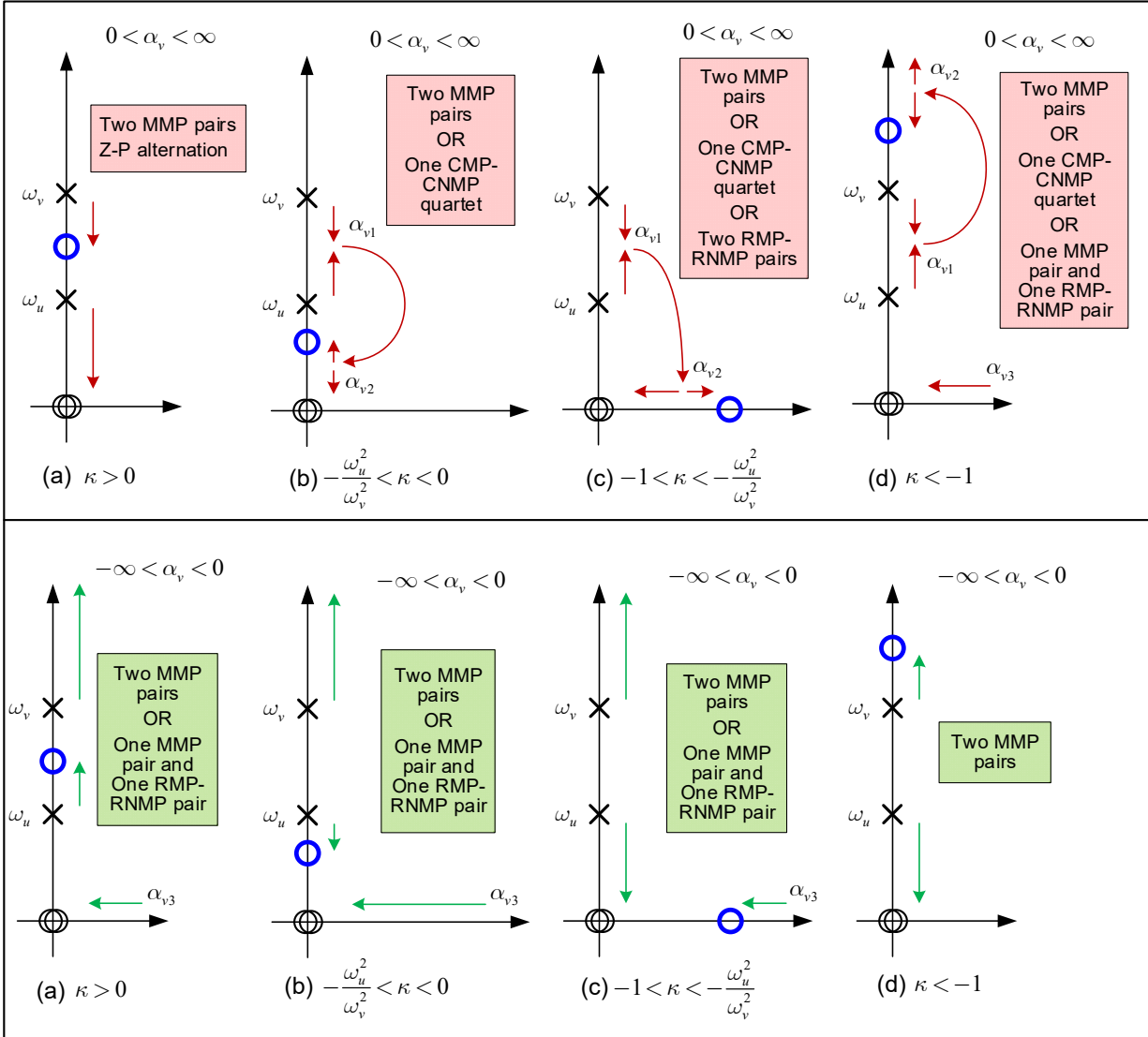


Fig 2-3 Zero loci of $G(s)$

Result 1: In a three-DoF undamped flexible LTI system given by Eq.(2-7), when $\alpha_v > 0$, the following conditions are individually sufficient and together necessary to guarantee the elimination of all NMP zeros:

Condition 1.1: $\kappa > 0$

OR

Condition 1.2: $(-\eta^2 < \kappa < 0)$ AND $((\alpha_v \leq \alpha_{v1})$ OR $(\alpha_v \geq \alpha_{v2}))$

OR

Condition 1.3: $(-1 < \kappa < -\eta^2)$ AND $(\alpha_v \leq \alpha_{v1})$

OR

Condition 1.4: $(\kappa < -1)$ AND $((\alpha_v \leq \alpha_{v1})$ OR $(\alpha_{v2} \leq \alpha_v \leq \alpha_{v3}))$

where

$$\alpha_{v1} \triangleq -\left(1-\eta^2\right) \frac{\left(\kappa-\eta^2\right)+\sqrt{-4 \kappa \eta^2}}{\left(\kappa+\eta^2\right)^2}, \alpha_{v2} \triangleq -\left(1-\eta^2\right) \frac{\left(\kappa-\eta^2\right)-\sqrt{-4 \kappa \eta^2}}{\left(\kappa+\eta^2\right)^2}$$

$$\alpha_{v3} \triangleq -\frac{1}{1+\kappa} \quad (2-11)$$

Proof: The individually sufficient conditions shown above are derived from the top panel of Fig 2-3 where $\alpha_v > 0$. The first condition i.e. Condition 1.1 is derived from case (a) of Fig 2-3. Case (a) shows that when the ratio of modal residues i.e. $\kappa > 0$, then there is no NMP zero in the zero loci. Condition 1.2 is derived from case (b) by selecting that range of α_v where the zero loci lies purely on the imaginary axis. Similarly, Condition 1.3 and Condition 1.4 are derived from case (c) and case (d) respectively.

Result 2: In a three-DoF undamped flexible LTI system given by Eq.(2-7), when $\alpha_v < 0$, the following conditions are individually sufficient and together necessary to guarantee the elimination of all NMP zeros:

Condition 2.1: $(\kappa > -1)$ AND $(\alpha_v \geq \alpha_{v3})$

OR

Condition 2.2: $(\kappa < -1)$ (2-12)

$$\text{where } \alpha_{v3} \triangleq -\frac{1}{1+\kappa}$$

Proof: The individually sufficient conditions **Result 2** are derived from the bottom panel of Fig 2-3 where $\alpha_v < 0$. Condition 2.1 is derived by combining case (a), case (b) and case (c) of the bottom panel and Condition 2.2 is derived from case (d).

Based on these results and Fig 2-3, the following conclusions can be drawn:

1. By varying α_u / α_v and α_v , all types of zeros (i.e. MMP, RMP-RNMP pair and CMP-CNMP quartet) are obtained in the zero loci of a three-DoF flexible system (with one rigid-body mode).
2. CNMP zeros occur in cases (b), (c) and (d) of the top panel where $(\alpha_u / \alpha_v) < 0$ and $0 < \alpha_v < \infty$. Therefore, the necessary condition for the existence of CNMP zeros is the alternating sequence of modal residue signs i.e. $\alpha_R > 0$ (already assumed to be +1), $\alpha_u < 0$ and $\alpha_v > 0$. This necessary condition is nevertheless not a sufficient condition. As seen in cases (b), (c) and (d) of the top panel, even when the necessary condition is satisfied, there exist values of α_v for which the zeros are either MMP or RMP-RNMP. These are the values of α_v before the break-away and after the re-join of the zero loci, given by Eq.(2-9).
3. Conversely, avoiding the alternating sequence of modal residue signs is a sufficient condition for the elimination of CNMP zeros. However, this is not a necessary condition for the elimination of CNMP zeros. The value of α_v can be tuned such that it does not lie between the

break-away and re-join points given by Eq.(2-9). This would guarantee that CNMP zeros do not occur in the system dynamics even in the presence of alternating modal residue signs.

4. Eq.(2-9) gives the break-away point of the zero loci from the imaginary axis and the subsequent re-join of the zero loci onto the imaginary axis or the real axis. This equation mathematically shows the precise conditions under which MMP zeros transition to a CMP-CNMP quartet and then back to either MMP zeros or a RMP-RNMP pair. These break-away and re-join points can be easily visualized in instances (b), (c) and (d) of the top panel (i.e. $0 < \alpha_v < \infty$) of Fig 2-3.
5. Based on Eq.(2-9), it can be mathematically observed that as $\eta (\triangleq \omega_u^2 / \omega_v^2)$ tends to 1, the values of α_v at which break-away and re-join occur tend to zero. Therefore, in the presence of alternating sequence of modal residue signs (represented by (b), (c) and (d) when $0 < \alpha_v < \infty$), if a three-DoF flexible system has two closely spaced flexible modes (given by η tending to 1), then the occurrence of CNMP zeros (in form of quartet) becomes very sensitive to small values of α_v . In the presence of closely spaced flexible modes, even a small non-zero value of α_v (modal residue associated with the flexible mode v), can lead to the presence of CNMP zeros in the system dynamics.
6. Eq.(2-10) gives the mathematical condition when MMP zeros transition into a RMP-RNMP pair. This point of transition only depends on the ratio of modal residues (κ) of the two flexible modes. If κ tends to -1, then the transition from MMP zeros to RMP-RNMP pair happens for very large values of α_v . In other words, the transition becomes insensitive to the value of α_v .
7. There are two cases, namely case (a) of the top panel and case (d) of the bottom panel where NMP zeros do not occur in the zero locus for any value of α_v . Case (a) of the top panel leads to a configuration of modal residue signs given by $\alpha_R > 0$, $\alpha_u > 0$ and $\alpha_v > 0$. This is in agreement

with [24] where it was shown that when all modal residues have the same sign, it only leads to MMP zeros in the system dynamics.

2.6 Conclusion

This chapter investigates the zero dynamics of an undamped three-DoF flexible system that consists of one rigid body mode and two flexible modes. Mathematical formulae are used to provide the necessary and sufficient conditions for the existence of every type of zero (MMP, RMP-RNMP pair and CMP-CNMP quartet) in the system. Particular emphasis is given to NMP zeros, which severely impact the closed loop performance of flexible systems. Based on this investigation, it is found that whenever CNMP zeros occur in the system dynamics, they always occur in a quartet of CMP-CNMP zeros and alternating signs of modal residues is a necessary condition for their occurrence. Therefore, in order to avoid CNMP zeros in the system dynamics, avoiding an alternating sequence of modal residue signs is a sufficient condition. The signs of modal residues are closely tied to the location of actuators and sensors on a flexible system through the mode shapes of the associated flexible modes [24]. The mathematical insight from this investigation can be combined with the knowledge of mode shapes of specific flexible systems that can be approximated by an undamped three-DoF flexible system model. This will enable optimal placement of actuators and sensors in order to avoid NMP zeros.

This investigation also reveals that the occurrence of CNMP zeros in undamped three-DoF flexible systems with closely spaced flexible modes is very sensitive to variations in the modal residues and by extension very sensitive to variations in physical parameters of the flexible systems [36]. This phenomenon is usually observed in the dynamics of flexure mechanisms that make use of symmetric/periodic building blocks (or flexure modules) to achieve large range of motion, high

constraint direction stiffness, and low sensitivity to thermal effects [39]. The symmetric/periodic structure gives rise to closely spaced flexible modes and a large range of motion gives rise to geometric non-linearities that lead to varying system parameters [36, 37].

In this chapter, we only presented an investigation on the zeros of an undamped flexible system. In the subsequent chapters, we will also investigate the zero dynamics of damped flexible systems and draw key physical insights on the impact of damping on zero dynamics. We will use these insights to choose actuator-sensor location and damping strategies to show how NMP zeros can be eliminated from the dynamics of large-range multi-axis flexure mechanisms.

Chapter 3 On the Zeros of Two and Three DoF Damped Flexible Systems

This chapter presents an investigation of the non-minimum phase (NMP) zeros in the single input single output (SISO) transfer function of two and three-DoF (degrees of freedom) damped flexible linear time-invariant (LTI) systems under the assumption of classical damping. It is well-known that when all the modal residue signs of any multi-DoF damped flexible LTI system are the same, NMP zeros never occur in the system dynamics for any value of system parameters including modal residue, modal frequency and modal damping ratio. However, when all the modal residue signs are not the same, then additional conditions in terms of the system parameters are required to guarantee the elimination of NMP zeros. In this chapter, the zero loci of a two and three-DoF damped flexible LTI system are developed to derive the sufficient and necessary conditions for the elimination of all NMP zeros. These conditions can be employed in the robust physical design of flexible systems, i.e., as long as these conditions are satisfied, the elimination of NMP zeros is guaranteed even when the system parameters undergo variations

3.1 Introduction and Background

Flexible system dynamics plays a vital role in the performance of several motion and vibration control applications such as space structures [2, 66], rotorcraft blades [5, 97], hard-disk drives [3, 4], flexure mechanisms [7, 39], and motion systems with transmission compliance [8, 98]. These applications often require the use of feedback and feedforward controls in an attempt to achieve high speed, low settling time, strong disturbance rejection, low sensitivity to modeling

uncertainties, and stability robustness. However, the presence of undamped poles and non-minimum phase (NMP) zero dynamics in the single input single output (SISO) transfer function lead to significant tradeoffs amongst these competing requirements. A zero is non-minimum phase (NMP) if it has a positive real component, and minimum phase (MP) if it has a non-positive real component.

One particular application example that highlights these tradeoffs is of flexure mechanisms used in high-precision high-speed positioning stages that exhibit undamped poles and ill-behaved zero dynamics such as non-minimum phase (NMP) behavior [36, 37, 39]. In these applications, the zeros are analytically and experimentally shown to transition from minimum phase (MP) to non-minimum phase (NMP) as a function of parameters such as mass asymmetry and motion stage operating point. This variability in the system's zero dynamics makes the flexible system all the more challenging to control. In such applications, it would be highly desirable to guarantee the absence of NMP zeros over the expected range of parameter variability via informed physical design. We refer to this as *robust physical design* of flexible systems.

The physical consequences of NMP zeros on control performance of flexible systems is well-documented in the literature [14, 16, 40, 41]. For example, a real NMP zero (i.e. with imaginary component = 0) guarantees the presence of undershoot in the step response [16]. It has been experimentally shown that the undershoot due to a real NMP zero and overshoot due to undamped poles limit the response time of a flexible one-link robot [41]. It is noteworthy that the presence of undershoot is only guaranteed for real NMP zeros; complex NMP zeros (i.e. with imaginary component $\neq 0$) may or may not lead to undershoot as numerically demonstrated in [19]. The presence of any NMP zero also leads to a tradeoff between closed-loop bandwidth and stability

robustness [14]. Poor stability robustness in flexible systems leads to undesired residual vibrations, especially in case of modeling uncertainty. This is experimentally shown in [40] where the presence of complex NMP zeros in the end-point positioning control of a cantilevered beam leads to residual vibrations.

Apart from the effect of NMP zeros on the control performance of flexible systems, these zeros are also linked to the vibration performance of flexible systems. Recent investigation in the dynamics of flexure mechanisms revealed that complex NMP zeros and mode localization occur together for the same values of physical parameters [36]. These two phenomena concurrently occur in flexible systems that exhibit closely spaced modes arising from their periodic structure as well as small parametric asymmetry. It is well-known that mode localization is responsible for localized vibration in large space structures and turbine blades which leads to their premature failure [32-34]. The above-noted correlation between complex NMP zeros and mode localization can offer a means to predict and eliminate mode localization, which can be of significant value in these applications. Furthermore, Mottershead [99] numerically demonstrated the presence of complex NMP zeros in multi-DoF flexible systems and showed that in open-loop response, vibration is not completely eliminated at the frequency of these zeros. Furthermore, Mottershead [100, 101] has shown that zeros of multi-DoF flexible systems placed on the imaginary axis exhibit no vibration at these zero frequencies. However, these papers do not demonstrate how complex NMP zeros can be moved to zeros on the imaginary axis.

These undesirable physical consequences of NMP zeros on the control and vibration performance of flexible systems motivate the need to systematically and comprehensively investigate the relationship between NMP zeros and the system parameters. Such an understanding can inform the design of flexible systems to intentionally eliminate NMP zeros.

Chapter 2 provided a comprehensive review of the research literature on zeros of linear time-invariant (LTI) flexible systems, dating back to the 1980s. This review reveals that comprehensive sufficient and necessary conditions for the elimination of NMP zeros had not been reported in the literature for damped LTI flexible systems. Furthermore, Chapter 2 investigated the zeros of a three-DoF (Degrees of Freedom) *undamped* flexible LTI system by employing modal decomposition of the SISO transfer function. Five different zero types were investigated – complex MP (CMP) i.e. imaginary component $\neq 0$, real MP (RMP) i.e. imaginary component = 0, marginal MP (MMP) i.e. real component = 0, complex NMP (CNMP), and real NMP (RNMP). Comprehensive sufficient and necessary conditions were then derived in terms of the system parameters, i.e. modal residues and frequencies, to guarantee the elimination of all NMP zeros. But this investigation did not consider any damping.

There is a well-established body of research on the effect of viscous damping on the poles of flexible systems [61, 63, 102-107] but less so on the zeros [35, 94, 108, 109] even though zeros also play an important role in the dynamic performance of the flexible systems as noted above. Pang [108] analytically studied the effect of viscous damping on the migration of zeros specifically for transverse vibration of an Euler-Bernoulli beam and showed that the zeros lie on the LHS of the imaginary axis. However, this study was only limited to a collocated transfer function for the specific system studied. This paper provided no commentary on whether the conclusions reached are applicable to any general collocated transfer function. Alberts [109] also analytically investigated the effect of viscous damping on non-collocated transfer functions for transverse vibration of Euler-Bernoulli beams and reported the existence of NMP zeros. Duffour [94] analytically investigated the zero dynamics of two- and three- DoF flexible systems with and without damping. However, this paper did not explore the complete parameter space of the flexible

systems. Hoagg [35] numerically demonstrated the presence of CNMP zeros in the non-located transfer function of a three-DoF damped flexible system for large value of damping ratio ($\zeta > 1.3$). These prior numerical and analytical investigations provide examples of specific flexible systems where NMP zeros are either present or absent in the presence of viscous damping. However, no general insights or conditions for the elimination of NMP zeros are provided.

Lin [60, 110] studied the zeros of general multi-DoF damped flexible systems, and reported a sufficient condition for the elimination of only NMP zeros. This sufficient condition stated that collocated transfer functions will guarantee the elimination of NMP zeros in flexible systems with any viscous damping. However, this sufficient condition does not address the zeros of non-located transfer functions. Williams [57] under the additional assumption of classical damping, derived another sufficient condition for collocated as well as non-located transfer functions: If all the modal residue signs are positive and all the poles are underdamped, then all the zeros will be CMP.

However, Williams [57] does not provide any result when all poles are not underdamped. Furthermore, when all the modal residue signs are not the same, finding the sufficient and necessary conditions for elimination of NMP zeros becomes far more complex. To the best of the authors' knowledge, there are no previously reported conditions for two and three-DoF damped flexible systems, even though these systems are common and effective as reduced-order models in investigating the dynamics of practical multi-DoF flexible systems. For example, Tohyama [92, 93] studied the zero dynamics of a transfer function associated with room acoustics, which is an infinite DoF system, using a three-DoF flexible system model to predict the occurrence of NMP zeros. Similarly, Duffour [94] investigated the self-excited instability in brake-disc like mechanical

systems in the presence of frictional contact by approximating the dynamics of the flexible system using two and three-DoF linearized models.

Accordingly, this chapter investigates the sufficient and necessary conditions for the elimination of NMP zeros in two and three-DoF damped flexible systems, when all modal residue signs are not the same. Classical damping is assumed, which has widespread application in engineering practice because of its conceptual simplicity and practical utility [111-113]. Section 3.2 demonstrates how this assumption enables modal decomposition of the system transfer function, leading to the subsequent investigation into zeros. The first novel contribution of this chapter, presented in Section 3.3, is a broader sufficient condition as compared to Williams [57] for any level of classical damping (underdamped, critically damped, or over-damped): If all the modal residue signs are the same, then the zeros of collocated as well as non-collocated transfer functions are guaranteed to be minimum phase (RMP or CMP). The second novel contribution, presented in Section 3.4, explicitly provides the sufficient and necessary conditions for the elimination of NMP zeros in terms of system parameters (i.e. modal residues, frequencies, and damping ratios) of a two-DoF flexible system using zero loci. The third novel contribution, presented in Section 3.5, explicitly provides the sufficient and necessary conditions for the elimination of NMP zeros in terms of system parameters (i.e. modal residues, frequencies, and damping ratios) of a three-DoF flexible system using zero loci. Section 3.4 and Section 3.5 also provides several observations and inferences about the behavior of zero dynamics for their respective systems. The fourth novel contribution is in Section 3.6, which provides a step by step procedure that employs the above-derived conditions to determine location and values of viscous damping so as to robustly eliminate NMP zeros in a three-DoF flexible system, leading to better control and vibration performance. Finally, Section 3.7 provides conclusion and subsequent research directions.

3.2 Zero Dynamics and Modal Decomposition

Consider the equation of motion of a multi-DoF viscously damped flexible LTI system as shown in Eq.(3-1).

$$\begin{aligned} [\mathbf{M}]_{n \times n} \ddot{w} + [\mathbf{C}]_{n \times n} \dot{w} + [\mathbf{K}]_{n \times n} w &= [\mathbf{B}]_{n \times 1} F \\ q &= [\mathbf{D}]_{1 \times n} w \end{aligned} \quad (3-1)$$

where, $[\mathbf{M}]$, $[\mathbf{C}]$, and $[\mathbf{K}]$ denote the mass, damping, and stiffness matrices, respectively; F denotes the force acting on the system through an input vector $[\mathbf{B}]$; and, q is the measured displacement and is a linear combination, captured by sensor vector $[\mathbf{D}]$, of the individual DoF displacements denoted by w .

If the $[\mathbf{M}]$, $[\mathbf{C}]$, and $[\mathbf{K}]$ matrices satisfy the following Caughey and O'Kelly criterion [59], the flexible system is referred to as "classically damped" system.

$$[\mathbf{C}][\mathbf{M}]^{-1}[\mathbf{K}] = [\mathbf{K}][\mathbf{M}]^{-1}[\mathbf{C}] \quad (3-2)$$

This classically damped modeling assumption is commonly used in engineering applications because of its conceptual and mathematical simplicity [111-113]. The natural modes of vibration (i.e. eigenvectors) of such a classically damped flexible system are real valued and exactly same as those of the corresponding undamped flexible system (when $[\mathbf{C}] = 0$). Due to this assumption, the mode shapes matrix $[\boldsymbol{\psi}]$ is used to diagonalize the $[\mathbf{M}]$, $[\mathbf{C}]$ and $[\mathbf{K}]$ matrices simultaneously to obtain modal mass (m_i^{modal}), modal damping (c_i^{modal}), and modal stiffness (k_i^{modal}), as follows:

$$\begin{aligned} [\boldsymbol{\psi}]^T [\mathbf{M}] [\boldsymbol{\psi}] &= \mathbf{diag}(m_1^{\text{modal}}, \dots, m_n^{\text{modal}}) \quad , \quad [\boldsymbol{\psi}]^T [\mathbf{C}] [\boldsymbol{\psi}] = \mathbf{diag}(c_1^{\text{modal}}, \dots, c_n^{\text{modal}}) \\ [\boldsymbol{\psi}]^T [\mathbf{K}] [\boldsymbol{\psi}] &= \mathbf{diag}(k_1^{\text{modal}}, \dots, k_n^{\text{modal}}) \end{aligned} \quad (3-3)$$

The SISO transfer function of this system can then be modally decomposed, i.e., written as the sum of n second order modes [83], as follows:

$$G(s) = \sum_{i=1}^n \frac{\alpha_i}{s^2 + 2\zeta_i \omega_i s + \omega_i^2} \quad (3-4)$$

$$\text{where, } \alpha_i = \frac{([\mathbf{D}][\boldsymbol{\Psi}])_i ([\boldsymbol{\Psi}]^T [\mathbf{B}])_i}{m_i^{\text{modal}}}, \zeta_i = \frac{c_i^{\text{modal}}}{2\sqrt{m_i^{\text{modal}} k_i^{\text{modal}}}}, \omega_i = \sqrt{\frac{k_i^{\text{modal}}}{m_i^{\text{modal}}}} \quad (3-5)$$

The total number of second order modes (n) in the modal decomposition of $G(s)$ is equal to the number of DoF of the flexible system. The roots of each second order mode in Eq.(3-4) lie on the LHS of the imaginary axis due to the presence of positive viscous damping. Each second order mode is characterized by three real valued system parameters namely, modal residue (α_i), modal frequency (ω_i), and modal damping ratio (ζ_i). The modal residue (α_i) can be expressed in terms of the input vector $[\mathbf{B}]$, which depends on actuator location, and the sensor vector $[\mathbf{D}]$, which depends on sensor location, as well as the mode shapes matrix ($[\boldsymbol{\Psi}]$), as shown in Eq.(3-5). The columns of the matrix $[\boldsymbol{\Psi}]$ are the mode shape vectors of the flexible system. Similarly, the modal damping ratio (ζ_i) and modal frequency (ω_i) can be expressed in terms of the modal damping, mass, and stiffness.

In this chapter, we use a set of mathematical and graphical tools, namely modal decomposition (as noted above) and zero loci (presented in Section 3.4 and Section 3.5), to generate granular insights into the behavior of different types of zeros as a function of system parameters (α_i , ω_i , and ζ_i). We are able to differentiate between different types of NMP zeros, and provide separate conditions to eliminate each specific type, e.g. all NMP zeros, or CNMP zeros only, or RNMP zeros only. For example, **Result 2** in *Section 3.4* provides sufficient conditions for the elimination

of only *CNMP* zeros in a two-DoF damped flexible system, **Result 3** provides sufficient and necessary conditions for the elimination of only *RNMP* zeros in such a system, and **Result 4** provides sufficient and necessary conditions for the elimination of all NMP zeros. The graphical insights also allow us to examine the robustness of the zero dynamics to parametric variations i.e. how close the zeros are to the imaginary axis where they can transition from minimum phase to non-minimum phase.

Thus, the conditions for elimination of various types of NMP zeros derived in this chapter, in terms of the system parameters, help inform physical design choices such as selection of viscous damping strategies and magnitude i.e. choice of $[C]$, actuator and sensor placement i.e. choice of $[B]$ and $[D]$, mass and stiffness distribution i.e. choice of $[M]$ and $[K]$. The relation between these systems parameters (α_i , ω_i , and ζ_i) and the physical design choices ($[M]$, $[C]$, $[K]$, $[B]$ and $[D]$) are given by Eq.(3-3) and Eq.(3-5). Physical design choices, thus informed, can lead to robust physical designs that guarantee the elimination of NMP zeros over a wide range of system parameters.

3.3 Multi-DoF Damped Flexible System

Result 1: In a multi-DoF damped flexible LTI system, a sufficient condition for the zeros of the SISO transfer function, $G(s)$ to be minimum phase (MP) is that all the modal residue signs are the same.

The zeros for $G(s)$ are found by solving Eq. (3-6).

$$\sum_{i=1}^n \frac{\alpha_i}{s^2 + 2\zeta_i\omega_i s + \omega_i^2} = 0 \quad (3-6)$$

It is assumed that $x+jy$ is one of the zeros of $G(s)$ obtained by solving Eq.(3-6). Substitute $x+jy$ into the i^{th} mode in order to rewrite it in the Euler form as shown below.

$$\frac{\alpha_i}{s^2 + 2\zeta_i\omega_i s + \omega_i^2} = \frac{\alpha_i}{\beta_i e^{j\theta_i}} \quad (3-7)$$

$$\text{where } \beta_i = \left| (x^2 - y^2 + 2\zeta_i\omega_i x + \omega_i^2) + 2j(xy + \zeta_i\omega_i y) \right|$$

$$\theta_i = \tan^{-1} \left(\frac{2xy + 2\zeta_i\omega_i y}{x^2 - y^2 + 2\zeta_i\omega_i x + \omega_i^2} \right)$$

Next, substitute the Euler form of the i^{th} mode in Eq.(3-6).

$$\sum_{i=1}^n \frac{\alpha_i}{\beta_i} e^{-j\theta_i} = 0 \Rightarrow \sum_{i=1}^n \frac{\alpha_i}{\beta_i} \cos(\theta_i) - j \sum_{i=1}^n \frac{\alpha_i}{\beta_i} \sin(\theta_i) = 0 \quad (3-8)$$

$$\Rightarrow \sum_{i=1}^n \frac{\alpha_i}{\beta_i} \cos(\theta_i) = 0 \text{ AND } \sum_{i=1}^n \frac{\alpha_i}{\beta_i} \sin(\theta_i) = 0 \quad (3-9)$$

Since all α_i are the same sign in this result, that sign can be assumed to be positive without any loss of generality. β_i is a positive quantity, by definition, as shown in Eq.(3-7). If it is assumed that the zero $x+jy$ does not lie on the real axis i.e. $y \neq 0$, then the $\sin(\theta)$ terms are not all zero. Therefore the $\sin(\theta)$ terms cannot all have the same sign in order to satisfy Eq.(3-9). The sign of $\sin(\theta)$ is given by the sign of the quantity $2y(x + \zeta_i\omega_i)$.

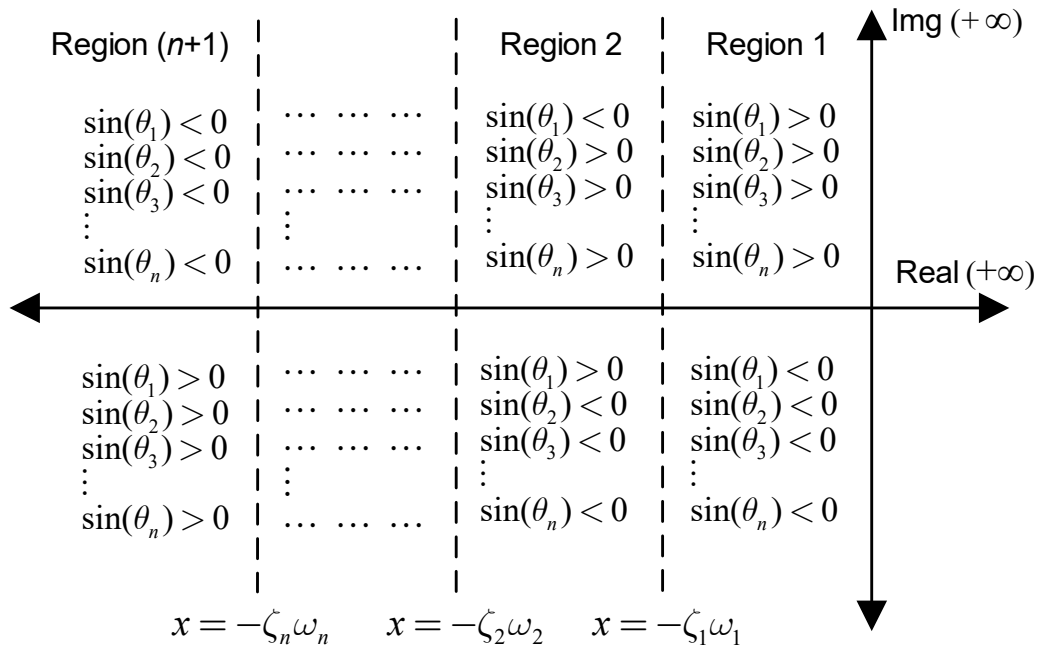


Fig 3-1 Sign of $\sin(\theta)$ when the zero $(x+jy)$ lies in various regions of the s-plane

Fig 3-1 illustrates the sign of $2y(x+\zeta_i\omega_i)$ when the zero $x+jy$ lies in different regions of the s-plane. For a multi-DoF damped flexible system that has n modes, the s-plane can be divided into $n+1$ regions defined by $x = -\zeta_i\omega_i$. If the zero $x+jy$ lies in Region 1 that extends from $x = -\zeta_1\omega_1$ to $x = +\infty$, then all the $\sin(\theta_i)$ terms will necessarily have the same sign which would not satisfy Eq.(3-9). Hence, any zero of $G(s)$ that does not lie on the real axis (i.e. $y \neq 0$) can never lie in Region 1. Since Region 1 includes the right hand side (RHS) of the s-plane, such zeros will always be minimum phase. However, the zero $x+jy$ can lie in Region 2 or for that matter in any region other than Region 1 and Region $n+1$, since the $\sin(\theta)$ terms do not have the same sign in these regions, as shown in Fig. 1, and therefore Eq.(3-9) can be satisfied.

If it is assumed that the zero $x+jy$ lies on the real axis i.e. $y = 0$ and as a consequence, all the $\sin(\theta)$ terms are equal to zero, then the above mentioned argument does not hold anymore for the $\sin(\theta)$ terms. In that case, one can observe the signs of the $\cos(\theta)$ terms in Eq.(3-9). The sign of

$\cos(\theta)$ is given by the sign of the quantity $(x^2 + 2\zeta_i\omega x + \omega^2)$ when $y = 0$. If the zero x lies on the RHS of the imaginary axis i.e. $x > 0$, then this quantity is always positive. As a consequence, all the $\cos(\theta)$ terms will be positive and Eq.(3-9) will not be satisfied. This leads to a contradiction that can only be resolved if $x < 0$ i.e. any real zero lies on the LHS of the imaginary axis and therefore is minimum phase.

Result 1 proves that when classical viscous damping is added to a flexible system, with all modal residue signs being the same, the zero dynamics will continue to remain minimum phase for any value of system parameters, which now additionally include modal damping ratios. Therefore, if the same sign of modal residues can be realized through physical design of a multi-DoF damped flexible system, then it will guarantee the absence of NMP zeros. This result holds for any level of damping (underdamped, critically damped, or over-damped) as opposed to the result derived by Williams [57] which only holds for underdamped flexible systems. However, when all the modal residue signs are not same, additional conditions are required to guarantee the elimination of NMP zeros. Hence, in the next sections, the NMP zero dynamics of two-DoF damped flexible systems will be investigated to determine those additional conditions (in terms of system parameters) for the elimination of NMP zeros when all the modal residue signs are not the same.

3.4 Two DoF Damped Flexible LTI Systems

The SISO transfer function of a two-DoF classically damped flexible system is expressed in its decomposed form below.

$$G_2(s) = \frac{\alpha_u}{s^2 + 2\zeta_u\omega_u s + \omega_u^2} + \frac{\alpha_v}{s^2 + 2\zeta_v\omega_v s + \omega_v^2} \quad (3-10)$$

The subscript ‘2’ in $G_2(s)$ stands for the number of modes (or the DoF). Furthermore, it is assumed without any loss of generality that $\omega_u < \omega_v$. $G_2(s)$ is expressed in terms of its numerator and denominator as shown below.

$$G_2(s) = \frac{N_2(s)}{D_2(s)} = \frac{\kappa(s^2 + 2\zeta_v\omega_v s + \omega_v^2) + (s^2 + 2\zeta_u\omega_u s + \omega_u^2)}{(s^2 + 2\zeta_u\omega_u s + \omega_u^2)(s^2 + 2\zeta_v\omega_v s + \omega_v^2)} \text{ where } \kappa \triangleq \frac{\alpha_u}{\alpha_v} \quad (3-11)$$

The zeros of $G_2(s)$ are investigated by studying the roots of its numerator $N_2(s)$. Of interest are the zeros when modal residues do not have the same sign, i.e., $\kappa (\triangleq \alpha_u / \alpha_v) < 0$. $N_2(s)$ is expressed in terms of $A_2(s)$ and $B_2(s)$ that are defined below. $A_2(s)$ and $B_2(s)$ have no physical meaning and simply serve as a mathematical tool.

$$N_2(s) = \kappa A_2(s) + B_2(s) \text{ where } \kappa \triangleq \frac{\alpha_u}{\alpha_v} \quad (3-12)$$

$$A_2(s) \triangleq (s^2 + 2\zeta_v\omega_v s + \omega_v^2) \quad B_2(s) \triangleq (s^2 + 2\zeta_u\omega_u s + \omega_u^2)$$

Next, we define a transfer function $T_2(s) = A_2(s) / B_2(s)$, which has no physical meaning and simply serves as a mathematical tool. The root locus of $T_2(s)$ is the zero locus of $G_2(s)$. Therefore, to obtain the zero locus of $G_2(s)$, we plot the root locus of $T_2(s)$ as a function of the ratio of modal residues (κ). Since, $\kappa < 0$ by definition in this section, the negative (i.e. complementary) root locus of $T_2(s)$ will be analyzed to derive the sufficient and necessary conditions to eliminate NMP zeros in $G_2(s)$. In order to do so, first the sufficient and necessary condition for the elimination of CNMP zeros is derived in **Result 2** followed by the sufficient and necessary conditions for the elimination of RNMP zeros in **Result 3**. Finally Result 4 provides the sufficient and necessary conditions for the elimination of all NMP zeros i.e. CNMP and RNMP zeros.

The zeros of $G_2(s)$ (or equivalently, the roots of $T_2(s)$) can be obtained by solving

$$\begin{aligned}
N_2(s) &= \kappa A_2(s) + B_2(s) = 0 \\
\Rightarrow \kappa &= \frac{B_2(s)}{A_2(s)} = -\frac{(s^2 + 2\zeta_u \omega_u s + \omega_u^2)}{(s^2 + 2\zeta_v \omega_v s + \omega_v^2)}
\end{aligned} \tag{3-13}$$

If $x + jy$ is part of the root locus of $T_2(s)$ and $\kappa < 0$, then

$$\begin{aligned}
(\angle \psi_u)_{s=x+jy} - (\angle \psi_v)_{s=x+jy} &= 360^\circ m \quad (m \text{ is an integer}) \\
(\angle \psi_u)_{s=x+jy} &\triangleq \angle (s^2 + 2\zeta_u \omega_u s + \omega_u^2)_{s=x+jy} \\
(\angle \psi_v)_{s=x+jy} &\triangleq \angle (s^2 + 2\zeta_v \omega_v s + \omega_v^2)_{s=x+jy}
\end{aligned} \tag{3-14}$$

Applying the tangent function to both sides of Eq.(3-14) and substituting Laplace variable 's' with Cartesian coordinates x and y , the root locus of $T_2(s)$ in the Cartesian form is given by

$$\begin{aligned}
\tan\left((\angle \psi_u)_{s=x+jy}\right) - \tan\left((\angle \psi_v)_{s=x+jy}\right) &= 0 \\
\Rightarrow y \left(\frac{2x + 2\zeta_u \omega_u}{x^2 - y^2 + 2\zeta_u \omega_u x + \omega_u^2} - \frac{2x + 2\zeta_v \omega_v}{x^2 - y^2 + 2\zeta_v \omega_v x + \omega_v^2} \right) &= 0
\end{aligned} \tag{3-15}$$

A few observations can be made here. The entire real axis (i.e. $y = 0$) is always a solution to Eq.(3-15). Therefore, the entire real axis is always a part of the root locus of $T_2(s)$. The real axis is divided into two the negative real axis where real minimum phase (RMP) zeros occur and the positive real axis where real non-minimum phase (RNMP) zeros occur.

There exists a critical value of κ for which the root locus $T_2(s)$ transitions from the negative real axis to the positive real axis or vice versa by passing through the origin. In the process, the zero changes from real minimum phase (RMP) to real non-minimum phase (RNMP), or vice versa. Mathematically, this value of κ can be found by substituting the Laplace variable $s = 0$ in Eq.(3-13)

$$\begin{aligned}
& \kappa A_2(s) + B_2(s) = 0 \\
\Rightarrow & \kappa \left(s^2 + 2\zeta_v \omega_v s + \omega_v^2 \right)_{s=0} + \left(s^2 + 2\zeta_u \omega_u s + \omega_u^2 \right)_{s=0} = 0 \quad (3-16) \\
\Rightarrow & \kappa \omega_v^2 + \omega_u^2 = 0 \quad \Rightarrow \quad \kappa = -\eta^2
\end{aligned}$$

There exists a critical value of κ for which the root locus $T_2(s)$ transitions from the negative real axis to the positive real axis or vice versa by passing through infinity. As a result, the zero changes from RMP to RNMP or vice versa. Mathematically, this corresponds to Eq.(3-13) having a single root.

$$\begin{aligned}
& (\kappa + 1)s^2 + 2(\kappa\zeta_v\omega_v + \zeta_u\omega_u)s + \kappa\omega_v^2 + \omega_u^2 = 0 \\
& \text{Setting coefficient of } s^2 \text{ to zero} \quad (3-17) \\
\Rightarrow & (\kappa + 1) = 0 \quad \Rightarrow \quad \kappa = -1
\end{aligned}$$

While the entire real axis is part of the root locus of $T_2(s)$ (or zero locus of $G_2(s)$), only a few points on the imaginary axis can be part of the root locus. The points of intersection of the root locus with the imaginary axis, if they exist, can be determined by substituting $x = 0$ in Eq.(3-15).

$$\begin{aligned}
& \frac{2\zeta_u\omega_u y}{-y^2 + \omega_u^2} - \frac{2\zeta_v\omega_v y}{-y^2 + \omega_v^2} = 0 \quad (3-18) \\
\Rightarrow & (\zeta_v\omega_v - \zeta_u\omega_u)y^2 + (\zeta_u\omega_u\omega_v^2 - \zeta_v\omega_v\omega_u^2) = 0
\end{aligned}$$

The sufficient condition to guarantee that the root locus of $T_2(s)$ does not cross the imaginary axis is to ensure that Eq.(3-18) does not have any real solutions for y . This can be ensured if

$$\frac{\zeta_u\omega_u\omega_v^2 - \zeta_v\omega_v\omega_u^2}{\zeta_u\omega_u - \zeta_v\omega_v} \leq 0 \quad \Rightarrow \quad \frac{(\chi - \eta)}{\left(\chi - \frac{1}{\eta}\right)} \leq 0 \quad (3-19)$$

Since $\eta < 1$ by definition (i.e. $\omega_u < \omega_v$), the above condition can be reduced to

$$\chi \geq \eta \quad \text{AND} \quad \chi \leq 1/\eta \quad \Rightarrow \quad \eta \leq \chi \leq 1/\eta \quad (3-20)$$

When Eq.(3-20) is satisfied, the root locus of $T_2(s)$ will not cross the imaginary axis. However, when $\chi < \eta$ or $\chi > 1/\eta$, Eq.(3-18) will have real solutions for y . Therefore, the root locus will cross the imaginary axis leading to transition of complex minimum phase (CMP) zeros to complex non-minimum phase (CNMP) zeros or vice versa. The critical value of κ when the root locus crosses the imaginary axis mathematically corresponds Eq.(3-13) having purely imaginary roots.

$$\begin{aligned} \kappa A_2(s) + B_2(s) &= 0 \\ \Rightarrow (\kappa + 1)s^2 + 2(\kappa\zeta_v\omega_v + \zeta_u\omega_u)s + \kappa\omega_v^2 + \omega_u^2 &= 0 \end{aligned} \quad (3-21)$$

Setting coefficient of s to zero

$$\Rightarrow (\kappa\zeta_v\omega_v + \zeta_u\omega_u) = 0 \quad \Rightarrow \quad \kappa = -\eta\chi$$

There also exists a critical value of κ for which CNMP zeros transition into RNMP zeros. This happens when the root locus meets the positive real axis. For this value of κ , there are two repeated roots of the Eq. (3-13) that are real positive. This value of κ is found by setting the discriminant of the quadratic equation in Eq.(3-13) to zero.

$$\begin{aligned} \kappa_1 &= \frac{(\eta^2 + 1 - 2\chi\eta\zeta_v^2) - \sqrt{(\eta^2 - 1)^2 + 4\eta^2\zeta_v^2\left(\chi - \frac{1}{\eta}\right)(\chi - \eta)}}{2(\zeta_v^2 - 1)} \\ \kappa_2 &= \frac{(\eta^2 + 1 - 2\chi\eta\zeta_v^2) + \sqrt{(\eta^2 - 1)^2 + 4\eta^2\zeta_v^2\left(\chi - \frac{1}{\eta}\right)(\chi - \eta)}}{2(\zeta_v^2 - 1)} \end{aligned} \quad (3-22)$$

Simple algebraic manipulation of the above critical values of κ will show that κ_1 is valid for the parameter space $\chi < \eta$ and κ_2 is valid for $\chi > 1/\eta$.

Having addressed how the root locus of $T_2(s)$, or equivalently the zero locus of $G_2(s)$, interacts with the real and imaginary axes of the s -plane, we can now construct the root locus of $T_2(s)$, or

equivalently the zero locus of $G_2(s)$, using this information. It should be noted that the three different parameter range of χ span all values of χ from 0 to $+\infty$, and therefore the zero loci shown in Fig 3-2 are a comprehensive depiction of the zeros of $G_2(s)$ for all possible system parameters as long as $\kappa < 0$. Note that since the zeros occur as pairs of complex conjugate, only one half of the zero loci, which is above the real axis is shown in Fig 3-2.

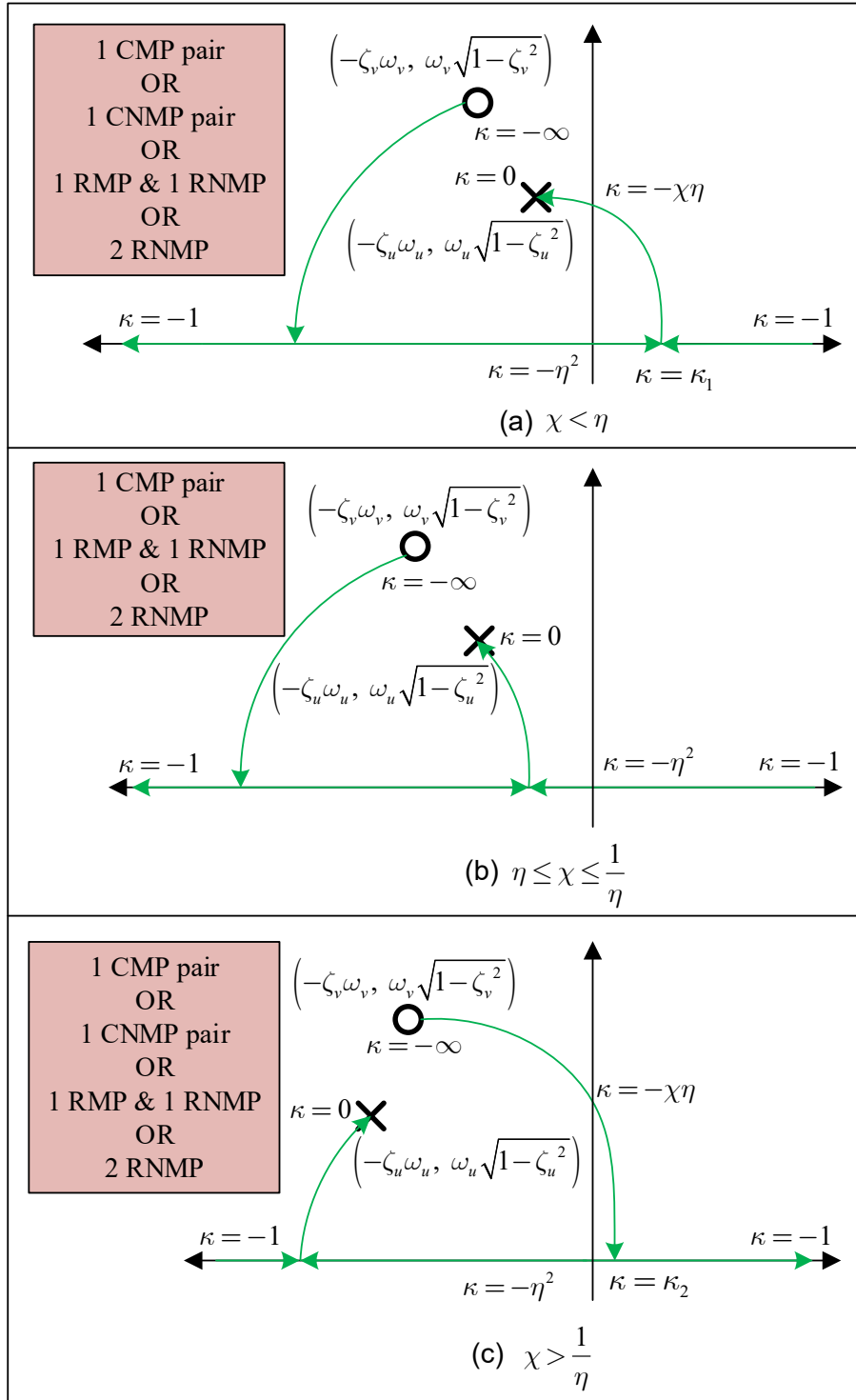


Fig 3-2 Zero Loci of $G_2(s)$ for different ranges of χ as κ varies from $-\infty$ to 0. Zeros and poles of

$T_2(s)$ provide the starting and ending locations, respectively, of these zero loci

3.4.1 Sufficient and Necessary Condition for eliminating CNMP Zeros

Result 2: In a two-DoF damped flexible LTI system given by Eq.(3-10), when the modal residue signs are not same ($\kappa < 0$), the following conditions are individually sufficient and together necessary to guarantee the elimination of CNMP zeros:

$$\text{Condition 2.1: } (\chi < \eta) \text{ AND } (\kappa \leq \kappa_1 \text{ OR } \kappa \geq -\chi\eta)$$

OR

$$\text{Condition 2.2: } \left(\eta \leq \chi \leq \frac{1}{\eta} \right) \quad (3-23)$$

OR

$$\text{Condition 2.3: } \left(\chi > \frac{1}{\eta} \right) \text{ AND } (\kappa \leq -\chi\eta \text{ OR } \kappa \geq \kappa_2)$$

Condition 2.1 is derived from Fig 3-2a. Fig 3-2a is valid for $\chi < \eta$. For $\chi < \eta$, Fig 3-2a shows that CNMP zeros are not part of the zero locus if $\kappa \geq -\chi\eta$. In this case the zero lies on the left hand side of the imaginary axis. Therefore, the zero can either be CMP or RMP (if the poles are overdamped) but never CNMP. Similarly, CNMP zeros do not occur again if $\kappa \leq \kappa_1$. In this case, it is evident from Fig 3-2a that the zero is either RNMP, RMP or CMP but never CNMP. Therefore, the graphical analysis of Fig 3-2a in this manner leads to Condition 2.1. Similarly, Fig 3-2b leads to Condition 2.2 and Fig 3-2c leads to Condition 2.3.

Based on **Result 2** and Fig 3-2, the following observations can be made about the CNMP zeros of a two-DoF damped flexible LTI system:

1. Each condition listed in **Result 2** is individually sufficient but not necessary. For example, Condition 2.1, by itself, is a sufficient condition. However, Condition 2.1, by itself, is not necessary

because even if this condition is not met, NMP zeros can still be eliminated via other non-overlapping conditions such as Condition 2.2 or Condition 2.3.

2. Each sufficient condition comprises of parameter ranges that are essential and broadest possible. For each of these conditions, one can write various inferior conditions with narrower parameter ranges that would also be sufficient conditions. For example, based on Condition 2.1, [$\chi < \eta$ AND $\kappa < -1$] is also a sufficient condition for the elimination of NMP zeros.

3. As shown by the zero loci of Fig 3-2, the entire range of the system parameters comprising of modal residues, frequencies, and damping ratios is covered in this analysis. Therefore, the conditions of **Result 2** form a complete list of all possible sufficient conditions. In other words, there are no other sufficient conditions for which one can guarantee the elimination of NMP zeros. As a result, these three conditions when considered together, i.e., [Condition 2.1 OR Condition 2.2 OR Condition 2.3], form a necessary condition for the elimination of CNMP zeros.

4. The mathematical form of the conditions in **Result 2** is the consequence of our choice of parameterization. The normalized parameters κ , χ , and η that are defined in terms of system parameters and used to provide the conditions in **Result 2** could have been defined differently. For example, instead of considering $\kappa (= \alpha_u / \alpha_v)$ as the varying parameter to plot the zero locus of $G_2(s)$, one could use a different varying parameter defined by α_v / α_u . The zero locus could have been plotted as a function of ratio of modal frequencies or modal damping ratios. While the resulting mathematical form of the conditions may be different in that case, the conditions would effectively be the same in terms system parameters. In other words, the conditions are unique.

5. It was shown previously [114] that a two-DoF undamped flexible system can never exhibit CNMP zeros for any value of system parameters (modal frequencies and residues). However, for

a two-DoF damped flexible system, Fig 3-2a and Fig 3-2c depict the presence of CNMP zeros for certain parameter ranges of χ and κ . This shows a potential disadvantage of adding damping to a two-DoF flexible system, which is intuitively unexpected because damping is generally beneficial [61].

3.4.2 Sufficient and Necessary Conditions for Eliminating RNMP zeros

Result 3: In a two-DoF damped flexible LTI system given by Eq.(3-10), when the modal residue signs are not same ($\kappa < 0$), the following conditions are individually sufficient and together necessary to guarantee the elimination of RNMP zeros:

$$\begin{aligned}
 &\text{Condition 3.1: } (\chi < \eta) \text{ AND } (\kappa \leq -1 \text{ OR } \kappa > \kappa_1) \\
 &\quad \text{OR} \\
 &\text{Condition 3.2: } \left(\eta \leq \chi \leq \frac{1}{\eta} \right) \text{ AND } (\kappa \leq -1 \text{ OR } \kappa \geq -\eta^2) \quad (3-24) \\
 &\quad \text{OR} \\
 &\text{Condition 3.3: } \left(\chi > \frac{1}{\eta} \right) \text{ AND } (\kappa < \kappa_2 \text{ OR } \kappa \geq -\eta^2)
 \end{aligned}$$

Condition 3.1 is derived from Fig 3-2a. It can be observed from Fig 3-2a, which is valid for $\chi < \eta$, that RNMP zero occur in the zero locus when $\kappa_1 \leq \kappa < -1$. Therefore, removing this parameter space of κ from its complete parameter space i.e. $-\infty$ to 0 gives the Condition 3.1 for which RNMP zeros do not occur in the zero locus of Fig 3-2a. Similarly, Fig 3-2b leads to Condition 3.2 and Fig 3-2c leads to Condition 3.3. Note that the general observation for **Result 2** i.e. bullet point (1) to (4) also hold true for **Result 3**.

3.4.3 Sufficient and Necessary Conditions for Eliminating all NMP zeros

Result 4: In a two-DoF damped flexible LTI system given by Eq.(3-10), when the modal residue signs are not same ($\kappa < 0$), the following conditions are individually sufficient and together necessary to guarantee the elimination of all NMP zeros.

$$\text{Condition 4.1: } (\chi < \eta) \text{ AND } (\kappa \leq -1 \text{ OR } \kappa \geq -\eta\chi)$$

OR

$$\text{Condition 4.2: } (\eta \leq \chi \leq 1/\eta) \text{ AND } (\kappa \leq -1 \text{ OR } \kappa \geq -\eta^2) \quad (3-25)$$

OR

$$\text{Condition 4.3: } (\chi > 1/\eta) \text{ AND } (\kappa \leq -\eta\chi \text{ OR } \kappa \geq -\eta^2)$$

Condition 4.1 is derived from Fig 3-2a. Referring to Fig 3-2a, where $\chi < \eta$, it can be seen that the zero locus remains on the LHS real axis when $\kappa < -1$ and crosses back into the LHS of the imaginary axis when $\kappa \geq -\eta\chi$. Condition 4.2 is derived from Fig 3-2b. In Fig 3-2b, which corresponds to the parameter range $\eta \leq \chi \leq 1/\eta$, there are no CNMP zeros in the transfer function $G_2(s)$. The zero locus flips from negative infinity to positive infinity on the real axis when $\kappa = -1$ and returns to the LHS real axis, crossing the origin when $\kappa = -\eta^2$. Thus, no NMP zeros will occur if $\kappa \leq -1$ or if $\kappa \geq -\eta^2$. Condition 4.3 is derived from Fig 3-2c. Fig 3-2c shows the zero locus of $G_2(s)$ when $\chi > 1/\eta$, and it can be seen that NMP zeros will not occur if $\kappa \leq -\eta\chi$ or if $\kappa \geq -\eta^2$. Note that the general observation for **Result 2** i.e. bullet point (1) to (4) also hold true for **Result 4**.

The graphical visualization in Fig 3-2 allows one to determine the sufficient and necessary conditions for the elimination of *specific* types of NMP zeros e.g. CNMP only, RNMP only, as

well as all NMP. For example, **Result 2** provides a sufficient and necessary condition for the elimination of CNMP zeros, while **Result 3** provides sufficient and necessary conditions for the elimination of RNMP zeros. Finally, **Result 4** provides sufficient and necessary conditions for the elimination of all NMP zeros. Furthermore, this graphical visualization allows one to examine the sensitivity of different types of NMP zeros to parametric variations, which helps inform the robustness of any choice of system parameters that avoid NMP zeros. For example, when the value of κ is close to $-\eta^2$, the RMP zero can flip to become a RNMP zero, and similarly when κ is close to $-\chi\eta$, CMP zeros can flip to become CNMP zeros.

3.5 Three-DoF Damped Flexible LTI Systems

The SISO transfer function of a three-DoF classically damped flexible system is given by $G_3(s)$:

$$G_3(s) = \frac{\alpha_R}{s^2 + 2\zeta_R\omega_R s + \omega_R^2} + \frac{\alpha_u}{s^2 + 2\zeta_u\omega_u s + \omega_u^2} + \frac{\alpha_v}{s^2 + 2\zeta_v\omega_v s + \omega_v^2}$$

where $\omega_R < \omega_u < \omega_v$. Two additional assumptions are made here. The natural frequency and damping ratio of the first flexible mode, ω_R and ζ_R , are assumed low enough to be set to zero. In previous modeling [36] and experimental work [37], CNMP zeros were reported in systems that have a low frequency rigid-body mode and at least two high frequency closely-spaced modes i.e. $\omega_R \ll \omega_u \approx \omega_v$. The CNMP zeros occurred very close to the frequency of the closely-spaced modes, much higher than the rigid-body mode. Furthermore, in many flexible systems damping is relatively low [61]. Thus, at the higher frequencies of interest, the ' ω_R^2 ' and the ' $2\zeta_R\omega_R s$ ' terms can be ignored in comparison to the ' s^2 ' term in the first mode. Motivated by practical examples, these

additional approximations limit the complexity of the mathematical and graphical analysis in this section, which in turn allows for better physical insights from the results.

Accordingly, the three-DoF damped flexible system investigated in this section can be expressed as $G_3(s) =$

$$\frac{N_3(s)}{D_3(s)} = \frac{\alpha_R}{s^2} + \frac{\alpha_u}{s^2 + 2\zeta_u\omega_u s + \omega_u^2} + \frac{\alpha_v}{s^2 + 2\zeta_v\omega_v s + \omega_v^2} \quad (3-26)$$

Furthermore, α_R can be set to +1 without any loss in generality. This reduces the number of system parameters that need to be carried through the subsequent mathematical steps. The zeros of $G_3(s)$ are investigated by studying the roots of its numerator, $N_3(s)$.

$$N_3(s) = \alpha_v s^2 \left[(1 + \kappa)s^2 + 2\zeta_v\omega_v(\chi\eta + \kappa)s + \omega_v^2(\eta^2 + \kappa) \right] + (s^2 + 2\zeta_u\omega_u s + \omega_u^2)(s^2 + 2\zeta_v\omega_v s + \omega_v^2)$$

$$\text{where } \eta \triangleq \frac{\omega_u}{\omega_v}, \chi \triangleq \frac{\zeta_u}{\zeta_v}, \text{ and } \kappa \triangleq \frac{\alpha_u}{\alpha_v} \quad (3-27)$$

$N_3(s)$ is expressed in a condensed form below in terms of α_v , $A_3(s)$ and $B_3(s)$.

$$N_3(s) = \alpha_v A_3(s) + B_3(s)$$

$$\text{where } A_3(s) \triangleq s^2 \left[(1 + \kappa)s^2 + 2\zeta_v\omega_v(\chi\eta + \kappa)s + \omega_v^2(\eta^2 + \kappa) \right] \quad (3-28)$$

$$B_3(s) \triangleq (s^2 + 2\zeta_u\omega_u s + \omega_u^2)(s^2 + 2\zeta_v\omega_v s + \omega_v^2)$$

A mathematical transfer function, $T_3(s) = A_3(s) / B_3(s)$, with no physical meaning is defined to capture the zero locus of $G_3(s)$. The root locus of $T_3(s)$ obtained by varying α_v , gives the zero locus of $G_3(s)$. When α_v is varied from 0 to $+\infty$, the positive root locus originates at the roots of $B_3(s)$ and terminates at the roots of $A_3(s)$. When α_v is varied from $-\infty$ to 0, the negative or complementary root locus goes from roots of $A_3(s)$ to the roots of $B_3(s)$. The goal of this section is to derive the sufficient and necessary conditions to eliminate all NMP zeros from $G_3(s)$ using its zero loci. First,

a set of sufficient conditions for the elimination of only CNMP zeros is derived in **Results 5** and **6**, followed by the sufficient and necessary conditions for the elimination of CNMP and RNMP zeros i.e. all NMP zeros in **Results 7** and **8**.

Table 3-1 shows all the possible modal residue signs for a three-DoF flexible system. The case when all the modal residues are positive has already been covered. In this section, the zero dynamics will be investigated for the remaining combinations (i.e. alternating signs and non-alternating) of modal residue signs.

Case	α_R	α_u	α_v	$\kappa (\triangleq \alpha_u / \alpha_v)$	Result
Same Signs	+	+	+	+	1
Alternating Signs	+	-	+	-	5,7
Non-Alternating Signs	+	+	-	-	6,8
	+	-	-	+	

Table 3-1 Combination of modal residue signs

Zeros of $G_3(s)$ are found by setting the numerator $N_3(s)$ in Eq.(3-28) to zero:

$$N_3(s) = \alpha_v A_3(s) + B_3(s) = 0 \Rightarrow \alpha_v = -\frac{B_3(s)}{A_3(s)} \quad (3-29)$$

A few key observations can be made here. Every point on the real axis of the s -plane (i.e. $y = 0$) is always a solution of Eq.(3-29). When $s = x$, the RHS of Eq.(3-29) i.e. $B_3(s) / A_3(s)$ is always a scalar with either a positive or negative sign. This means that for some positive or negative value of α_v , this equation will always be true. Therefore, the entire real axis is part of the root locus. There exists a critical value of α_v referred to as α_v^∞ for which the root locus flips from the negative real axis to the positive real axis, or vice versa by passing through infinity. This corresponds to the transition of the RMP zero of $G_3(s)$ into its RNMP zero, or vice versa. Mathematically, this condition corresponds to a loss in order of $N_3(s)$, and therefore α_v^∞ can be derived by setting the coefficient of s^4 in $N_3(s)$, given in Eq.(3-27), to zero.

$$\alpha_v^\infty = -\frac{1}{1+\kappa} \quad (3-30)$$

While the entire real axis of the s -plane is part of the root locus, only certain points on the imaginary axis can be part of the root locus. These points can be determined by applying the angle condition to Eq.(3-29), rearranging the terms, taking tangent on both sides, and setting $s = jy$.

$$\begin{aligned} (\angle B_3(s) - \angle A_3(s)) &= m180^\circ \quad (m \text{ is any integer}) \\ \tan(\angle B_3(s))_{s=jy} &= \tan(m180^\circ + \angle A_3(s))_{s=jy} \\ \Rightarrow \tan(\angle B_3(s))_{s=jy} &= \tan(\angle A_3(s))_{s=jy} \\ \Rightarrow y(ay^4 + by^2 + c) &= 0 \end{aligned} \quad (3-31)$$

$$\text{where } a \triangleq \kappa\eta(2\zeta_v\omega_v)\left(\frac{1}{\kappa\eta} + \chi\right), \quad c \triangleq \frac{\kappa}{\eta^3}(2\zeta_v\omega_u^4\omega_v)\left(\frac{\eta^3}{\kappa} + \chi\right)$$

$$b \triangleq (4\zeta_v\omega_u^2\omega_v)(\lambda\zeta_v^2 - \delta), \quad \lambda \triangleq 2\chi\left(\frac{\kappa}{\eta} + \chi\right), \quad \text{and } \delta \triangleq \frac{\kappa}{\eta}\left(\frac{\eta}{\kappa} + \chi\right)$$

Eq.(3-31) can have five real solutions in y , which correspond to five potential locations where the root locus of $T_3(s)$ intersects the imaginary axis. Note that $y = 0$ is always a solution to Eq.(3-31), which means that the root locus always passes through the origin of the s -plane. This is to be expected since $s = 0$ is also a root of $A_3(s)$, which corresponds to the root locus location for $\alpha_v = \pm\infty$. The other locations where the root locus crosses the imaginary axis correspond to the non-zero real solutions in y of Eq.(3-31). The mathematical conditions for which such crossings may or may not exist are given by:

Condition I: $b^2 - 4ac < 0$

$$\text{Condition II: } b^2 - 4ac \geq 0 \quad \text{AND} \quad \frac{-b + \sqrt{b^2 - 4ac}}{2a} < 0 \quad (3-32)$$

$$\text{Condition III: } b^2 - 4ac \geq 0 \quad \text{AND} \quad \frac{-b - \sqrt{b^2 - 4ac}}{2a} < 0$$

Given the fourth order polynomial in Eq.(3-31), the root locus can cross the imaginary axis at a maximum of two sets of conjugate locations. Each set of conjugate location has a corresponding α_v that are referred to as α_{v1}^{img} and α_{v2}^{img} . The value of α_{v1}^{img} and α_{v2}^{img} when the root locus crosses the imaginary axis can be found by setting $s = jy$ in the expression for $N_3(s)$ in Eq.(3-27) and equating $N_3(s)$ to 0.

$$\alpha_{v1}^{img} = \frac{\omega_u \omega_v (\chi + \eta) - (1 + \chi \eta) y_1^2}{(\chi \eta + \kappa) y_1^2} \quad \text{where } y_1^2 = \frac{-b + \sqrt{b^2 - 4ac}}{2a} \quad (3-33)$$

$$\alpha_{v2}^{img} = \frac{\omega_u \omega_v (\chi + \eta) - (1 + \chi \eta) y_2^2}{(\chi \eta + \kappa) y_2^2} \quad \text{where } y_2^2 = \frac{-b - \sqrt{b^2 - 4ac}}{2a}$$

If Condition I is true OR [Condition II AND Condition III] are true, then there are no non-zero real solutions in y . If Condition I is not true, AND Condition II is not true AND Condition III is true, then the root locus will cross the imaginary axis at one set of conjugate locations given by $s = \pm jy_1$ and corresponding $\alpha_v = \alpha_{v1}^{img}$. If Condition I is not true, AND Condition II is true AND Condition III is not true, then the root locus will cross the imaginary axis at one set of conjugate locations given by $s = \pm jy_2$ and corresponding $\alpha_v = \alpha_{v2}^{img}$. If Condition I is not true, AND [both Condition II AND Condition III] are also not true, then the root locus will cross the imaginary axis at two sets of conjugate locations given by $s = \pm jy_1$ (corresponding $\alpha_v = \alpha_{v1}^{img}$) and $s = \pm jy_2$ (corresponding $\alpha_v = \alpha_{v2}^{img}$). Thus, the above conditions determine the number of instances where the root locus crosses the imaginary axis, which in turn informs the shape of the root locus. These

crossings can happen for positive or negative values of α_v i.e. α_{v1}^{img} and α_{v2}^{img} can either be positive or negative. The detailed derivation of when α_{v1}^{img} and α_{v2}^{img} are positive or negative will be provided below.

Having addressed how the root locus of $T_3(s)$, or equivalently the zero locus of $G_3(s)$, interacts with the real and imaginary axes of the s-plane, we next proceed to divide the parameter space, reduce the conditions from Eq.(3-32) to parameter ranges, and plot the resulting zero loci for various combination of parameter ranges. The steps are as follows:

1. The parameter space of the modal residues ratio i.e. κ is divided into $(\kappa < -1)$, $(-1 < \kappa < -\eta^2)$, $(-\eta^2 < \kappa < 0)$ and $(\kappa > 0)$. These four ranges span all values of κ from $-\infty$ to $+\infty$ and they were used for the analysis of NMP zeros in the analogous three-DoF *undamped* flexible system. Using the same parameter ranges of κ in here allows for a direct comparison between the NMP zero dynamics of the *undamped* and damped systems. This leads to inferences on how the addition of damping changes the zero loci and the resulting condition for the elimination of NMP zeros. These inferences are discussed in **Result 5** and **Result 6**.
2. The mathematical inequalities given by Condition I, Condition II, and Condition III are solved separately for all four parameter ranges of κ . This gives the non-overlapping parameter ranges of χ and ζ_v for each parameter range of κ where these conditions are or are not satisfied. These ranges are then used to draw the multiple unique zero loci of $G_3(s)$, as shown in Fig. 3-5.
3. Detailed steps on the derivation of these parameter ranges will be discussed below.

The derivation for the parameter ranges starts from here:

Firstly, we derive the parameters ranges of χ and ζ_v for each parameter range of κ for which Condition I of Eq.(3-32) is satisfied.

$$\begin{aligned}
& b^2 - 4ac < 0 \\
& \Rightarrow [4\zeta_v \omega_u^2 \omega_v]^2 [\lambda \zeta_v^2 - \delta]^2 - 4ac < 0 \\
& \text{Let } [\zeta_v \omega_u^2 \omega_v] = \phi \\
& \Rightarrow 16\phi^2 [\lambda \zeta_v^2 - \delta]^2 - 4ac < 0 \\
& \Rightarrow [2\phi\{\lambda \zeta_v^2 - \delta\}]^2 - [\sqrt{ac}]^2 < 0 \\
& \Rightarrow -\frac{\sqrt{ac}}{2\phi} < \lambda \zeta_v^2 - \delta < \frac{\sqrt{ac}}{2\phi} \\
& \Rightarrow \delta - \frac{\sqrt{ac}}{2\phi} < \lambda \zeta_v^2 < \delta + \frac{\sqrt{ac}}{2\phi}
\end{aligned}$$

Multiplying and dividing $\lambda \zeta_v^2$ by λ and using modulus to represent both signs of λ

$$\begin{aligned}
& \Rightarrow \lambda \delta - |\lambda| \frac{\sqrt{ac}}{2\phi} < \lambda^2 \zeta_v^2 < \lambda \delta + |\lambda| \frac{\sqrt{ac}}{2\phi} \\
& \Rightarrow \frac{1}{|\lambda|} \sqrt{\lambda \delta - |\lambda| \frac{\sqrt{ac}}{2\phi}} < \zeta_v < \frac{1}{|\lambda|} \sqrt{\lambda \delta + |\lambda| \frac{\sqrt{ac}}{2\phi}} \\
& \Rightarrow \zeta_{v,\min} < \zeta_v < \zeta_{v,\max} \tag{3-34}
\end{aligned}$$

$$\text{where } \zeta_{v,\min} \triangleq \frac{1}{|\kappa + \eta\chi| \sqrt{2\chi}} \sqrt{(\kappa + \eta\chi)(\kappa\chi + \eta) - |\kappa + \eta\chi| \sqrt{\frac{(\eta^3 + \kappa\chi)(1 + \kappa\eta\chi)}{\eta}}}$$

$$\text{AND } \zeta_{v,\max} \triangleq \frac{1}{|\kappa + \eta\chi| \sqrt{2\chi}} \sqrt{(\kappa + \eta\chi)(\kappa\chi + \eta) + |\kappa + \eta\chi| \sqrt{\frac{(\eta^3 + \kappa\chi)(1 + \kappa\eta\chi)}{\eta}}}$$

Range of κ	Range of χ for which the radicand in Eq.(3-34) are positive	Range of ζ_v for which Condition I of Eq.(3-32) is satisfied
$\kappa < 1$	$\frac{-1}{\eta\kappa} < \chi < -\frac{\kappa}{\eta}$	$\zeta_{v,\min} < \zeta_v < \zeta_{v,\max}$

$-1 < \kappa < -\eta^2$	Upper and Lower limit do not exist for any value of χ	Limit does not exist
$-\eta^2 < \kappa < 0$	$-\frac{\kappa}{\eta} < \chi < -\frac{\eta^3}{\kappa}$	$\zeta_{v,\min} < \zeta_v < \zeta_{v,\max}$
$\kappa > 0$	For all values of χ	$\zeta_v < \zeta_{v,\max}$

Table 3-2 Range of χ and ζ_v for which Condition (I) of Eq.(3-32) is satisfied.

Now, we find the parameter ranges of χ and ζ_v for each parameter range of κ for which Condition II and Condition III of Eq.(3-32) are satisfied separately. Condition II and Condition III can only be true for certain combination of signs of a , b , and c as shown below. The combination of signs of a , b , and c in Eq.(3-35) is a necessary condition for Condition II and Condition III in Eq.(3-32) to hold true. Hence, we evaluate Condition II and Condition III only for these combination of signs of a , b , and c .

$$\text{Condition II: } b^2 - 4ac \geq 0 \quad \text{AND} \quad \frac{-b + \sqrt{b^2 - 4ac}}{2a} < 0 \Rightarrow \quad \text{IIA. } a > 0, b > 0, c > 0$$

$$\text{IIB. } a < 0, b > 0, c > 0$$

$$\text{IIC. } a < 0, b < 0, c > 0$$

$$\text{IID. } a < 0, b < 0, c < 0$$

$$\text{Condition III: } b^2 - 4ac \geq 0 \quad \text{AND} \quad \frac{-b - \sqrt{b^2 - 4ac}}{2a} < 0 \Rightarrow \quad \text{IIIA. } a > 0, b > 0, c > 0$$

$$\text{IIIB. } a > 0, b > 0, c < 0$$

$$\text{IIIC. } a < 0, b < 0, c < 0$$

$$\text{IIID. } a > 0, b < 0, c < 0$$

(3-35)

In order to evaluate Condition II and Condition III separately, we first consider the parameter range of ($\kappa < -1$) as shown below:

Parameter Range of κ ($\kappa < -1$)

Condition II: $b^2 - 4ac \geq 0$ AND $\frac{-b + \sqrt{b^2 - 4ac}}{2a} < 0$ (from Eq.(3-32))

Note that for $\kappa < -1$ and $\eta < 1$ (because we have assumed $\omega_u < \omega_v$ without any loss of generality), the following inequality holds true:

$$-\frac{\eta^3}{\kappa} < -\frac{\eta}{\kappa} < -\frac{1}{\kappa\eta} < -\frac{\kappa}{\eta} \tag{3-36}$$

κ	# No.	a	c	b	λ and δ	Range of χ where the signs of a, b & c are satisfied (range is hashed if it exists)	ζ_v
$\kappa < -1$	IIA	$a > 0$	$c > 0$	$b > 0$	$\lambda > 0, \delta > 0$		No sol
					$\lambda > 0, \delta < 0$		No sol
					$\lambda < 0, \delta < 0$		No sol

Table 3-3 Range of χ and ζ_v for which Condition (IIA) of Eq.(3-35) is satisfied

κ	# No.	a	c	b	λ and δ	Range of χ where the signs of a, b & c are satisfied (range is hashed if it exists)	ζ_v
$\kappa < -1$	IIB & IIC	$a < 0$	$c > 0$	$b > < 0$	$\lambda > 0,$ $\delta > 0$		No sol
					$\lambda > 0,$ $\delta < 0$		No sol
					$\lambda < 0,$ $\delta < 0$		No sol
					$\lambda < 0,$ $\delta > 0$		No sol

Table 3- 4 Range of χ and ζ_v for which Conditions (IIB, IIC) of Eq.(3-35) is satisfied. The sign of b is irrelevant in these cases as the sign of a and c cannot be satisfied simultaneously

κ	# No.	a	c	b	λ and δ	Range of χ where the signs of a, b & c are satisfied (range is hashed if it exists)	ζ_v
$\kappa < -1$	IID	$a < 0$	$c < 0$	$b < 0$	$\lambda > 0,$ $\delta > 0$		No sol
					$\lambda < 0,$ $\delta < 0$		$\zeta_v > \frac{\sqrt{\lambda\delta}}{ \lambda }$
					$\lambda < 0,$ $\delta > 0$		No sol

Table 3-5 Range of χ and ζ_v for which Condition (IID) of Eq.(3-35) is satisfied

Condition III: $b^2 - 4ac \geq 0$ AND $\frac{-b - \sqrt{b^2 - 4ac}}{2a} < 0$ (From Eq.(3-32))

κ	# No.	a	c	b	λ and δ	Range of χ where the signs of a, b & c are satisfied (range is hashed if it exists)	ζ_v
$\kappa < -1$	IIIA	$a > 0$	$c > 0$	$b > 0$	$\lambda > 0,$ $\delta > 0$		No sol
					$\lambda > 0,$ $\delta < 0$		No sol
					$\lambda < 0,$ $\delta < 0$		No sol

Table 3-6 Range of χ and ζ_v for which Condition (IIIA) of Eq.(3-35) is satisfied

κ	# No.	a	c	b	λ and δ	Range of χ where the signs of a, b & c are satisfied (range is hashed if it exists)	ζ_v
$\kappa < -1$	IIIB	$a > 0$	$c < 0$	$b > 0$	$\lambda > 0,$ $\delta > 0$		No sol
					$\lambda > 0,$ $\delta < 0$		No sol
					$\lambda < 0,$ $\delta < 0$		$\zeta_v < \frac{\sqrt{\lambda\delta}}{ \lambda }$

Table 3-7 Range of χ and ζ_v for which Condition (IIIB) of Eq.(3-35) is satisfied

κ	# No.	a	c	b	λ and δ	Range of χ where the signs of a, b & c are satisfied (range is hashed if it exists)	ζ_v
$\kappa < -1$	III C	$a < 0$	$c < 0$	$b < 0$	$\lambda > 0$, $\delta > 0$		No sol
					$\lambda < 0$, $\delta < 0$		$\zeta_v > \frac{\sqrt{\lambda\delta}}{ \lambda }$
					$\lambda < 0$, $\delta > 0$		No sol

Table 3-8 Range of χ and ζ_v for which Condition (IIIC) of Eq.(3-35) is satisfied

κ	# No.	a	c	b	λ and δ	Range of χ where the signs of a, b & c are satisfied (range is hashed if it exists)	ζ_v
$\kappa < -1$	III D	$a > 0$	$c < 0$	$b < 0$	$\lambda > 0$, $\delta > 0$		No sol
					$\lambda < 0$, $\delta < 0$		$\zeta_v > \frac{\sqrt{\lambda\delta}}{ \lambda }$
					$\lambda < 0$, $\delta > 0$		for all values of ζ_v

Table 3-9 Range of χ and ζ_v for which Condition (IIID) of Eq.(3-35) is satisfied.

For the parameter range of $(\kappa < -1)$, Table 3-2, Table 3-3 – Table 3-5, and Table 3-6 – Table 3-9 provide the solution for Condition I, Condition II and Condition III of Eq.(3-32) respectively.

Based on these tables, we can provide the following parameter ranges of χ and ζ_v :

a) $\chi < -\frac{\eta^3}{\kappa}$

Based on Eq.(3-36) and Table 3-2, Condition I of Eq.(3-32) is not true for this range of χ . Based on Table 3-3 – Table 3-5, Condition II of Eq.(3-32) is also not true for this range of χ . Similarly, based on Table 3-6 – Table 3-9, Condition III of Eq.(3-32) is also not true for this range of χ . This

implies that the zero locus of $G_3(s)$ will cross the imaginary axis at two sets of conjugate locations at $\alpha_v = \alpha_{v1}^{img}$ and $\alpha_v = \alpha_{v2}^{img}$ (given in Eq.(3-33)).

In order to ascertain the sign of α_{v1}^{img} and α_{v2}^{img} , we plot the zero locus of $G_3(s)$ numerically for certain values of system parameters that satisfy the condition ($\kappa < -1$) and ($\chi < -\eta^3/\kappa$). Comparing the two distinct values of α_v (where the zero locus crosses the imaginary axis) from the numerically plotted zero locus with the values of α_{v1}^{img} and α_{v2}^{img} from Eq.(3-33) leads to the observation that $\alpha_{v1}^{img} > 0$ and $\alpha_{v2}^{img} < 0$. Although this observation has been made numerically for one set of system parameters that satisfy the condition ($\kappa < -1$) and ($\chi < -\eta^3/\kappa$), it holds true for any combination of system parameters that satisfy ($\kappa < -1$) and ($\chi < -\eta^3/\kappa$). The proof for this as follows.

The expression for α_{v1}^{img} and α_{v2}^{img} are given by Eq.(3-37) as shown below.

$$\begin{aligned} \alpha_{v1}^{img} &= \frac{\omega_u \omega_v (\chi + \eta) - (1 + \chi\eta)y_1^2}{(\chi\eta + \kappa)y_1^2} \text{ where } y_1^2 = \frac{-b + \sqrt{b^2 - 4ac}}{2a} \\ \alpha_{v2}^{img} &= \frac{\omega_u \omega_v (\chi + \eta) - (1 + \chi\eta)y_2^2}{(\chi\eta + \kappa)y_2^2} \text{ where } y_2^2 = \frac{-b - \sqrt{b^2 - 4ac}}{2a} \end{aligned} \quad (3-37)$$

From numerical simulation, we observed that $\alpha_{v1}^{img} > 0$ and $\alpha_{v2}^{img} < 0$ for one set of system parameters that satisfy the condition ($\kappa < -1$) and ($\chi < -\eta^3/\kappa$). If α_{v1}^{img} and α_{v2}^{img} have to change sign for another set of system parameters that satisfy the condition ($\kappa < -1$) and ($\chi < -\eta^3/\kappa$), then either the numerator or the denominator of α_{v1}^{img} and α_{v2}^{img} should change signs but not both at the same time. If the numerators of α_{v1}^{img} and α_{v2}^{img} have to change sign then they will have to pass through 0 for some set of system parameters that satisfy the condition ($\kappa < -1$) and ($\chi < -\eta^3/\kappa$). This would mean that α_{v1}^{img} and α_{v2}^{img} will have to be equal to 0 for this set of system parameters.

However, if α_{v1}^{img} and α_{v2}^{img} are equal to 0, this means that for $\alpha_v = 0$ the zero locus should cross the imaginary axis. But for $\alpha_v = 0$ the zero locus passes through the damped poles that lie strictly on the open left half s -plane and not on the imaginary axis as shown in Fig 3-5a. Therefore, α_{v1}^{img} and α_{v2}^{img} cannot be equal to 0. Hence the numerators of α_{v1}^{img} and α_{v2}^{img} cannot change signs. The denominator of α_{v1}^{img} and α_{v2}^{img} cannot change sign because $\chi < -\kappa/\eta$ for any set of system parameters that satisfy $(\kappa < -1)$ and $(\chi < -\eta^3/\kappa)$ (refer to Eq.(3-36)). Hence, α_{v1}^{img} and α_{v2}^{img} cannot change signs for any set of system parameters that satisfy the condition $(\kappa < -1)$ and $(\chi < -\eta^3/\kappa)$. Therefore, $\alpha_{v1}^{img} > 0$ and $\alpha_{v2}^{img} < 0$ for any set of system parameters that satisfy the condition $(\kappa < -1)$ and $(\chi < -\eta^3/\kappa)$.

On further investigation, it was found that there exists an upper bound on α_{v1}^{img} given by Eq.(3-38). Since $\chi\eta + \kappa < 0$ (from Eq.(3-36))

$$\Rightarrow \alpha_{v1}^{img} + \frac{(1 + \chi\eta)}{(\chi\eta + \kappa)} < 0 \Rightarrow \alpha_{v1}^{img} < -\frac{(1 + \chi\eta)}{(\chi\eta + \kappa)} \quad (3-38)$$

Now, we have completely characterized the intersection of the zero locus of $G_3(s)$ with the imaginary axis for case (a) which is depicted graphically Fig 3-5a. This allows us to find sufficient condition for the elimination of only CNMP zeros for case (a) as shown below:

$$\begin{aligned} \alpha_v &\leq \alpha_{v1}^{img} \text{ if } \alpha_v > 0 \\ \alpha_v &\geq \alpha_{v2}^{img} \text{ if } \alpha_v < 0 \end{aligned} \quad (3-39)$$

Note that Eq.(3-39) is only a sufficient condition for the elimination of CNMP zeros and not a necessary one. This is evident from Fig 3-5a where for positive $\alpha_v > \alpha_{v1}^{img}$ i.e. Eq.(3-39) is not satisfied, the zeros of $G_3(s)$ can be RNMP instead of CNMP. Therefore, in order to find the necessary and sufficient condition for the elimination of only CNMP zeros and only RNMP zeros,

we characterize the intersection of the zero locus of $G_3(s)$ with the positive real axis. Zeros of $G_3(s)$ are found by setting the numerator $N_3(s)$ in Eq.(3-28) to zero:

$$N_3(s) = d_1s^4 + d_2s^3 + d_3s^2 + d_4s + d_5 = 0$$

$$\text{where } d_1 = (1 + \alpha_v(1 + \kappa)), \quad d_2 = (2\zeta_u\omega_u + 2\zeta_v\omega_v + 2\zeta_v\omega_v\alpha_v(\kappa + \chi\eta)) \quad (3-40)$$

$$d_3 = (\omega_u^2 + \omega_v^2 + 4\zeta_u\zeta_v\omega_u\omega_v + \alpha_v\omega_v^2(\kappa + \eta^2)), \quad d_4 = (2\zeta_u\omega_u\omega_v^2 + 2\zeta_v\omega_v\omega_u^2), \quad d_5 = \omega_u^2\omega_v^2$$

In order to find the intersection of the zero locus of $G_3(s)$ with the positive real axis, we set $s = x$ in Eq.(3-40) and find the repeated roots of Eq.(3-40). This is done by setting the discriminant in Eq. (3-40) to zero. The discriminant of the fourth order polynomial equation is given below:

$$\Delta = 256d_1^3d_5^3 - 192d_1^2d_2d_4d_5^2 - 128d_1^2d_3^2d_5^2 + 144d_1^2d_3d_4^2d_5^2 - 27d_1^2d_4^2 + 144d_1d_2^2d_3d_5^2$$

$$- 6d_1d_2^2d_4^2d_5 - 80d_1d_2d_3^2d_4d_5 + 18d_1d_2d_3d_4^3 + 16d_1d_3^4d_5 - 4d_1d_3^3d_4^2$$

$$- 27d_2^4d_5^2 + 18d_2^3d_3d_4d_5 - 4d_2^3d_4^3 - 4d_2^3d_3^3d_5 + d_2^2d_3^2d_4^2 \quad (3-41)$$

Eq.(3-41) leads to a 5th order polynomial in α_v which cannot be solved analytically as proven by the Abel – Ruffini theorem [115]. This theorem conclusively proved that the roots of a 5th or higher degree polynomial in x cannot be expressed in analytical closed forms in terms of the coefficients of the polynomial. Therefore, we cannot analytically characterize the intersection of the zero locus of $G_3(s)$ with the positive real axis like we did in the two-DoF case in the previous section. Therefore, it will not be possible to find the necessary and sufficient conditions for the elimination of only CNMP zeros and only RNMP zeros for a three-DoF damped flexible system. However, we can attempt to find the number of times the zero locus meets with the positive real axis in order to provide at least some insight into how the zero locus interacts with the positive real axis.

In order to do so, we take into account certain facts that we know about the zero locus

1. The real axis is always part of the zero locus of $G_3(s)$ irrespective of whether $\alpha_v > 0$ or $\alpha_v < 0$

2. $T_3(s)$ has 2 pairs of zeros of which one pair always lies at the origin

Based on these facts, we solve for the repeated roots of $N_3(s)$ in Eq.(3-29) since when the zero locus of $G_3(s)$ meets the positive real axis, we get repeated roots in s . For a fourth order polynomial, following scenarios are possible for the meeting points of the zero locus of $G_3(s)$ with the positive real axis as described below and shown graphically in Fig 3-3.

1. Scenario I: Zero meeting points of the zero locus of $G_3(s)$ with the positive real axis .
2. Scenario II: One meeting points (with two repeated roots for s) of the zero locus of $G_3(s)$ with the positive real axis.
3. Scenario III: One meeting points (with three repeated roots for s) of the zero locus of $G_3(s)$ with the positive real axis.
4. Scenario IV: One meeting points (with four repeated roots for s) of the zero locus of $G_3(s)$ with the positive real axis.
5. Scenario V: Two meeting points (with two repeated roots for s for each meeting point) of the zero locus of $G_3(s)$ with the positive real axis.

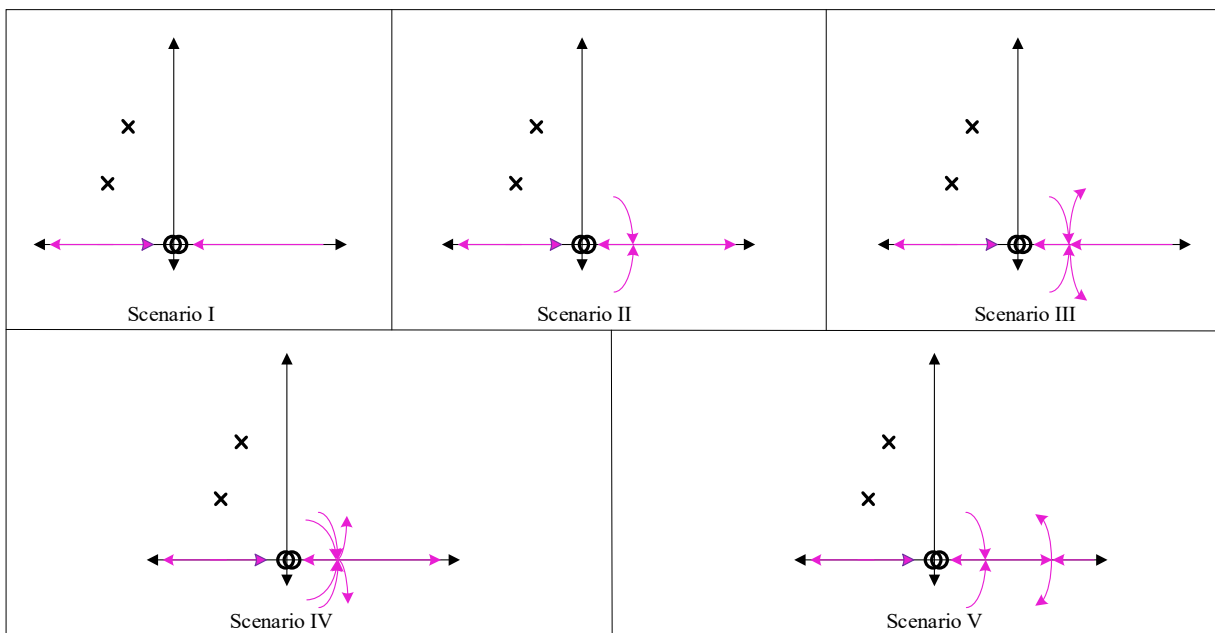


Fig 3-3 Scenarios for the meeting points on the real axis by the zero locus of $G_3(s)$

Now we have to ascertain for case (a) where the conditions ($\kappa < -1$) and ($\chi < -\eta^3/\kappa$) are satisfied, which of the five scenarios for the meeting point of the zero locus of $G_3(s)$ with the positive real axis are possible. In order to do so, we make use of following five facts about the zero locus:

1. Position of zeros of $T_3(s)$ - To find the location of the zeros of $T_3(s)$, as previously discussed below Eq.(3-28), the root locus of $T_3(s)$ is the zero locus of $G_3(s)$. The zeros of $T_3(s)$ are the roots of $A_3(s)$ given by Eq.(3-28). It can be observed from Eq.(3-28) that two of the zeros of $T_3(s)$ are at the origin. This is graphically depicted in Fig 3-5a. In order to find the location of the other zeros of $T_3(s)$, we analyze the roots of the equation below which is derived from expression of $A_3(s)$ from Eq.(3-28).

$$(1 + \kappa)s^2 + 2\zeta_v\omega_v(\chi\eta + \kappa)s + \omega_v^2(\eta^2 + \kappa) = 0 \quad (3-42)$$

$$\text{Product of roots} = \frac{\omega_v^2(\eta^2 + \kappa)}{(1 + \kappa)}, \quad \text{Sum of roots} = -\frac{2\zeta_v\omega_v(\chi\eta + \kappa)}{(1 + \kappa)}$$

Given the condition that ($\kappa < -1$) and ($\chi < -\eta^3/\kappa$) and Eq.(3-36), we can conclude the following:

$$\text{Product of roots} = \frac{\omega_v^2(\eta^2 + \kappa)}{(1 + \kappa)} > 0, \quad \text{Sum of roots} = -\frac{2\zeta_v\omega_v(\chi\eta + \kappa)}{(1 + \kappa)} < 0 \quad (3-43)$$

Therefore, for case (a), based on Eq.(3-43), the roots of Eq.(3-42) will lie on the left hand side (LHS) of the imaginary axis. They can either be real or occur as a pair of complex conjugates.

Fig 3-5a graphically depicts the location of these zeros on the LHS of the imaginary axis.

2. Intersection of zero locus of $G_3(s)$ with the imaginary axis - We have already shown that the zero locus of $G_3(s)$ will cross the imaginary axis at two sets of conjugate locations at $\alpha_v = \alpha_v l^{img}$

and $\alpha_v = \alpha_{v2}^{img}$ (given in Eq.(3-33)) as shown in Fig 3-5a. It is also known that $\alpha_{v1}^{img} > 0$ and $\alpha_{v2}^{img} < 0$ for any set of system parameters that satisfy the condition ($\kappa < -1$) and ($\chi < -\eta^3/\kappa$).

3. Relative position of intersection of positive zero locus ($\alpha_v > 0$) and negative zero locus ($\alpha_v < 0$) with the imaginary axis - From Eq.(3-33), it is known that

$$y_1^2 = \frac{-b + \sqrt{b^2 - 4ac}}{2a} > 0 \quad \text{AND} \quad y_2^2 = \frac{-b - \sqrt{b^2 - 4ac}}{2a} > 0 \quad (3-44)$$

In Eq.(3-44), based on the sign of a , it can be shown that

$$\begin{aligned} y_1^2 &> y_2^2 \text{ if } a > 0 \\ y_1^2 &< y_2^2 \text{ if } a < 0 \end{aligned} \quad (3-45)$$

Substituting for a from Eq.(3-31), it can be shown that

$$\begin{aligned} y_1^2 &> y_2^2 \text{ if } \chi < -1/\kappa\eta \\ y_1^2 &< y_2^2 \text{ if } \chi > -1/\kappa\eta \end{aligned} \quad (3-46)$$

Therefore, for case (a), from Eq.(3-46) we can say that $y_1^2 > y_2^2$. Since, from Eq.(3-37), α_{v1}^{img} corresponds to y_1^2 and α_{v2}^{img} corresponds to y_2^2 , the point of intersection of the zero locus of $G_3(s)$ corresponding to α_{v1}^{img} is higher than the point of intersection of the zero locus of $G_3(s)$ corresponding to α_{v2}^{img} .

4. Which portion of the positive real axis belongs to the positive or negative zero locus - For a certain value of α_v , the zero locus of $G_3(s)$ approaches negative infinity along the real axis and flips over to positive infinity, or vice versa, as seen in Fig 3-5a. Mathematically, this condition corresponds to a loss in order of $N_3(s)$ in Eq.(3-28), and therefore the corresponding value of α_v can be derived by setting the coefficient of s^4 for $N_3(s)$ in Eq.(3-28) to zero. This gives

$$\alpha_v^\infty = -\frac{1}{1+\kappa} \quad (3-47)$$

Therefore, for case (a), from Eq.(3-47), we can say that the portion of the positive real axis corresponding to α_v^∞ belongs to positive zero locus of $G_3(s)$. Further, since there are no zeros of $T_3(s)$ lying on the positive real axis, the entire positive real axis is covered by the positive zero locus of $G_3(s)$.

5. Angle of arrival of positive and negative zero locus at the zeros of $T_3(s)$ present at the origin -

The angle of arrival to zeros of a root locus are given by

$$q\psi_{arr} = \sum \phi_i - \sum \psi_i + 180^\circ + 360^\circ(l-1) \quad \text{for positive zero locus}$$

$$q\psi_{arr} = \sum \phi_i - \sum_{i \neq l, arr} \psi_i + 360^\circ(l-1) \quad \text{for negative zero locus}$$

where

$$\sum \phi_i = \text{sum of angles to all the poles} \quad (3-48)$$

$$\sum \psi_i = \text{sum of angles to the remaining zeros}$$

q = multiplicity of the zero where arrival angle is calculated

$l = 1, 2, \dots, q$

Therefore, for case (a), from Eq.(3-48), the angle of arrival for the positive zero locus of $G_3(s)$ to the zeros of $T_3(s)$ at the origin is determined to be 0° and 180° . The angle of arrival for the negative zero locus of $G_3(s)$ to the zeros of $T_3(s)$ at the origin is determined to be 90° and -90° .

Based on all these facts, we can conclude that for case (a), only Scenario II is possible for the zero locus of $G_3(s)$ to meet the positive real axis. The table below shows which of the above facts were used to eliminate the scenarios that are not possible for both $\alpha_v > 0$ and $\alpha_v < 0$.

Sign of α_v	Scenario I	Scenario II	Scenario III	Scenario IV	Scenario V
$\alpha_v > 0$	2	-	2	2	2
$\alpha_v < 0$	2	4	4	4	4

Table 3-10 Facts used to eliminate different scenarios for meeting points of the zero locus of

$G_3(s)$ on the positive real axis that are not possible for case (a)

Based on the above discussion, for parameter space ($\kappa < -1$) and ($\chi < -\eta^3/\kappa$), Fig 3-5a captures the intersection of the zero locus with the imaginary and positive real axis. The derivation process shown above is quite tedious to follow. Therefore, a flowchart is shown below that captures the various steps in the derivation, the intent behind these steps i.e. why and how these steps are carried out i.e how. Even though this flowchart is based on the steps shown in the derivation of (a), it will remain common for all the subsequent derivations in this section.

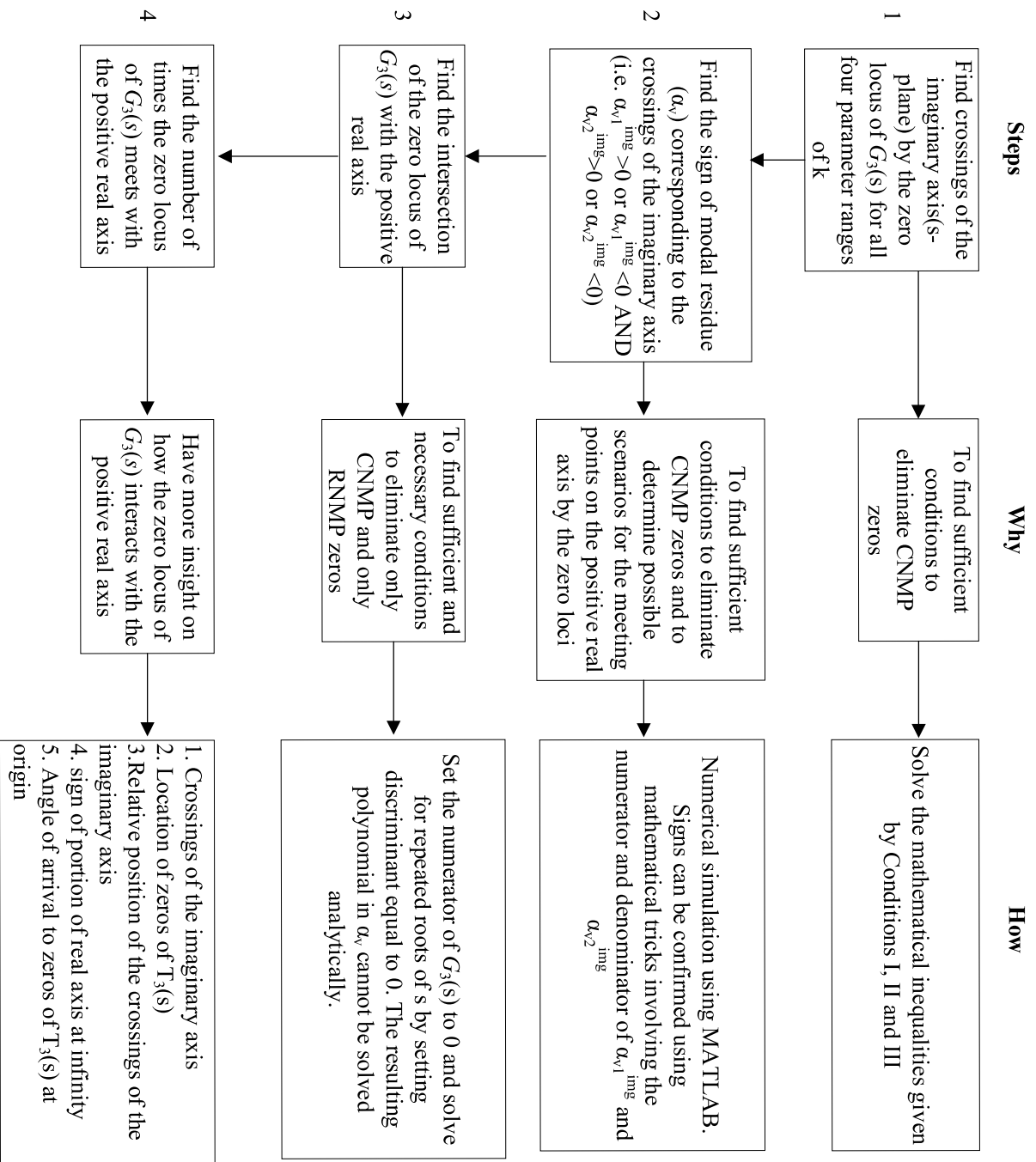


Fig 3-4 Flowchart showing the entire process of characterization of zeros for case (a)

$$\text{b) } -\frac{\eta^3}{\kappa} \leq \chi \leq \frac{1}{\kappa\eta}$$

Based on Eq.(3-36) and Table 3-2, Condition I of Eq.(3-32) is not true for this range of χ . Based on Table 3-3 – Table 3-5, Condition II of Eq.(3-32) is also not true for this range of χ . Based on Table 3-6 – Table 3-9, Condition III of Eq.(3-32) is true for this range of χ . This implies that the zero locus of $G_3(s)$ will cross the imaginary axis at one set of conjugate locations at $\alpha_v = \alpha_{v1}^{img}$ (given in Eq. (3-33)) as shown in Fig 3-5b.

In order to ascertain the sign of α_{v1}^{img} , we plot the zero locus of $G_3(s)$ numerically for certain values of systems parameters that satisfy the condition ($\kappa < -1$) and ($-\eta^3/\kappa \leq \chi \leq -1/\kappa\eta$). Comparing the value of α_v (where the zero locus crosses the imaginary axis) from the numerically plotted zero locus with the values of α_{v1}^{img} from Eq.(3-33) leads to the observation that $\alpha_{v1}^{img} > 0$. Although this observation has been made numerically for one set of system parameters that satisfy the condition ($\kappa < -1$) and ($-\eta^3/\kappa \leq \chi \leq -1/\kappa\eta$), it holds true for any combination of system parameters that satisfy ($\kappa < -1$) and ($-\eta^3/\kappa \leq \chi \leq -1/\kappa\eta$). The proof for this as follows.

The expression for α_{v1}^{img} and α_{v2}^{img} are given by Eq.(3-33). From numerical simulation, we observed that $\alpha_{v1}^{img} > 0$ for one set of system parameters that satisfy the condition ($\kappa < -1$) and ($-\eta^3/\kappa \leq \chi \leq -1/\kappa\eta$). If α_{v1}^{img} has to change sign for another set of system parameters that satisfy the condition ($\kappa < -1$) and ($-\eta^3/\kappa \leq \chi \leq -1/\kappa\eta$), then either the numerator or the denominator of α_{v1}^{img} should change sign but not both at the same time. If the numerator of α_{v1}^{img} has to change sign, then it will have to pass through 0 for some set of system parameters that satisfy the condition ($\kappa < -1$) and ($-\eta^3/\kappa \leq \chi \leq -1/\kappa\eta$). This would mean that α_{v1}^{img} will have to be equal to 0 for this

set of system parameters. However, if α_{v1}^{img} is equal to 0, this means that for $\alpha_v = 0$ the zero locus should cross the imaginary axis. But for $\alpha_v = 0$ the zero locus passes through the damped poles that lie strictly on the open left half s -plane and not on the imaginary axis as shown in Fig 3-5b. Therefore, α_{v1}^{img} cannot be equal to 0. Hence the numerator of α_{v1}^{img} cannot change sign. The denominator of α_{v1}^{img} cannot change sign because $\chi < -\kappa/\eta$ for any set of system parameters that satisfy $(\kappa < -1)$ and $(-\eta^3/\kappa \leq \chi \leq -1/\kappa\eta)$ (refer to Eq.(3-36)). Hence, α_{v1}^{img} cannot change sign for any set of system parameters that satisfy the condition $(\kappa < -1)$ and $(-\eta^3/\kappa \leq \chi \leq -1/\kappa\eta)$. Therefore, $\alpha_{v1}^{img} > 0$ for any set of system parameters that satisfy the condition $(\kappa < -1)$ and $(-\eta^3/\kappa \leq \chi \leq -1/\kappa\eta)$. On further investigation, it was found that there exists an upper bound on α_{v1}^{img} given by Eq.(3-38).

Now, we have completely characterized the intersection of the zero locus of $G_3(s)$ with the imaginary axis for case (b) which is depicted graphically in Fig 3-5b. This allows us to find sufficient condition for the elimination of only CNMP zeros for case (b) as shown below:

$$\begin{aligned} \alpha_v &\leq \alpha_{v1}^{img} \text{ if } \alpha_v > 0 \\ \alpha_v &< 0 \end{aligned} \tag{3-49}$$

Note that Eq.(3-49) is only a sufficient condition for the elimination of CNMP zeros and not a necessary one. This is evident from Fig 3-5b where for positive $\alpha_v > \alpha_{v1}^{img}$ i.e. Eq.(3-49) is not satisfied, the zeros of $G_3(s)$ can be RNMP instead of CNMP. Therefore, in order to find the necessary and sufficient condition for the elimination of only CNMP zeros and only RNMP zeros, we characterize the intersection of the zero locus of $G_3(s)$ with the positive real axis. Zeros of $G_3(s)$ are found by setting the numerator $N_3(s)$ in Eq.(3-28) to zero. In order to find the intersection of the zero locus of $G_3(s)$ with the positive real axis, we set $s = x$ in Eq.(3-40) and find the repeated

roots of Eq.(3-40). This is done by setting the discriminant in Eq.(3-40) to zero. The discriminant of the fourth order polynomial equation is given in Eq.(3-41). Eq.(3-41) leads to a 5th order polynomial in α_v which cannot be solved analytically as discussed in the previous case.

Therefore, we cannot analytically characterize the intersection of the zero locus of $G_3(s)$ with the positive real axis like we did in the two-DoF case in the previous section. Therefore, it will not be possible to find the necessary and sufficient conditions for the elimination of only CNMP zeros and only RNMP zeros for a three-DoF damped flexible system. However, we can attempt to find the number of times the zero locus meets with the positive real axis in order to provide at least some insight into how the zero locus interacts with the positive real axis.

In order to do so, we take into account certain facts that we know about the zero locus

1. The real axis is always part of the zero locus of $G_3(s)$ irrespective of whether $\alpha_v > 0$ or $\alpha_v < 0$
2. $T_3(s)$ has 2 pairs of zeros of which one pair always lies at the origin

Based on these facts, we solve for the repeated roots of $N_3(s)$ in Eq.(3-28) since when the zero locus of $G_3(s)$ meets the positive real axis, we get repeated roots in s . For a fourth order polynomial, five scenarios are possible for the meeting points of the zero locus of $G_3(s)$ with the positive real axis as described in case (a) and shown graphically in Fig 3-3.

Now we have to ascertain for case (b) where the conditions ($\kappa < -1$) and ($-\eta^3/\kappa \leq \chi \leq -1/\kappa\eta$) are satisfied, which of the five scenarios for the meeting point of the zero locus of $G_3(s)$ with the positive real axis are possible. In order to do so, we make use of following five facts about the zero locus:

1. Position of zeros of $T_3(s)$ - To find the location of the zeros of $T_3(s)$, as previously discussed below Eq.(3-28), the root locus of $T_3(s)$ is the zero locus of $G_3(s)$. The zeros of $T_3(s)$ are the roots of $A_3(s)$ given by Eq.(3-28). It can be observed from Eq.(3-28) that two of the zeros of

$T_3(s)$ are at the origin. This is graphically depicted in Fig 3-5b. In order to find the location of the other zeros of $T_3(s)$, we analyze the roots of Eq.(3-42) which is derived from expression of $A_3(s)$ from Eq.(3-28). Given the condition that $(\kappa < -1)$ and $(-\eta^3/\kappa \leq \chi \leq -1/\kappa\eta)$ and Eq.(3-36), we can conclude the following

$$\text{Product of roots} = \frac{\omega_v^2 (\eta^2 + \kappa)}{(1 + \kappa)} > 0, \text{ Sum of roots} = -\frac{2\zeta_v \omega_v (\chi\eta + \kappa)}{(1 + \kappa)} < 0 \quad (3-50)$$

Therefore, for case (b), based on Eq.(3-50), the roots of Eq.(3-42) will lie on the left hand side (LHS) of the imaginary axis. They can either be real or occur as a pair of complex conjugates. Fig 3-5b graphically depicts the location of these zeros on the LHS of the imaginary axis.

2. Intersection of zero locus of $G_3(s)$ with the imaginary axis - We have already shown that the zero locus of $G_3(s)$ will cross the imaginary axis at one set of conjugate locations at $\alpha_v = \alpha_{vI}^{img}$ (given in Eq.(3-33)) as shown in Fig 3-5b. It is also known that $\alpha_{vI}^{img} > 0$ for any set of system parameters that satisfy the condition $(\kappa < -1)$ and $(-\eta^3/\kappa \leq \chi \leq -1/\kappa\eta)$.
3. Which portion of the positive real axis belongs to the positive or negative zero locus - For case (b), from Eq.(3-46), we can say that the portion of the positive real axis corresponding to α_v^∞ belongs to positive zero locus of $G_3(s)$. Further, since there are no zeros of $T_3(s)$ lying on the positive real axis, the entire positive real axis is covered by the positive zero locus of $G_3(s)$.
4. Angle of arrival of positive and negative zero locus at the zeros of $T_3(s)$ present at the origin - For case (b), from Eq.(3-48), the angle of arrival for the positive zero locus of $G_3(s)$ to the zeros of $T_3(s)$ at the origin is determined to be 0° and 180° . The angle of arrival for the negative zero locus of $G_3(s)$ to the zeros of $T_3(s)$ at the origin is determined to be 90° and -90° .

Based on all these facts, we can conclude that for case (b), only Scenario II is possible for the zero locus of $G_3(s)$ to meet the positive real axis. The table below shows which of the above facts were used to eliminate the scenarios that are not possible for both $\alpha_v > 0$ and $\alpha_v < 0$.

Sign of α_v	Scenario I	Scenario II	Scenario III	Scenario IV	Scenario V
$\alpha_v > 0$	3	-	2	2	2
$\alpha_v < 0$	3	3	3	3	3

Table 3-11 Facts used to eliminate different scenarios for meeting points of the zero locus of $G_3(s)$ on the positive real axis that are not possible for case (b)

$$c) \quad -\frac{1}{\kappa\eta} < \chi < -\frac{\kappa}{\eta}, \zeta_v < \zeta_{v,\min}$$

Based on Eq.(3-36) and Table 3-2, Condition I of Eq.(3-32) is not true for this range of χ . Based on Table 3-3 – Table 3-5, Condition II of Eq.(3-32) is also not true for this range of χ . Similarly, based on Table 3-6 – Table 3-9, Condition III of Eq.(3-32) is also not true for this range of χ and ζ_v . This implies that the zero locus of $G_3(s)$ will cross the imaginary axis at two sets of conjugate locations at $\alpha_v = \alpha_{v1}^{img}$ and $\alpha_v = \alpha_{v2}^{img}$ (given in Eq.(3-33)) as shown in Fig 3-5c1, Fig 3-5c2 and Fig 3-5c3.

In order to ascertain the sign of α_{v1}^{img} and α_{v2}^{img} , we plot the zero locus of $G_3(s)$ numerically for certain values of system parameters that satisfy the condition ($\kappa < -1$) and ($-1/\kappa\eta < \chi < -\kappa/\eta, \zeta_v < \zeta_{v,\min}$). Comparing the two distinct values of α_v (where the zero locus crosses the imaginary axis) from the numerically plotted zero locus with the values of α_{v1}^{img} and α_{v2}^{img} from Eq.(3-33) leads to the observation that $\alpha_{v1}^{img} > 0$ and $\alpha_{v2}^{img} > 0$. Although this observation has been made numerically for one set of system parameters that satisfy the condition

$(\kappa < -1)$ and $(-1/\kappa\eta < \chi < -\kappa/\eta, \zeta_v < \zeta_{v,min})$, it holds true for any combination of system parameters that satisfy $(\kappa < -1)$ and $(-1/\kappa\eta < \chi < -\kappa/\eta, \zeta_v < \zeta_{v,min})$. The proof for this as follows. The expression for α_{v1}^{img} and α_{v2}^{img} are given by Eq.(3-33). From numerical simulation, we observed that $\alpha_{v1}^{img} > 0$ and $\alpha_{v2}^{img} > 0$ for one set of system parameters that satisfy the condition $(\kappa < -1)$ and $(-1/\kappa\eta < \chi < -\kappa/\eta, \zeta_v < \zeta_{v,min})$. If α_{v1}^{img} and α_{v2}^{img} have to change sign for another set of system parameters that satisfy the condition $(\kappa < -1)$ and $(-1/\kappa\eta < \chi < -\kappa/\eta, \zeta_v < \zeta_{v,min})$, then either the numerator or the denominator of α_{v1}^{img} and α_{v2}^{img} should change signs but not both at the same time. If the numerators of α_{v1}^{img} and α_{v2}^{img} have to change sign then they will have to pass through 0 for some set of system parameters that satisfy the condition $(\kappa < -1)$ and $(-1/\kappa\eta < \chi < -\kappa/\eta, \zeta_v < \zeta_{v,min})$. This would mean that α_{v1}^{img} and α_{v2}^{img} will have to be equal to 0 for this set of system parameters. However, if α_{v1}^{img} and α_{v2}^{img} are equal to 0, this means that for $\alpha_v = 0$ the zero locus should cross the imaginary axis. But for $\alpha_v = 0$ the zero locus passes through the damped poles that lie strictly on the open left half s -plane and not on the imaginary axis as shown in Fig 3-5c1, Fig 3-5c2 and Fig 3-5c3. Therefore, α_{v1}^{img} and α_{v2}^{img} cannot be equal to 0. Hence the numerators of α_{v1}^{img} and α_{v2}^{img} cannot change signs. The denominator of α_{v1}^{img} and α_{v2}^{img} cannot change sign because $\chi < -\kappa/\eta$ for any set of system parameters that satisfy $(\kappa < -1)$ and $(-1/\kappa\eta < \chi < -\kappa/\eta, \zeta_v < \zeta_{v,min})$ (refer to Eq.(3-36)). Hence, α_{v1}^{img} and α_{v2}^{img} cannot change signs for any set of system parameters that satisfy the condition $(\kappa < -1)$ and $(-1/\kappa\eta < \chi < -\kappa/\eta, \zeta_v < \zeta_{v,min})$. Therefore, $\alpha_{v1}^{img} > 0$ and $\alpha_{v2}^{img} > 0$ for any set of system parameters that satisfy the condition $(\kappa < -1)$ and $(-1/\kappa\eta < \chi < -\kappa/\eta, \zeta_v < \zeta_{v,min})$. On further investigation, it was found that there exists an upper bound on α_{v1}^{img} given by Eq.(3-38).

Now, we have completely characterized the intersection of the zero locus of $G_3(s)$ with the imaginary axis for case (c) which is depicted graphically in Fig 3-5c1, Fig 3-5c2 and Fig 3-5c3. This allows us to find sufficient condition for the elimination of only CNMP zeros for case (c) as shown below:

$$\begin{aligned} \alpha_v \leq \alpha_{v1}^{img} \text{ AND } \alpha_v \geq \alpha_{v2}^{img} \text{ if } \alpha_v > 0 \\ \alpha_v < 0 \end{aligned} \quad (3-51)$$

Note that Eq.(3-51) is only a sufficient condition for the elimination of CNMP zeros and not a necessary one. This is evident from Fig 3-5c2 and Fig 3-5c3 where for positive $\alpha_v > \alpha_{v1}^{img}$ i.e. Eq.(3-51) is not satisfied, the zeros of $G_3(s)$ can be RNMP instead of CNMP. Therefore, in order to find the necessary and sufficient condition for the elimination of only CNMP zeros and only RNMP zeros, we characterize the intersection of the zero locus of $G_3(s)$ with the positive real axis. Zeros of $G_3(s)$ are found by setting the numerator $N_3(s)$ in Eq.(3-28) to zero. In order to find the intersection of the zero locus of $G_3(s)$ with the positive real axis, we set $s = x$ in Eq.(3-40) and find the repeated roots of Eq.(3-40). This is done by setting the discriminant in Eq.(3-40) to zero. The discriminant of the fourth order polynomial equation is given in Eq.(3-41). Eq.(3-41) leads to a 5th order polynomial in α_v which cannot be solved analytically as discussed in case(a).

Therefore, we cannot analytically characterize the intersection of the zero locus of $G_3(s)$ with the positive real axis like we did in the two-DoF case in the previous section. Therefore, it will not be possible to find the necessary and sufficient conditions for the elimination of only CNMP zeros and only RNMP zeros for a three-DoF damped flexible system. However, we can attempt to find the number of times the zero locus meets with the positive real axis in order to provide at least some insight into how the zero locus interacts with the positive real axis.

In order to do so, we take into account certain facts that we know about the zero locus

1. The real axis is always part of the zero locus of $G_3(s)$ irrespective of whether $\alpha_v > 0$ or $\alpha_v < 0$
2. $T_3(s)$ has 2 pairs of zeros of which one pair always lies at the origin

Based on these facts, we solve for the repeated roots of $N_3(s)$ in Eq.(3-29) since when the zero locus of $G_3(s)$ meets the positive real axis, we get repeated roots in s . For a fourth order polynomial, five scenarios are possible for the meeting points of the zero locus of $G_3(s)$ with the positive real axis as described in case (a) and shown graphically in Fig 3-3.

Now we have to ascertain for case (c) where the conditions ($\kappa < -1$) and ($-1/\kappa\eta < \chi < -\kappa/\eta$, $\zeta_v < \zeta_{v,min}$) are satisfied, which of the five scenarios for the meeting point of the zero locus of $G_3(s)$ with the positive real axis are possible. In order to do so, we make use of following five facts about the zero locus:

1. Position of zeros of $T_3(s)$ - To find the location of the zeros of $T_3(s)$, as previously discussed below Eq.(3-28), the root locus of $T_3(s)$ is the zero locus of $G_3(s)$. The zeros of $T_3(s)$ are the roots of $A_3(s)$ given by Eq.(3-28). It can be observed from Eq.(3-28) that two of the zeros of $T_3(s)$ are at the origin. This is graphically depicted in Fig 3-5c1, Fig 3-5c2 and Fig 3-5c3. In order to find the location of the other zeros of $T_3(s)$, we analyze the roots of Eq.(3-42) which is derived from expression of $A_3(s)$ from Eq.(3-28). Given the condition that ($\kappa < -1$) and ($-1/\kappa\eta < \chi < -\kappa/\eta$, $\zeta_v < \zeta_{v,min}$) and Eq.(3-36), we can conclude the following

$$\text{Product of roots} = \frac{\omega_v^2 (\eta^2 + \kappa)}{(1 + \kappa)} > 0, \text{ Sum of roots} = -\frac{2\zeta_v \omega_v (\chi\eta + \kappa)}{(1 + \kappa)} < 0$$

(3-52)Therefore, for case (c), based on Eq.(3-52), the roots of Eq.(3-42) will lie on the left hand side (LHS) of the imaginary axis. They can either be real or occur as a pair of complex conjugates. Fig 3-5c1, Fig 3-5c2 and Fig 3-5c3 graphically depicts the location of these zeros on the LHS of the imaginary axis.

2. Intersection of zero locus of $G_3(s)$ with the imaginary axis - We have already shown that the zero locus of $G_3(s)$ will cross the imaginary axis at two sets of conjugate locations at $\alpha_v = \alpha_{v1}^{img}$ and $\alpha_v = \alpha_{v2}^{img}$ (given in Eq.(3-33)) as shown in Fig 3-5c1, Fig 3-5c2 and Fig 3-5c3. It is also known that $\alpha_{v1}^{img} > 0$ and $\alpha_{v2}^{img} > 0$ for any set of system parameters that satisfy the condition $(\kappa < -1)$ and $(-1/\kappa\eta < \chi < -\kappa/\eta, \zeta_v < \zeta_{v,min})$.
3. Relative position of intersection of positive zero locus ($\alpha_v > 0$) and negative zero locus ($\alpha_v < 0$) with the imaginary axis - For case (c), from Eq.(3-46) we can say that $y_1^2 < y_2^2$. Since, from Eq.(3-37), α_{v1}^{img} corresponds to y_1^2 and α_{v2}^{img} corresponds to y_2^2 , the point of intersection of the zero locus of $G_3(s)$ corresponding to α_{v2}^{img} is higher than the point of intersection of the zero locus of $G_3(s)$ corresponding to α_{v1}^{img} .
4. Which portion of the positive real axis belongs to the positive or negative zero locus - For case (c), from Eq.(3-47), we can say that the portion of the positive real axis corresponding to α_v^∞ belongs to positive zero locus of $G_3(s)$. Further, since there are no zeros of $T_3(s)$ lying on the positive real axis, the entire positive real axis is covered by the positive zero locus of $G_3(s)$.
5. Angle of arrival of positive and negative zero locus at the zeros of $T_3(s)$ present at the origin - For case (c), from Eq.(3-48), the angle of arrival for the positive zero locus of $G_3(s)$ to the zeros of $T_3(s)$ at the origin is determined to be 0° and 180° . The angle of arrival for the negative zero locus of $G_3(s)$ to the zeros of $T_3(s)$ at the origin is determined to be 90° and -90° .

Based on all these facts, we can conclude that for case (c), Scenario I, Scenario III and Scenario V are possible for the zero locus of $G_3(s)$ to meet the positive real axis. The table below shows which of the above facts were used to eliminate the scenarios that are not possible for both $\alpha_v > 0$ and $\alpha_v < 0$.

Sign of α_v	Scenario I	Scenario II	Scenario III	Scenario IV	Scenario V
$\alpha_v > 0$	-	2	-	1,2	-
$\alpha_v < 0$	-	4	-	4	-

Table 3-12 Facts used to eliminate different scenarios for meeting points of the zero locus of

$G_3(s)$ on the positive real axis that are not possible for case (c)

$$d) \quad -\frac{1}{\kappa\eta} < \chi < -\frac{\kappa}{\eta}, \zeta_v = \zeta_{v,\min}$$

Based on Eq.(3-36) and Table 3-2, Condition I of Eq.(3-32) is not true for this range of χ . Based on Table 3-3 – Table 3-5, Condition II of Eq.(3-32) is also not true for this range of χ . Similarly, based on Table 3-6 – Table 3-9, Condition III of Eq.(3-32) is also not true for this range of χ and ζ_v . This implies that the zero locus of $G_3(s)$ will cross the imaginary axis at two sets of conjugate locations at $\alpha_v = \alpha_{v1}^{img}$ and $\alpha_v = \alpha_{v2}^{img}$ (given in Eq.(3-33)) as shown in Fig 3-5d. However, we see that this is a limiting case where the zero locus goes from crossing the imaginary axis to not crossing the imaginary axis as ζ_v becomes greater than $\zeta_{v,\min}$. Hence, $\alpha_{v1}^{img} = \alpha_{v2}^{img}$ and the two sets of conjugate locations where the zero locus of $G_3(s)$ crosses the imaginary axis are the same.

In order to ascertain the sign of α_{v1}^{img} and α_{v2}^{img} , we plot the zero locus of $G_3(s)$ numerically for certain values of system parameters that satisfy the condition ($\kappa < -1$) and ($-1/\kappa\eta < \chi < -\kappa/\eta$, $\zeta_v = \zeta_{v,\min}$). Comparing the two distinct values of α_v (where the zero locus crosses the imaginary axis) from the numerically plotted zero locus with the values of α_{v1}^{img} and α_{v2}^{img} from Eq.(3-33) leads to the observation that $\alpha_{v1}^{img} > 0$ and $\alpha_{v2}^{img} > 0$. Although this observation has been made numerically for one set of system parameters that satisfy the condition

$(\kappa < -1)$ and $(-1/\kappa\eta < \chi < -\kappa/\eta, \zeta_v = \zeta_{v,min})$, it holds true for any combination of system parameters that satisfy $(\kappa < -1)$ and $(-1/\kappa\eta < \chi < -\kappa/\eta, \zeta_v = \zeta_{v,min})$. The proof for this as follows. The expression for α_{v1}^{img} and α_{v2}^{img} are given by Eq.(3-33). From numerical simulation, we observed that $\alpha_{v1}^{img} > 0$ and $\alpha_{v2}^{img} > 0$ for one set of system parameters that satisfy the condition $(\kappa < -1)$ and $(-1/\kappa\eta < \chi < -\kappa/\eta, \zeta_v = \zeta_{v,min})$. If α_{v1}^{img} and α_{v2}^{img} have to change sign for another set of system parameters that satisfy the condition $(\kappa < -1)$ and $(-1/\kappa\eta < \chi < -\kappa/\eta, \zeta_v = \zeta_{v,min})$, then either the numerator or the denominator of α_{v1}^{img} and α_{v2}^{img} should change signs but not both at the same time. If the numerators of α_{v1}^{img} and α_{v2}^{img} have to change sign then they will have to pass through 0 for some set of system parameters that satisfy the condition $(\kappa < -1)$ and $(-1/\kappa\eta < \chi < -\kappa/\eta, \zeta_v = \zeta_{v,min})$. This would mean that α_{v1}^{img} and α_{v2}^{img} will have to be equal to 0 for this set of system parameters. However, if α_{v1}^{img} and α_{v2}^{img} are equal to 0, this means that for $\alpha_v = 0$ the zero locus should cross the imaginary axis. But for $\alpha_v = 0$ the zero locus passes through the damped poles that lie strictly on the open left half s -plane and not on the imaginary axis as shown in Fig 3-5d. Therefore, α_{v1}^{img} and α_{v2}^{img} cannot be equal to 0. Hence the numerators of α_{v1}^{img} and α_{v2}^{img} cannot change signs. The denominator of α_{v1}^{img} and α_{v2}^{img} cannot change sign because $\chi < -\kappa/\eta$ for any set of system parameters that satisfy $(\kappa < -1)$ and $(-1/\kappa\eta < \chi < -\kappa/\eta, \zeta_v = \zeta_{v,min})$ (refer to Eq.(3-36)). Hence, α_{v1}^{img} and α_{v2}^{img} cannot change signs for any set of system parameters that satisfy the condition $(\kappa < -1)$ and $(-1/\kappa\eta < \chi < -\kappa/\eta, \zeta_v = \zeta_{v,min})$. Therefore, $\alpha_{v1}^{img} > 0$ and $\alpha_{v2}^{img} < 0$ for any set of system parameters that satisfy the condition $(\kappa < -1)$ and $(-1/\kappa\eta < \chi < -\kappa/\eta, \zeta_v = \zeta_{v,min})$. On further investigation, it was found that there exists an upper bound on α_{v1}^{img} given by Eq.(3-38).

We have completely characterized the intersection of the zero locus of $G_3(s)$ with the imaginary axis for case (d) which is depicted graphically in Fig 3-5d. This allows us to find sufficient condition for the elimination of only CNMP zeros for case (d) as shown below:

$$\begin{aligned}\alpha_v &\geq 0 \\ \alpha_v &\leq 0\end{aligned}\tag{3-53}$$

Note that Eq.(3-53) is a sufficient and necessary condition for the elimination of only CNMP zeros. This is evident from Fig 3-5d where Eq.(3-53) is always satisfied. For this case, we can also find necessary and sufficient conditions for the elimination of only RNMP zeros. From Fig 3-5d, it is evident that when $\alpha_v > \alpha_v^\infty$, the zero locus of $G_3(s)$ approaches negative infinity along the real axis and flips over to positive infinity thereby leading to RNMP zeros. This allows us to find sufficient condition for the elimination of only RNMP zeros for case (d) as shown below:

$$\alpha_v < \alpha_v^\infty\tag{3-54}$$

Since the two sets of conjugate locations where the zero locus of $G_3(s)$ crosses the imaginary axis are the same, the zero locus of $G_3(s)$ goes back to the left-hand side (LHS) of imaginary axis after touching the imaginary axis. Therefore, since there are no CNMP zeros present for this case, only Scenario I is possible for the meeting point of the zero locus of $G_3(s)$ with the positive real axis.

$$\text{e) } -\frac{1}{\kappa\eta} < \chi < -\frac{\kappa}{\eta}, \zeta_v > \zeta_{v,\min}$$

Based on Eq.(3-36) and Table 3-2, Condition I of Eq.(3-32) is true for this range of χ . Based on Table 3-3 – Table 3-5, Condition II of Eq.(3-32) is also true for this range of χ . Similarly, based on Table 3-6 – Table 3-9, Condition III of Eq.(3-32) is also true for this range of χ and ζ_v . This implies that the zero locus of $G_3(s)$ will not cross the imaginary axis as shown in Fig 3-5e. This

allows us to find sufficient condition for the elimination of only CNMP zeros for case (e) as shown below:

$$\begin{aligned}\alpha_v &\geq 0 \\ \alpha_v &\leq 0\end{aligned}\tag{3-55}$$

Note that Eq.(3-55) is a sufficient and necessary condition for the elimination of only CNMP zeros. For this case, we can also find necessary and sufficient conditions for the elimination of only RNMP zeros. From Fig 3-5e, it is evident that when $\alpha_v > \alpha_v^\infty$, the zero locus of $G_3(s)$ approaches negative infinity along the real axis and flips over to positive infinity thereby leading to RNMP zeros. This allows us to find sufficient condition for the elimination of only RNMP zeros for case (e) as shown below:

$$\alpha_v < \alpha_v^\infty\tag{3-56}$$

Since there are no CNMP zeros present for this case, only Scenario I is possible for the meeting point of the zero locus of $G_3(s)$ with the positive real axis.

f) $\chi \geq -\frac{\kappa}{\eta}$

Based on Eq.(3-36) and Table 3-2, Condition I of Eq.(3-32) is not true for this range of χ . Based on Table 3-3 – Table 3-5, Condition II of Eq.(3-32) is also not true for this range of χ . Similarly, based on Table 3-6 – Table 3-9, Condition III of Eq.(3-32) is also not true for this range of χ . This implies that the zero locus of $G_3(s)$ will cross the imaginary axis at two sets of conjugate locations at $\alpha_v = \alpha_{v1}^{img}$ and $\alpha_v = \alpha_{v2}^{img}$ (given in Eq.(3-33)) as shown in Fig 3-5f1, Fig 3-5f2 and Fig 3-5f3.

In order to ascertain the sign of α_{v1}^{img} and α_{v2}^{img} , we plot the zero locus of $G_3(s)$ numerically for certain values of system parameters that satisfy the condition ($\kappa < -1$) and ($\chi \geq -\kappa/\eta$). Comparing

the two distinct values of α_v (where the zero locus crosses the imaginary axis) from the numerically plotted zero locus with the values of α_{v1}^{img} and α_{v2}^{img} from Eq.(3-33) leads to the observation that $\alpha_{v1}^{img} > 0$ and $\alpha_{v2}^{img} < 0$. Although this observation has been made numerically for one set of system parameters that satisfy the condition $(\kappa < -1)$ and $(\chi \geq -\kappa/\eta)$, it holds true for any combination of system parameters that satisfy $(\kappa < -1)$ and $(\chi \geq -\kappa/\eta)$. The proof for this is as follows.

The expression for α_{v1}^{img} and α_{v2}^{img} are given by Eq.(3-33). From numerical simulation, we observed that $\alpha_{v1}^{img} > 0$ and $\alpha_{v2}^{img} < 0$ for one set of system parameters that satisfy the condition $(\kappa < -1)$ and $(\chi \geq -\kappa/\eta)$. If α_{v1}^{img} and α_{v2}^{img} have to change sign for another set of system parameters that satisfy the condition $(\kappa < -1)$ and $(\chi \geq -\kappa/\eta)$, then either the numerator or the denominator of α_{v1}^{img} and α_{v2}^{img} should change signs but not both at the same time. If the numerators of α_{v1}^{img} and α_{v2}^{img} have to change sign then they will have to pass through 0 for some set of system parameters that satisfy the condition $(\kappa < -1)$ and $(\chi \geq -\kappa/\eta)$. This would mean that α_{v1}^{img} and α_{v2}^{img} will have to be equal to 0 for this set of system parameters. However, if α_{v1}^{img} and α_{v2}^{img} are equal to 0, this means that for $\alpha_v = 0$ the zero locus should cross the imaginary axis. But for $\alpha_v = 0$ the zero locus passes through the damped poles that lie strictly on the open left half s -plane and not on the imaginary axis as shown in Fig 3-5f1, Fig 3-5f2 and Fig 3-5f3. Therefore, α_{v1}^{img} and α_{v2}^{img} cannot be equal to 0. Hence the numerators of α_{v1}^{img} and α_{v2}^{img} cannot change signs. The denominator of α_{v1}^{img} and α_{v2}^{img} cannot change sign because $\chi \geq -\kappa/\eta$ for any set of system parameters that satisfy $(\kappa < -1)$ and $(\chi \geq -\kappa/\eta)$ (refer to Eq.(3-36)). When χ is equal to $-\kappa/\eta$, it is seen from numerical simulation that α_{v1}^{img} and α_{v2}^{img} have finite values such that $\alpha_{v1}^{img} > 0$ and $\alpha_{v2}^{img} < 0$. Hence, α_{v1}^{img} and α_{v2}^{img} cannot change signs for any set of system

parameters that satisfy the condition ($\kappa < -1$) and ($\chi \geq -\kappa/\eta$). Therefore, $\alpha_{v1}^{img} > 0$ and $\alpha_{v2}^{img} < 0$ for any set of system parameters that satisfy the condition ($\kappa < -1$) and ($\chi \geq -\kappa/\eta$). On further investigation, it was found that there exists an upper bound on α_{v1}^{img} given by Eq.(3-57).

Since $\chi\eta + \kappa \geq 0$ (from Eq.(3-36))

$$\alpha_{v1}^{img} - \frac{\omega_u \omega_v (\chi + \eta)}{(\chi\eta + \kappa) y_1^2} < 0 \Rightarrow \alpha_{v1}^{img} \leq \frac{\omega_u \omega_v (\chi + \eta)}{(\chi\eta + \kappa) y_1^2} \quad (3-57)$$

Now, we have completely characterized the intersection of the zero locus of $G_3(s)$ with the imaginary axis for case (f) which is depicted graphically in Fig 3-5f1, Fig 3-5f2 and Fig 3-5f3. This allows us to find sufficient condition for the elimination of only CNMP zeros for case (f) as shown below:

$$\begin{aligned} \alpha_v &\leq \alpha_{v1}^{img} \text{ if } \alpha_v > 0 \\ \alpha_v &\geq \alpha_{v2}^{img} \text{ if } \alpha_v < 0 \end{aligned} \quad (3-58)$$

Note that Eq.(3-58) is only a sufficient condition for the elimination of CNMP zeros and not a necessary one. This is evident from Fig 3-5f2 and Fig 3-5f3 where for positive $\alpha_v > \alpha_{v1}^{img}$ i.e. Eq.(3-58) is not satisfied, the zeros of $G_3(s)$ can be RNMP instead of CNMP. Therefore, in order to find the necessary and sufficient condition for the elimination of only CNMP zeros and only RNMP zeros, we characterize the intersection of the zero locus of $G_3(s)$ with the positive real axis. Zeros of $G_3(s)$ are found by setting the numerator $N_3(s)$ in Eq.(3-28) to zero. In order to find the intersection of the zero locus of $G_3(s)$ with the positive real axis, we set $s = x$ in Eq.(3-40) and find the repeated roots of Eq.(3-40). This is done by setting the discriminant in Eq.(3-40) to zero. The discriminant of the fourth order polynomial equation is given in Eq.(3-41). Eq.(3-41) leads to a 5th order polynomial in α_v which cannot be solved analytically as discussed in case(a).

Therefore, we cannot analytically characterize the intersection of the zero locus of $G_3(s)$ with the positive real axis like we did in the two-DoF case in the previous section. Therefore, it will not be possible to find the necessary and sufficient conditions for the elimination of only CNMP zeros and only RNMP zeros for a three-DoF damped flexible system. However, we can attempt to find the number of times the zero locus meets with the positive real axis in order to provide at least some insight into how the zero locus interacts with the positive real axis.

In order to do so, we take into account certain facts that we know about the zero locus

1. The real axis is always part of the zero locus of $G_3(s)$ irrespective of whether $\alpha_v > 0$ or $\alpha_v < 0$
2. $T_3(s)$ has 2 pairs of zeros of which one pair always lies at the origin

Based on these facts, we solve for the repeated roots of $N_3(s)$ in Eq.(3-29) since when the zero locus of $G_3(s)$ meets the positive real axis, we get repeated roots in s . For a fourth order polynomial, five scenarios are possible for the meeting points of the zero locus of $G_3(s)$ with the positive real axis as described in case (a) and shown graphically in Fig 3-3. Now we have to ascertain for case (f) where the conditions ($\kappa < -1$) and ($\chi \geq -\kappa/\eta$) are satisfied, which of the five scenarios for the meeting point of the zero locus of $G_3(s)$ with the positive real axis are possible. In order to do so, we make use of following five facts about the zero locus:

1. Position of zeros of $T_3(s)$ - To find the location of the zeros of $T_3(s)$, as previously discussed below Eq.(3-28), the root locus of $T_3(s)$ is the zero locus of $G_3(s)$. The zeros of $T_3(s)$ are the roots of $A_3(s)$ given by Eq.(3-28). It can be observed from Eq.(3-28) that two of the zeros of $T_3(s)$ are at the origin. In order to find the location of the other zeros of $T_3(s)$, we analyze the roots of Eq.(3-42) which is derived from expression of $A_3(s)$ from Eq.(3-28). Given the condition that ($\kappa < -1$) and ($\chi \geq -\kappa/\eta$) and Eq.(3-36), we can conclude the following:

$$\text{Product of roots} = \frac{\omega_v^2 (\eta^2 + \kappa)}{(1 + \kappa)} > 0, \text{ Sum of roots} = -\frac{2\zeta_v \omega_v (\chi\eta + \kappa)}{(1 + \kappa)} \geq 0 \quad (3-59)$$

Therefore, based on Eq.(3-59), the roots of Eq.(3-42) will lie on the right hand side (RHS) of the imaginary axis. They can either be real or occur as a pair of complex conjugates. Fig 3-5f1, Fig 3-5f2 and Fig 3-5f3 graphically depicts the location of these zeros on the RHS of the imaginary axis.

2. Intersection of zero locus of $G_3(s)$ with the imaginary axis - We have already shown that the zero locus of $G_3(s)$ will cross the imaginary axis at two sets of conjugate locations at $\alpha_v = \alpha_{v1}^{img}$ and $\alpha_v = \alpha_{v2}^{img}$ (given in Eq.(3-33)) as shown in Fig 3-5f1, Fig 3-5f2 and Fig 3-5f3. It is also known that $\alpha_{v1}^{img} > 0$ and $\alpha_{v2}^{img} < 0$ for any set of system parameters that satisfy the condition $(\kappa < -1)$ and $(\chi \geq -\kappa/\eta)$.
3. Relative position of intersection of positive zero locus ($\alpha_v > 0$) and negative zero locus ($\alpha_v < 0$) with the imaginary axis - For case (f), from Eq.(3-46) we can say that $y_1^2 < y_2^2$. Since, from Eq.(3-37), α_{v1}^{img} corresponds to y_1^2 and α_{v2}^{img} corresponds to y_2^2 , the point of intersection of the zero locus of $G_3(s)$ corresponding to α_{v2}^{img} is higher than the point of intersection of the zero locus of $G_3(s)$ corresponding to α_{v1}^{img} .
4. Which portion of the positive real axis belongs to the positive or negative zero locus - For case (f), from Eq.(3-47), we can say that the portion of the positive real axis corresponding to α_v^∞ belongs to positive zero locus of $G_3(s)$. Further, since there are no zeros of $T_3(s)$ lying on the positive real axis, the entire positive real axis is covered by the positive zero locus of $G_3(s)$.
5. Angle of arrival of positive and negative zero locus at the zeros of $T_3(s)$ present at the origin - For case (f), from Eq.(3-48), the angle of arrival for the positive zero locus of $G_3(s)$ to the zeros

of $T_3(s)$ at the origin is determined to be 0° and 180° . The angle of arrival for the negative zero locus of $G_3(s)$ to the zeros of $T_3(s)$ at the origin is determined to be 90° and -90° .

Based on all these facts, we can conclude that for case (f), Scenario I, Scenario III and Scenario V are possible for the zero locus of $G_3(s)$ to meet the positive real axis. The table below shows which of the above facts were used to eliminate the scenarios that are not possible for both $\alpha_v > 0$ and $\alpha_v < 0$.

Sign of α_v	Scenario I	Scenario II	Scenario III	Scenario IV	Scenario V
$\alpha_v > 0$	-	2	-	1,2	-
$\alpha_v < 0$	-	4	-	4	-

Table 3-13 Facts used to eliminate different scenarios for meeting points of the zero locus of $G_3(s)$ on the positive real axis that are not possible for case (f)

Parameter Range of κ : ($-1 \leq \kappa \leq -\eta^2$)

$$\text{Condition II: } b^2 - 4ac \geq 0 \quad \text{AND} \quad \frac{-b + \sqrt{b^2 - 4ac}}{2a} < 0 \quad (\text{from Eq.(3-32)})$$

Note that for $-1 \leq \kappa \leq -\eta^2$ and $\eta < 1$ (because we have assumed $\omega_u < \omega_v$ without any loss of generality), the parameter space of χ can be written in two ways because under the condition that $-1 < \kappa < -\eta^2$, it cannot be ascertained if $-\kappa/\eta > -\eta/\kappa$ or $-\kappa/\eta < -\eta/\kappa$. Hence, the parameter space can be written in two ways

$$-\frac{\eta^3}{\kappa} < -\frac{\kappa}{\eta} < -\frac{\eta}{\kappa} < -\frac{1}{\kappa\eta} \quad \text{OR} \quad -\frac{\eta^3}{\kappa} < -\frac{\eta}{\kappa} < -\frac{\kappa}{\eta} < -\frac{1}{\kappa\eta} \quad (3-60)$$

κ	# No.	a	c	b	λ and δ	Range of χ where the signs of a, b & c are satisfied (range is hashed if it exists)	ζ_v
$-1 < \kappa < -\eta^2$	IIA	$a > 0$	$c > 0$	$b > 0$	$\lambda > 0, \delta > 0$		No sol
					$\lambda > 0, \delta < 0$		
					$\lambda < 0, \delta < 0$		

Table 3-14 Range of χ and ζ_v for which Condition (IIA) of Eq.(3-35) is satisfied

κ	# No.	a	c	b	λ and δ	Range of χ where the signs of a, b & c are satisfied (range is hashed if it exists)	ζ_v
$-1 < \kappa < -\eta^2$	IIB & IIC	$a < 0$	$c > 0$	$b > 0$	$\lambda > 0, \delta > 0$		No sol
					$\lambda > 0, \delta < 0$		No sol
					$\lambda < 0, \delta < 0$		No sol
					$\lambda < 0, \delta > 0$		No sol

Table 3-15 Range of χ and ζ_v for which Condition (IIB) and (IIC) of Eq.(3-35) is satisfied

κ	# No.	a	c	b	λ and δ	Range of χ where the signs of a, b & c are satisfied (range is hashed if it exists)	ζ_v
$-1 < \kappa < -\eta^2$	IID	$a < 0$	$c < 0$	$b < 0$	$\lambda > 0, \delta > 0$		No sol

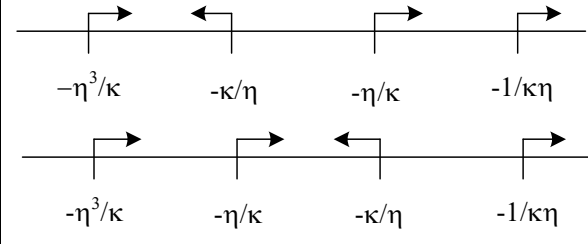
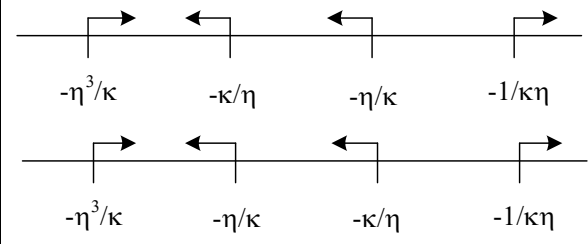
					$\lambda < 0, \delta < 0$		No sol
					$\lambda < 0, \delta > 0$		No sol

Table 3-16 Range of χ and ζ_v for which Condition (IID) of Eq.(3-35) is satisfied

Condition III: $b^2 - 4ac \geq 0$ AND $\frac{-b - \sqrt{b^2 - 4ac}}{2a} < 0$

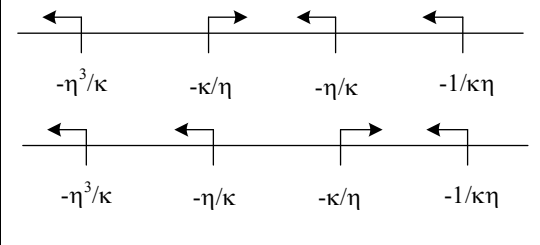
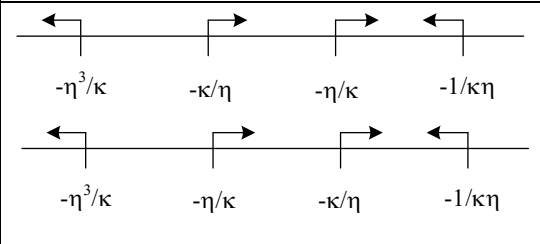
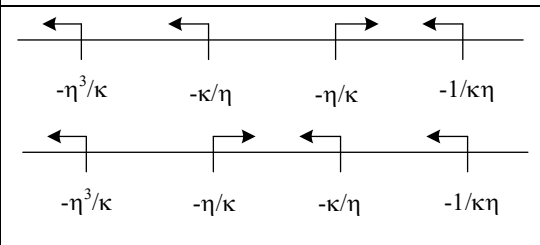
κ	# No.	a	c	b	λ and δ	Range of χ where the signs of a, b & c are satisfied (range is hashed if it exists)	ζ_v
$-1 < \kappa < -\eta^2$	IIIA	$a > 0$	$c > 0$	$b > 0$	$\lambda > 0, \delta > 0$		No sol
					$\lambda > 0, \delta < 0$		No sol
					$\lambda < 0, \delta < 0$		No sol

Table 3-17 Range of χ and ζ_v for which Condition (IIIA) of Eq.(3-35) is satisfied

κ	# No.	a	c	b	λ and δ	Range of χ where the signs of a, b & c are satisfied (range is hashed if it exists)	ζ_v
$1 < \kappa < -\eta^2$	III B	$a > 0$	$c < 0$	$b > 0$	$\lambda > 0, \delta > 0$		$\zeta_v > \frac{\sqrt{\delta\lambda}}{ \lambda }$
					$\lambda > 0, \delta < 0$		For all values of ζ_v
					$\lambda < 0, \delta < 0$		$\zeta_v < \frac{\sqrt{\delta\lambda}}{ \lambda }$

Table 3-18 Range of χ and ζ_v for which Condition (IIIB) of Eq.(3-35) is satisfied

κ	# No.	a	c	b	λ and δ	Range of χ where the signs of a, b & c are satisfied (range is hashed if it exists)	ζ_v
$-1 < \kappa < -\eta^2$	IIIC	$a < 0$	$c < 0$	$b < 0$	$\lambda > 0, \delta > 0$		No sol
					$\lambda < 0, \delta < 0$		No sol
					$\lambda < 0, \delta > 0$		No sol

Table 3-19 Range of χ and ζ_v for which Condition (IIIC) of Eq.(3-35) is satisfied

κ	# No.	a	c	b	λ and δ	Range of χ where the signs of a , b & c are satisfied (range is hashed if it exists)	ζ_v
$-1 < \kappa < -\eta^2$	III D	$a > 0$	$c < 0$	$b < 0$	$\lambda > 0, \delta > 0$		$\zeta_v < \frac{\sqrt{\delta\lambda}}{ \lambda }$
					$\lambda < 0, \delta < 0$		$\zeta_v > \frac{\sqrt{\delta\lambda}}{ \lambda }$
					$\lambda < 0, \delta > 0$		for all values of ζ_v

Table 3-20 Range of χ and ζ_v for which Condition (IIID) of Eq.(3-35) is satisfied

For the parameter range of $(-1 \leq \kappa \leq -\eta^2)$, Table 3-2, Table 3-14 – Table 3-16, and Table 3-17 – Table 3-20 provide the solution for Condition I, Condition II and Condition III of Eq.(3-32) respectively. Based on these tables, we can provide the following parameter ranges of χ and ζ_v :

g) $\chi < -\frac{\eta^3}{\kappa}$

Based on Eq.(3-60) and Table 3-2, Condition I of Eq.(3-32) is not true for this range of χ . Based on Table 3-14 – Table 3-16, Condition II of Eq.(3-32) is also not true for this range of χ . Similarly, based on Table 3-17 – Table 3-20, Condition III of Eq.(3-32) is also not true for this range of χ . This implies that the zero locus of $G_3(s)$ will cross the imaginary axis at two sets of conjugate locations at $\alpha_v = \alpha_{v1}^{img}$ and $\alpha_v = \alpha_{v2}^{img}$ (given in Eq.(3-33)) as shown in Fig 3-5g.

In order to ascertain the sign of α_{v1}^{img} and α_{v2}^{img} , we plot the zero locus of $G_3(s)$ numerically for certain values of system parameters that satisfy the condition $(-1 \leq \kappa \leq -\eta^2)$ and $(\chi < -\eta^3/\kappa)$. Comparing the two distinct values of α_v (where the zero locus crosses the imaginary axis) from the numerically plotted zero locus with the values of α_{v1}^{img} and α_{v2}^{img} from Eq.(3-33) leads to the observation that $\alpha_{v1}^{img} > 0$ and $\alpha_{v2}^{img} < 0$. Although this observation has been made numerically for one set of system parameters that satisfy the condition $(-1 \leq \kappa \leq -\eta^2)$ and $(\chi < -\eta^3/\kappa)$, it holds true for any combination of system parameters that satisfy $(-1 \leq \kappa \leq -\eta^2)$ and $(\chi < -\eta^3/\kappa)$. The proof for this is as follows

The expression for α_{v1}^{img} and α_{v2}^{img} are given by Eq.(3-33). From numerical simulation, we observed that $\alpha_{v1}^{img} > 0$ and $\alpha_{v2}^{img} < 0$ for one set of system parameters that satisfy the condition $(-1 \leq \kappa \leq -\eta^2)$ and $(\chi < -\eta^3/\kappa)$. If α_{v1}^{img} and α_{v2}^{img} have to change sign for another set of system parameters that satisfy the condition $(-1 \leq \kappa \leq -\eta^2)$ and $(\chi < -\eta^3/\kappa)$, then either the numerator or the denominator of α_{v1}^{img} and α_{v2}^{img} should change signs but not both at the same time. If the numerators of α_{v1}^{img} and α_{v2}^{img} have to change sign then they will have to pass through 0 for some set of system parameters that satisfy the condition $(-1 \leq \kappa \leq -\eta^2)$ and $(\chi < -\eta^3/\kappa)$. This would mean that α_{v1}^{img} and α_{v2}^{img} will have to be equal to 0 for this set of system parameters. However, if α_{v1}^{img} and α_{v2}^{img} are equal to 0, this means that for $\alpha_v = 0$ the zero locus should cross the imaginary axis. But for $\alpha_v = 0$ the zero locus passes through the damped poles that lie strictly on the open left half s -plane and not on the imaginary axis as shown in Fig 3-5g. Therefore, α_{v1}^{img} and α_{v2}^{img} cannot be equal to 0. Hence the numerators of α_{v1}^{img} and α_{v2}^{img} cannot change signs. The denominator of α_{v1}^{img} and α_{v2}^{img} cannot change sign because $\chi < -\kappa/\eta$ for any set of system

parameters that satisfy $(-1 \leq \kappa \leq -\eta^2)$ and $(\chi < -\eta^3/\kappa)$ (refer to Eq.(3-60)). Hence, α_{v1}^{img} and α_{v2}^{img} cannot change signs for any set of system parameters that satisfy the condition $(-1 \leq \kappa \leq -\eta^2)$ and $(\chi < -\eta^3/\kappa)$. Therefore, $\alpha_{v1}^{img} > 0$ and $\alpha_{v2}^{img} < 0$ for any set of system parameters that satisfy the condition $(-1 \leq \kappa \leq -\eta^2)$ and $(\chi < -\eta^3/\kappa)$. On further investigation, it was found that there exists an upper bound on α_{v1}^{img} given by Eq.(3-61). Since $\chi\eta + \kappa < 0$ (from Eq.(3-60))

$$\Rightarrow \alpha_{v1}^{img} + \frac{(1 + \chi\eta)}{(\chi\eta + \kappa)} < 0 \Rightarrow \alpha_{v1}^{img} < -\frac{(1 + \chi\eta)}{(\chi\eta + \kappa)} \quad (3-61)$$

Now, we have completely characterized the intersection of the zero locus of $G_3(s)$ with the imaginary axis for case (g) which is depicted graphically in Fig 3-5g. This allows us to find sufficient condition for the elimination of only CNMP zeros for case (g) as shown below:

$$\begin{aligned} \alpha_v &\leq \alpha_{v1}^{img} \text{ if } \alpha_v > 0 \\ \alpha_v &\geq \alpha_{v2}^{img} \text{ if } \alpha_v < 0 \end{aligned} \quad (3-62)$$

Note that Eq.(3-62) is only a sufficient condition for the elimination of CNMP zeros and not a necessary one. This is evident from Fig 3-5g where for positive $\alpha_v > \alpha_{v1}^{img}$ i.e. Eq.(3-62) is not satisfied, the zeros of $G_3(s)$ can be RNMP instead of CNMP. Therefore, in order to find the necessary and sufficient condition for the elimination of only CNMP zeros and only RNMP zeros, we characterize the intersection of the zero locus of $G_3(s)$ with the positive real axis. Zeros of $G_3(s)$ are found by setting the numerator $N_3(s)$ in Eq.(3-28) to zero. In order to find the intersection of the zero locus of $G_3(s)$ with the positive real axis, we set $s = x$ in Eq.(3-40) and find the repeated roots of Eq.(3-40). This is done by setting the discriminant in Eq.(3-40) to zero. The discriminant of the fourth order polynomial equation is given in Eq.(3-41). Eq.(3-41) leads to a 5th order polynomial in α_v which cannot be solved analytically as discussed in case(a).

Therefore, we cannot analytically characterize the intersection of the zero locus of $G_3(s)$ with the positive real axis like we did in the two-DoF case in the previous section. Therefore, it will not be possible to find the necessary and sufficient conditions for the elimination of only CNMP zeros and only RNMP zeros for a three-DoF damped flexible system. However, we can attempt to find the number of times the zero locus meets with the positive real axis in order to provide at least some insight into how the zero locus interacts with the positive real axis.

In order to do so, we take into account certain facts that we know about the zero locus

1. The real axis is always part of the zero locus of $G_3(s)$ irrespective of whether $\alpha_v > 0$ or $\alpha_v < 0$
2. $T_3(s)$ has 2 pairs of zeros of which one pair always lies at the origin

Based on these facts, we solve for the repeated roots of $N_3(s)$ in Eq.(3-28) since when the zero locus of $G_3(s)$ meets the positive real axis, we get repeated roots in s . For a fourth order polynomial, five scenarios are possible for the meeting points of the zero locus of $G_3(s)$ with the positive real axis as described in case a) and shown graphically in Fig 3-3. Now we have to ascertain for case (g) where the conditions $(-1 \leq \kappa \leq -\eta^2)$ and $(\chi < -\eta^3/\kappa)$ are satisfied, which of the five scenarios for the meeting point of the zero locus of $G_3(s)$ with the positive real axis are possible. In order to do so, we make use of following five facts about the zero locus:

1. Position of zeros of $T_3(s)$ - To find the location of the zeros of $T_3(s)$, as previously discussed below Eq.(3-28), the root locus of $T_3(s)$ is the zero locus of $G_3(s)$. The zeros of $T_3(s)$ are the roots of $A_3(s)$ given by Eq.(3-28). It can be observed from Eq.(3-28) that two of the zeros of $T_3(s)$ are at the origin. This is graphically depicted in Fig 3-5g. In order to find the location of the other zeros of $T_3(s)$, we analyze the roots of Eq. which is derived from expression of $A_3(s)$ from Eq.(3-28).

$$(1 + \kappa)s^2 + 2\zeta_v\omega_v(\chi\eta + \kappa)s + \omega_v^2(\eta^2 + \kappa) = 0$$

$$\text{Product of roots} = \frac{\omega_v^2(\eta^2 + \kappa)}{(1 + \kappa)}, \text{ Sum of roots} = -\frac{2\zeta_v\omega_v(\chi\eta + \kappa)}{(1 + \kappa)} \quad (3-63)$$

Given the condition that $(-1 \leq \kappa \leq -\eta^2)$ and $(\chi < -\eta^3/\kappa)$ and Eq.(3-60), we can conclude the following:

$$\text{Product of roots} = \frac{\omega_v^2(\eta^2 + \kappa)}{(1 + \kappa)} \leq 0, \text{ Sum of roots} = -\frac{2\zeta_v\omega_v(\chi\eta + \kappa)}{(1 + \kappa)} > 0 \quad (3-64)$$

Therefore, based on Eq.(3-64), the roots of Eq.(3-63) can only be real with one zero lying on positive real axis and the other on negative real axis. In the limiting case when $\kappa = -\eta^2$, there is one zero at the origin and the other on positive real axis. In the limiting case when $\kappa = -1$, there is one zero at $+\infty$ and the other on negative real axis. Fig 3-5g graphically depicts the location of these zeros.

2. Intersection of zero locus of $G_3(s)$ with the imaginary axis - We have already shown that the zero locus of $G_3(s)$ will cross the imaginary axis at two sets of conjugate locations at $\alpha_v = \alpha_{v1}^{img}$ and $\alpha_v = \alpha_{v2}^{img}$ (given in Eq.(3-33)) as shown in Fig 3-5g. It is also known that $\alpha_{v1}^{img} > 0$ and $\alpha_{v2}^{img} < 0$ for any set of system parameters that satisfy the condition $(-1 \leq \kappa \leq -\eta^2)$ and $(\chi < -\eta^3/\kappa)$.
3. Relative position of intersection of positive zero locus ($\alpha_v > 0$) and negative zero locus ($\alpha_v < 0$) with the imaginary axis - For case (g), from Eq.(3-46) we can say that $y_1^2 > y_2^2$. Since, from Eq.(3-37), α_{v1}^{img} corresponds to y_1^2 and α_{v2}^{img} corresponds to y_2^2 , the point of intersection of the zero locus of $G_3(s)$ corresponding to α_{v1}^{img} is higher than the point of intersection of the zero locus of $G_3(s)$ corresponding to α_{v2}^{img} .

4. Which portion of the positive real axis belongs to the positive or negative zero locus - For case (g), from Eq.(3-47), we can say that the portion of the positive real axis corresponding to α_v^∞ belongs to negative zero locus of $G_3(s)$. Further, since there is a zero of $T_3(s)$ lying on the positive real axis, the portion of the positive real axis that lies to the right of this zero of $T_3(s)$ is covered by the negative zero locus of $G_3(s)$ and the portion of the positive real axis that lies to the left of this zero of $T_3(s)$ is covered by the positive zero locus of $G_3(s)$.
5. Angle of arrival of positive and negative zero locus at the zeros of $T_3(s)$ present at the origin - For case (g), from Eq.(3-48), the angle of arrival for the positive zero locus of $G_3(s)$ to the zeros of $T_3(s)$ at the origin is determined to be 0° and 180° . The angle of arrival for the negative zero locus of $G_3(s)$ to the zeros of $T_3(s)$ at the origin is determined to be -90° and 90° . However, for the limiting case when $\kappa = -\eta^2$, the zero of $T_3(s)$ on the negative real axis moves to the origin (leading to three zeros of $T_3(s)$ at the origin) . For this case, the angle of arrival for the positive zero locus of $G_3(s)$ to the zeros of $T_3(s)$ at the origin is determined to be -60° , 60° and 180° and the angle of arrival for the negative zero locus of $G_3(s)$ to the zeros of $T_3(s)$ at the origin is determined to be -120° , 0° and 120° .

Based on all these facts, we can conclude that for case (g), Scenario II is possible for the zero locus of $G_3(s)$ to meet the positive real axis. The table below shows which of the above facts were used to eliminate the scenarios that are not possible for both $\alpha_v > 0$ and $\alpha_v < 0$.

Sign of α_v	Scenario I	Scenario II	Scenario III	Scenario IV	Scenario V
$\alpha_v > 0$	4	-	2,3	1,2	2,3
$\alpha_v < 0$	4	4	4	4	4

Table 3- 21 Facts used to eliminate different scenarios for meeting points of the zero locus of

$G_3(s)$ on the positive real axis that are not possible for case (g)

$$\text{h) } -\frac{\eta^3}{\kappa} \leq \chi \leq -\frac{1}{\kappa\eta}$$

Based on Eq.(3-60) and Table 3-2, Condition I of Eq.(3-32) is not true for this range of χ . Based on Table 3-14 – Table 3-16, Condition II of Eq.(3-32) is also not true for this range of χ . Based on Table 3-17 – Table 3-20, Condition III of Eq.(3-32) is true for this range of χ . This implies that the zero locus of $G_3(s)$ will cross the imaginary axis at one sets of conjugate locations at $\alpha_v = \alpha_{v1}^{img}$ (given in Eq.(3-33)) as shown in Fig 3-5h1 and Fig 3-5h2.

In order to ascertain the sign of α_{v1}^{img} , we plot the zero locus of $G_3(s)$ numerically for certain values of system parameters that satisfy the condition $(-1 \leq \kappa \leq -\eta^2)$ and $(-\eta^3/\kappa \leq \chi \leq -1/\kappa\eta)$. Comparing the value of α_v (where the zero locus crosses the imaginary axis) from the numerically plotted zero locus with the values of α_{v1}^{img} from Eq.(3-33) leads to the observation that $\alpha_{v1}^{img} > 0$. Although this observation has been made numerically for one set of system parameters that satisfy the condition $(-1 \leq \kappa \leq -\eta^2)$ and $(-\eta^3/\kappa \leq \chi \leq -1/\kappa\eta)$, it holds true for any combination of system parameters that satisfy $(-1 \leq \kappa \leq -\eta^2)$ and $(-\eta^3/\kappa \leq \chi \leq -1/\kappa\eta)$. The proof for this is as follows: The expression for α_{v1}^{img} is given by Eq.(3-33). From numerical simulation, we observed that $\alpha_{v1}^{img} > 0$ for one set of system parameters that satisfy the condition $(-1 \leq \kappa \leq -\eta^2)$ and $(-\eta^3/\kappa \leq \chi \leq -1/\kappa\eta)$. If α_{v1}^{img} has to change sign for another set of system

parameters that satisfy the condition $(-1 \leq \kappa \leq -\eta^2)$ and $(-\eta^3/\kappa \leq \chi \leq -1/\kappa\eta)$, then either the numerator or the denominator of $\alpha_{v_l}^{img}$ should change signs but not both at the same time. If the numerator of $\alpha_{v_l}^{img}$ has to change sign then it will have to pass through 0 for some set of system parameters that satisfy the condition $(-1 \leq \kappa \leq -\eta^2)$ and $(-\eta^3/\kappa \leq \chi \leq -1/\kappa\eta)$. This would mean that $\alpha_{v_l}^{img}$ will have to be equal to 0 for this set of system parameters. However, if $\alpha_{v_l}^{img}$ is equal to 0, this means that for $\alpha_v = 0$ the zero locus should cross the imaginary axis. But for $\alpha_v = 0$ the zero locus passes through the damped poles that lie strictly on the open left half s -plane and not on the imaginary axis as shown in Fig 3-5h1 and Fig 3-5h2. Therefore, $\alpha_{v_l}^{img}$ cannot be equal to 0. Hence the numerator of $\alpha_{v_l}^{img}$ cannot change sign. For checking the sign of denominator, this case can be analyzed by sub-dividing it into two sub-cases, one where $\chi < -\kappa/\eta$ and one where $\chi \geq -\kappa/\eta$. For both these sub-cases, the denominator of $\alpha_{v_l}^{img}$ cannot change sign because for the first sub-case, $\chi < -\kappa/\eta$ for any set of system parameters that satisfy $(-1 \leq \kappa \leq -\eta^2)$ and $(-\eta^3/\kappa \leq \chi < -\kappa/\eta)$ (refer to Eq.(3-60)). Similarly, for the second sub-case, the denominator of $\alpha_{v_l}^{img}$ cannot change sign because $\chi \geq -\kappa/\eta$ for any set of system parameters that satisfy $(-1 \leq \kappa \leq -\eta^2)$ and $(-\kappa/\eta \leq \chi \leq -1/\kappa\eta)$ (refer to Eq.(3-60)). When χ is equal to $-\kappa/\eta$, it is seen from numerical simulation that $\alpha_{v_l}^{img}$ has a finite value such that $\alpha_{v_l}^{img} > 0$. Hence, $\alpha_{v_l}^{img}$ cannot change sign for any set of system parameters that satisfy the condition $(-\eta^3/\kappa \leq \chi \leq -1/\kappa\eta)$. Therefore, $\alpha_{v_l}^{img} > 0$ for any set of system parameters that satisfy the condition $(-\eta^3/\kappa \leq \chi \leq -1/\kappa\eta)$. On further investigation, it was found that there exists an upper bound on $\alpha_{v_l}^{img}$ given by Eq.(3-61) when $(\chi < -\kappa/\eta)$ and an upper bound given by Eq.(3-57) when $(\chi \geq -\kappa/\eta)$.

Now, we have completely characterized the intersection of the zero locus of $G_3(s)$ with the imaginary axis for case (h) which is depicted graphically in Fig 3-5h1 and Fig 3-5h2. This allows us to find sufficient condition for the elimination of only CNMP zeros for case (h) as shown below:

$$\begin{aligned} \alpha_v &\leq \alpha_{v1}^{img} \text{ if } \alpha_v > 0 \\ \alpha_v &< 0 \end{aligned} \tag{3-65}$$

Note that Eq.(3-65) is only a sufficient condition for the elimination of CNMP zeros and not a necessary one. This is evident from Fig 3-5h2 where for positive $\alpha_v > \alpha_{v1}^{img}$ i.e. Eq.(3-65) is not satisfied, the zeros of $G_3(s)$ can be RNMP instead of CNMP. Therefore, in order to find the necessary and sufficient condition for the elimination of only CNMP zeros and only RNMP zeros, we characterize the intersection of the zero locus of $G_3(s)$ with the positive real axis. Zeros of $G_3(s)$ are found by setting the numerator $N_3(s)$ in Eq.(3-28) to zero. In order to find the intersection of the zero locus of $G_3(s)$ with the positive real axis, we set $s = x$ in Eq.(3-40) and find the repeated roots of Eq.(3-40). This is done by setting the discriminant in Eq.(3-40) to zero. The discriminant of the fourth order polynomial equation is given in Eq.(3-41). Eq.(3-41) leads to a 5th order polynomial in α_v which cannot be solved analytically as discussed in case(a).

Therefore, we cannot analytically characterize the intersection of the zero locus of $G_3(s)$ with the positive real axis like we did in the two-DoF case in the previous section. Therefore, it will not be possible to find the necessary and sufficient conditions for the elimination of only CNMP zeros and only RNMP zeros for a three-DoF damped flexible system. However, we can attempt to find the number of times the zero locus meets with the positive real axis in order to provide at least some insight into how the zero locus interacts with the positive real axis.

In order to do so, we take into account certain facts that we know about the zero locus

1. The real axis is always part of the zero locus of $G_3(s)$ irrespective of whether $\alpha_v > 0$ or $\alpha_v < 0$

2. $T_3(s)$ has 2 pairs of zeros of which one pair always lies at the origin

Based on these facts, we solve for the repeated roots of $N_3(s)$ in Eq.(3-28) since when the zero locus of $G_3(s)$ meets the positive real axis, we get repeated roots in s . For a fourth order polynomial, five scenarios are possible for the meeting points of the zero locus of $G_3(s)$ with the positive real axis as described in case (a) and shown graphically in Fig 3-3. Now we have to ascertain for case (h) where the conditions $(-1 \leq \kappa \leq -\eta^2)$ and $(-\eta^3/\kappa \leq \chi \leq -1/\kappa\eta)$ are satisfied, which of the five scenarios for the meeting point of the zero locus of $G_3(s)$ with the positive real axis are possible. In order to do so, we make use of following five facts about the zero locus:

1. Position of zeros of $T_3(s)$ - To find the location of the zeros of $T_3(s)$, as previously discussed below Eq.(3-28), the root locus of $T_3(s)$ is the zero locus of $G_3(s)$. The zeros of $T_3(s)$ are the roots of $A_3(s)$ given by Eq.(3-28). It can be observed from Eq.(3-28) that two of the zeros of $T_3(s)$ are at the origin. This is graphically depicted in Fig 3-5h1 and Fig 3-5h2. In order to find the location of the other zeros of $T_3(s)$, we analyze the roots of Eq.(3-63) which is derived from expression of $A_3(s)$ from Eq.(3-28). Given the condition that $(-1 \leq \kappa \leq -\eta^2)$ and $(-\eta^3/\kappa \leq \chi \leq -1/\kappa\eta)$ and Eq.(3-60), we can conclude the following:

$$\text{Product of roots} = \frac{\omega_v^2 (\eta^2 + \kappa)}{(1 + \kappa)} \leq 0 \quad (3-66)$$

We cannot tell anything about the sign of $(\kappa + \chi\eta)$ and therefore cannot comment on the sum of the roots. Therefore, based on Eq.(3-66), the roots of Eq.(3-63) can only be real with one zero lying on positive real axis and the other on negative real axis. In the limiting case when $\kappa = -\eta^2$, there is one zero at the origin and the other on negative real axis (which goes to the

origin when $\chi = \eta$). In the limiting case when $\kappa = -1$, there is one zero at $+\infty$ and the other on negative real axis. Fig 3-5h1 and Fig 3-5h2 graphically depicts the location of these zeros.

2. Intersection of zero locus of $G_3(s)$ with the imaginary axis - We have already shown that the zero locus of $G_3(s)$ will cross the imaginary axis at one sets of conjugate locations at $\alpha_v = \alpha_{v1}^{img}$ (given in Eq.(3-33)) as shown in Fig 3-5h1 and Fig 3-5h2. It is also known that $\alpha_{v1}^{img} > 0$ for any set of system parameters that satisfy the condition $(-1 \leq \kappa \leq -\eta^2)$ and $(-\eta^3/\kappa \leq \chi \leq -1/\kappa\eta)$.
3. Which portion of the positive real axis belongs to the positive or negative zero locus - For case (h), from Eq.(3-47), we can say that the portion of the positive real axis corresponding to α_v^∞ belongs to negative zero locus of $G_3(s)$. Further, since there is a zero of $T_3(s)$ lying on the positive real axis (or the origin), the portion of the positive real axis that lies to the right of this zero of $T_3(s)$ is covered by the negative zero locus of $G_3(s)$ and the portion of the positive real axis that lies to the left of this zero of $T_3(s)$ is covered by the positive zero locus of $G_3(s)$.
4. Angle of arrival of positive and negative zero locus at the zeros of $T_3(s)$ present at the origin - For case (h), from Eq.(3-48), the angle of arrival for the positive zero locus of $G_3(s)$ to the zeros of $T_3(s)$ at the origin is determined to be 0° and 180° . The angle of arrival for the negative zero locus of $G_3(s)$ to the zeros of $T_3(s)$ at the origin is determined to be -90° and 90° . This can be seen in Fig 3-5h2. However, for the limiting case when $\kappa = -\eta^2$, the zero of $T_3(s)$ on the positive real axis moves to the origin (leading to three zeros of $T_3(s)$ at the origin). For this case, the angle of arrival for the positive zero locus of $G_3(s)$ to the zeros of $T_3(s)$ at the origin is determined to be -120° , 0° and 120° and the angle of arrival for the negative zero locus of $G_3(s)$ to the zeros of $T_3(s)$ at the origin is determined to be -60° , 60° and 180° . This can be seen in Fig 3-5h1. When $\kappa = -\eta^2$ and further when $\chi = \eta$, all zeros of $T_3(s)$ are at the origin. For this

case, the angle of arrival for the positive zero locus of $G_3(s)$ to the zeros of $T_3(s)$ at the origin is determined to be -135° , -45° and 45° , 135° and the angle of arrival for the negative zero locus of $G_3(s)$ to the zeros of $T_3(s)$ at the origin is determined to be -90° , 0° , 90° and 180° .

Based on all these facts, we can conclude that for case (h), Scenario I and Scenario II are possible for the zero locus of $G_3(s)$ to meet the positive real axis. The table below shows which of the above facts were used to eliminate the scenarios that are not possible for both $\alpha_v > 0$ and $\alpha_v < 0$.

Sign of α_v	Scenario I	Scenario II	Scenario III	Scenario IV	Scenario V
$\alpha_v > 0$	-	-	1,2	1,2	1,2
$\alpha_v < 0$	-	2	2	2	2

Table 3- 22 Facts used to eliminate different scenarios for meeting points of the zero locus of $G_3(s)$ on the positive real axis that are not possible for case (h)

i) $-\frac{1}{\kappa\eta} < \chi$

Based on Eq.(3-60) and Table 3-2, Condition I of Eq.(3-32) is not true for this range of χ . Based on Table 3-14 – Table 3-16, Condition II of Eq.(3-32) is also not true for this range of χ . Similarly, based on Table 3-17 – Table 3-20, Condition III of Eq.(3-32) is also not true for this range of χ . This implies that the zero locus of $G_3(s)$ will cross the imaginary axis at two sets of conjugate locations at $\alpha_v = \alpha_{v1}^{img}$ and $\alpha_v = \alpha_{v2}^{img}$ (given in Eq.(3-33)) as shown in Fig 3-5i1 and Fig 3-5i2.

In order to ascertain the sign of α_{v1}^{img} and α_{v2}^{img} , we plot the zero locus of $G_3(s)$ numerically for certain values of system parameters that satisfy the condition $(-1 \leq \kappa \leq -\eta^2)$ and $(\chi > -1/\kappa\eta)$. Comparing the two distinct values of α_v (where the zero locus crosses the imaginary axis) from the numerically plotted zero locus with the values of α_{v1}^{img} and α_{v2}^{img} from Eq.(3-33)

leads to the observation that $\alpha_{v1}^{img} > 0$ and $\alpha_{v2}^{img} < 0$. Although this observation has been made numerically for one set of system parameters that satisfy the condition $(-1 \leq \kappa \leq -\eta^2)$ and $(\chi > -I/\kappa\eta)$, it holds true for any combination of system parameters that satisfy $(-1 \leq \kappa \leq -\eta^2)$ and $(\chi > -I/\kappa\eta)$. The proof for this is as follows.

The expression for α_{v1}^{img} and α_{v2}^{img} are given by Eq.(3-33). From numerical simulation, we observed that $\alpha_{v1}^{img} > 0$ and $\alpha_{v2}^{img} < 0$ for one set of system parameters that satisfy the condition $(-1 \leq \kappa \leq -\eta^2)$ and $(\chi > -I/\kappa\eta)$. If α_{v1}^{img} and α_{v2}^{img} have to change sign for another set of system parameters that satisfy the condition $(-1 \leq \kappa \leq -\eta^2)$ and $(\chi > -I/\kappa\eta)$, then either the numerator or the denominator of α_{v1}^{img} and α_{v2}^{img} should change signs but not both at the same time. If the numerators of α_{v1}^{img} and α_{v2}^{img} have to change sign then they will have to pass through 0 for some set of system parameters that satisfy the condition $(-1 \leq \kappa \leq -\eta^2)$ and $(\chi > -I/\kappa\eta)$. This would mean that α_{v1}^{img} and α_{v2}^{img} will have to be equal to 0 for this set of system parameters. However, if α_{v1}^{img} and α_{v2}^{img} are equal to 0, this means that for $\alpha_v = 0$ the zero locus should cross the imaginary axis. But for $\alpha_v = 0$ the zero locus passes through the damped poles that lie strictly on the open left half s -plane and not on the imaginary axis as shown in Fig 3-5i1 and Fig 3-5i2. Therefore, α_{v1}^{img} and α_{v2}^{img} cannot be equal to 0. Hence the numerators of α_{v1}^{img} and α_{v2}^{img} cannot change signs. The denominator of α_{v1}^{img} and α_{v2}^{img} cannot change sign because $\chi > -\kappa/\eta$ for any set of system parameters that satisfy $(-1 \leq \kappa \leq -\eta^2)$ and $(\chi > -I/\kappa\eta)$ (refer to Eq.(3-60)). Hence, α_{v1}^{img} and α_{v2}^{img} cannot change signs for any set of system parameters that satisfy the condition $(-1 \leq \kappa \leq -\eta^2)$ and $(\chi > -I/\kappa\eta)$. Therefore, $\alpha_{v1}^{img} > 0$ and $\alpha_{v2}^{img} < 0$ for any set of system

parameters that satisfy the condition $(-1 \leq \kappa \leq -\eta^2)$ and $(\chi > -1/\kappa\eta)$. On further investigation, it was found that there exists an upper bound on α_v given by Eq.(3-57).

Now, we have completely characterized the intersection of the zero locus of $G_3(s)$ with the imaginary axis for case (i) which is depicted graphically in Fig 3-5i1 and Fig 3-5i2. This allows us to find sufficient condition for the elimination of only CNMP zeros for case (i) as shown below:

$$\begin{aligned} \alpha_v &\leq \alpha_{v1}^{img} \text{ if } \alpha_v > 0 \\ \alpha_v &\geq \alpha_{v2}^{img} \text{ if } \alpha_v < 0 \end{aligned} \quad (3-67)$$

Note that Eq.(3-67) is only a sufficient condition for the elimination of CNMP zeros and not a necessary one. This is evident from Fig 3-5i1 and Fig 3-5i2 where for positive $\alpha_v > \alpha_{v1}^{img}$ i.e. Eq.(3-67) is not satisfied, the zeros of $G_3(s)$ can be RNMP instead of CNMP. Therefore, in order to find the necessary and sufficient condition for the elimination of only CNMP zeros and only RNMP zeros, we characterize the intersection of the zero locus of $G_3(s)$ with the positive real axis. Zeros of $G_3(s)$ are found by setting the numerator $N_3(s)$ in Eq.(3-28) to zero. In order to find the intersection of the zero locus of $G_3(s)$ with the positive real axis, we set $s = x$ in Eq.(3-40) and find the repeated roots of Eq.(3-40). This is done by setting the discriminant in Eq.(3-40) to zero. The discriminant of the fourth order polynomial equation is given in Eq.(3-41). Eq.(3-41) leads to a 5th order polynomial in α_v which cannot be solved analytically as discussed in case(a).

Therefore, we cannot analytically characterize the intersection of the zero locus of $G_3(s)$ with the positive real axis like we did in the two-DoF case in the previous section. Therefore, it will not be possible to find the necessary and sufficient conditions for the elimination of only CNMP zeros and only RNMP zeros for a three-DoF damped flexible system. However, we can attempt to find

the number of times the zero locus meets with the positive real axis in order to provide at least some insight into how the zero locus interacts with the positive real axis.

In order to do so, we take into account certain facts that we know about the zero locus

1. The real axis is always part of the zero locus of $G_3(s)$ irrespective of whether $\alpha_v > 0$ or $\alpha_v < 0$
2. $T_3(s)$ has 2 pairs of zeros of which one pair always lies at the origin

Based on these facts, we solve for the repeated roots of $N_3(s)$ in Eq.(3-28) since when the zero locus of $G_3(s)$ meets the positive real axis, we get repeated roots in s . For a fourth order polynomial, five scenarios are possible for the meeting points of the zero locus of $G_3(s)$ with the positive real axis as described in case (a) and shown graphically in Fig 3-3. Now we have to ascertain for case (i) where the conditions $(-1 \leq \kappa \leq -\eta^2)$ and $(\chi > -1/\kappa\eta)$ are satisfied, which of the five scenarios for the meeting point of the zero locus of $G_3(s)$ with the positive real axis are possible. In order to do so, we make use of following five facts about the zero locus:

1. Position of zeros of $T_3(s)$ - To find the location of the zeros of $T_3(s)$, as previously discussed below Eq.(3-28), the root locus of $T_3(s)$ is the zero locus of $G_3(s)$. The zeros of $T_3(s)$ are the roots of $A_3(s)$ given by Eq.(3-28). It can be observed from Eq.(3-28) that two of the zeros of $T_3(s)$ are at the origin. This is graphically depicted in Fig 3-5i1 and Fig 3-5i2. In order to find the location of the other zeros of $T_3(s)$, we analyze the roots of Eq.(3-63) which is derived from expression of $A_3(s)$ from Eq.(3-28). Given the condition that $(-1 \leq \kappa \leq -\eta^2)$ and $(\chi > -1/\kappa\eta)$ and Eq.(3-60), we can conclude the following:

$$\text{Product of roots} = \frac{\omega_v^2 (\eta^2 + \kappa)}{(1 + \kappa)} \leq 0, \quad \text{Sum of roots} = -\frac{2\zeta_v \omega_v (\chi\eta + \kappa)}{(1 + \kappa)} < 0 \quad (3-68)$$

Therefore, based on Eq.(3-68), the roots of Eq.(3-63) can only be real with one zero lying on positive real axis and the other on negative real axis. In the limiting case when $\kappa = -\eta^2$, there is

one zero at the origin and the other on negative real axis. In the limiting case when $\kappa = -1$, there is one zero at $-\infty$ and the other on positive real axis. Fig 3-5i1 and Fig 3-5i2 graphically depicts the location of these zeros.

2. Intersection of zero locus of $G_3(s)$ with the imaginary axis - We have already shown that the zero locus of $G_3(s)$ will cross the imaginary axis at two sets of conjugate locations at $\alpha_v = \alpha_{v1}^{img}$ and $\alpha_v = \alpha_{v2}^{img}$ (given in Eq.(3-33)) as shown in Fig 3-5i1 and Fig 3-5i2. It is also known that $\alpha_{v1}^{img} > 0$ and $\alpha_{v2}^{img} < 0$ for any set of system parameters that satisfy the condition $(-1 \leq \kappa \leq -\eta^2)$ and $(\chi > -1/\kappa\eta)$
3. Relative position of intersection of positive zero locus ($\alpha_v > 0$) and negative zero locus ($\alpha_v < 0$) with the imaginary axis - For case (i), from Eq.(3-46) we can say that $y_1^2 < y_2^2$. Since, from Eq.(3-37), α_{v1}^{img} corresponds to y_1^2 and α_{v2}^{img} corresponds to y_2^2 , the point of intersection of the zero locus of $G_3(s)$ corresponding to α_{v2}^{img} is higher than the point of intersection of the zero locus of $G_3(s)$ corresponding to α_{v1}^{img} .
4. Which portion of the positive real axis belongs to the positive or negative zero locus - For case (i), from Eq.(3-47), we can say that the portion of the positive real axis corresponding to α_v^∞ belongs to negative zero locus of $G_3(s)$. Further, since there is a zero of $T_3(s)$ lying on the positive real axis (or at the origin), the portion of the positive real axis that lies to the right of this zero of $T_3(s)$ is covered by the negative zero locus of $G_3(s)$ and the portion of the positive real axis that lies to the left of this zero of $T_3(s)$ is covered by the positive zero locus of $G_3(s)$.
5. Angle of arrival of positive and negative zero locus at the zeros of $T_3(s)$ present at the origin - For case (i), from Eq.(3-48), the angle of arrival for the positive zero locus of $G_3(s)$ to the zeros of $T_3(s)$ at the origin is determined to be 0° and 180° . The angle of arrival for the negative zero

locus of $G_3(s)$ to the zeros of $T_3(s)$ at the origin is determined to be -90° and 90° . This can be seen in Fig 3-5i2. However, for the limiting case when $\kappa = -\eta^2$, the zero of $T_3(s)$ on the positive real axis moves to the origin (leading to three zeros of $T_3(s)$ at the origin) . For this case, the angle of arrival for the positive zero locus of $G_3(s)$ to the zeros of $T_3(s)$ at the origin is determined to be -120° , 0° and 120° and the angle of arrival for the negative zero locus of $G_3(s)$ to the zeros of $T_3(s)$ at the origin is determined to be -60° , 60° and 180° . This can be seen in Fig 3-5i1.

Based on all these facts, we can conclude that for case (i), Scenario II and Scenario V are possible for the zero locus of $G_3(s)$ to meet the positive real axis. The table below shows which of the above facts were used to eliminate the scenarios that are not possible for both $\alpha_v > 0$ and $\alpha_v < 0$.

Sign of α_v	Scenario I	Scenario II	Scenario III	Scenario IV	Scenario V
$\alpha_v > 0$	5	4	4	4	-
$\alpha_v < 0$	5	-	1,2	1,2	-

Table 3- 23 Facts used to eliminate different scenarios for meeting points of the zero locus of $G_3(s)$ on the positive real axis that are not possible for case (i)

Parameter Range of κ : ($-\eta^2 < \kappa < 0$)

Condition II: $b^2 - 4ac \geq 0$ AND $\frac{-b + \sqrt{b^2 - 4ac}}{2a} < 0$ (From Eq.(3-32))

Note that for $-\eta^2 < \kappa < 0$ and $\eta < 1$ (because we have assumed $\omega_u < \omega_v$ without any loss of generality), the following inequality holds true:

$$-\frac{\kappa}{\eta} < -\frac{\eta^3}{\kappa} < -\frac{\eta}{\kappa} < -\frac{1}{\kappa\eta} \quad (3-69)$$

κ	# No.	a	c	b	λ and δ	Range of χ where the signs of a, b & c are satisfied (range is hashed if it exists)	ζ_v
-	II A	$a > 0$	$c > 0$	$b > 0$	$\lambda > 0, \delta > 0$		$\zeta_v > \frac{\sqrt{\delta\lambda}}{ \lambda }$
					$\lambda > 0, \delta < 0$		No sol
					$\lambda < 0, \delta < 0$		No sol

Table 3-24 Range of χ and ζ_v for which Condition (IIA) of Eq.(3-35) is satisfied

κ	# No.	a	c	b	λ and δ	Range of χ where the signs of a, b & c are satisfied (range is hashed if it exists)	ζ_v
-	IIB & IIC	$a < 0$	$c > 0$	$b > < 0$	$\lambda > 0, \delta > 0$		No sol
					$\lambda > 0, \delta < 0$		No sol
					$\lambda < 0, \delta < 0$		No sol
					$\lambda < 0, \delta > 0$		No sol

Table 3-25 Range of χ and ζ_v for which Condition (IIB) and (IIC) of Eq.(3-35) is satisfied

κ	# No.	a	c	b	λ and δ	Range of χ where the signs of a, b & c are satisfied (range is hashed if it exists)	ζ_v
-	IID	$a < 0$	$c < 0$	$b < 0$	$\lambda > 0, \delta > 0$		No sol
					$\lambda < 0, \delta < 0$		No sol
					$\lambda < 0, \delta > 0$		No sol

Table 3-26 Range of χ and ζ_v for which Condition (IID) of Eq.(3-35) is satisfied

Condition III: $b^2 - 4ac \geq 0$ AND $\frac{-b - \sqrt{b^2 - 4ac}}{2a} < 0$

κ	# No.	a	c	b	λ and δ	Range of χ where the signs of a, b & c are satisfied (range is hashed if it exists)	ζ_v
$\eta^2 < \kappa < 0$	III A	$a > 0$	$c > 0$	$b > 0$	$\lambda > 0, \delta > 0$		$\zeta_v > \frac{\sqrt{\delta\lambda}}{ \lambda }$
					$\lambda > 0, \delta < 0$		No sol
					$\lambda < 0, \delta < 0$		No sol

Table 3-27 Range of χ and ζ_v for which Condition (IIIA) of Eq.(3-35) is satisfied

κ	# No.	a	c	b	λ and δ	Range of χ where the signs of a, b & c are satisfied (range is hashed if it exists)	ζ_v
$\eta^2 < \kappa < 0$	III B	$a > 0$	$c < 0$	$b > 0$	$\lambda > 0, \delta > 0$		$\zeta_v > \frac{\sqrt{\delta\lambda}}{ \lambda }$
					$\lambda > 0, \delta < 0$		for all values of ζ_v
					$\lambda < 0, \delta < 0$		No sol

Table 3-28 Range of χ and ζ_v for which Condition (IIIB) of Eq.(3-35) is satisfied

κ	# No.	a	c	b	λ and δ	Range of χ where the signs of a, b & c are satisfied (range is hashed if it exists)	ζ_v
$\eta^2 < \kappa < 0$	IIIC	$a < 0$	$c < 0$	$b < 0$	$\lambda > 0, \delta > 0$		No sol
					$\lambda < 0, \delta < 0$		No sol
					$\lambda < 0, \delta > 0$		No sol

Table 3-29 Range of χ and ζ_v for which Condition (IIIC) of Eq.(3-35) is satisfied

κ	# No.	a	c	b	λ and δ	Range of χ where the signs of a, b & c are satisfied (range is hashed if it exists)	ζ_v
$-\eta^2 < \kappa < 0$	III D	$a > 0$	$c < 0$	$b < 0$	$\lambda > 0, \delta > 0$		$\zeta_v < \frac{\sqrt{\delta\lambda}}{ \lambda }$
					$\lambda < 0, \delta < 0$		No sol
					$\lambda < 0, \delta > 0$		No sol

Table 3-30 Range of χ and ζ_v for which Condition (IIID) of Eq.(3-35) is satisfied

For the parameter range of $(-\eta^2 \leq \kappa \leq 0)$, Table 3-2, Table 3-24 – Table 3-26, and Table 3-27 – Table 3-30 provide the solution for Condition I, Condition II and Condition III of Eq.(3-32) respectively. Based on these tables, we can provide the following parameter ranges of χ and ζ_v :

j) $\chi \leq -\frac{\kappa}{\eta}$

Based on Eq.(3-69) and Table 3-2, Condition I of Eq.(3-32) is not true for this range of χ . Based on Table 3-24 – Table 3-26, Condition II of Eq.(3-32) is also not true for this range of χ . Similarly, based on Table 3-27 – Table 3-30, Condition III of Eq.(3-32) is also not true for this range of χ . This implies that the zero locus of $G_3(s)$ will cross the imaginary axis at two sets of conjugate locations at $\alpha_v = \alpha_{v1}^{img}$ and $\alpha_v = \alpha_{v2}^{img}$ (given in Eq.(3-33)) as shown in Fig 3-5j1, Fig 3-5j2 and Fig 3-5j3.

In order to ascertain the sign of α_{v1}^{img} and α_{v2}^{img} , we plot the zero locus of $G_3(s)$ numerically for certain values of system parameters that satisfy the condition $(-\eta^2 < \kappa < 0)$ and $(\chi \leq -\kappa/\eta)$. Comparing the two distinct values of α_v (where the zero locus crosses the imaginary

axis) from the numerically plotted zero locus with the values of α_{v1}^{img} and α_{v2}^{img} from Eq.(3-33) leads to the observation that $\alpha_{v1}^{img} > 0$ and $\alpha_{v2}^{img} < 0$. Although this observation has been made numerically for one set of system parameters that satisfy the condition $(-\eta^2 < \kappa < 0)$ and $(\chi \leq -\kappa/\eta)$, it holds true for any combination of system parameters that satisfy $(-\eta^2 < \kappa < 0)$ and $(\chi \leq -\kappa/\eta)$. The proof for this is as follows: The expression for α_{v1}^{img} and α_{v2}^{img} are given by Eq.(3-33). From numerical simulation, we observed that $\alpha_{v1}^{img} > 0$ and $\alpha_{v2}^{img} < 0$ for one set of system parameters that satisfy the condition $(-\eta^2 < \kappa < 0)$ and $(\chi \leq -\kappa/\eta)$. If α_{v1}^{img} and α_{v2}^{img} have to change sign for another set of system parameters that satisfy the condition $(-\eta^2 < \kappa < 0)$ and $(\chi \leq -\kappa/\eta)$, then either the numerator or the denominator of α_{v1}^{img} and α_{v2}^{img} should change signs but not both at the same time. If the numerators of α_{v1}^{img} and α_{v2}^{img} have to change sign then they will have to pass through 0 for some set of system parameters that satisfy the condition $(-\eta^2 < \kappa < 0)$ and $(\chi \leq -\kappa/\eta)$. This would mean that α_{v1}^{img} and α_{v2}^{img} will have to be equal to 0 for this set of system parameters. However, if α_{v1}^{img} and α_{v2}^{img} are equal to 0, this means that for $\alpha_v = 0$ the zero locus should cross the imaginary axis. But for $\alpha_v = 0$ the zero locus passes through the damped poles that lie strictly on the open left half s -plane and not on the imaginary axis as shown in Fig 3-5j1, Fig 3-5j2 and Fig 3-5j3. Therefore, α_{v1}^{img} and α_{v2}^{img} cannot be equal to 0. Hence the numerators of α_{v1}^{img} and α_{v2}^{img} cannot change signs. The denominator of α_{v1}^{img} and α_{v2}^{img} cannot change sign because $\chi \leq -\kappa/\eta$ for any set of system parameters that satisfy $(-\eta^2 < \kappa < 0)$ and $(\chi \leq -\kappa/\eta)$ (refer to Eq.(3-69)). When χ is equal to $-\kappa/\eta$, it is seen from numerical simulation that α_{v1}^{img} and α_{v2}^{img} have finite values such that $\alpha_{v1}^{img} > 0$ and $\alpha_{v2}^{img} < 0$. Hence, α_{v1}^{img} and α_{v2}^{img} cannot change signs for any set of system parameters that satisfy the condition $(-\eta^2 < \kappa < 0)$ and

($\chi \leq -\kappa/\eta$). Therefore, $\alpha_{v1}^{img} > 0$ and $\alpha_{v2}^{img} < 0$ for any set of system parameters that satisfy the condition ($-\eta^2 < \kappa < 0$) and ($\chi \leq -\kappa/\eta$). On further investigation, it was found that there exists an upper bound on α_{v1}^{img} given by Eq.(3-61).

Now, we have completely characterized the intersection of the zero locus of $G_3(s)$ with the imaginary axis for case (j) which is depicted graphically in Fig 3-5j1, Fig 3-5j2 and Fig 3-5j3. This allows us to find sufficient condition for the elimination of only CNMP zeros for case (j) as shown below:

$$\begin{aligned} \alpha_v &\leq \alpha_{v1}^{img} \text{ if } \alpha_v > 0 \\ \alpha_v &\geq \alpha_{v2}^{img} \text{ if } \alpha_v < 0 \end{aligned} \tag{3-70}$$

Note that Eq.(3-70) is only a sufficient condition for the elimination of CNMP zeros and not a necessary one. This is evident from Fig 3-5j2 and Fig 3-5j3 where for positive $\alpha_v > \alpha_{v1}^{img}$ i.e. Eq.(3-70) is not satisfied, the zeros of $G_3(s)$ can be RNMP instead of CNMP. Therefore, in order to find the necessary and sufficient condition for the elimination of only CNMP zeros and only RNMP zeros, we characterize the intersection of the zero locus of $G_3(s)$ with the positive real axis. Zeros of $G_3(s)$ are found by setting the numerator $N_3(s)$ in Eq.(3-28) to zero. In order to find the intersection of the zero locus of $G_3(s)$ with the positive real axis, we set $s = x$ in Eq.(3-40) and find the repeated roots of Eq.(3-40). This is done by setting the discriminant in Eq.(3-40) to zero. The discriminant of the fourth order polynomial equation is given in Eq.(3-41). Eq.(3-41) leads to a 5th order polynomial in α_v which cannot be solved analytically as discussed in case(a).

Therefore, we cannot analytically characterize the intersection of the zero locus of $G_3(s)$ with the positive real axis like we did in the two-DoF case in the previous section. Therefore, it will not be possible to find the necessary and sufficient conditions for the elimination of only CNMP zeros

and only RNMP zeros for a three-DoF damped flexible system. However, we can attempt to find the number of times the zero locus meets with the positive real axis in order to provide at least some insight into how the zero locus interacts with the positive real axis.

In order to do so, we take into account certain facts that we know about the zero locus

1. The real axis is always part of the zero locus of $G_3(s)$ irrespective of whether $\alpha_v > 0$ or $\alpha_v < 0$
2. $T_3(s)$ has 2 pairs of zeros of which one pair always lies at the origin

Based on these facts, we solve for the repeated roots of $N_3(s)$ in Eq.(3-29) since when the zero locus of $G_3(s)$ meets the positive real axis, we get repeated roots in s . For a fourth order polynomial, five scenarios are possible for the meeting points of the zero locus of $G_3(s)$ with the positive real axis as described in case (a) and shown graphically in Fig 3-3. Now we have to ascertain for case (j) where the conditions $(-\eta^2 < \kappa < 0)$ and $(\chi \leq -\kappa/\eta)$ are satisfied, which of the five scenarios for the meeting point of the zero locus of $G_3(s)$ with the positive real axis are possible. In order to do so, we make use of following five facts about the zero locus:

1. Position of zeros of $T_3(s)$ - To find the location of the zeros of $T_3(s)$, as previously discussed below Eq.(3-28), the root locus of $T_3(s)$ is the zero locus of $G_3(s)$. The zeros of $T_3(s)$ are the roots of $A_3(s)$ given by Eq.(3-28). It can be observed from Eq.(3-28) that two of the zeros of $T_3(s)$ are at the origin. This is graphically depicted in Fig 3-5j1, Fig 3-5j2 and Fig 3-5j3. In order to find the location of the other zeros of $T_3(s)$, we analyze the roots of Eq.(3-63) which is derived from expression of $A_3(s)$ from Eq.(3-28). Given the condition that $(-\eta^2 < \kappa < 0)$ and $(\chi \leq -\kappa/\eta)$ and Eq.(3-69), we can conclude the following:

$$\text{Product of roots} = \frac{\omega_v^2 (\eta^2 + \kappa)}{(1 + \kappa)} > 0, \text{ Sum of roots} = -\frac{2\zeta_v \omega_v (\chi \eta + \kappa)}{(1 + \kappa)} \geq 0 \quad (3-71)$$

Therefore, based on Eq.(3-71), the roots of Eq.(3-63) will lie on the right hand side (RHS) of the imaginary axis. They can either be real or occur as a pair of complex conjugates. Fig 3-5j1, Fig 3-5j2 and Fig 3-5j3 graphically depicts the location of these zeros on the RHS of the imaginary axis.

2. Intersection of zero locus of $G_3(s)$ with the imaginary axis - We have already shown that the zero locus of $G_3(s)$ will cross the imaginary axis at two sets of conjugate locations at $\alpha_v = \alpha_{v1}^{img}$ and $\alpha_v = \alpha_{v2}^{img}$ (given in Eq.(3-33)) as shown in Fig 3-5j1, Fig 3-5j2 and Fig 3-5j3. It is also known that $\alpha_{v1}^{img} > 0$ and $\alpha_{v2}^{img} < 0$ for any set of system parameters that satisfy the condition $(-\eta^2 < \kappa < 0)$ and $(\chi \leq -\kappa/\eta)$.
3. Relative position of intersection of positive zero locus ($\alpha_v > 0$) and negative zero locus ($\alpha_v < 0$) with the imaginary axis - For case (j), from Eq.(3-46) we can say that $y_1^2 > y_2^2$. Since, from Eq.(3-37), α_{v1}^{img} corresponds to y_1^2 and α_{v2}^{img} corresponds to y_2^2 , the point of intersection of the zero locus of $G_3(s)$ corresponding to α_{v1}^{img} is higher than the point of intersection of the zero locus of $G_3(s)$ corresponding to α_{v2}^{img} .
4. Which portion of the positive real axis belongs to the positive or negative zero locus - For case (j), from Eq.(3-47), we can say that the portion of the positive real axis corresponding to α_v^∞ belongs to negative zero locus of $G_3(s)$.
5. Angle of arrival of positive and negative zero locus at the zeros of $T_3(s)$ present at the origin - For case (j), from Eq.(3-48), the angle of arrival for the positive zero locus of $G_3(s)$ to the zeros of $T_3(s)$ at the origin is determined to be -90° and 90° . The angle of arrival for the negative zero locus of $G_3(s)$ to the zeros of $T_3(s)$ at the origin is determined to be 0° and 180° .

Based on all these facts, we can conclude that for case (j), Scenario I, Scenario III and Scenario V are possible for the zero locus of $G_3(s)$ to meet the positive real axis. The table below shows which of the above facts were used to eliminate the scenarios that are not possible for both $\alpha_v > 0$ and $\alpha_v < 0$.

Sign of α_v	Scenario I	Scenario II	Scenario III	Scenario IV	Scenario V
$\alpha_v > 0$	-	4	4	4	-
$\alpha_v < 0$	-	2	-	2	-

Table 3-31 Facts used to eliminate different scenarios for meeting points of the zero locus of $G_3(s)$ on the positive real axis that are not possible for case (j)

$$\text{k) } -\frac{\kappa}{\eta} < \chi < -\frac{\eta^3}{\kappa}, \zeta_v < \zeta_{v,\min}$$

Based on Eq.(3-69) and Table 3-2, Condition I of Eq.(3-32) is not true for this range of χ . Based on Table 3-24 – Table 3-26, Condition II of Eq.(3-32) is also not true for this range of χ . Similarly, based on Table 3-27 – Table 3-30, Condition III of Eq.(3-32) is also not true for this range of χ and ζ_v . This implies that the zero locus of $G_3(s)$ will cross the imaginary axis at two sets of conjugate locations at $\alpha_v = \alpha_{v1}^{img}$ and $\alpha_v = \alpha_{v2}^{img}$ (given in Eq.(3-33)) as shown in Fig 3-5k.

In order to ascertain the sign of α_{v1}^{img} and α_{v2}^{img} , we plot the zero locus of $G_3(s)$ numerically for certain values of system parameters that satisfy the condition $(-\eta^2 < \kappa < 0)$ and $(-\kappa/\eta < \chi < -\eta^3/\kappa, \zeta_v < \zeta_{v,\min})$. Comparing the two distinct values of α_v (where the zero locus crosses the imaginary axis) from the numerically plotted zero locus with the values of α_{v1}^{img} and α_{v2}^{img} from Eq.(3-33) leads to the observation that $\alpha_{v1}^{img} > 0$ and $\alpha_{v2}^{img} > 0$. Although this observation has been made numerically for one set of system parameters that satisfy the condition

$(-\eta^2 < \kappa < 0)$ and $(-\kappa/\eta < \chi < -\eta^3/\kappa, \zeta_v < \zeta_{v,min})$, it holds true for any combination of system parameters that satisfy $(-\eta^2 < \kappa < 0)$ and $(-\kappa/\eta < \chi < -\eta^3/\kappa, \zeta_v < \zeta_{v,min})$. The proof for this is as follows: The expression for α_{v1}^{img} and α_{v2}^{img} are given by Eq.(3-33). From numerical simulation, we observed that $\alpha_{v1}^{img} > 0$ and $\alpha_{v2}^{img} > 0$ for one set of system parameters that satisfy the condition $(-\eta^2 < \kappa < 0)$ and $(-\kappa/\eta < \chi < -\eta^3/\kappa, \zeta_v < \zeta_{v,min})$. If α_{v1}^{img} and α_{v2}^{img} have to change sign for another set of system parameters that satisfy the condition $(-\eta^2 < \kappa < 0)$ and $(-\kappa/\eta < \chi < -\eta^3/\kappa, \zeta_v < \zeta_{v,min})$, then either the numerator or the denominator of α_{v1}^{img} and α_{v2}^{img} should change signs but not both at the same time. If the numerators of α_{v1}^{img} and α_{v2}^{img} have to change sign then they will have to pass through 0 for some set of system parameters that satisfy the condition $(-\eta^2 < \kappa < 0)$ and $(-\kappa/\eta < \chi < -\eta^3/\kappa, \zeta_v < \zeta_{v,min})$. This would mean that α_{v1}^{img} and α_{v2}^{img} will have to be equal to 0 for this set of system parameters. However, if α_{v1}^{img} and α_{v2}^{img} are equal to 0, this means that for $\alpha_v = 0$ the zero locus should cross the imaginary axis. But for $\alpha_v = 0$ the zero locus passes through the damped poles that lie strictly on the open left half s -plane and not on the imaginary axis as shown in Fig 3-5k. Therefore, α_{v1}^{img} and α_{v2}^{img} cannot be equal to 0. Hence the numerators of α_{v1}^{img} and α_{v2}^{img} cannot change signs. The denominator of α_{v1}^{img} and α_{v2}^{img} cannot change sign because $\chi > -\kappa/\eta$ for any set of system parameters that satisfy $(-\eta^2 < \kappa < 0)$ and $(-\kappa/\eta < \chi < -\eta^3/\kappa, \zeta_v < \zeta_{v,min})$ (refer to Eq.(3-69)). Hence, α_{v1}^{img} and α_{v2}^{img} cannot change signs for any set of system parameters that satisfy the condition $(-\eta^2 < \kappa < 0)$ and $(-\kappa/\eta < \chi < -\eta^3/\kappa, \zeta_v < \zeta_{v,min})$. Therefore, $\alpha_{v1}^{img} > 0$ and $\alpha_{v2}^{img} > 0$ for any set of system parameters that satisfy the condition $(-\eta^2 < \kappa < 0)$ and $(-\kappa/\eta < \chi < -\eta^3/\kappa, \zeta_v < \zeta_{v,min})$. On further investigation, it was found that there exists an upper bound on α_{v1}^{img} given by Eq.(3-57).

Now, we have completely characterized the intersection of the zero locus of $G_3(s)$ with the imaginary axis for case (k) which is depicted graphically in Fig 3-5k. This allows us to find sufficient condition for the elimination of only CNMP zeros for case (k) as shown below:

$$\begin{aligned} \alpha_v \leq \alpha_{v1}^{img} \text{ AND } \alpha_v \geq \alpha_{v2}^{img} \text{ if } \alpha_v > 0 \\ \alpha_v < 0 \end{aligned} \quad (3-72)$$

Note that Eq.(3-72) is only a sufficient condition for the elimination of CNMP zeros and not a necessary one. This is evident from Fig 3-5k where for positive $\alpha_v > \alpha_{v1}^{img}$ i.e. Eq.(3-72) is not satisfied, the zeros of $G_3(s)$ can be RNMP instead of CNMP. Therefore, in order to find the necessary and sufficient condition for the elimination of only CNMP zeros and only RNMP zeros, we characterize the intersection of the zero locus of $G_3(s)$ with the positive real axis. Zeros of $G_3(s)$ are found by setting the numerator $N_3(s)$ in Eq.(3-28) to zero. In order to find the intersection of the zero locus of $G_3(s)$ with the positive real axis, we set $s = x$ in Eq.(3-40) and find the repeated roots of Eq.(3-40). This is done by setting the discriminant in Eq.(3-40) to zero. The discriminant of the fourth order polynomial equation is given in Eq.(3-41). Eq.(3-41) leads to a 5th order polynomial in α_v which cannot be solved analytically as discussed in case(a).

Therefore, we cannot analytically characterize the intersection of the zero locus of $G_3(s)$ with the positive real axis like we did in the two-DoF case in the previous section. Therefore, it will not be possible to find the necessary and sufficient conditions for the elimination of only CNMP zeros and only RNMP zeros for a three-DoF damped flexible system. However, we can attempt to find the number of times the zero locus meets with the positive real axis in order to provide at least some insight into how the zero locus interacts with the positive real axis.

In order to do so, we take into account certain facts that we know about the zero locus

1. The real axis is always part of the zero locus of $G_3(s)$ irrespective of whether $\alpha_v > 0$ or $\alpha_v < 0$

2. $T_3(s)$ has 2 pairs of zeros of which one pair always lies at the origin

Based on these facts, we solve for the repeated roots of $N_3(s)$ in Eq.(3-28) since when the zero locus of $G_3(s)$ meets the positive real axis, we get repeated roots in s . For a fourth order polynomial, five scenarios are possible for the meeting points of the zero locus of $G_3(s)$ with the positive real axis as described in case (a) and shown graphically in Fig 3-3. Now we have to ascertain for case (k) where the conditions $(-\eta^2 < \kappa < 0)$ and $(-\kappa/\eta < \chi < -\eta^3/\kappa, \zeta_v < \zeta_{v,min})$ are satisfied, which of the five scenarios for the meeting point of the zero locus of $G_3(s)$ with the positive real axis are possible. In order to do so, we make use of following five facts about the zero locus:

1. Position of zeros of $T_3(s)$ - To find the location of the zeros of $T_3(s)$, as previously discussed below Eq.(3-28), the root locus of $T_3(s)$ is the zero locus of $G_3(s)$. The zeros of $T_3(s)$ are the roots of $A_3(s)$ given by Eq.(3-28). It can be observed from Eq.(3-28) that two of the zeros of $T_3(s)$ are at the origin. This is graphically depicted in Fig 3-5k. In order to find the location of the other zeros of $T_3(s)$, we analyze the roots of Eq.(3-63) which is derived from expression of $A_3(s)$ from Eq.(3-28). Given the condition that $(-\eta^2 < \kappa < 0)$ and $(-\kappa/\eta < \chi < -\eta^3/\kappa, \zeta_v < \zeta_{v,min})$ and Eq.(3-69), we can conclude the following:

$$\text{Product of roots} = \frac{\omega_v^2 (\eta^2 + \kappa)}{(1 + \kappa)} > 0, \text{ Sum of roots} = -\frac{2\zeta_v \omega_v (\chi \eta + \kappa)}{(1 + \kappa)} < 0 \quad (3-73)$$

Therefore, based on Eq.(3-73), the roots of Eq.(3-63) will lie on the left hand side (LHS) of the imaginary axis. They can either be real or occur as a pair of complex conjugates. Fig 3-5k graphically depicts the location of these zeros on the LHS of the imaginary axis.

2. Intersection of zero locus of $G_3(s)$ with the imaginary axis - We have already shown that the zero locus of $G_3(s)$ will cross the imaginary axis at two sets of conjugate locations at $\alpha_v = \alpha_{v1}^{img}$ and $\alpha_v = \alpha_{v2}^{img}$ (given in Eq.(3-33)) as shown in Fig 3-5k. It is also known that $\alpha_{v1}^{img} > 0$ and

$\alpha_{v2}^{img} > 0$ for any set of system parameters that satisfy the condition $(-\eta^2 < \kappa < 0)$ and $(-\kappa/\eta < \chi < -\eta^3/\kappa, \zeta_v < \zeta_{v,min})$.

3. Relative position of intersection of positive zero locus ($\alpha_v > 0$) and negative zero locus ($\alpha_v < 0$) with the imaginary axis - For case (k), from Eq.(3-46) we can say that $y_1^2 > y_2^2$. Since, from Eq.(3-37), α_{v1}^{img} corresponds to y_1^2 and α_{v2}^{img} corresponds to y_2^2 , the point of intersection of the zero locus of $G_3(s)$ corresponding to α_{v1}^{img} is higher than the point of intersection of the zero locus of $G_3(s)$ corresponding to α_{v2}^{img} .
4. Which portion of the positive real axis belongs to the positive or negative zero locus - For case (k), from Eq.(3-47), we can say that the portion of the positive real axis corresponding to α_v^∞ belongs to negative zero locus of $G_3(s)$. Further, since there are no zeros of $T_3(s)$ lying on the positive real axis, the entire positive real axis is covered by the negative zero locus of $G_3(s)$.
5. Angle of arrival of positive and negative zero locus at the zeros of $T_3(s)$ present at the origin - For case (c), from Eq.(3-48), the angle of arrival for the positive zero locus of $G_3(s)$ to the zeros of $T_3(s)$ at the origin is determined to be -90° and 90° . The angle of arrival for the negative zero locus of $G_3(s)$ to the zeros of $T_3(s)$ at the origin is determined to be 0° and 180° .

Based on all these facts, we can conclude that for case (k), Scenario I is possible for the zero locus of $G_3(s)$ to meet the positive real axis. The table below shows which of the above facts were used to eliminate the scenarios that are not possible for both $\alpha_v > 0$ and $\alpha_v < 0$.

Sign of α_v	Scenario I	Scenario II	Scenario III	Scenario IV	Scenario V
$\alpha_v > 0$	-	4	4	4	4
$\alpha_v < 0$	-	2	2	2	2

Table 3-32 Facts used to eliminate different scenarios for meeting points of the zero locus of

$G_3(s)$ on the positive real axis that are not possible for case (k)

$$1) \quad -\frac{\kappa}{\eta} < \chi < -\frac{\eta^3}{\kappa}, \zeta_v = \zeta_{v,\min}$$

Based on Eq.(3-69) and Table 3-2, Condition I of Eq.(3-32) is not true for this range of χ . Based on Table 3-24 – Table 3-26, Condition II of Eq.(3-32) is also not true for this range of χ . Similarly, based on Table 3-27 – Table 3-30, Condition III of Eq.(3-32) is also not true for this range of χ and ζ_v . This implies that the zero locus of $G_3(s)$ will cross the imaginary axis at two sets of conjugate locations at $\alpha_v = \alpha_{v1}^{img}$ and $\alpha_v = \alpha_{v2}^{img}$ (given in Eq.(3-33)) as shown in Fig 3-51. However, we see that this is a limiting case where the zero locus goes from crossing the imaginary axis to not crossing the imaginary axis as ζ_v becomes greater than $\zeta_{v,\min}$. Hence, $\alpha_{v1}^{img} = \alpha_{v2}^{img}$ and the two sets of conjugate locations where the zero locus of $G_3(s)$ crosses the imaginary axis are the same.

In order to ascertain the sign of α_{v1}^{img} and α_{v2}^{img} , we plot the zero locus of $G_3(s)$ numerically for certain values of system parameters that satisfy the condition $(-\eta^2 < \kappa < 0)$ and $(-\kappa/\eta < \chi < -\eta^3/\kappa, \zeta_v = \zeta_{v,\min})$. Comparing the two distinct values of α_v (where the zero locus crosses the imaginary axis) from the numerically plotted zero locus with the values of α_{v1}^{img} and α_{v2}^{img} from Eq.(3-33) leads to the observation that $\alpha_{v1}^{img} > 0$ and $\alpha_{v2}^{img} > 0$. Although this observation has been made numerically for one set of system parameters that satisfy the condition

$(-\eta^2 < \kappa < 0)$ and $(-\kappa/\eta < \chi < -\eta^3/\kappa, \zeta_v = \zeta_{v,min})$, it holds true for any combination of system parameters that satisfy $(-\eta^2 < \kappa < 0)$ and $(-\kappa/\eta < \chi < -\eta^3/\kappa, \zeta_v = \zeta_{v,min})$. The proof for this is as follows: The expression for α_{v1}^{img} and α_{v2}^{img} are given by Eq.(3-33). From numerical simulation, we observed that $\alpha_{v1}^{img} > 0$ and $\alpha_{v2}^{img} > 0$ for one set of system parameters that satisfy the condition $(-\eta^2 < \kappa < 0)$ and $(-\kappa/\eta < \chi < -\eta^3/\kappa, \zeta_v = \zeta_{v,min})$. If α_{v1}^{img} and α_{v2}^{img} have to change sign for another set of system parameters that satisfy the condition $(-\eta^2 < \kappa < 0)$ and $(-\kappa/\eta < \chi < -\eta^3/\kappa, \zeta_v = \zeta_{v,min})$, then either the numerator or the denominator of α_{v1}^{img} and α_{v2}^{img} should change signs but not both at the same time. If the numerators of α_{v1}^{img} and α_{v2}^{img} have to change sign then they will have to pass through 0 for some set of system parameters that satisfy the condition $(-\eta^2 < \kappa < 0)$ and $(-\kappa/\eta < \chi < -\eta^3/\kappa, \zeta_v = \zeta_{v,min})$. This would mean that α_{v1}^{img} and α_{v2}^{img} will have to be equal to 0 for this set of system parameters. However, if α_{v1}^{img} and α_{v2}^{img} are equal to 0, this means that for $\alpha_v = 0$ the zero locus should cross the imaginary axis. But for $\alpha_v = 0$ the zero locus passes through the damped poles that lie strictly on the open left half s -plane and not on the imaginary axis as shown in Fig 3-51. Therefore, α_{v1}^{img} and α_{v2}^{img} cannot be equal to 0. Hence the numerators of α_{v1}^{img} and α_{v2}^{img} cannot change signs. The denominator of α_{v1}^{img} and α_{v2}^{img} cannot change sign because $\chi > -\kappa/\eta$ for any set of system parameters that satisfy $(-\eta^2 < \kappa < 0)$ and $(-\kappa/\eta < \chi < -\eta^3/\kappa, \zeta_v = \zeta_{v,min})$ (refer to Eq.(3-69)). Hence, α_{v1}^{img} and α_{v2}^{img} cannot change signs for any set of system parameters that satisfy the condition $(-\eta^2 < \kappa < 0)$ and $(-\kappa/\eta < \chi < -\eta^3/\kappa, \zeta_v = \zeta_{v,min})$. Therefore, $\alpha_{v1}^{img} > 0$ and $\alpha_{v2}^{img} > 0$ for any set of system parameters that satisfy the condition $(-\eta^2 < \kappa < 0)$ and $(-\kappa/\eta < \chi < -\eta^3/\kappa, \zeta_v = \zeta_{v,min})$. On further investigation, it was found that there exists an upper bound on α_{v1}^{img} given by Eq.(3-57).

Now, we have completely characterized the intersection of the zero locus of $G_3(s)$ with the imaginary axis for case (l) which is depicted graphically in Fig 3-51. This allows us to find sufficient and necessary condition for the elimination of only CNMP zeros for case (l) as shown below:

$$\begin{aligned}\alpha_v &\geq 0 \\ \alpha_v &\leq 0\end{aligned}\tag{3-74}$$

Note that Eq.(3-74) is a sufficient and necessary condition for the elimination of only CNMP zeros. This is evident from Fig 3-51 where Eq.(3-74) is always satisfied. For this case, we can also find necessary and sufficient conditions for the elimination of only RNMP zeros. From Fig 3-51, it is evident that when $\alpha_v < \alpha_v^\infty$, the zero locus of $G_3(s)$ approaches negative infinity along the real axis and flips over to positive infinity thereby leading to RNMP zeros. This allows us to find sufficient condition for the elimination of only RNMP zeros for case (n) as shown below:

$$\alpha_v > \alpha_v^\infty\tag{3-75}$$

Since the two sets of conjugate locations where the zero locus of $G_3(s)$ crosses the imaginary axis are the same, the zero locus of $G_3(s)$ goes back to the left-hand side (LHS) of imaginary axis after touching the imaginary axis. Therefore, since there are no CNMP zeros present for this case, only Scenario I is possible for the meeting point of the zero locus of $G_3(s)$ with the positive real axis.

$$\text{m) } -\frac{\kappa}{\eta} < \chi < -\frac{\eta^3}{\kappa}, \zeta_v > \zeta_{v,\min}$$

Based on Eq.(3-69) and Table 3-2, Condition I of Eq.(3-32) is true for this range of χ . Based on Table 3-24 – Table 3-26, Condition II of Eq.(3-32) is also true for this range of χ . Similarly, based on Table 3-27 – Table 3-30, Condition III of Eq.(3-32) is also true for this range of χ and ζ_v . This

implies that the zero locus of $G_3(s)$ will not cross the imaginary axis as shown in Fig 3-5m. This allows us to find sufficient condition for the elimination of only CNMP zeros for case (m) as shown below:

$$\begin{aligned}\alpha_v &\geq 0 \\ \alpha_v &\leq 0\end{aligned}\tag{3-76}$$

Note that Eq.(3-76) is a sufficient and necessary condition for the elimination of only CNMP zeros. For this case, we can also find necessary and sufficient conditions for the elimination of only RNMP zeros. From Fig 3-5m, it is evident that when $\alpha_v < \alpha_v^\infty$, the zero locus of $G_3(s)$ approaches negative infinity along the real axis and flips over to positive infinity thereby leading to RNMP zeros. This allows us to find sufficient condition for the elimination of only RNMP zeros for case (m) as shown below:

$$\alpha_v > \alpha_v^\infty\tag{3-77}$$

Since there are no CNMP zeros present for this case, only Scenario I is possible for the meeting point of the zero locus of $G_3(s)$ with the positive real axis.

$$\text{n) } -\frac{\eta^3}{\kappa} \leq \chi \leq -\frac{1}{\kappa\eta}$$

Based on Eq.(3-69) and Table 3-2, Condition I of Eq.(3-32) is not true for this range of χ . Based on Table 3-24 – Table 3-26, Condition II of Eq.(3-32) is also not true for this range of χ . Based on Table 3-27 – Table 3-30, Condition III of Eq.(3-32) is true for this range of χ . This implies that the zero locus of $G_3(s)$ will cross the imaginary axis at one set of conjugate locations at $\alpha_v = \alpha_v^{img}$ (given in Eq.(3-33)) as shown in Fig 3-5n.

In order to ascertain the sign of α_{vI}^{img} , we plot the zero locus of $G_3(s)$ numerically for certain values of systems parameters that satisfy the condition $(-\eta^2 < \kappa < 0)$ and $(-\eta^3/\kappa \leq \chi \leq -1/\kappa\eta)$. Comparing the value of α_v (where the zero locus crosses the imaginary axis) from the numerically plotted zero locus with the values of α_{vI}^{img} from Eq.(3-33) leads to the observation that $\alpha_{vI}^{img} > 0$. Although this observation has been made numerically for one set of system parameters that satisfy the condition $(-\eta^2 < \kappa < 0)$ and $(-\eta^3/\kappa \leq \chi \leq -1/\kappa\eta)$, it holds true for any combination of system parameters that satisfy $(-\eta^2 < \kappa < 0)$ and $(-\eta^3/\kappa \leq \chi \leq -1/\kappa\eta)$. The proof for this is as follows: The expression for α_{vI}^{img} is given by Eq.(3-33). From numerical simulation, we observed that $\alpha_{vI}^{img} > 0$ for one set of system parameters that satisfy the condition $(-\eta^2 < \kappa < 0)$ and $(-\eta^3/\kappa \leq \chi \leq -1/\kappa\eta)$. If α_{vI}^{img} has to change sign for another set of system parameters that satisfy the condition $(-\eta^2 < \kappa < 0)$ and $(-\eta^3/\kappa \leq \chi \leq -1/\kappa\eta)$, then either the numerator or the denominator of α_{vI}^{img} should change sign but not both at the same time. If the numerator of α_{vI}^{img} has to change sign, then it will have to pass through 0 for some set of system parameters that satisfy the condition $(-\eta^2 < \kappa < 0)$ and $(-\eta^3/\kappa \leq \chi \leq -1/\kappa\eta)$. This would mean that α_{vI}^{img} will have to be equal to 0 for this set of system parameters. However, if α_{vI}^{img} is equal to 0, this means that for $\alpha_v = 0$ the zero locus should cross the imaginary axis. But for $\alpha_v = 0$ the zero locus passes through the damped poles that lie strictly on the open left half s -plane and not on the imaginary axis as shown in Fig 3-5n. Therefore, α_{vI}^{img} cannot be equal to 0. Hence the numerator of α_{vI}^{img} cannot change sign. The denominator of α_{vI}^{img} cannot change sign because $\chi > -\kappa/\eta$ for any set of system parameters that satisfy $(-\eta^2 < \kappa < 0)$ and $(-\eta^3/\kappa \leq \chi \leq -1/\kappa\eta)$ (refer to Eq.(3-69)). Hence, α_{vI}^{img} cannot change sign for any set of system

parameters that satisfy the condition $(-\eta^2 < \kappa < 0)$ and $(-\eta^3/\kappa \leq \chi \leq -1/\kappa\eta)$. Therefore, $\alpha_{v1}^{img} > 0$ for any set of system parameters that satisfy the condition $(-\eta^2 < \kappa < 0)$ and $(-\eta^3/\kappa \leq \chi \leq -1/\kappa\eta)$. On further investigation, it was found that there exists an upper bound on α_{v1}^{img} given by Eq.(3-57).

Now, we have completely characterized the intersection of the zero locus of $G_3(s)$ with the imaginary axis for case (n) which is depicted graphically in Fig 3-5n. This allows us to find sufficient condition for the elimination of only CNMP zeros for case (n) as shown below:

$$\begin{aligned} \alpha_v &\leq \alpha_{v1}^{img} \text{ if } \alpha_v > 0 \\ \alpha_v &< 0 \end{aligned} \tag{3-78}$$

Note that Eq.(3-78) is only a sufficient condition for the elimination of CNMP zeros and not a necessary one. This is evident from Fig 3-5n where for positive $\alpha_v > \alpha_{v1}^{img}$ i.e. Eq.(3-78) is not satisfied, the zeros of $G_3(s)$ can be RNMP instead of CNMP. Therefore, in order to find the necessary and sufficient condition for the elimination of only CNMP zeros and only RNMP zeros, we characterize the intersection of the zero locus of $G_3(s)$ with the positive real axis. Zeros of $G_3(s)$ are found by setting the numerator $N_3(s)$ in Eq.(3-28) to zero. In order to find the intersection of the zero locus of $G_3(s)$ with the positive real axis, we set $s = x$ in Eq.(3-40) and find the repeated roots of Eq.(3-40). This is done by setting the discriminant in Eq.(3-40) to zero. The discriminant of the fourth order polynomial equation is given in Eq.(3-41). Eq.(3-41) leads to a 5th order polynomial in α_v which cannot be solved analytically as discussed in case(a).

Therefore, we cannot analytically characterize the intersection of the zero locus of $G_3(s)$ with the positive real axis like we did in the two-DoF case in the previous section. Therefore, it will not be possible to find the necessary and sufficient conditions for the elimination of only CNMP zeros

and only RNMP zeros for a three-DoF damped flexible system. However, we can attempt to find the number of times the zero locus meets with the positive real axis in order to provide at least some insight into how the zero locus interacts with the positive real axis.

In order to do so, we take into account certain facts that we know about the zero locus

1. The real axis is always part of the zero locus of $G_3(s)$ irrespective of whether $\alpha_v > 0$ or $\alpha_v < 0$
2. $T_3(s)$ has 2 pairs of zeros of which one pair always lies at the origin

Based on these facts, we solve for the repeated roots of $N_3(s)$ in Eq.(3-28) since when the zero locus of $G_3(s)$ meets the positive real axis, we get repeated roots in s . For a fourth order polynomial, five scenarios are possible for the meeting points of the zero locus of $G_3(s)$ with the positive real axis as described in case (a) and shown graphically in Fig 3-3. Now we have to ascertain for case (n) where the conditions $(-\eta^2 < \kappa < 0)$ and $(-\eta^3/\kappa \leq \chi \leq -1/\kappa\eta)$ are satisfied, which of the five scenarios for the meeting point of the zero locus of $G_3(s)$ with the positive real axis are possible. In order to do so, we make use of following five facts about the zero locus:

1. Position of zeros of $T_3(s)$ - To find the location of the zeros of $T_3(s)$, as previously discussed below Eq.(3-28), the root locus of $T_3(s)$ is the zero locus of $G_3(s)$. The zeros of $T_3(s)$ are the roots of $A_3(s)$ given by Eq.(3-28). It can be observed from Eq.(3-28) that two of the zeros of $T_3(s)$ are at the origin. This is graphically depicted in Fig 3-5n. In order to find the location of the other zeros of $T_3(s)$, we analyze the roots of Eq.(3-63) which is derived from expression of $A_3(s)$ from Eq.(3-28). Given the condition that $(-\eta^2 < \kappa < 0)$ and $(-\eta^3/\kappa \leq \chi \leq -1/\kappa\eta)$ and Eq.(3-69), we can conclude the following:

$$\text{Product of roots} = \frac{\omega_v^2 (\eta^2 + \kappa)}{(1 + \kappa)} > 0, \text{ Sum of roots} = -\frac{2\zeta_v \omega_v (\chi\eta + \kappa)}{(1 + \kappa)} < 0 \quad (3-79)$$

Therefore, based on Eq.(3-79), the roots of Eq.(3-63) will lie on the left hand side (LHS) of the imaginary axis. They can either be real or occur as a pair of complex conjugates. Fig 3-5n graphically depicts the location of these zeros on the LHS of the imaginary axis.

2. Intersection of zero locus of $G_3(s)$ with the imaginary axis - We have already shown that the zero locus of $G_3(s)$ will cross the imaginary axis at one set of conjugate locations at $\alpha_v = \alpha_v^{img}$ (given in Eq.(3-33)) as shown in Fig 3-5n. It is also known that $\alpha_v^{img} > 0$ for any set of system parameters that satisfy the condition $(-\eta^2 < \kappa < 0)$ and $(-\eta^3/\kappa \leq \chi \leq -1/\kappa\eta)$.
3. Which portion of the positive real axis belongs to the positive or negative zero locus - For case (n), from Eq.(3-47), we can say that the portion of the positive real axis corresponding to α_v^∞ belongs to negative zero locus of $G_3(s)$. Further, since there are no zeros of $T_3(s)$ lying on the positive real axis, the entire positive real axis is covered by the negative zero locus of $G_3(s)$.
4. Angle of arrival of positive and negative zero locus at the zeros of $T_3(s)$ present at the origin - For case (n), from Eq.(3-48), the angle of arrival for the positive zero locus of $G_3(s)$ to the zeros of $T_3(s)$ at the origin is determined to be -90° and 90° . The angle of arrival for the negative zero locus of $G_3(s)$ to the zeros of $T_3(s)$ at the origin is determined to be 0° and 180° .

Based on all these facts, we can conclude that for case (n), Scenario I is possible for the zero locus of $G_3(s)$ to meet the positive real axis. The table below shows which of the above facts were used to eliminate the scenarios that are not possible for both $\alpha_v > 0$ and $\alpha_v < 0$.

Sign of α_v	Scenario I	Scenario II	Scenario III	Scenario IV	Scenario V
$\alpha_v > 0$	-	3	3	3	3
$\alpha_v < 0$	-	2	2	2	2

Table 3-33 Facts used to eliminate different scenarios for meeting points of the zero locus of $G_3(s)$ on the positive real axis that are not possible for case (n)

o) $\chi > -\frac{1}{\kappa\eta}$

Based on Eq.(3-69) and Table 3-2, Condition I of Eq.(3-32) is not true for this range of χ . Based on Table 3-24 – Table 3-26, Condition II of Eq.(3-32) is also not true for this range of χ . Similarly, based on Table 3-27 – Table 3-30, Condition III of Eq.(3-32) is also not true for this range of χ . This implies that the zero locus of $G_3(s)$ will cross the imaginary axis at two sets of conjugate locations at $\alpha_v = \alpha_{v1}^{img}$ and $\alpha_v = \alpha_{v2}^{img}$ (given in Eq.(3-33)) as shown in Fig 3-5o.

In order to ascertain the sign of α_{v1}^{img} and α_{v2}^{img} , we plot the zero locus of $G_3(s)$ numerically for certain values of system parameters that satisfy the condition $(-\eta^2 < \kappa < 0)$ and $(\chi > -1/\kappa\eta)$. Comparing the two distinct values of α_v (where the zero locus crosses the imaginary axis) from the numerically plotted zero locus with the values of α_{v1}^{img} and α_{v2}^{img} from Eq.(3-33) leads to the observation that $\alpha_{v1}^{img} > 0$ and $\alpha_{v2}^{img} < 0$. Although this observation has been made numerically for one set of system parameters that satisfy the condition $(-\eta^2 < \kappa < 0)$ and $(\chi > -1/\kappa\eta)$, it holds true for any combination of system parameters that satisfy $(-\eta^2 < \kappa < 0)$ and $(\chi > -1/\kappa\eta)$. The proof for this as shown below: The expression for α_{v1}^{img} and α_{v2}^{img} are given by Eq.(3-33). From numerical simulation, we observed that $\alpha_{v1}^{img} > 0$ and $\alpha_{v2}^{img} < 0$ for one set of system parameters that satisfy the condition $(-\eta^2 < \kappa < 0)$ and $(\chi > -1/\kappa\eta)$. If α_{v1}^{img} and α_{v2}^{img} have to change sign for another set of system parameters that satisfy the condition $(-\eta^2 < \kappa < 0)$ and $(\chi > -1/\kappa\eta)$, then either the numerator or the denominator of α_{v1}^{img} and α_{v2}^{img} should change signs but not both at the same time. If the numerators of α_{v1}^{img} and α_{v2}^{img} have to change sign then

they will have to pass through 0 for some set of system parameters that satisfy the condition $(-\eta^2 < \kappa < 0)$ and $(\chi > -1/\kappa\eta)$. This would mean that α_{v1}^{img} and α_{v2}^{img} will have to be equal to 0 for this set of system parameters. However, if α_{v1}^{img} and α_{v2}^{img} are equal to 0, this means that for $\alpha_v = 0$ the zero locus should cross the imaginary axis. But for $\alpha_v = 0$ the zero locus passes through the damped poles that lie strictly on the open left half s -plane and not on the imaginary axis as shown in Fig 3-5o. Therefore, α_{v1}^{img} and α_{v2}^{img} cannot be equal to 0. Hence the numerators of α_{v1}^{img} and α_{v2}^{img} cannot change signs. The denominator of α_{v1}^{img} and α_{v2}^{img} cannot change sign because $\chi > -\kappa/\eta$ for any set of system parameters that satisfy $(-\eta^2 < \kappa < 0)$ and $(\chi > -1/\kappa\eta)$ (refer to Eq.(3-69)). Hence, α_{v1}^{img} and α_{v2}^{img} cannot change signs for any set of system parameters that satisfy the condition $(-\eta^2 < \kappa < 0)$ and $(\chi > -1/\kappa\eta)$. Therefore, $\alpha_{v1}^{img} > 0$ and $\alpha_{v2}^{img} < 0$ for any set of system parameters that satisfy the condition $(-\eta^2 < \kappa < 0)$ and $(\chi > -1/\kappa\eta)$. On further investigation, it was found that there exists an upper bound on α_{v1}^{img} given by Eq.(3-57).

Now, we have completely characterized the intersection of the zero locus of $G_3(s)$ with the imaginary axis for case (o) which is depicted graphically in Fig 3-5o. This allows us to find sufficient condition for the elimination of only CNMP zeros for case (o) as shown below:

$$\begin{aligned} \alpha_v &\leq \alpha_{v1}^{img} \text{ if } \alpha_v > 0 \\ \alpha_v &\geq \alpha_{v2}^{img} \text{ if } \alpha_v < 0 \end{aligned} \tag{3-80}$$

Note that Eq.(3-80) is only a sufficient condition for the elimination of CNMP zeros and not a necessary one. This is evident from Fig 3-5o where for positive $\alpha_v > \alpha_{v1}^{img}$ i.e. Eq.(3-80) is not satisfied, the zeros of $G_3(s)$ can be RNMP instead of CNMP. Therefore, in order to find the necessary and sufficient condition for the elimination of only CNMP zeros and only RNMP zeros, we characterize the intersection of the zero locus of $G_3(s)$ with the positive real axis. Zeros of $G_3(s)$

are found by setting the numerator $N_3(s)$ in Eq.(3-28) to zero. In order to find the intersection of the zero locus of $G_3(s)$ with the positive real axis, we set $s = x$ in Eq.(3-40) and find the repeated roots of Eq.(3-40). This is done by setting the discriminant in Eq.(3-40) to zero. The discriminant of the fourth order polynomial equation is given in Eq.(3-41). Eq.(3-41) leads to a 5th order polynomial in α_v which cannot be solved analytically as discussed in case(a).

Therefore, we cannot analytically characterize the intersection of the zero locus of $G_3(s)$ with the positive real axis like we did in the two-DoF case in the previous section. Therefore, it will not be possible to find the necessary and sufficient conditions for the elimination of only CNMP zeros and only RNMP zeros for a three-DoF damped flexible system. However, we can attempt to find the number of times the zero locus meets with the positive real axis in order to provide at least some insight into how the zero locus interacts with the positive real axis.

In order to do so, we take into account certain facts that we know about the zero locus

1. The real axis is always part of the zero locus of $G_3(s)$ irrespective of whether $\alpha_v > 0$ or $\alpha_v < 0$
2. $T_3(s)$ has 2 pairs of zeros of which one pair always lies at the origin

Based on these facts, we solve for the repeated roots of $N_3(s)$ in Eq.(3-28) since when the zero locus of $G_3(s)$ meets the positive real axis, we get repeated roots in s . For a fourth order polynomial, five scenarios are possible for the meeting points of the zero locus of $G_3(s)$ with the positive real axis as described in case (a) and shown graphically in Fig 3-3. Now we have to ascertain for case (o) where the conditions $(-\eta^2 < \kappa < 0)$ and $(\chi > -l/\kappa\eta)$ are satisfied, which of the five scenarios for the meeting point of the zero locus of $G_3(s)$ with the positive real axis are possible. In order to do so, we make use of following five facts about the zero locus:

1. Position of zeros of $T_3(s)$ - To find the location of the zeros of $T_3(s)$, as previously discussed below Eq.(3-28), the root locus of $T_3(s)$ is the zero locus of $G_3(s)$. The zeros of $T_3(s)$ are the

roots of $A_3(s)$ given by Eq.(3-28). It can be observed from Eq.(3-28) that two of the zeros of $T_3(s)$ are at the origin. This is graphically depicted in Fig 3-5o. In order to find the location of the other zeros of $T_3(s)$, we analyze the roots of Eq.(3-63) which is derived from expression of $A_3(s)$ from Eq.(3-28). Given the condition that $(-\eta^2 < \kappa < 0)$ and $(\chi > -1/\kappa\eta)$ and Eq.(3-69), we can conclude the following:

$$\text{Product of roots} = \frac{\omega_v^2 (\eta^2 + \kappa)}{(1 + \kappa)} > 0, \text{ Sum of roots} = -\frac{2\zeta_v \omega_v (\chi\eta + \kappa)}{(1 + \kappa)} < 0 \quad (3-81)$$

Therefore, based on Eq.(3-81), the roots of Eq.(3-63) will lie on the left hand side (LHS) of the imaginary axis. They can either be real or occur as a pair of complex conjugates. Fig 3-5o graphically depicts the location of these zeros on the LHS of the imaginary axis.

2. Intersection of zero locus of $G_3(s)$ with the imaginary axis - We have already shown that the zero locus of $G_3(s)$ will cross the imaginary axis at two set of conjugate locations at $\alpha_v = \alpha_{v1}^{img}$ and $\alpha_v = \alpha_{v2}^{img}$ (given in Eq.(3-33)) as shown in Fig 3-5o. It is also known that $\alpha_{v1}^{img} > 0$ and $\alpha_{v2}^{img} < 0$ for any set of system parameters that satisfy the condition $(-\eta^2 < \kappa < 0)$ and $(\chi > -1/\kappa\eta)$.
3. Relative position of intersection of positive zero locus ($\alpha_v > 0$) and negative zero locus ($\alpha_v < 0$) with the imaginary axis - For case (o), from Eq.(3-46) we can say that $y_1^2 < y_2^2$. Since, from Eq.(3-37), α_{v1}^{img} corresponds to y_1^2 and α_{v2}^{img} corresponds to y_2^2 , the point of intersection of the zero locus of $G_3(s)$ corresponding to α_{v2}^{img} is higher than the point of intersection of the zero locus of $G_3(s)$ corresponding to α_{v1}^{img} .
4. Which portion of the positive real axis belongs to the positive or negative zero locus - For case (o), from Eq.(3-47), we can say that the portion of the positive real axis corresponding to α_v^∞

belongs to negative zero locus of $G_3(s)$. Further, since there are no zeros of $T_3(s)$ lying on the positive real axis, the entire positive real axis is covered by the negative zero locus of $G_3(s)$.

5. Angle of arrival of positive and negative zero locus at the zeros of $T_3(s)$ present at the origin -
 For case (o), from Eq.(3-48), the angle of arrival for the positive zero locus of $G_3(s)$ to the zeros of $T_3(s)$ at the origin is determined to be -90° and 90° . The angle of arrival for the negative zero locus of $G_3(s)$ to the zeros of $T_3(s)$ at the origin is determined to be 0° and 180° .

Parameter Range of κ : $\kappa > 0$

Note that for the case of $\kappa > 0$, the sign of a , c , λ and δ will be unconditionally positive. This can be easily seen from Eq.(3-31). This reduces the number of combination of signs of a , b and c for which there are no real solutions of y . These combinations of signs are given in Eq.(3-35). We just pick those combinations from Eq.(3-35) that have $a > 0$ and $c > 0$. They happen to be IIA and IIIA for condition II and condition III respectively. Since both IIA and IIIA are exactly the same, condition II and condition III are analyzed collectively below.

κ	# No.	a	c	b	λ and δ	Range of χ where the signs of a , b & c are satisfied (range is hashed if it exists)	ζ_v
$\kappa > 0$	IIA, IIIA	$a > 0$	$c > 0$	$b > 0$	$\lambda > 0,$ $\delta > 0$	For all values of χ	$\zeta_v > \frac{\sqrt{\lambda\delta}}{ \lambda }$

Table 3-34 Range of χ and ζ_v for which Condition (IIA,IIIA) of Eq.(3-35) is satisfied

p) $\kappa > 0$

Based on Table 3-2, Condition I of Eq.(3-32) is true for this range of χ . Based on Table 3-34, Condition II and Condition III of Eq.(3-32) is also true for this range of χ . This implies that the zero locus of $G_3(s)$ will not cross the imaginary axis as shown in Fig 3-5p.

This allows us to find sufficient condition for the elimination of only CNMP zeros for case (p) as shown below:

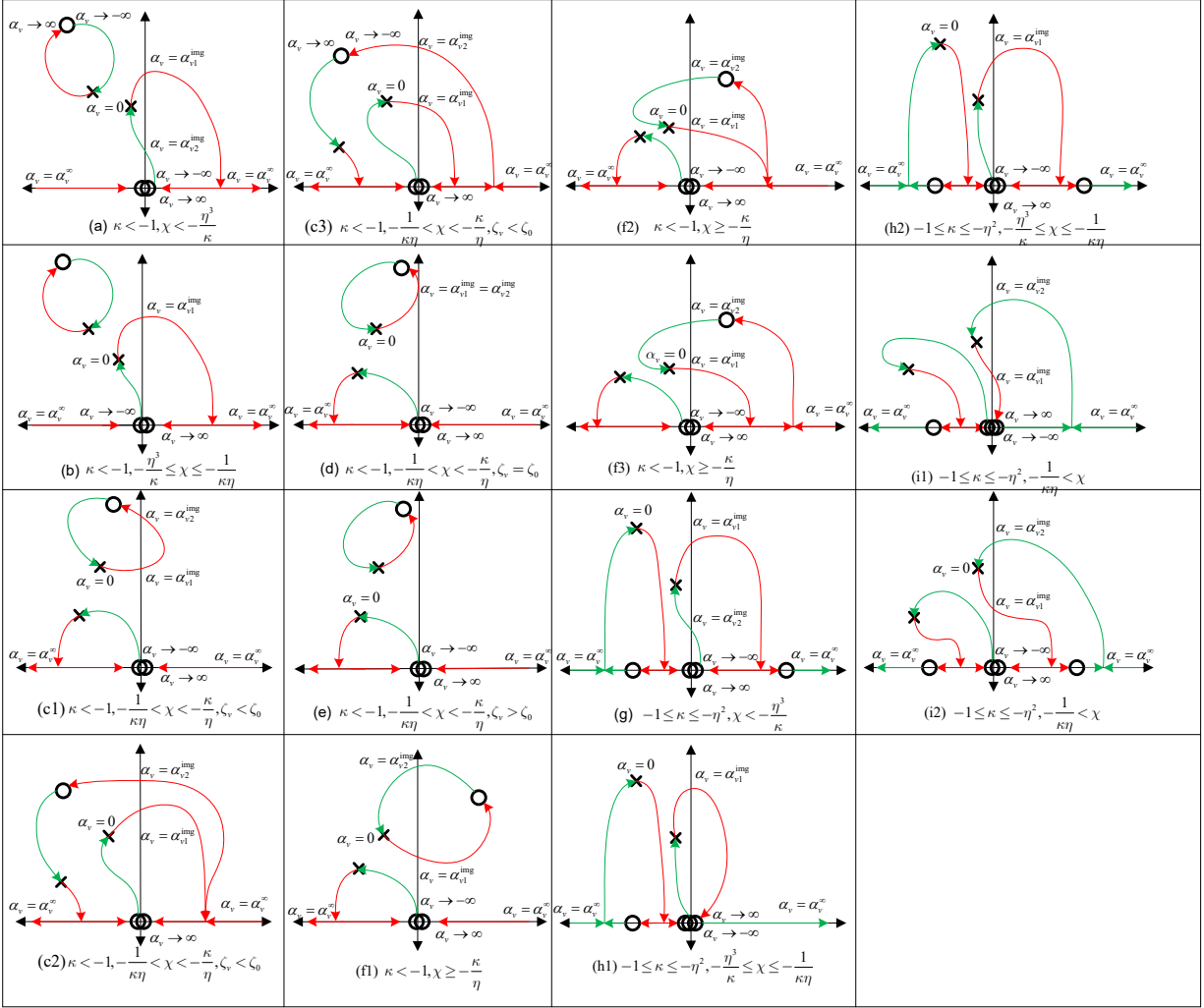
$$\begin{aligned}\alpha_v &\geq 0 \\ \alpha_v &\leq 0\end{aligned}\tag{3-82}$$

Note that Eq.(3-82) is a sufficient and necessary condition for the elimination of only CNMP zeros. For this case, we can also find necessary and sufficient conditions for the elimination of only RNMP zeros. From Fig 3-5p, it is evident that when $\alpha_v < \alpha_v^\infty$, the zero locus of $G_3(s)$ approaches negative infinity along the real axis and flips over to positive infinity thereby leading to RNMP zeros. This allows us to find sufficient condition for the elimination of only RNMP zeros for case (p) as shown below:

$$\alpha_v > \alpha_v^\infty\tag{3-83}$$

Since there are no CNMP zeros present for this case, only Scenario I is possible for the meeting point of the zero locus of $G_3(s)$ with the positive real axis.

The derivation of the parameter ranges is over.



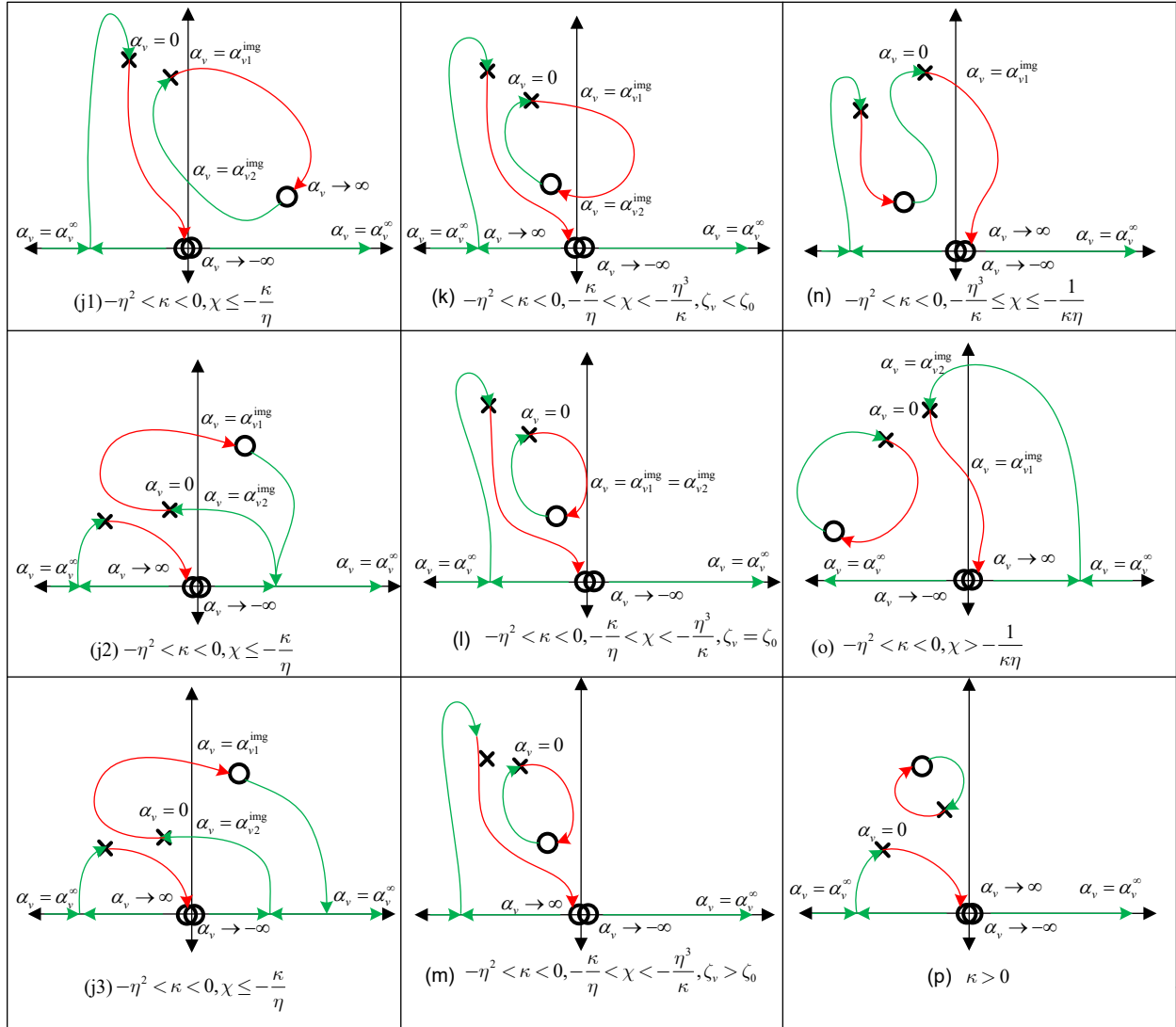


Fig 3-5 Zero Loci of $G_3(s)$ for different ranges of κ , χ and ζ_v as α_v varies from $-\infty$ to 0 (green curve) and 0 to $+\infty$ (red curve). The parameter ranges of κ , χ and ζ_v are given below each sub figure.

In each of the sub figures i.e. (a) to (p), the green curve which corresponds to the negative zero locus starts from the roots of $A_3(s)$ (represented by circle in above figure) as α_v starts from $-\infty$ and terminates at the roots of $B_3(s)$ (represented by cross in above figure) as α_v becomes equal to 0. In each of the sub figures i.e. (a) to (p), the red curve which corresponds to the positive zero

locus starts from the roots of $B_3(s)$ as α_v starts from 0 and terminates at the roots of $A_3(s)$ as α_v tends to $+\infty$. The portion of the zero locus (positive or negative) that lies strictly on the right hand side (RHS) of the imaginary axis leads to NMP zeros of $G_3(s)$. The analytical expression for α_v where the zero locus crosses the imaginary axis i.e. α_{v1}^{img} and α_{v2}^{img} is given in Eq.(3-33). The analytical expression for α_v where the zero locus tends to $+/-\infty$ on the real axis i.e. α_{v^∞} is given by Eq.(3-30).

The zero loci of Fig 3-5 span the entire range of all the parameters: κ ($-\infty$ to $+\infty$), χ (0 to $+\infty$), ζ_v (0 to $+\infty$), η (0 to $+\infty$), and α_v ($-\infty$ to $+\infty$). For example, when ($\kappa < -1$), there are six non-overlapping parameter ranges of χ and ζ_v that lead to six unique zero loci depicted by Fig 3-5a-f. In these zero loci, Fig 3-5c and Fig 3-5f is divided into three parts i.e. c1, c2, c3 and f1, f2, and f3 which depict all possible intersection of the zero locus with the positive real axis for the same parameter ranges of χ and ζ_v . The value of α_v ranges from $-\infty$ to $+\infty$ in each of these zero loci. Based on the Table 3-1, the positive zero loci in Fig 3-5 will be used to find the conditions for the eliminations of NMP zeros for the case of alternating sign of modal residues ($\alpha_v > 0$). Similarly, the negative zero loci in Fig 3-5 will be used to do the same for the case of non-alternating sign of modal residues ($\alpha_v < 0$). This separation of mathematical conditions between alternating and non-alternating modal residue signs is done to allow a direct comparison between the results obtained in this chapter and those obtained in the previous chapter for a three-DoF *undamped* flexible system.

3.5.1 Sufficient Condition for eliminating CNMP Zeros

Result 5: In a three-DoF damped flexible LTI system given by Eq.(3-26), when the signs of the modal residues are alternating (i.e. $\alpha_v > 0$), the ratio of modal residues (κ), ratio of modal damping

ratios (χ) and modal damping ratio (ζ_v) should satisfy the following inequalities to eliminate CNMP zeros for any positive value of modal residue α_v .

$$\text{Condition 5.1: } (\kappa < -1) \text{ AND } \left(-\frac{1}{\kappa\eta} < \chi < -\frac{\kappa}{\eta} \right) \text{ AND } (\zeta_v \geq \zeta_0)$$

OR

$$\text{Condition 5.2: } (-\eta^2 < \kappa < 0) \text{ AND } \left(-\frac{\kappa}{\eta} < \chi < -\frac{\eta^3}{\kappa} \right) \text{ AND } (\zeta_v \geq \zeta_0) \quad (3-84)$$

$$\text{where } \zeta_0 \triangleq \frac{\sqrt{(\kappa + \eta\chi)(\kappa\chi + \eta) - |\kappa + \eta\chi|} \sqrt{\frac{(\eta^3 + \kappa\chi)(1 + \kappa\eta\chi)}{\eta}}}{\sqrt{2\chi} |\kappa + \eta\chi|}$$

Condition 5.1 is derived from Fig 3-5(d-e). It can be seen that when the parameter ranges of κ , χ , and ζ_v in Fig 3-5(d-e) are satisfied, the positive zero loci (i.e. the red curve) do not cross the imaginary axis. Hence, for these parameter ranges, $G_3(s)$ does not exhibit CNMP zeros. Similarly, Condition 5.2 is derived from Fig 3-5(l-m). When Condition 1.1 and Condition 1.2 are not met, Fig 3-5(a-c), Fig 3-5(f-k), and Fig 3-5(n-o) depict the positive zero loci crossing the imaginary axis at non-zero frequencies, indicating the presence of CNMP zeros.

Based on **Result 5** and the red curves ($\alpha_v > 0$) in the zero loci of Fig 3-5 the following observations can be made about the CNMP zero dynamics of the three-DoF damped flexible system:

1. Each of the conditions given in **Result 5**, i.e. Condition 5.1 and Condition 5.2, is individually sufficient for the elimination of CNMP zeros. Also, these sufficient conditions are not unique or necessary. Even when these sufficient conditions are not satisfied, Fig 3-5(a-c), Fig 3-5(f-k), and Fig 3-5(n-o) show that one can guarantee the absence of CNMP zeros by selecting ranges of α_v for which the zeros never lie on the RHS of the s-plane (excluding the RHS real axis). This

requires the exact solution for α_v when the zero locus intersects with the positive real axis and it was shown in the preceding proof that it is not possible to find the closed form solution for α_v for which the zero locus intersects with the positive real axis. Hence, it is not possible to provide the sufficient and necessary condition for the elimination of CNMP zeros for a three-DoF damped flexible system. Only a few sufficient conditions i.e. Condition 5.1 and Condition 5.2 can be provided.

2. It was shown previously that for a three-DoF *undamped* flexible system with alternating modal residue signs, the sufficient and necessary condition to eliminate CNMP zeros is to tune the value of α_v such that it lies within a certain range. However, as shown in Fig 3-5d, Fig 3-5e, Fig 3-5l, Fig 3-5m and **Result 5**, the addition of viscous damping leads to sufficient conditions in terms of κ , χ , and ζ_v that guarantee the elimination of CNMP zeros for any value of α_v . Therefore, these sufficient conditions guarantee the elimination of CNMP zeros for a wider range of system parameters, especially when the modal residue α_v undergoes large variation.

Result 6: In a three-DoF damped flexible LTI system given by Eq.(3-26), when the signs of the modal residues are non-alternating (i.e. $\alpha_v < 0$), the ratio of modal residues (κ) and ratio of modal damping ratios (χ) should satisfy the following mathematical inequalities to eliminate CNMP zeros for any negative value of the modal residue α_v .

$$\text{Condition 6.1: } (\kappa < -1) \text{ AND } \left(-\frac{\eta^3}{\kappa} \leq \chi \leq -\frac{\kappa}{\eta} \right)$$

OR

$$\text{Condition 6.2: } (-1 \leq \kappa \leq -\eta^2) \text{ AND } \left(-\frac{\eta^3}{\kappa} \leq \chi \leq -\frac{1}{\kappa\eta} \right)$$

OR

(3-85)

$$\text{Condition 6.3: } (-\eta^2 < \kappa < 0) \text{ AND } \left(-\frac{\kappa}{\eta} \leq \chi \leq -\frac{1}{\kappa\eta} \right)$$

OR

$$\text{Condition 6.4: } (\kappa > 0)$$

Condition 6.1, Condition 6.2, Condition 6.3, and Condition 6.4 are derived from Fig 3-5(b-e), Fig 3-5h, Fig 3-5(k-n), Fig 3-5p respectively. When the parameter ranges in these conditions are satisfied, their corresponding negative zero loci (i.e. green curve) in Fig 3-5 do not cross the imaginary axis at non-zero frequencies. Therefore, the absence of CNMP zeros is guaranteed. When these conditions are not met, Fig 3-5a, Fig 3-5(f-g), Fig 3-5(i-j), and Fig 3-5o depict the negative zero loci crossing the imaginary axis at non-zero frequencies, indicating the presence of CNMP zeros.

Based on **Result 6** and the green curves ($\alpha_v < 0$) in the zero loci of Fig 3-5, the following observations can be made about the CNMP zero dynamics of the three-DoF damped flexible system:

1. It was shown previously that the sequence of non-alternating modal residue signs ($\alpha_R > 0$, $\alpha_u > 0$, $\alpha_v < 0$) is a sufficient condition that guarantees the elimination of CNMP zeros for any negative value of modal residue (α_v) in a three-DoF *undamped* flexible system. However, Fig 3-5a, Fig 3-5(f-g), Fig 3-5(i-j), and Fig 3-5o depict the presence of CNMP zeros for some parameter

ranges of κ and χ . This shows a potential drawback of adding viscous damping to a three-DoF *undamped* flexible system. Therefore, one key advantage of the sufficient conditions in **Result 6** is that it guarantees the elimination of CNMP zeros in the presence of viscous damping even if the modal residue (α_v) undergoes large variation.

2. Condition 6.4 is derived from Fig 3-5p and implies that the non-alternating modal residue signs is a sufficient condition that guarantees the elimination of CNMP zeros for any negative value of modal residue (α_v). This is unlike Conditions 6.1, 6.2, and 6.3, which also hold true for non-alternating modal residue signs, but they require additional conditions on χ to guarantee the elimination of CNMP zeros.

3.5.2 Sufficient and Necessary Conditions for Eliminating all NMP zeros

The sufficient conditions in **Result 5** and **Result 6** that guarantee the elimination of CNMP zeros do not guarantee the elimination of RNMP zeros. This can be seen, for example, in Fig 3-5(d-e) for alternating signs of modal residues and Fig 3-5(k-n) for non-alternating signs. In fact, in each zero locus plot of $G_3(s)$ in Fig 3-5, the positive real axis is always part of the zero locus for some range of values of α_v , which confirms the presence of RNMP zeros. In this section, we will determine the sufficient and necessary conditions for eliminating all NMP zeros i.e. CNMP *as well as* RNMP zeros such that the zeros of $G_3(s)$ always lie on or to the left of the imaginary axis. Therefore, it is indeed possible to report the sufficient and necessary condition for the elimination of all NMP zeros even in the absence of the closed form solution of α_v for which the zero locus intersects with the positive real axis. Based on Fig 3-5, **Result 7** and **Result 8** provide the sufficient and necessary conditions for the elimination of all NMP zeros for alternating and non-alternating modal residue signs, respectively.

Result 7: In a three-DoF damped flexible LTI system given by Eq.(3-26), when the modal residue signs are alternating ($\alpha_v > 0$), the following conditions are individually sufficient, and together necessary, to guarantee the elimination of all NMP zeros.

$$\text{Condition 7.1: } (\kappa < -1) \text{ AND } \left(\chi \leq -\frac{1}{\kappa\eta} \right) \text{ AND } (\alpha_v \leq \alpha_{v1}^{\text{img}})$$

OR

$$\text{Condition 7.2: } (\kappa < -1) \text{ AND } \left(-\frac{1}{\kappa\eta} < \chi < -\frac{\kappa}{\eta} \right) \text{ AND } (\zeta_v < \zeta_0) \text{ AND } \left(\begin{array}{l} \{ \alpha_v \leq \alpha_{v1}^{\text{img}} \text{ OR } \alpha_v \geq \alpha_{v2}^{\text{img}} \} \\ \text{AND } \{ \alpha_v \leq \alpha_v^\infty \} \end{array} \right)$$

OR

$$\text{Condition 7.3: } (\kappa < -1) \text{ AND } \left(-\frac{1}{\kappa\eta} < \chi < -\frac{\kappa}{\eta} \right) \text{ AND } (\zeta_v \geq \zeta_0) \text{ AND } (\alpha_v \leq \alpha_v^\infty)$$

OR

$$\text{Condition 7.4: } (\kappa < -1) \text{ AND } \left(\chi \geq -\frac{\kappa}{\eta} \right) \text{ AND } (\alpha_v \leq \min \{ \alpha_{v1}^{\text{img}}, \alpha_v^\infty \})$$

OR

$$\text{Condition 7.5: } (-1 \leq \kappa \leq -\eta^2) \text{ AND } (\alpha_v \leq \alpha_{v1}^{\text{img}})$$

OR

$$\text{Condition 7.6: } (-\eta^2 < \kappa < 0) \text{ AND } \left(\chi \leq -\frac{\kappa}{\eta} \right) \text{ AND } (\alpha_v \leq \alpha_{v1}^{\text{img}})$$

OR

$$\text{Condition 7.7: } (-\eta^2 < \kappa < 0) \text{ AND } \left(-\frac{\kappa}{\eta} < \chi < -\frac{\eta^3}{\kappa} \right) \text{ AND } (\zeta_v < \zeta_0) \\ \text{AND } (\alpha_v \leq \alpha_{v1}^{img} \text{ OR } \alpha_v \geq \alpha_{v2}^{img})$$

OR

(3-86)

$$\text{Condition 7.8: } (-\eta^2 < \kappa < 0) \text{ AND } \left(-\frac{\kappa}{\eta} < \chi < -\frac{\eta^3}{\kappa} \right) \text{ AND } (\zeta_v \geq \zeta_0)$$

OR

$$\text{Condition 7.9: } (-\eta^2 < \kappa < 0) \text{ AND } \left(\chi \geq -\frac{\eta^3}{\kappa} \right) \text{ AND } (\alpha_v \leq \alpha_{v1}^{img})$$

Each sufficient condition in **Result 7** is derived from the positive zero loci in Fig 3-5. For example, when $(\kappa < -1)$ AND $(\chi < -\eta^3/\kappa)$ in Fig 3-5a, CNMP and RNMP zeros will not occur if $\alpha_v \leq \alpha_{v1}^{img}$. Similarly, in Fig 3-5b, when $(\kappa < -1)$ AND $(-\eta^3/\kappa \leq \chi \leq -1/\kappa\eta)$, then again CNMP and RNMP zeros will not occur if $\alpha_v \leq \alpha_{v1}^{img}$. Therefore, combining the parameter range of χ from Fig 3-5a and Fig 3-5b leads to Condition 7.1 i.e. $(\kappa < -1)$ AND $(\chi \leq -1/\kappa\eta)$ AND $(\alpha_v \leq \alpha_{v1}^{img})$. Similarly, other sufficient conditions are also derived from the positive zero loci of Fig 3-5. The correspondence between each sufficient condition and Fig 3-5 is as follows: Condition 7.1 \rightarrow Fig 3-5a and Fig 3-5b, Condition 7.2 \rightarrow Fig 3-5c, Condition 7.3 \rightarrow Fig 3-5d and Fig 3-5e, Condition 7.4 \rightarrow Fig 3-5f, Condition 7.5 \rightarrow Fig 3-5g, Fig 3-5h and Fig 3-5i, Condition 7.6 \rightarrow Fig 3-5j, Condition 7.7 \rightarrow Fig 3-5k, Condition 7.8 \rightarrow Fig 3-5l and Fig 3-5m, and Condition 7.9 \rightarrow Fig 3-5n and Fig 3-5o. Note that when we refer to Fig 3-5c, we refer to all its parts i.e. Fig 3-5c1, Fig 3-5c2, and Fig 3-5c3 because all these parts give the final condition i.e. Condition 7.2. This is true for all other subplots that have multiple parts.

Based on **Result 7** and Fig 3-5, the following observations can be made about the NMP zero dynamics of a three-DoF damped flexible LTI system:

1. Each condition listed in **Result 7** is individually sufficient but not necessary. For example, Condition 7.1, by itself, is a sufficient condition. However, Condition 7.1, by itself, is not necessary because even if this condition is not met, NMP zeros can still be eliminated via other non-overlapping conditions such as Condition 7.2 or Condition 7.3.

2. Each sufficient condition comprises of parameter ranges that are essential and broadest possible. For each of these conditions, one can write various inferior conditions with narrower parameter ranges that would also be sufficient conditions. For example, based on Condition 7.1, $[(\kappa < -2) \text{ AND } (\chi \leq -1/\kappa\eta) \text{ AND } (\alpha_v \leq \alpha_{vI}^{\text{img}})]$ is also a sufficient condition for the elimination of NMP zeros.

3. As shown by the zero loci of Fig 3-5, the entire range of the system parameters comprising of modal residues, frequencies, and damping ratios is covered in this analysis. Therefore, **Result 7** is a complete list of all possible sufficient conditions. In other words, there are no other sufficient conditions for which one can guarantee the elimination of NMP zeros. As a result, these nine conditions when considered together, i.e., [Condition 7.1 OR Condition 7.2 OR Condition 7.3 OR Condition 7.4 OR Condition 7.5 OR Condition 7.6 OR Condition 7.7 OR Condition 7.8 OR Condition 7.9], form a necessary condition for the elimination of NMP zeros.

4. The mathematical form of the conditions is the consequence of our choice of parameterization. The normalized parameters κ , χ , and η that are defined in terms of system parameters and used to provide the conditions could have been defined differently. For example, instead of using α_v as the varying parameter to plot the zero locus of $G_3(s)$, one could use a different varying parameter, for example α_u . The zero locus could have been plotted as a function of modal frequencies or

modal damping ratios. While the resulting mathematical form of the conditions may be different in that case, the conditions would effectively be the same in terms of system parameters. In other words, the conditions are unique.

5. The graphical visualization in Fig 3-5 allows one to determine the sufficient and necessary conditions for the elimination of *specific* types of NMP zeros e.g. CNMP only, RNMP only, as well as all NMP. For example, **Result 5** provides a sufficient condition for the elimination of CNMP zeros, while **Result 7** provides sufficient and necessary conditions for the elimination of all NMP zeros. Furthermore, this graphical visualization allows one to examine the sensitivity of different types of NMP zeros to parametric variations, which helps inform the robustness of any choice of system parameters that avoid NMP zeros. For example, when the value of α_v is close to α_{v1}^{img} in Fig 3-5a, the CMP zero can flip to become a CNMP zero, and similarly when α_v is close to α_v^∞ , RMP zero can flip to become RNMP zero in Fig 3-5a.

6. Condition 7.8 is the only sufficient condition that guarantees the elimination of all NMP zeros for any positive value of modal residue, α_v or any negative value of modal residue α_u . Such condition becomes useful in situations where the modal residues α_v or α_u undergo large variations and can enable robust physical design [36]. The application of Condition 7.8 in eliminating NMP zeros is demonstrated via a case study in the subsequent section.

Result 8: In a three-DoF damped flexible LTI system given by Eq.(3-26), when the modal residue signs are non-alternating ($\alpha_v < 0$), the following conditions are individually sufficient, and together necessary, to guarantee the elimination of all NMP zeros.

$$\text{Condition 8.1: } (\kappa < -1) \text{ AND } \left(\chi < -\frac{\eta^3}{\kappa} \right) \text{ AND } (\alpha_v \geq \alpha_{v2}^{\text{img}})$$

OR

$$\text{Condition 8.2: } (\kappa < -1) \text{ AND } \left(-\frac{\eta^3}{\kappa} \leq \chi \leq -\frac{\kappa}{\eta} \right)$$

OR

$$\text{Condition 8.3: } (\kappa < -1) \text{ AND } \left(\chi > -\frac{\kappa}{\eta} \right) \text{ AND } (\alpha_v \geq \alpha_{v2}^{\text{img}})$$

OR

$$\text{Condition 8.4: } (-1 \leq \kappa \leq -\eta^2) \text{ AND } \left(\chi < -\frac{\eta^3}{\kappa} \right) \text{ AND } (\alpha_v \geq \max \{ \alpha_{v2}^{\text{img}}, \alpha_v^\infty \})$$

OR

$$\text{Condition 8.5: } (-1 \leq \kappa \leq -\eta^2) \text{ AND } \left(-\frac{\eta^3}{\kappa} \leq \chi \leq -\frac{1}{\kappa\eta} \right) \text{ AND } (\alpha_v \geq \alpha_v^\infty)$$

OR

$$\text{Condition 8.6: } (-1 \leq \kappa \leq -\eta^2) \text{ AND } \left(\chi > -\frac{1}{\kappa\eta} \right) \text{ AND } (\alpha_v \leq \alpha_v^\infty \text{ OR } \alpha_v \geq \alpha_{v2}^{\text{img}})$$

OR

$$\text{Condition 8.7: } (-\eta^2 < \kappa < 0) \text{ AND } \left(\chi < -\frac{\kappa}{\eta} \right) \text{ AND } (\alpha_v \geq \max \{ \alpha_{v2}^{\text{img}}, \alpha_v^\infty \})$$

OR

$$\text{Condition 8.8: } (-\eta^2 < \kappa < 0) \text{ AND } \left(-\frac{\kappa}{\eta} \leq \chi \leq -\frac{1}{\kappa\eta} \right) \text{ AND } (\alpha_v \geq \alpha_v^\infty)$$

OR

$$\text{Condition 8.9: } (-\eta^2 < \kappa < 0) \text{ AND } \left(\chi > -\frac{1}{\kappa\eta} \right) \text{ AND } (\alpha_v \leq \alpha_v^\infty \text{ OR } \alpha_v \geq \alpha_{v2}^{\text{img}})$$

OR

$$\text{Condition 8.10: } (\kappa > 0) \text{ AND } (\alpha_v \geq \alpha_v^\infty) \tag{3-87}$$

Each sufficient condition in **Result 8** is derived from the negative zero loci in Fig 3-5. For example, in Fig 3-5a, when $(\kappa < -1)$ AND $(\chi < -\eta^3/\kappa)$, RNMP zeros are not part of the zero locus. Therefore, they do not occur for any value of α_v . CNMP zeros are part of the zero locus but they only occur when CMP zeros cross the imaginary axis for $\alpha_v < \alpha_{v2}^{img}$. This leads to Condition 8.1 for the elimination of all NMP zeros i.e. $[(\kappa < -1)$ AND $(\chi < -\eta^3/\kappa)$ AND $(\alpha_v \geq \alpha_{v2}^{img})]$. Similarly, other sufficient conditions are also derived from the negative zero loci of Fig 3-5. The correspondence between each sufficient condition and Fig 3-5 is as follows: Condition 8.1 \rightarrow Fig 3-5a, Condition 8.2 \rightarrow Fig 3-5(b-e), Condition 8.3 \rightarrow Fig 3-5f, Condition 8.4 \rightarrow Fig 3-5g, Condition 8.5 \rightarrow Fig 3-5h, Condition 8.6 \rightarrow Fig 3-5i, Condition 8.7 \rightarrow Fig 3-5j, Condition 8.8 \rightarrow Fig 3-5(k-n), Condition 8.9 \rightarrow Fig 3-5o, and Condition 8.10 \rightarrow Fig 3-5p.

Based on **Result 8** and Fig 3-5, the following observations can be made about the NMP zero dynamics of a three-DoF damped flexible system:

1. The general observations made for **Result 7** above i.e. bullet point (1) to point (5) also hold true for **Result 8** when the modal residue signs are not alternating.
2. Condition 8.2 is the only condition that holds true for any negative value of modal residue α_v or any positive value of α_u and any positive value of modal damping ratio ζ_v or ζ_u . Therefore, such a condition becomes useful when the modal residue α_v or α_u and/or modal damping ratio ζ_v or ζ_u undergo large variations and can enable robust physical design [36].
3. Condition 8.10 is the only condition that holds true for any value of modal damping ratios ζ_v and/or ζ_u . Therefore, such a condition becomes useful when modal damping ratios undergo large variations and can enable robust physical design.

3.6 Case Study of Three-DoF Flexible System

This section demonstrates how the results from previous section can be used to determine the location, value of viscous dampers and sensor placement in a three-DoF flexible system in order to eliminate NMP zeros in its transfer function and also place zeros on the imaginary axis. Furthermore, it will be demonstrated that the elimination of NMP zeros is robust to parametric variations in sensor placement.

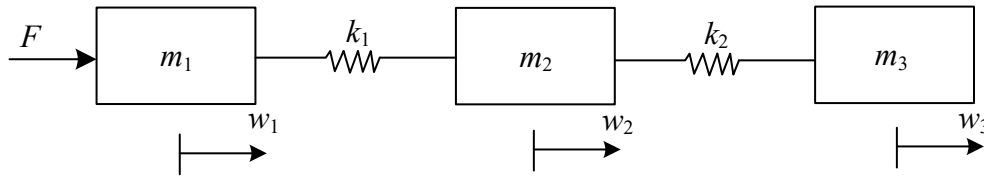


Fig 3-6 Three-DoF undamped flexible system

Consider the three-DoF flexible system shown in Fig 3-6. For illustration, the physical parameters of this system are chosen as $m_1 = m_3 = 1$ kg, $m_2 = 10$ kg, $k_1 = k_2 = 1$ N/m. The force, F is applied at m_1 and the measured displacement, q is the linear combination of the displacement of m_1 and m_3 i.e. $q = w_1 + 3w_3$. The equations of motion of the undamped three-DoF flexible system is given below.

$$[\mathbf{M}] \begin{bmatrix} \ddot{w}_1 \\ \ddot{w}_2 \\ \ddot{w}_3 \end{bmatrix} + [\mathbf{K}] \begin{bmatrix} w_1 \\ w_2 \\ w_3 \end{bmatrix} = [\mathbf{B}]F, \quad q = [\mathbf{D}] \begin{bmatrix} w_1 \\ w_2 \\ w_3 \end{bmatrix} \quad \text{where } [\mathbf{M}] = \begin{bmatrix} m_1 & 0 & 0 \\ 0 & m_2 & 0 \\ 0 & 0 & m_3 \end{bmatrix} \quad (3-88)$$

$$[\mathbf{K}] = \begin{bmatrix} k_1 & -k_1 & 0 \\ -k_1 & k_1 + k_2 & -k_2 \\ 0 & -k_2 & k_2 \end{bmatrix}, \quad [\mathbf{B}] = \begin{bmatrix} 1 \\ 0 \\ 0 \end{bmatrix}, \quad [\mathbf{D}] = [1 \quad 0 \quad 3]$$

The transfer function from applied force, F to measured displacement, q is given below along with its poles and zeros.

$$\frac{q(s)}{F(s)} = \frac{s^4 + 1.2s^2 + 0.4}{s^6 + 2.2s^4 + 1.2s^2} \quad (3-89)$$

$$\text{Poles: } p_{1,2} = 0, p_{3,4} = \pm 1j, p_{5,6} = \pm 1.1j, \text{ Zeros: } z_{1,2,3,4} = \pm 0.127 \pm 0.785j$$

This system exhibits a CMP-CNMP zero quartet. Our goal is to add viscous damping (location and value) to the flexible system so as to eliminate NMP zeros from the transfer function. The equations of motion of the resulting three-DoF damped flexible system (Fig 3-7) are given below.

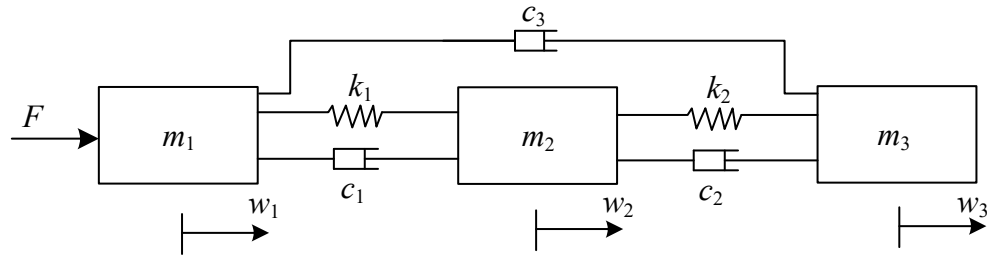


Fig 3-7 Three-DoF damped flexible system

$$[\mathbf{M}] \begin{bmatrix} \ddot{w}_1 \\ \ddot{w}_2 \\ \ddot{w}_3 \end{bmatrix} + [\mathbf{C}] \begin{bmatrix} \dot{w}_1 \\ \dot{w}_2 \\ \dot{w}_3 \end{bmatrix} + [\mathbf{K}] \begin{bmatrix} w_1 \\ w_2 \\ w_3 \end{bmatrix} = [\mathbf{B}]F, q = [\mathbf{D}] \begin{bmatrix} w_1 \\ w_2 \\ w_3 \end{bmatrix} \text{ where } [\mathbf{C}] = \begin{bmatrix} c_1 + c_3 & -c_1 & -c_3 \\ -c_1 & c_1 + c_2 & -c_2 \\ -c_3 & -c_2 & c_2 + c_3 \end{bmatrix} \quad (3-90)$$

In this chapter, we have assumed that the flexible system is ‘classically damped’. This means that the mass matrix $[\mathbf{M}]$, stiffness matrix $[\mathbf{K}]$, and damping matrix $[\mathbf{C}]$ should satisfy the Caughey and O’Kelly criterion given in Eq.(3-2). Applying Eq.(3-2) to the $[\mathbf{M}]$, $[\mathbf{K}]$, and $[\mathbf{C}]$ from Eq.(3-88) and Eq.(3-90) and using the numerical values of $m_1 = m_3 = 1 \text{ kg}$, $m_2 = 10 \text{ kg}$, $k_1 = k_2 = 1 \text{ N/m}$ leads to the following condition on the viscous dampers c_1 , c_2 , and c_3 .

$$c_1 = c_2 \text{ AND } c_3 \text{ can be any arbitrary value} \quad (3-91)$$

The result that c_3 can be any arbitrary value tells us that for any value of c_3 , Eq.(3-2) is satisfied. Therefore, we choose $c_3 = 0$ to keep the ensuing mathematical analysis simple. Since, the Caughey

and O'Kelly criterion is satisfied, the $[\mathbf{M}]$, $[\mathbf{C}]$, and $[\mathbf{K}]$ matrices can be simultaneously diagonalized to obtain the modal mass, modal damping and modal stiffness diagonal matrices as demonstrated in Eq.(3-3). The modal mass, damping and stiffness matrices are then used to construct the decomposed form of the transfer function as demonstrated in Eq.(3-4) and Eq.(3-5). The decomposed transfer function in terms of the viscous damper, c_1 is given below. Note that we already know that $c_2 = c_1$ and we have chosen $c_3 = 0$.

$$\frac{q(s)}{F(s)} = \frac{\alpha_R}{s^2} + \frac{\alpha_u}{s^2 + 2\zeta_u\omega_u s + \omega_u^2} + \frac{\alpha_v}{s^2 + 2\zeta_v\omega_v s + \omega_v^2} = \frac{0.33}{s^2} + \frac{-1}{s^2 + c_1 s + 1} + \frac{1.67}{s^2 + 1.2c_1 s + 1.21} \quad (3-92)$$

Comparing the LHS and RHS of the above equation provides the relationship between c_1 , ζ_u and ζ_v .

$$\zeta_u = 0.5c_1 \text{ AND } \zeta_v = 0.547c_1 \quad (3-93)$$

The modal residue signs in Eq.(3-92) are alternating with $\alpha_v > 0$. According to Table 3-1 we should use **Result 7** to eliminate all NMP zeros in the transfer function with alternating modal residue signs. There are 9 distinct conditions in **Result 7** and we have to choose the appropriate condition for our current system. From Eq.(3-92), the value of κ , η and χ can be readily found as shown below. Since, both ζ_u and ζ_v are proportional to c_1 , as evident in Eq.(3-93), their ratio i.e. χ is independent of it.

$$\kappa \left(\triangleq \frac{\alpha_u}{\alpha_v} \right) = -0.6, \quad \eta \left(\triangleq \frac{\omega_u}{\omega_v} \right) = 0.91, \text{ and } \chi \left(\triangleq \frac{\zeta_u}{\zeta_v} \right) = 0.914 \quad (3-94)$$

Based on the values of κ , η and χ , it can be inferred that the following two inequalities are simultaneously satisfied.

$$\left(-\eta^2 < \kappa < 0 \right) \text{ AND } \left(-\frac{\kappa}{\eta} < \chi < -\frac{\eta^3}{\kappa} \right) \quad (3-95)$$

In **Result 7**, only Condition 7.7 and Condition 7.8 are applicable to our current system since they satisfy Eq.(3-95).

$$\begin{aligned} \text{Condition 7.7: } & \left(-\eta^2 < \kappa < 0\right) \text{AND} \left(-\frac{\kappa}{\eta} < \chi < -\frac{\eta^3}{\kappa}\right) \text{AND} (\zeta_v < \zeta_0) \\ & \text{AND} (\alpha_v \leq \alpha_{v1}^{\text{img}} \text{ OR } \alpha_v \geq \alpha_{v2}^{\text{img}}) \end{aligned} \quad (3-96)$$

OR

$$\text{Condition 7.8: } \left(-\eta^2 < \kappa < 0\right) \text{AND} \left(-\frac{\kappa}{\eta} < \chi < -\frac{\eta^3}{\kappa}\right) \text{AND} (\zeta_v \geq \zeta_0)$$

In order to completely satisfy Condition 3.8, we only need to additionally satisfy $\zeta_v \geq \zeta_0$. This will give us the value of c_1 that will guarantee the elimination of NMP zeros in the transfer function in Eq.(3-92). However, in order to satisfy Condition 7.7, we will have to modify the value of α_v which can only be done by modifying the mass matrix, stiffness matrix, actuator or sensor location. Since, our goal is to eliminate NMP zeros by simply adding viscous damping, we decide to satisfy Condition 3.8. Using the expression of ζ_0 from Eq.(3-84) along with the numerical value of κ , η and χ from Eq.(3-94) leads to the following result.

$$\zeta_v \geq 0.2350 \quad (3-97)$$

Eq.(3-93) is used along with Eq.(3-97) to find the range of values for c_1 for which the transfer function in Eq.(3-92) will not have any NMP zeros.

$$c_1 \geq 0.4296 \quad (3-98)$$

Therefore, selecting $c_1 = c_2 = 0.5$ and $c_3 = 0$ leads to a transfer function of the three-DoF damped flexible system that does not exhibit any NMP zeros as shown below. Note that this transfer function is simply obtained by substituting $c_1 = 0.5$ in Eq.(3-92).

$$\frac{q(s)}{F(s)} = \frac{s^4 + 0.6s^3 + 1.3s^2 + 0.4s + 0.4}{s^6 + 1.1s^3 + 2.5s^4 + 1.2s^3 + 1.2s^2}$$

$$\text{Poles : } p_{1,2} = 0, p_{3,4} = -0.2500 \pm 0.9682j, p_{5,6} = -0.3000 \pm 1.0536j \quad (3-99)$$

$$\text{Zeros : } z_{1,2} = -0.2700 \pm 0.7210j, z_{3,4} = -0.0300 \pm 0.8210j$$

Since, the damped flexible system satisfies Condition 7.8, Fig 3-5m (from which Condition 7.8 was derived) predicts that its transfer function will exhibit two pairs of CMP zeros. This is shown to be true in Eq.(3-99) where $z_{1,2}$ and $z_{3,4}$ denote the two CMP zero pairs. Not only that, one of the CMP zero pair i.e. $z_{1,2}$ is placed very close to the pole pair i.e. $p_{1,2}$ leading to approximate pole-zero cancellation and effectively eliminating any ‘vibration’ at the $p_{1,2}$ frequency. The other CMP zero pair i.e. $z_{3,4}$ is located very close to the imaginary axis leading to improved ‘vibration isolation’ at its frequency. This improvement in the ‘vibration performance’ of the damped system achieved via the elimination of NMP zeros is shown via a Bode plot in Fig 3-8a.

Note that the zero pair $z_{3,4}$ is not exactly located on the imaginary axis. If further ‘vibration isolation’ is desired by placing $z_{3,4}$ exactly on the imaginary axis, it can also be easily achieved based on the graphical insight obtained from Fig 3-5l. According to the positive zero locus in Fig 3-5l, if $(\zeta_v = \zeta_0)$ AND $(\alpha_v = \alpha_{v1}^{img} = \alpha_{v2}^{img})$ are satisfied, then $z_{3,4}$ will lie exactly on the imaginary axis. In order to satisfy $(\zeta_v = \zeta_0)$, choose $c_1 = 0.4296$ (see Eq.(3-97) and Eq.(3-98)). Choosing $(\zeta_v = \zeta_0)$ automatically ensure that $\alpha_{v1}^{img} = \alpha_{v2}^{img}$ (see Fig 3-5l). Finally, $\alpha_v = \alpha_{v1}^{img}$ can be ensured by modifying the value of α_v . One of the ways to modify the value of α_v is by altering the sensor vector $[\mathbf{D}]$, which is parameterized as follows:

$$[\mathbf{D}] = [1 + \varepsilon_1 \quad \varepsilon_2 \quad 3] \quad (3-100)$$

The value of ε_1 and ε_2 is found by using the relationship between α_v and $[\mathbf{D}]$, given in Eq.(3-5) and imposing the two conditions shown below. The condition on $\kappa (= \alpha_u / \alpha_v)$ is to make sure

that value of ζ_0 and α_v ^{img} that were calculated for a constant $\kappa = -0.6$ (see Eq.(3-94)) do not change as α_v is changed.

$$(\alpha_v = \alpha_{v1}^{img}) \text{ AND } (\kappa = -0.6) \quad (3-101)$$

Solving the conditions in Eq.(3-101) for the two unknowns ε_1 and ε_2 leads to the following sensor vector.

$$[\mathbf{D}] = [0.92 \quad -1.2 \quad 3] \quad (3-102)$$

The zeros of the transfer function $q(s) / F(s)$ with the new sensor vector from Eq.(3-102) and $c_1 = 0.4296$ are as follows:

$$z_{1,2} = -0.2674 \pm 0.7801j, z_{3,4} = \pm 0.6590j \quad (3-103)$$

It can be clearly seen that the zero pair $z_{3,4}$ is now on the imaginary axis as intended. The ensuing improvement in vibration isolation due to the tuning of the viscous damper c_1 and sensor vector $[\mathbf{D}]$ is shown via a Bode plot in Fig 3-8b. Therefore, by informed choice of the damping matrix $[\mathbf{C}]$ and sensor vector $[\mathbf{D}]$, the CNMP zeros of the three-DoF *undamped* flexible system can be converted into MP zeros of its *damped* counterpart lying exactly on the imaginary axis.

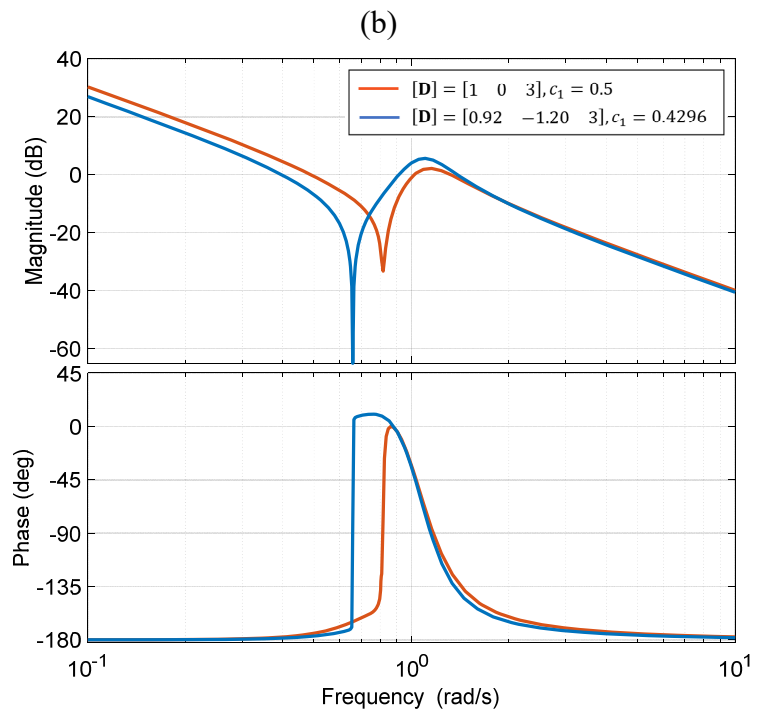
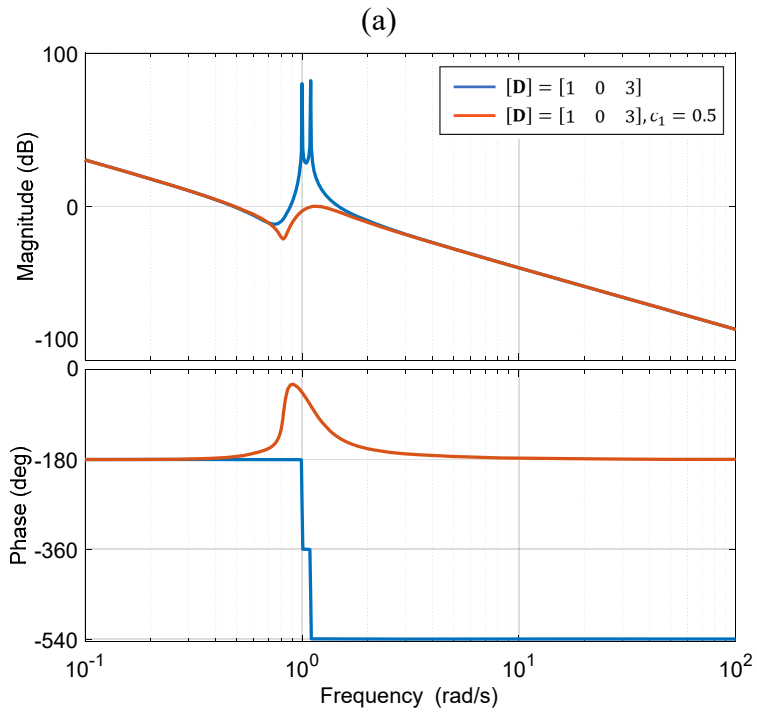


Fig 3-8 Bode plots of: a) Undamped vs. damped system with tuned damping to eliminate NMP zeros, b) Damped system with tuned damping and sensor vector to place the zero on the imaginary axis

To investigate the robustness of the damped system obtained using the proposed technique for a fixed c_1 that satisfies Eq. (3-98), Bode plots of the damped system with variations in the sensor vector $[\mathbf{D}]$ are shown in Fig 3-9. Variation in the sensor vector is generally caused by uncertainty in sensor placement. It can be observed from the Bode plots that even in the presence of finite perturbations (up to 10 %) in the sensor parameters, the designed damping matrix $[\mathbf{C}]$ still ensures that all the zeros of the flexible system remain MP. This is because even in the presence of this sensor parameter variation, the inequalities in Condition 7.8 are still satisfied. It should be noted that this level of robustness exists for $c_1 = c_2 = 0.5$, which is very close to the minimum required value of damping given in Eq.(3-98). If a more robust design is needed for a given application, then larger damping values can be chosen to ensure an even wider safety margin. Thus, this case study highlights that the new sufficient and necessary conditions derived in this chapter can be effectively used to enable *robust physical design* of three-DoF flexible systems.

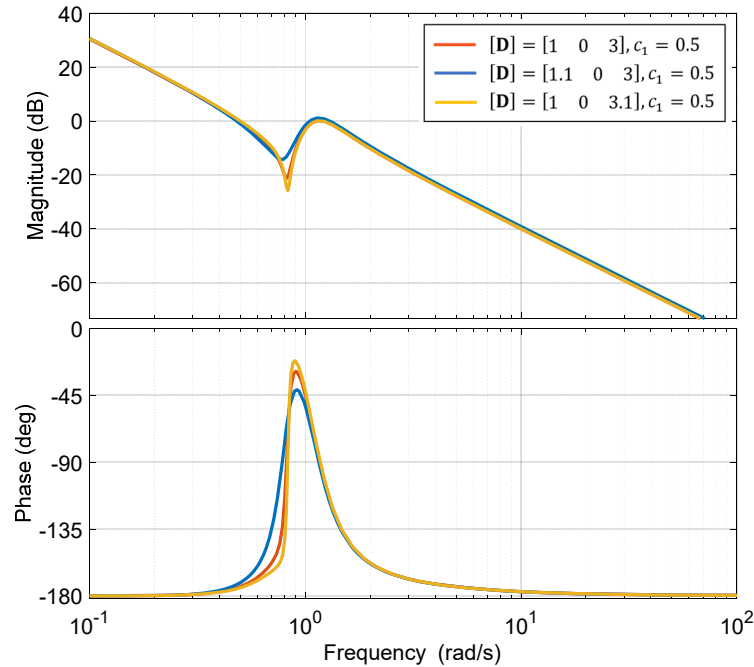


Fig 3-9 Robust elimination of NMP zeros under variation in sensor vector

3.7 Conclusion

In this chapter, the sufficient and necessary conditions for the elimination of NMP zeros in the transfer functions of two-DoF and three-DoF damped flexible LTI systems are presented under the assumption of classical damping when all the modal residue signs are not same. No such results exist in the prior literature.

In the case of a two-DoF damped flexible LTI system, **Result 4** provides a *complete set* of all possible sufficient conditions for the elimination of all NMP zeros. This *complete* set of sufficient conditions when imposed together also serves as the necessary condition for elimination of NMP zeros. Similarly, **Result 7** and **Result 8** provide the sufficient and necessary conditions for the elimination of NMP zeros in a three-DoF damped flexible LTI system (with one rigid body mode and two flexible modes) when the modal residue signs are alternating and non-alternating, respectively. These conditions enable informed physical design choices such as selection of

viscous damping strategies and magnitude, actuator and sensor placement, mass and stiffness distribution, etc. These choices can lead to robust physical designs that guarantee the elimination of NMP zeros over a wide range of system parameters, as shown via a case study in the previous section.

The mathematical and graphical tools used in this chapter (i.e. modal decomposition and zero loci) provide a more granular understanding of the NMP zeros as compared to other purely mathematical techniques such as the Routh-Hurwitz criterion. These tools allow one to derive conditions for the elimination of *specific* types of zeros as well as provide graphical insights into the behavior of the zeros as system parameters are varied. For example, **Results 2, 5 and 6** provide sufficient conditions for elimination of specifically CNMP zeros. The graphical insights offered by the zero loci allow one to examine the robustness of the zero dynamics to parametric variations i.e. how close the CMP or RMP zeros are to the imaginary axis where they can transition from minimum phase to non-minimum phase.

There are two key limitations of the modeling work presented in this chapter. First, the results and design insights are restricted to classically damped flexible systems. Second, the conditions for the elimination of NMP zeros have been investigated only for low DoF (two and three) damped flexible LTI systems. This was done to keep the parameter space small enough in order to find the *complete set* of all possible sufficient conditions, which in turn lead to the necessary condition. In the subsequent chapters, we will derive analytical conditions to eliminate NMP zeros in multi-DoF damped flexible systems with arbitrary number of DoFs (modes). To do so, we will investigate techniques to reduce the size of the parameter space of an n -DoF damped flexible system from $3n$ system parameters to fewer composite parameters.

Chapter 4 Non-minimum Phase Zeros of Multi-DoF Undamped Flexible Systems

This chapter investigates the non-minimum phase (NMP) zeros in the transfer function, between actuated load input and measured displacement output, of a multi-degree of freedom (DoF) undamped flexible system. The transfer function of an undamped flexible system can be modally decomposed into second order modes where each mode is characterized by two system parameters – modal residue and modal frequency. It is well known that when all the modal residue signs are the same, all the zeros of the undamped flexible system are minimum phase (MP). However, it may not be possible to always guarantee the same sign for all modal residues, given practical constraints on actuator and sensor placements. This chapter presents a sufficient condition for the elimination of NMP zeros when all modal residue signs are not the same. Therefore, it enables a wider design space in terms of actuator–sensor placement and mass–stiffness distribution in order to eliminate NMP zeros. We start by deriving results that elucidate the distribution of zeros with respect to the poles on the real and imaginary axes of the s -plane. These results are then used to derive a sufficient condition for the elimination of only complex non-minimum phase zeros in terms of the sequence of modal residue signs. Once this sufficient condition is met, the sufficient condition for the elimination of all NMP zeros is derived i.e. complex and real non-minimum phase zeros.

4.1 Introduction and Motivation

Position control of the end effector is required in several machineries that exhibit flexible

system dynamics such as space structures [1, 2, 66], rotorcraft blades [5, 97, 116], hard-disk drives [3, 4, 74], flexure mechanisms [7, 39, 75, 117], and motion systems with transmission compliance [8, 98, 118], among others. In these applications, the position of the end effector is controlled through feedback and feedforward control strategies to simultaneously achieve high speed, low settling time, good disturbance rejection, and stability robustness. Oftentimes, given the practical constraints on the cost of additional actuators and sensors and the available space to accommodate them within the machines, it is highly desirable to achieve the above mentioned dynamic performance with the help of a single actuator and a single sensor. Therefore, in this chapter we will limit the discussion to the dynamics of single input single output (SISO) flexible systems.

The presence of non-minimum phase (NMP) zeros in the transfer function severely limits the dynamic performance that can be achieved through feedback and feedforward control strategies in SISO systems [14, 15, 18, 119-121]. A zero is non-minimum phase (NMP) if it has a positive real component, and minimum phase (MP) if it has a non-positive real component. NMP zeros occur very frequently in the dynamics of flexible systems. Chapter 2 provides a comprehensive review of the linear time invariant (LTI) flexible systems that exhibit NMP zeros in their transfer functions. In this review, we identified two types of NMP zeros: complex NMP (CNMP) where the imaginary component $\neq 0$, and real NMP (RNMP) where the imaginary component $= 0$; and three types of MP zeros: complex MP (CMP) where the imaginary component $\neq 0$, real MP (RMP) where the imaginary component $= 0$, and marginal MP (MMP) where real component $= 0$.

The zeros of a multi-degree of freedom (DoF) flexible linear time invariant (LTI) systems depend on its physical parameters i.e. mass and stiffness distribution, actuator and sensor locations, and damping. Therefore, there is a need to investigate the effect of these physical parameters on

NMP zeros to be able to eliminate these zeros. The effect of the various physical parameters on NMP zeros is mathematically involved, and requires a step by step approach. Therefore, we first study the effects of mass-stiffness distribution and actuator-sensor location on NMP zeros in undamped multi-DoF flexible systems in this chapter. Then in the subsequent chapter, we investigate the effect of proportional viscous damping on NMP zeros in damped multi-DoF flexible systems. This sequential approach to investigating undamped and damped flexible systems provides a more comprehensive, systematic, and insightful understanding of how physical parameters affect NMP zeros.

The transfer function of a multi-DoF undamped flexible LTI system can be modally decomposed into second order modes where each mode is characterized by two system parameters – modal residue and modal frequency, as described in Chapter 2. The modal residue and modal frequency depend on the mass-stiffness distribution and actuator-sensor location. Martin [43] and Gevarter [44] showed that when all the modal residue signs are the same, all the zeros of the multi-DoF undamped flexible LTI system are marginally minimum phase (MMP) and are interlaced with the poles on the imaginary axis. It was demonstrated that a flexible system with this interlacing property can be easily stabilized in closed loop using proportional or proportional derivative feedback control [43, 44]. Furthermore, it was also shown that this distribution of the zeros with respect to the poles is robust to the variations in system parameters caused by modelling uncertainties or unmodelled dynamics, as long all the modal residue signs remain the same [43, 45, 46, 122]. This makes the same sign for all modal residues a desirable trait to aim for when one designs a multi-DoF undamped flexible LTI system. Collocated actuator-sensor configuration is the only known technique that guarantees the same sign for all modal residues when a single actuator and single sensor are used [123, 124]. However, certain trajectory tracking applications

such as tracking the tip displacement of a flexible link robot while providing input torque at its root requires a non-collocated actuator-sensor configuration [47]. This non-collocated actuator sensor configuration can lead to the occurrence of NMP zeros in the transfer functions of multi-DoF undamped flexible LTI systems [41]. If multiple sensors are allowed as opposed to a single sensor, then different researchers have proposed different linear combinations of outputs from multiple sensors in order to achieve the same sign for all modal residues. This technique guaranteed the elimination of NMP zeros in multi-DoF undamped flexible LTI systems with non-collocated actuator sensor configurations [47, 48, 125] when multiple sensors are used. However, for a SISO system, it may not be always possible to guarantee the same sign for all modal residues via collocated actuator-sensor placement due to various practical constraints on the location of the actuator and sensor [7, 39, 126]. Fortunately, the same sign for all modal residues is only a sufficient condition, and not a necessary one for the elimination of NMP zeros. This motivates the need to investigate the distribution of zeros with respect to the poles when all the modal residue signs are not the same, and for such systems it is useful to derive one or more sufficient conditions, in terms of the system parameters – modal residue and modal frequency, to eliminate NMP zeros.

The zero dynamics of multi-DoF undamped flexible LTI systems when all modal residue signs are not the same has been less thoroughly studied analytically. However, there are several numerical studies for specific multi-DoF undamped flexible LTI systems [36, 37, 39, 87, 89, 92, 93]. These flexible LTI systems employ a single actuator and sensor in non-collocated configurations which lead to all modal residue signs not being the same. A detailed review of the literature on NMP zeros of multi-DoF undamped flexible LTI systems when all modal residue signs are not the same is provided in Chapter 2. A brief summary is provided here. The transfer functions of certain flexure mechanism based motion stages [36, 37, 39] have demonstrated the

transition of two pairs of marginally minimum phase (MMP) zeros into a quartet of complex minimum phase (CMP) – complex non-minimum phase (CNMP) zeros, for small changes in the mass distribution and operating position of the motion stages. It was numerically demonstrated that these NMP zeros can be eliminated by tuning the mass distribution and keeping all other physical parameters constant. This elimination of NMP zeros via numerical simulation was only shown for a given set of physical parameters. No underlying physical explanation or general sufficient condition was provided that could guarantee the elimination of these NMP zeros for a different set of physical parameters. Spector [87] and Lee [89] carried out numerical investigation of the transfer function of a pinned-free beam model and free-free beam model respectively and identified the migration of the zeros on the real and imaginary axis due to variation in sensor position. But they could not provide any general conclusion or design insights to eliminate NMP zeros other than collocation of the actuator and sensor. Tohyama and Lyon [92, 93] investigated the zero dynamics of room acoustics using a three-DoF flexible system model whose transfer function could be modally decomposed into two flexible modes and a constant remainder. By varying the remainder, they identified NMP zeros in the system. These studies, however, only investigated the variation in the remainder without investigating the effect of varying the modal residues and frequencies associated with the other two modes. As a result, they could not provide a comprehensive list of all possible ways to eliminate NMP zeros in a three-DoF flexible system. The key gap in these prior publications is that they are system specific and investigate the NMP zeros over a limited range of parameters of the flexible systems. Therefore, the prior publications do not provide any meaningful conclusions in the form of necessary and/or sufficient conditions for the absence of NMP zeros in a general multi-DoF undamped flexible LTI system when all modal residue signs are not the same.

In Chapter 2, we carried out an analytical investigation of the zeros of a three-DoF undamped flexible LTI system by constructing zero loci that comprehensively covered all possible distribution of the zeros with respect to the poles for any value of system parameters. Based on these zero loci, the necessary and sufficient conditions for the elimination of NMP zeros were derived. But while it is possible to construct all possible zero loci that span the entire parameter space and use them to derive the necessary and sufficient conditions for the elimination of NMP zeros for low-DoF undamped flexible systems, this process becomes mathematically tedious and impractical as the number of DoFs increase. Therefore, there remains a need to find sufficient conditions for the elimination of NMP zeros in any general multi-DoF undamped flexible system when all modal residue signs are not the same.

This chapter addresses this need by making two novel contributions. The first novel contribution is a non-unique sufficient condition for the elimination of all NMP zeros in multi-DoF undamped flexible LTI systems in terms of the system parameters – modal residue and modal frequency, without the overly restrictive requirement of all modal residue signs being the same. The second novel contribution is a step by step design strategy (demonstrated via a case study) to choose physical parameters that satisfy the sufficient condition for the elimination of NMP zeros. This chapter is organized as follows: Section 4.2 derives and presents some important mathematical results on the distribution of the zeros with respect to the poles on the real and imaginary axis of the s -plane. Section 4.3 makes use of these results to derive the sufficient condition for the elimination of NMP zeros. Section 4.4 provides a case study based on a four-DoF undamped flexible system to demonstrate the utility of this sufficient condition to make informed choices about actuator-sensor placement and mass-stiffness distribution. Section 4.5 provides a conclusion and briefly motivates the research direction in the subsequent chapters.

4.2 Parity of Number of Zeros on the Real and Imaginary axis

Consider the equations of motion of an undamped multi-DoF flexible system given by:

$$\begin{aligned} [\mathbf{M}]_{n \times n} \ddot{w} + [\mathbf{K}]_{n \times n} w &= [\mathbf{B}]_{n \times 1} F \\ q &= [\mathbf{D}]_{1 \times n} w \end{aligned} \quad (4-1)$$

where, $[\mathbf{M}]$ and $[\mathbf{K}]$ denote the mass, and stiffness matrices, respectively; F denotes the force acting on the system through an input vector $[\mathbf{B}]$; and, q is the measured displacement and is a linear combination, captured by sensor vector $[\mathbf{D}]$, of the individual DoF displacements denoted by w . The mode shape matrix $[\boldsymbol{\psi}]$ is used to diagonalize the $[\mathbf{M}]$ and $[\mathbf{K}]$ matrices simultaneously to obtain modal mass (m_i^{modal}) and modal stiffness (k_i^{modal}), as follows:

$$\begin{aligned} [\boldsymbol{\psi}]^T [\mathbf{M}] [\boldsymbol{\psi}] &= \text{diag}(m_1^{\text{modal}}, \dots, m_n^{\text{modal}}), \quad [\boldsymbol{\psi}]^T [\mathbf{K}] [\boldsymbol{\psi}] = \text{diag}(k_1^{\text{modal}}, \dots, k_n^{\text{modal}}) \\ \text{where } \text{diag}(\) &\text{ represents a diagonal matrix} \end{aligned} \quad (4-2)$$

The transfer function, between the input force, F and the measured displacement output, q of the multi-DoF undamped flexible LTI system is given below where the coefficients in the numerator and denominator are all real valued.

$$\begin{aligned} G(s) &= \frac{q(s)}{F(s)} = \frac{b_m s^{2m} + \dots + b_1 s^2 + b_0}{a_n s^{2n} + \dots + a_1 s^2 + a_0} = \sum_{i=1}^n \frac{\alpha_i}{s^2 + \omega_i^2} \\ \text{where, } \alpha_i &= \frac{([\mathbf{D}][\boldsymbol{\psi}])_i ([\boldsymbol{\psi}]^T [\mathbf{B}])_i}{m_i^{\text{modal}}}, \quad \omega_i = \sqrt{\frac{k_i^{\text{modal}}}{m_i^{\text{modal}}}} \end{aligned} \quad (4-3)$$

The modal decomposition of the transfer function $G(s)$ is also given by Eq.(4-3) where $\alpha_i \neq 0$ for any i from 1 to n , and $\omega_1 < \omega_2 < \dots < \omega_n$. The total number of second order modes in the modal decomposition is n , which is also the DoF of the system. ω_i and α_i are the modal frequency and the modal residue of the i^{th} mode, respectively. All the modal frequencies and residues are referred

to as the system parameters in this chapter. The modal residue (α_i) is expressed in terms of input vector $[\mathbf{B}]$, which depends on the actuator location, and sensor vector $[\mathbf{D}]$, which depends on the sensor location, as well as mode shape matrix $[\boldsymbol{\psi}]$, which depend on mass-stiffness distribution i.e. $[\mathbf{M}]$ and $[\mathbf{K}]$. The modal frequency only depends on the mass-stiffness distribution. $G(s)$ represents a physical system (as opposed to a mathematical system), and is therefore strictly proper (i.e. $m < n$). The numerator of $G(s)$ is referred to as $N(s)$ and its denominator is referred to as $D(s)$ as shown below:

$$N(s) = b_m s^{2m} + \dots + b_1 s^2 + b_0, \quad D(s) = a_n s^{2n} + \dots + a_1 s^2 + a_0 \quad (4-4)$$

Since, the coefficients of the numerator $N(s)$, given by b_i , are real as well as $N(s)$ is an even function in s i.e. $N(s) = N(-s)$, the roots of $N(s)$ (or zeros of $G(s)$) will be symmetric about the real and imaginary axis. Hence the zeros of $G(s)$ will either be real or complex conjugate pairs and it is sufficient to focus on the first quadrant of the s -plane including the positive real axis and the positive imaginary axis.

The distribution of the zeros of the transfer function $G(s)$ on the imaginary and real axis of the s -plane is given in terms of the parity of the number of the zeros i.e. odd or even number of zeros between two points, $s = c_1$ and $s = c_2$, either both on the real axis or both on the imaginary axis with $|c_1| < |c_2|$. The choice of c_1 and c_2 divides the imaginary and the real axis into four distinct segments for which the parity of the number of zeros is investigated. These segments are graphically illustrated in Fig 4-1 and described below:

1. Segment 1: Parity of number of zeros between $c_1 = j\omega_f$ and $c_2 = j\omega_{f+1}$ on the imaginary axis for any f from 1 to $n-1$.

2. Segment 2: Parity of number of zeros between $c_1 = j\omega_n$ (pole corresponding to the last mode of $G(s)$) and $c_2 = +j\infty$ on the imaginary axis.

3. Segment 3: Parity of number of zeros between $c_1 = \text{origin}$ and $c_2 = +\infty$ on the real axis.

4. Segment 4: Parity of number of zeros between $c_1 = \text{origin}$ and $c_2 = j\omega_1$ (pole corresponding to the first mode of $G(s)$) on the imaginary axis.

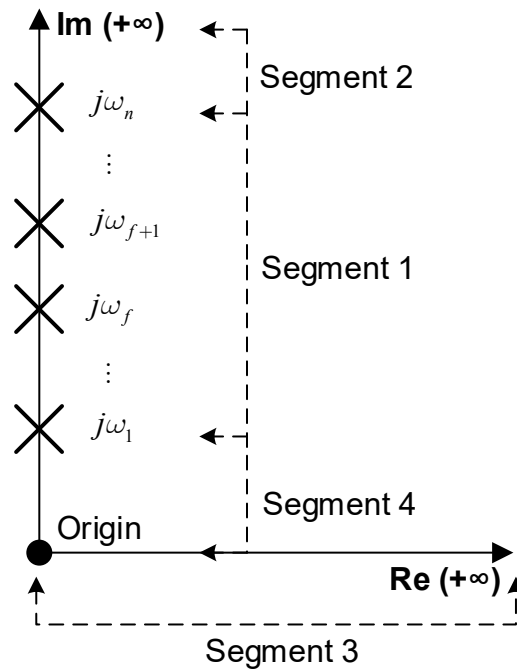


Fig 4-1 Imaginary and real axis divided into four distinct segments

When seeking to find the parity of the number of zeros between two points, c_1 and c_2 , the sign of $N(s)$, given by Eq.(4-3), will be sought at both points. Since $N(s)$ is a continuous function in s , examining its sign at points c_1 and c_2 tells us how many times $N(s)$ can become zero between these two points. An odd number of zeros occur between points c_1 and c_2 if the sign of $N(c_1)N(c_2) < 0$ and an even number of zeros occur between points c_1 and c_2 if the sign of $N(c_1)N(c_2) > 0$. The opposite statements are also true i.e. if there are odd number of zeros between points c_1 and c_2 then $N(c_1)N(c_2) < 0$ and if there are even number of zeros between points c_1 and c_2 then $N(c_1)N(c_2) > 0$.

For the case where $N(c_1)N(c_2) = 0$ because $N(c_1) = 0$ and/or $N(c_2) = 0$, they will be replaced by their respective limiting cases as shown below. If $c_2 \rightarrow \infty$ it implies that $N(c_2) \rightarrow \infty$, then it will be replaced by its limiting case as shown below.

$$\text{If } N(c_1) = 0 \Rightarrow \text{Replace } \text{sgn}(N(c_1)) \text{ with } \lim_{s \rightarrow c_1^+} \text{sgn}(N(s)) \quad (4-5)$$

$$\text{If } N(c_2) = 0 \text{ or } \rightarrow \infty \Rightarrow \text{Replace } \text{sgn}(N(c_2)) \text{ with } \lim_{s \rightarrow c_2^-} \text{sgn}(N(s))$$

4.2.1 Parity of number of zeros between $j\omega_f$ and $j\omega_{f+1}$

Result 1: In a multi-DoF undamped flexible LTI system with a transfer function given by Eq.(4-3), the parity of number of zeros between any two of its consecutive poles, given by $j\omega_f$ and $j\omega_{f+1}$ for any f from 1 to $n-1$, is given by:

$$\text{sgn}\left\{\left(\alpha_f\right)\left(\alpha_{f+1}\right)\right\} > 0 \Leftrightarrow \text{Odd no. of zeros between } j\omega_f \text{ and } j\omega_{f+1} \quad (4-6)$$

$$\text{sgn}\left\{\left(\alpha_f\right)\left(\alpha_{f+1}\right)\right\} < 0 \Leftrightarrow \text{Even no. of zeros between } j\omega_f \text{ and } j\omega_{f+1}$$

Proof: Express the transfer function $G(s)$ as the sum of three transfer functions:

$$G(s) = G_{f,f+1}(s) + \frac{\alpha_f}{s^2 + \omega_f^2} + \frac{\alpha_{f+1}}{s^2 + \omega_{f+1}^2} \text{ where } G_{f,f+1}(s) = \frac{N_{f,f+1}(s)}{D_{f,f+1}(s)} = \sum_{i=1, i \neq f, f+1}^n \left(\frac{\alpha_i}{s^2 + \omega_i^2} \right) \quad (4-7)$$

Next, the numerator of $G(s)$, given by $N(s)$, is evaluated at $s = j\omega_f$ and $s = j\omega_{f+1}$.

$$\Rightarrow N(s) = N_{f,f+1}(s)(s^2 + \omega_f^2)(s^2 + \omega_{f+1}^2) + D_{f,f+1}(s)\left[\alpha_f(s^2 + \omega_{f+1}^2) + \alpha_{f+1}(s^2 + \omega_f^2)\right]$$

$$\Rightarrow N(j\omega_f) = D_{f,f+1}(j\omega_f)\left[\alpha_f(\omega_{f+1}^2 - \omega_f^2)\right]$$

$$\Rightarrow N(j\omega_{f+1}) = -D_{f,f+1}(j\omega_{f+1})\left[\alpha_{f+1}(\omega_{f+1}^2 - \omega_f^2)\right]$$

(4-8)

Taking the product of $N(j\omega_f)$ and $N(j\omega_{f+1})$ and evaluating the sign of the product leads to:

$$\begin{aligned}
N(j\omega_f)N(j\omega_{f+1}) &= -(\alpha_f\alpha_{f+1})(D_{f,f+1}(j\omega_f)D_{f,f+1}(j\omega_{f+1}))(\omega_{f+1}^2 - \omega_f^2)^2 \\
\Rightarrow \text{sgn}(N(j\omega_f)N(j\omega_{f+1})) &= -\text{sgn}(\alpha_f\alpha_{f+1})\text{sgn}(D_{f,f+1}(j\omega_f)D_{f,f+1}(j\omega_{f+1}))
\end{aligned} \tag{4-9}$$

It can be observed that

$$\begin{aligned}
D_{f,f+1}(s) &= \prod_{i=1, i \neq f, f+1}^n (s^2 + \omega_i^2) \\
\Rightarrow \text{sgn}(D_{f,f+1}(j\omega_f)) &= \text{sgn}(D_{f,f+1}(j\omega_{f+1})) = \prod_{i=1}^{f-1} (-1) \prod_{i=f+2}^n (1)
\end{aligned} \tag{4-10}$$

Substituting Eq.(4-10) in Eq.(4-9), we get: $\text{sgn}(N(j\omega_f)N(j\omega_{f+1})) = -\text{sgn}(\alpha_f\alpha_{f+1})$

This directly leads to **Result 1** expressed in Eq.(4-6), which is restated below:

$$\text{sgn}(\alpha_f\alpha_{f+1}) < 0 \Leftrightarrow \text{sgn}(N(j\omega_f)N(j\omega_{f+1})) > 0 \Leftrightarrow \text{Even no. of zeros between } j\omega_f \text{ and } j\omega_{f+1}$$

$$\text{sgn}(\alpha_f\alpha_{f+1}) > 0 \Leftrightarrow \text{sgn}(N(j\omega_f)N(j\omega_{f+1})) < 0 \Leftrightarrow \text{Odd no. of zeros between } j\omega_f \text{ and } j\omega_{f+1}$$

4.2.2 Parity of number of zeros between $j\omega_n$ and $j\infty$

Result 2: In a multi-DoF undamped flexible LTI system whose transfer function is given by Eq.(4-3), the parity of number of zeros between the last pole, given by $j\omega_n$, and positive infinity on the imaginary axis, $j\infty$, is given below:

$$(-1)^{n-1+m} \operatorname{sgn}\{(b_m)(\alpha_n)\} < 0 \Leftrightarrow \text{Odd no. of zeros between } j\omega_n \text{ and } j\infty$$

$$(-1)^{n-1+m} \operatorname{sgn}\{(b_m)(\alpha_n)\} > 0 \Leftrightarrow \text{Even no. of zeros between } j\omega_n \text{ and } j\infty$$

$$\text{where } b_m = \sum_{i=1}^n \alpha_i e_{n-1-m}(\omega_1, \omega_2, \dots, \omega_{i-1}, \omega_{i+1}, \dots, \omega_{n-1}, \omega_n) \quad (4-11)$$

where $m \in (0, n-1)$ is the greatest positive integer

such that $b_m \neq 0$ and e_{n-1-m} represents the $(n-1-m)$ th elementary symmetric polynomial in $(n-1)$ variables.

Proof: Express the transfer function $G(s)$ as the sum of two transfer functions.

$$G(s) = G_n(s) + \frac{\alpha_n}{s^2 + \omega_n^2} \quad \text{where } G_n(s) = \frac{N_n(s)}{D_n(s)} = \sum_{i=1}^{n-1} \frac{\alpha_i}{s^2 + \omega_i^2} \quad (4-12)$$

Next, the sign of the numerator of $G(s)$, given by $N(s)$ is evaluated at $s = j\omega_n$.

$$\begin{aligned} N(s) &= N_n(s)(s^2 + \omega_n^2) + \alpha_n D_n(s) \Rightarrow N(j\omega_n) = \alpha_n D_n(j\omega_n) \\ &\Rightarrow \operatorname{sgn}(N(j\omega_n)) = \operatorname{sgn}(\alpha_n) \operatorname{sgn}(D_n(j\omega_n)) \end{aligned} \quad (4-13)$$

It is observed that

$$D_n(j\omega_n) = \prod_{i=1}^{n-1} (\omega_i^2 - \omega_n^2) \Rightarrow \operatorname{sgn}(D_n(j\omega_n)) = \prod_{i=1}^{n-1} \operatorname{sgn}(\omega_i^2 - \omega_n^2) = \prod_{i=1}^{n-1} (-1) = (-1)^{n-1} \quad (4-14)$$

Substituting Eq.(4-14) into Eq.(4-13) yields

$$\operatorname{sgn}(N(j\omega_n)) = (-1)^{n-1} \operatorname{sgn}(\alpha_n) \quad (4-15)$$

Now the sign of $N(s)$ is evaluated at $s = j\infty$. It is impossible to directly evaluate the sign of $N(s)$ at $s = j\infty$, because $N(s) \rightarrow \infty$. Therefore, the limit of $N(s)$ is considered as below, by making a change of variables and substituting for c_2 in Eq.(4-5).

$$\lim_{y \rightarrow \infty} \operatorname{sgn}(N(jy)) = \lim_{y \rightarrow \infty} \operatorname{sgn}\left(\sum_{i=1}^m b_i (-1)^i (y)^{2i}\right) \quad (4-16)$$

As y tends to infinity, the term with the highest power of y in Eq.(4-16) which is y^{2m} will dominate.

This leads to

$$\lim_{y \rightarrow \infty} \operatorname{sgn}(N(jy)) = (-1)^m \operatorname{sgn}(b_m) \quad (4-17)$$

Using Vieta's formulae and binomial expansion, an expression for b_m can be derived in terms of the elementary symmetric polynomials, which are defined as follows.

$$e_0(x_1, x_2, \dots, x_n) = 1, \quad e_1(x_1, x_2, \dots, x_n) = \sum_{1 \leq i \leq n} x_i, \quad e_2(x_1, x_2, \dots, x_n) = \sum_{1 \leq i < k \leq n} x_i x_k \text{ and so forth, until}$$

$$e_n(x_1, x_2, \dots, x_n) = \prod_{1 \leq i \leq n} x_i \quad (4-18)$$

The expression for b_m is stated below.

$$b_m = \sum_{i=1}^n \alpha_i e_{n-1-m}(\omega_1, \omega_2, \dots, \omega_{i-1}, \omega_{i+1}, \dots, \omega_{n-1}, \omega_n) \quad (4-19)$$

Taking the product of the signs of $N(s)$ at $s = j\omega_n$ and $s = j\infty$ using Eq.(4-15) and Eq.(4-17) gives Eq.(4-11), restated here:

$$\operatorname{sgn}(N(j\omega_n)) \lim_{s \rightarrow j\infty} \operatorname{sgn}(N(s)) = (-1)^{n-1+m} \operatorname{sgn}\{(b_m)(\alpha_n)\}$$

Therefore,

$$(-1)^{n-1+m} \operatorname{sgn}\{(b_m)(\alpha_n)\} < 0 \Leftrightarrow \text{Odd no. of zeros between } j\omega_n \text{ and } j\infty$$

$$(-1)^{n-1+m} \operatorname{sgn}\{(b_m)(\alpha_n)\} > 0 \Leftrightarrow \text{Even no. of zeros between } j\omega_n \text{ and } j\infty$$

The term $2(n-m)$ is the relative degree of the transfer function of $G(s)$ and b_m corresponds to the highest power of s in the numerator as shown in Eq.(4-3). It has been shown previously that the relative degree of transfer functions of collinear lumped parameter undamped flexible systems

depends only on actuator and sensor location and is independent of the other physical parameters such as mass and stiffness distribution [35]. For such systems, **Result 2** can be useful in evaluating the effect of mass and stiffness distribution on the parity of number of zeros in Segment 2 for a given actuator and sensor location. Certain flexure mechanisms exhibit a relative degree of 2 irrespective of mass and stiffness distribution and actuator and sensor location [36, 39]. For such systems, **Result 2** can be useful in evaluating the effect of mass and stiffness distribution and actuator and sensor location on the parity of number of zeros in Segment 2. A change in the parity of number of zeros in Segment 2 indicates that odd number of zeros have migrated from Segment 1 to Segment 2, or vice versa, which suggests pole-zero flipping close to the frequency ω_n . Alternatively, it could indicate that odd number of zeros have migrated from Segment 2 to Segment 3, or vice versa, leading to transition from marginally minimum phase (MMP) zeros to real non-minimum phase (RNMP) zeros or vice-versa.

4.2.3 Parity of number of zeros between 0 and ∞ on the real axis

Result 3: In a multi-DoF undamped flexible LTI system whose transfer function is given by Eq.(4-3), the parity of number of zeros between the origin and positive infinity on the real axis is given below:

$$\text{sgn} \left\{ (b_{q^*})(b_m) \right\} < 0 \Leftrightarrow \text{Odd no. of zeros between } 0 \text{ and } +\infty$$

$$\text{sgn} \left\{ (b_{q^*})(b_m) \right\} > 0 \Leftrightarrow \text{Even no. of zeros between } 0 \text{ and } +\infty$$

$$\text{where } b_{q^*} = \sum_{i=1}^n \alpha_i e_{n-1-q^*}(\omega_1, \omega_2, \dots, \omega_{i-1}, \omega_{i+1}, \dots, \omega_{n-1}, \omega_n) \quad (4-20)$$

where $q^* \in (0, n-1)$ is the smallest positive integer

such that $b_{q^*} \neq 0$ and e_{n-1-q^*} represents the $(n-1-q^*)$ th elementary symmetric polynomial in $(n-1)$ variables.

Proof: The sign of $N(s)$ is evaluated at $s = \infty$.

$$\lim_{x \rightarrow \infty} \text{sgn}(N(x)) = \lim_{x \rightarrow \infty} \text{sgn} \left(\sum_{i=1}^m b_i x^{2i} \right) \quad (4-21)$$

As x tends to infinity, the term with the highest power of x in Eq.(4-21) which is x^{2m} will dominate.

This leads to Eq.(4-22).

$$\lim_{x \rightarrow \infty} \text{sgn}(N(x)) = \text{sgn}(b_m) \quad (4-22)$$

Eq.(4-19) provides the expression for b_m . We evaluate the sign of $N(s)$ at the origin by substituting $c_1 = 0$ into Eq.(4-5).

$$\lim_{x \rightarrow 0^+} \text{sgn}(N(x)) = \lim_{x \rightarrow 0} \text{sgn} \left(\sum_{i=0}^m b_i x^{2i} \right) \quad (4-23)$$

It can be observed that

$$x^k \gg x^{k+1} \text{ as } x \rightarrow 0 \quad (4-24)$$

Thus, the term with the lowest power of x in Eq.(4-23) which is x^{2q^*} will dominate due to Eq.(4-24)

. This leads to:

$$\lim_{x \rightarrow 0^+} \text{sgn}(N(x)) = \text{sgn}(b_{q^*}) \quad (4-25)$$

Note that an expression for the coefficient b_{q^*} can be obtained by substituting q^* for m in Eq.(4-19)

$$b_{q^*} = \sum_{i=1}^n \alpha_i e_{n-1-q^*}(\omega_1, \omega_2, \dots, \omega_{i-1}, \omega_{i+1}, \dots, \omega_{n-1}, \omega_n) \quad (4-26)$$

Taking the product of the sign or sign limits at 0 and ∞ using Eq.(4-22) and Eq.(4-25) yields Eq.(4-20), restated below:

$$\text{sgn} \left\{ \left(b_{q^*} \right) \left(b_m \right) \right\} < 0 \Leftrightarrow \text{Odd no. of zeros between } 0 \text{ and } \infty$$

$$\text{sgn} \left\{ \left(b_{q^*} \right) \left(b_m \right) \right\} > 0 \Leftrightarrow \text{Even no. of zeros between } 0 \text{ and } \infty$$

There are certain classes of multi-DoF undamped flexible LTI system for which $q^* = 0$ for any actuator and sensor location and mass stiffness distribution [35, 36, 39]. A change in the parity of number of zeros in Segment 3 indicates that odd number of zeros have migrated from Segment 2 to Segment 3, or vice versa, leading to transition from MMP to RNMP zeros or vice-versa. Alternatively, it could indicate that odd number of zeros have migrated from Segment 4 to Segment 3, or vice-versa, again leading to transition from MMP to RNMP zeros or vice-versa.

4.2.4 Parity of number of zeros between 0 and $j\omega_1$ on the imaginary axis

Result 4: In a multi-DoF undamped flexible LTI system whose transfer function is given by Eq.(4-3), the parity of number of zeros between the origin and the first pole, given by $j\omega_1$ on the imaginary axis, is given below:

$$(-1)^{q^*} \text{sgn} \left\{ \left(b_{q^*} \right) \left(\alpha_1 \right) \right\} < 0 \Leftrightarrow \text{Odd no. of zeros between } j0 \text{ and } j\omega_1 \quad (4-27)$$

$$(-1)^{q^*} \text{sgn} \left\{ \left(b_{q^*} \right) \left(\alpha_1 \right) \right\} > 0 \Leftrightarrow \text{Even no. of zeros between } j0 \text{ and } j\omega_1$$

Proof: The transfer function $G(s)$ is expressed as the sum of two transfer functions as shown in Eq.(4-28).

$$G(s) = G_1(s) + \frac{\alpha_1}{s^2 + \omega_1^2} \text{ where } G_1(s) = \frac{N_1(s)}{D_1(s)} = \sum_{i=2}^n \frac{\alpha_i}{s^2 + \omega_i^2} \quad (4-28)$$

Next, the sign of the numerator of $G(s)$, given by $N(s)$ is evaluated at $s = j\omega_1$.

$$\begin{aligned} N(s) &= N_1(s)(s^2 + \omega_1^2) + \alpha_1 D_1(s) \Rightarrow N(j\omega_1) = \alpha_1 D_1(j\omega_1) \\ &\Rightarrow \text{sgn}(N(j\omega_1)) = \text{sgn}(\alpha_1) \text{sgn}(D_1(j\omega_1)) \end{aligned} \quad (4-29)$$

It can be observed that

$$D_1(j\omega_1) = \prod_{i=2}^n (\omega_i^2 - \omega_1^2) \Rightarrow \text{sgn}(D_1(j\omega_1)) = \prod_{i=2}^n (1) = 1 \quad (4-30)$$

Substituting Eq.(4-30) into Eq.(4-29) yields

$$\text{sgn}(N(j\omega_1)) = \text{sgn}(\alpha_1) \quad (4-31)$$

Now the sign of $N(s)$ will be evaluated at $j0$, by substituting for c_1 in Eq.(4-5)

$$\lim_{y \rightarrow 0^+} \text{sgn}(N(jy)) = \lim_{y \rightarrow 0^+} \text{sgn}\left(\sum_{i=0}^m b_i (jy)^{2i}\right) = \lim_{y \rightarrow 0^+} \text{sgn}\left(\sum_{i=0}^m (-1)^i b_i y^{2i}\right) \quad (4-32)$$

Based on the procedure followed in Eq.(4-23) and Eq.(4-24) in *Section 4.2.3*, Eq.(4-32) can then be simplified to

$$\lim_{y \rightarrow 0^+} \text{sgn}(N(jy)) = (-1)^q \text{sgn}(b_q^*) \quad (4-33)$$

Taking the product of the sign or sign limits at $j0$ and $j\omega_1$ using Eq.(4-31) and Eq.(4-33) yields Eq.(4-27), restated below:

$$(-1)^{q^*} \operatorname{sgn} \left\{ \left(b_{q^*} \right) (\alpha_1) \right\} < 0 \Leftrightarrow \text{Odd no. of zeros between } j0 \text{ and } j\omega_1$$

$$(-1)^{q^*} \operatorname{sgn} \left\{ \left(b_{q^*} \right) (\alpha_1) \right\} > 0 \Leftrightarrow \text{Even no. of zeros between } j0 \text{ and } j\omega_1$$

A change in the parity of number of zeros in Segment 4 indicates that odd number of zeros have migrated from Segment 4 to Segment 1, or vice-versa, which suggests pole-zero flipping close to the frequency ω_1 . Alternatively, it could indicate that odd number of zeros have migrated from Segment 4 to Segment 3, or vice-versa, leading to transition from MMP to RNMP zeros or vice-versa.

4.3 Multi-DoF Undamped Flexible Systems

In this section, a non-unique sufficient condition is provided to guarantee the elimination of all NMP zeros from the transfer functions of multi-DoF undamped flexible LTI systems. In order to do so, first a sufficient condition for the elimination of only CNMP zeros is derived in Section 4.3.1 i.e. **Result 5**. Following that, under the condition that **Result 5** is satisfied, the sufficient condition for the elimination of all NMP (CNMP and RNMP) zeros is derived in Section 4.3.2 i.e. **Result 6**. Note that in order for **Result 6** to be satisfied, **Result 5** must be satisfied first. Therefore, if **Result 6** is satisfied, it is implied that **Result 5** has also been satisfied thereby guaranteeing the elimination of all NMP zeros i.e. CNMP and RNMP zeros. However, the converse is not true i.e. **Result 5** can be satisfied without satisfying **Result 6**. Therefore, **Result 6** is the non-unique sufficient condition for the elimination of all NMP zeros in multi-DoF undamped flexible systems.

A sufficient condition for the elimination of only CNMP zeros (Section 4.3.1) is derived first because if collinear lumped parameter undamped flexible LTI systems exhibit NMP zeros in their transfer functions, those zeros occur only as CNMP zeros [35]. Because of their mathematical

simplicity, collinear lumped parameter models can be effectively used to investigate the dynamics of multi DoF undamped flexible systems in various applications e.g. the longitudinal and torsional vibration of building foundations [127], the torsional vibration of a drill string [128] and a hybrid powertrain [129], and acoustic properties of 1-D metamaterials [130]. Therefore, the sufficient condition for the elimination of only CNMP zeros will have practical relevance in several motion and vibration control applications where collinear lumped parameter models are used. Moreover, **Result 6** will be widely applicable to any multi-DoF undamped flexible LTI system (collinear or non-collinear lumped parameter) for the elimination of all NMP zeros i.e. CNMP and RNMP zeros.

4.3.1 A Sufficient Condition to eliminate only CNMP zeros

Result 5: In a multi-DoF undamped flexible LTI system whose transfer function is given by Eq.(4-3), a sufficient condition for the elimination of only CNMP zeros is:

$$r \leq \text{No. of modal residue sign changes} \leq r+1 \quad \text{where } r = (n - m - 1) + q^* \quad (4-34)$$

Proof: Note that in Eq.(4-34), No.” is abbreviation for “Number”. Given a sequence of modal residue signs, the number of times the sign changes in that sequence is defined as the number of modal residue sign changes. For example, consider a four-DoF undamped flexible system whose sequence of the modal residue signs is given by (+ - - +). For this sequence of modal residue signs, the number of modal residue sign changes = 2.

A new parameter r is defined in Eq.(4-34) which is the sum of number of zero pairs at infinity i.e. $(n-m-1)$ and the number of zero pairs at the origin i.e. q^* . Note that m is defined as the greatest positive integer such that $b_m \neq 0$ in Eq.(4-3) (refer to *Section 4.2.2*) and q^* is also defined as the smallest positive integer such that $b_{q^*} \neq 0$ in Eq.(4-3) (refer to *Section 4.2.3*). It is known from

existing literature that $q^* = 0$ and the value of m is independent of mass and stiffness distribution and depends only on the actuator and sensor location for certain classes of multi-DoF undamped flexible LTI systems [35, 36, 39]. For such undamped flexible systems, the value of r is fixed for a given actuator and sensor location. This allows one to make informed choices of mass and stiffness distribution in order to satisfy Eq.(4-34), thus guaranteeing the elimination of only CNMP zeros. This will be demonstrated via a case study in *Section 4.4*.

It was stated in *Section 4.2* that the distribution of the zeros is symmetric about the real axis. Therefore, we will only refer to the poles and zeros on the top half of the s-plane. Consider a n -DoF ($n > 1$) undamped flexible system whose transfer function is given by Eq.(4-3).

$$\text{No. of poles} = n \Rightarrow \text{Total no. of zeros} \leq (n-1)$$

$$\text{Since, there are } (n-m-1) \text{ zeros at infinity and } q^* \text{ at origin} \Rightarrow \text{No. of MMP zeros} \leq (n-r-1) \quad (4-35)$$

It is known from Chapter 2 that a CNMP zero always occurs along with a CMP zero in the transfer functions of multi-DoF undamped flexible systems and two MMP zeros coalesce on the imaginary axis to give rise to a pair of CMP-CNMP zeros. Therefore, a single CMP-CNMP zero pair is numerically equivalent to two MMP zeros. Therefore, if at least one pair of CMP-CNMP zeros occurs, the number of MMP zeros in Eq.(4-35) is modified to:

$$\text{No. of MMP zeros} \leq (n-r-3) \quad (4-36)$$

From **Result 1** (*Section 4.2.1*), it is known that if two adjacent poles i.e. $j\omega_i$ and $j\omega_{i+1}$ have the same sign of modal residues i.e. $\text{sgn}(\alpha_i) = \text{sgn}(\alpha_{i+1})$ then there is atleast one MMP zero trapped between these two poles i.e. $\omega_i < z_i < \omega_{i+1}$. This leads to:

$$\left(\begin{array}{l} \text{No. of same sign adjacent} \\ \text{modal residue pairs} \end{array} \right) \leq \left(\begin{array}{l} \text{No. of MMP} \\ \text{zeros} \end{array} \right) \quad (4-37)$$

Combining Eq.(4-36) and Eq.(4-37) leads to the condition for the existence of at least one CMP-CNMP zero pair.

$$\left(\begin{array}{l} \text{No. of same sign adjacent} \\ \text{modal residue pairs} \end{array} \right) \leq (n-r-3) \quad (4-38)$$

Therefore, a sufficient condition for the complete elimination of CNMP zeros is given by Eq.(4-39)

$$\left(\begin{array}{l} \text{No. of same sign adjacent} \\ \text{modal residue pairs} \end{array} \right) \geq (n-r-2) \quad (4-39)$$

Eq.(4-39) provides a lower limit on the number of same sign adjacent modal residue pairs in order to guarantee the absence of CNMP zeros. However, there is an upper limit on this quantity for a given n -DoF flexible system with total r zeros at infinity ($(n-m-1)$ zeros) and the origin (q^* zeros). This upper limit comes from Eq.(4-35) and Eq.(4-37) as shown below.

$$\begin{aligned} \text{Eq.(4-37)} &\Rightarrow \left(\begin{array}{l} \text{No. of same sign adjacent} \\ \text{modal residue pairs} \end{array} \right) \leq \left(\begin{array}{l} \text{No. of MMP} \\ \text{zeros} \end{array} \right) \\ \text{AND Eq.(4-35)} &\Rightarrow \left(\begin{array}{l} \text{No. of MMP} \\ \text{zeros} \end{array} \right) \leq (n-r-1) \\ &\Rightarrow \left(\begin{array}{l} \text{No. of same sign adjacent} \\ \text{modal residue pairs} \end{array} \right) \leq (n-r-1) \end{aligned} \quad (4-40)$$

Combining Eq.(4-39) and Eq.(4-40) provides the sufficient condition for the elimination of only CNMP zeros.

$$(n-r-2) \leq \left(\begin{array}{l} \text{No. of same sign adjacent} \\ \text{modal residue pairs} \end{array} \right) \leq (n-r-1) \quad (4-41)$$

Since a n -DoF undamped flexible system has $(n-1)$ adjacent modal residue pairs, Eq.(4-42) holds true for this system.

$$\left(\begin{array}{l} \text{No. of same sign adjacent} \\ \text{modal residue pairs} \end{array} \right) + \left(\begin{array}{l} \text{No. of modal residue} \\ \text{sign changes} \end{array} \right) = n - 1 \quad (4-42)$$

Therefore, the sufficient condition in Eq.(4-41) can be written in terms of the number of modal residue sign changes as shown in Eq.(4-34) and restated below.

$$r \leq \text{No. of modal residue sign changes} \leq r+1$$

To demonstrate an example of what the modal residue sign sequence looks like when Eq.(4-34) is satisfied, we present the case when $r = 0$ i.e. there are no zeros at infinity and the origin. The transfer functions of certain flexure mechanisms demonstrate this behavior [36, 39]. In this case Eq.(4-34) leads to the inference that the number of modal residue sign changes can either be 0 or 1. Assume that the first modal residue sign is positive, then the following sequence of modal residue signs guarantee the elimination of only CNMP zeros.

1. Number of modal residue sign changes = 0 implies that all n modal residue signs are positive. Therefore the modal residue sign sequence is given by $(+ + + \dots +)_n$. This sequence of modal residue signs is very well known in the existing literature: all modal residue signs are same. It naturally falls out of **Result 5**.

2. Number of modal residue sign changes = 1 implies that first l ($l \geq 1$) modal residues are positive and the remaining $(n-l)$ modal residues are negative. Therefore, the modal residue sign sequence is given by $((+ + + \dots +)_l (- - - \dots -)_{n-l})$. This sequence of modal residue signs is new and has not been reported in the existing literature. This demonstrates that **Result 5** can provide all possible sequence of modal residue signs for the elimination of CNMP zeros.

4.3.2 A Sufficient Condition for the elimination of all NMP zeros

Result 6: In a multi-DoF undamped flexible LTI system whose transfer function is given by Eq.(4-3) and it satisfies **Result 5**, RNMP zeros do not occur in the transfer function if the number of modal residue sign changes = r . Therefore, the elimination of all NMP zeros is guaranteed. However, one RNMP zero may occur when the number of modal residue sign changes = $r+1$. Therefore, the mathematical condition which eliminates this RNMP zero thereby guaranteeing the elimination of all NMP zeros when the number of modal residue sign changes = $r+1$ is given by:

$$\text{sgn} \left\{ \left(b_{q^*} \right) \left(b_m \right) \right\} > 0 \quad (4-43)$$

Proof: When Eq.(4-34) is satisfied to guarantee the elimination of only CNMP zeros, the number of modal residue sign changes can either be r or $r+1$. In this section, we will mathematically demonstrate that when number of modal residue sign changes = r , it also guarantees the elimination of RNMP zeros. Therefore, this condition becomes a sufficient condition for the elimination of all NMP zeros i.e. CNMP and RNMP zeros. For the special case of $r = 0$, this condition leads to the trivial case where all the modal residues have the same sign. This case has been extensively studied in the existing literature as discussed in *Section 4.1*. However, when $r \neq 0$, (which can be the case for collinear lumped parameter undamped flexible LTI systems), this sufficient condition leads to a non-trivial modal residue sign sequence which will be demonstrated in *Section 4.4* through a case study.

Furthermore, we will mathematically demonstrate in this section that when the number of modal residue sign changes = $r+1$, one RNMP zero may exist in the transfer function. Therefore, an additional mathematical condition is required to guarantee the elimination of this RNMP zero which is given by Eq.(4-43). It was stated in *Section 4.2* that the distribution of zeros is also

symmetric about the imaginary axis. Therefore, a RNMP zero occurs along with a RMP zero as a pair. For subsequent discussion, we will only refer to the RNMP zero of this pair.

Consider the case when the number of modal residue sign changes = r . This case leads to a lower limit on the number of MMP zeros as shown in Eq.(4-44).

$$\begin{aligned} \text{Eq.(4-42)} &\Rightarrow \left(\begin{array}{c} \text{No. of same sign adjacent} \\ \text{modal residue pairs} \end{array} \right) = (n-r-1), \\ \text{AND Eq.(4-37)} &\Rightarrow \left(\begin{array}{c} \text{No. of same sign adjacent} \\ \text{modal residue pairs} \end{array} \right) \leq \left(\begin{array}{c} \text{No. of MMP} \\ \text{zeros} \end{array} \right) \quad (4-44) \\ &\Rightarrow \left(\begin{array}{c} \text{No. of MMP} \\ \text{zeros} \end{array} \right) \geq n-r-1 \end{aligned}$$

The upper limit on the number of MMP zeros is given by Eq.(4-35). Considering Eq.(4-35) and Eq.(4-44) together, we come to the conclusion that the upper limit and lower limit on the number of MMP zeros is the same. Thus, the number of MMP zeros is given by Eq.(4-45)

$$\left(\begin{array}{c} \text{No. of MMP} \\ \text{zeros} \end{array} \right) = (n-r-1) \quad (4-45)$$

The transfer function of a n -DoF undamped flexible LTI system has $(n-1)$ zeros. There are total r zeros at infinity and the origin and the remaining $(n-r-1)$ zeros have been shown to be MMP zeros. Therefore, RNMP zeros cannot exist in the transfer function when the number of modal residue sign changes = r .

In fact, the distribution of MMP zeros with respect to the poles on the imaginary axis is fixed for the case when the number of modal residue sign changes = r . There are $(n-r-1)$ MMP zeros and $(n-r-1)$ same sign adjacent modal residue pairs. Therefore, it follows from **Result 1** that there is one MMP zero trapped between two adjacent poles $j\omega_i$ and $j\omega_{i+1}$ that have the same sign of

modal residues i.e. $\text{sgn}(\alpha_i) = \text{sgn}(\alpha_{i+1})$. For the special case of $r = 0$, this leads to the well-known and extensively studied pole-zero interlacing property when all modal residue signs are the same [43, 45, 46, 122].

Consider the case when the number of modal residue sign changes = $r+1$. This case leads to a lower limit on the number of MMP zeros as shown in Eq.(4-46)

$$\begin{aligned} \text{Eq.(4-42)} &\Rightarrow \left(\begin{array}{c} \text{No. of same sign adjacent} \\ \text{modal residue pairs} \end{array} \right) = (n-r-2) \\ \text{AND Eq.(4-37)} &\Rightarrow \left(\begin{array}{c} \text{No. of same sign adjacent} \\ \text{modal residue pairs} \end{array} \right) \leq \left(\begin{array}{c} \text{No. of MMP} \\ \text{zeros} \end{array} \right) \\ &\Rightarrow \left(\begin{array}{c} \text{No. of MMP} \\ \text{zeros} \end{array} \right) \geq n-r-2 \end{aligned} \quad (4-46)$$

The upper limit on the number of MMP zeros is given by Eq.(4-35). Considering Eq.(4-35) and Eq.(4-46) together leads to the following inequality in Eq.(4-47).

$$n-r-2 \leq \left(\begin{array}{c} \text{No. of MMP} \\ \text{zeros} \end{array} \right) \leq n-r-1 \quad (4-47)$$

It was mathematically shown in the previous paragraphs that if the number of MMP zeros is $(n-r-1)$, RNMP zeros will not exist in the transfer function. However, Eq.(4-47) suggests that the number of MMP zero can be either $(n-r-1)$ or $(n-r-2)$. When the number of MMP zeros is $(n-r-2)$, there is one extra zero which can exist as a RNMP zero. Therefore, a mathematical condition is needed to guarantee that this extra zero does not exist as a RNMP zero.

Result 1 proved that there are odd/even number of MMP zeros between any two adjacent poles $j\omega_i$ and $j\omega_{i+1}$ that have the same/opposite modal residue signs. Therefore, when the number of same sign adjacent modal residue pairs is $(n-r-2)$, the odd/even number of MMP zeros between any

two adjacent poles $j\omega_i$ and $j\omega_{i+1}$ that have the same/opposite modal residue sign cannot be anything but 1/0 otherwise it violates the upper limit on the number of MMP zeros as shown in Eq.(4-47). Therefore, this implies that when the number of same sign adjacent modal residue pairs is $(n-r-2)$ and the maximum number of MMP zeros possible is $(n-r-1)$, then there are $(n-r-2)$ MMP zeros in Segment 1 (refer to Fig. 2) i.e. between $j\omega_1$ (pole corresponding to the first mode) and $j\omega_n$ (pole corresponding to the last mode) in such a way that there is one MMP zero between two adjacent poles $j\omega_i$ and $j\omega_{i+1}$ that have the same modal residue sign i.e. $\text{sgn}(\alpha_i) = \text{sgn}(\alpha_{i+1})$.

The total number of zeros is $(n-1)$, out of which total r zeros are at infinity and the origin and $(n-r-2)$ zeros are MMP zeros that lie in Segment 1. Therefore, there is one zero whose location is still not certain. This zero can lie in either Segment 2, Segment 3 or Segment 4. Since a single zero indicates an odd number of zeros, **Result 2**, **Result 3** and **Result 4** can be used to determine the mathematical conditions for which this zero lies in Segment 2, Segment 3 and Segment 4 respectively. These mathematical conditions are given below.

$$\text{MMP zero in Segment 2} \Rightarrow (-1)^{n-1+m} \text{sgn}\{(b_m)(\alpha_n)\} < 0$$

$$\text{RNMP zero in Segment 3} \Rightarrow \text{sgn}\{(b_{q^*})(b_m)\} < 0 \quad (4-48)$$

$$\text{MMP zero in Segment 4} \Rightarrow (-1)^q \text{sgn}\{(b_{q^*})(\alpha_1)\} < 0$$

Eq.(4-48) provides the mathematical condition for which the zero lies in Segment 3 as a RNMP zero. When this condition is not satisfied, as shown by Eq.(4-43) (restated below), it leads to the elimination of that one RNMP zero thereby guaranteeing the absence of all NMP zeros i.e. CNMP and RNMP zeros. This concludes the proof for **Result 6**.

$$\text{sgn}\{(b_{q^*})(b_m)\} > 0$$

Note that when Eq.(4-43) is satisfied i.e. the zero does not lie in Segment 3 as a RNMP zero. Then it should either lie in Segment 2 or Segment 4 as a MMP zero. It can be easily shown that if Eq.(4-43) is satisfied, then either one of the mathematical conditions corresponding to the zero lying in either Segment 2 or Segment 4 as a MMP zero is also satisfied as shown in Eq.(4-49).

$$\operatorname{sgn} \left\{ \left(b_{q^*} \right) \left(b_m \right) \right\} > 0 \Leftrightarrow \left(\begin{array}{l} \text{MMP zero in Segment 2} \Leftrightarrow (-1)^{n-1+m} \operatorname{sgn} \left\{ \left(b_m \right) \left(\alpha_n \right) \right\} < 0 \\ \text{OR} \\ \text{MMP zero in Segment 4} \Leftrightarrow (-1)^q \operatorname{sgn} \left\{ \left(b_{q^*} \right) \left(\alpha_1 \right) \right\} < 0 \end{array} \right) \quad (4-49)$$

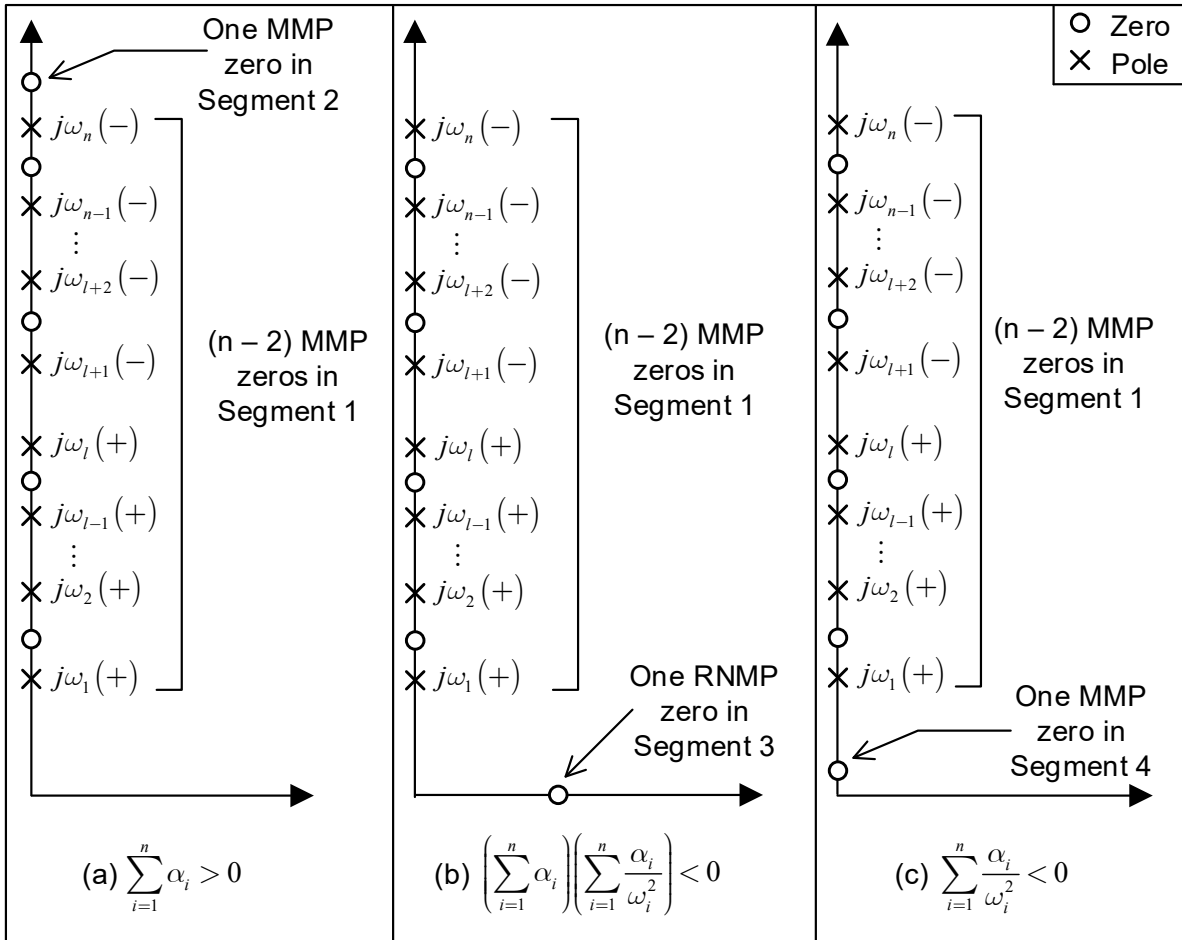


Fig 4-2 Distribution of zeros w.r.t the poles when $r = 0$ and number of modal residue sign change = 1 (a) Zero is in Segment 2 as MMP (b) Zero is in Segment 3 as RNMP (c) Zero is in Segment 4 as MMP

To demonstrate an example of the distribution of zeros with respect to the poles when **Result 6** is satisfied and when it is not satisfied, we present the case when $r = 0$ and **Result 5** is already assumed to be satisfied. In this case, when the number of modal residue sign changes = 0, it leads to the trivial case of all modal residue signs being the same which leads to pole-zero interlacing which was discussed in the prior art in Section 4.1. When the number of modal residue sign changes = 1, Fig 4-2 demonstrates the distribution of the zero with respect to the poles. The sign next to the poles indicates the sign of the corresponding modal residue in Fig 4-2.

The mathematical conditions in Fig 4-2 are derived from Eq.(4-48) when $r = 0$. This means $m = n-1$ and $q^* = 0$ from Eq.(4-34) because $m \leq n-1$ (Eq.(4-11)) and $q^* \geq 0$ (Eq.(4-20)). Since, **Result 5** is assumed to be satisfied, Fig 4-2a, Fig 4-2b, and Fig 4-2c do not exhibit CNMP zeros for any value of system parameters. Fig 4-2a and Fig 4-2c depict the case when Eq.(4-43) is satisfied leading to no RNMP zeros. There are $(n-2)$ MMP zeros in Segment 1 in Fig 4-2a and Fig 4-2c. The $(n-1)^{\text{th}}$ MMP zero lies in Segment 2 in Fig 4-2a and Segment 4 in Fig 4-2c since they satisfy the corresponding conditions in Eq.(4-48). Fig 4-2b depicts the case when Eq.(4-43) is not satisfied leading to the presence of a RNMP zero in Segment 3. The remaining $(n-2)$ MMP zeros still lie in Segment 1. Fig 4-2 will prove to be useful in selecting parameters of a multi-DoF undamped flexible LTI system in order to eliminate all NMP zeros when $r = 0$ which happens to the case for certain flexure mechanisms [36, 39].

Section 4.3 provides a non-unique sufficient condition i.e. **Result 6** for the elimination of all NMP zeros in multi-DoF undamped flexible LTI systems in terms of the system parameters –

modal residue and modal frequency without the narrow assumption of all modal residue signs being the same. In fact, this sufficient condition subsumes the already known sufficient condition that ‘all modal residue signs are same’ as well as provide other possible sequences of modal residue signs to eliminate NMP zeros. Therefore, it opens up a wider design space in terms of actuator–sensor placement and mass–stiffness distribution in order to eliminate NMP zeros.

4.4 Case Study: Four DoF Undamped Flexible System

Here we provide a case study to demonstrate the use of the sufficient condition i.e. **Result 5** derived in Section 4.3.1 to inform the choice of physical parameters in an undamped flexible system.

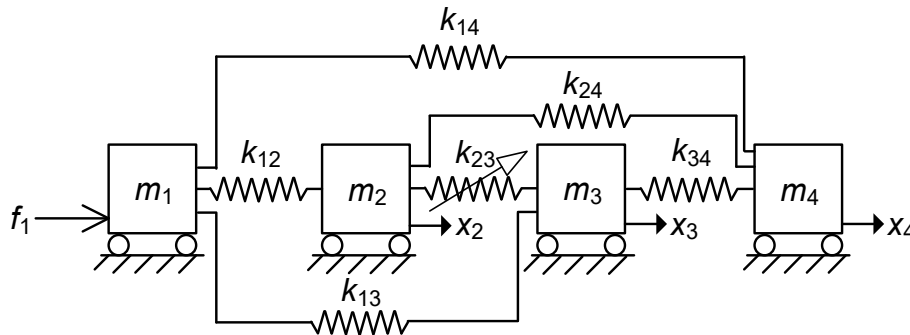


Fig 4-3 Four-doF collinear lumped parameter undamped flexible LTI system

Consider a four-DoF collinear lumped parameter undamped flexible LTI system as shown in Fig 4-3. Since, this undamped flexible system is collinear lumped parameter, its transfer function will not exhibit RNMP zeros for any value of springs and masses, as noted previously in the second paragraph of Section 4.3. However, this flexible system can still exhibit CNMP zeros. Therefore, only **Result 5** needs to be satisfied for this flexible system to eliminate CNMP zeros. Note that a collinear lumped parameter flexible system is any lumped parameter flexible system where each mass can only move in a single direction as shown in Fig 4-3. Hence, it represents a large class of

flexible systems and its study is of great practical importance as discussed in the second paragraph of Section 4.3. For this numerical example adapted from [40], $m_1 = m_2 = m_3 = m_4 = 1$, $k_{12} = k_{34} = 100$, $k_{13} = k_{14} = k_{24} = 200$, and $k_{23} = 100 + \Delta k$ where Δk lies between -100 and $+\infty$. In this section, we will examine three transfer functions between force input and displacement output: $G_{12}(s) = x_2(s)/f_1(s)$, $G_{13}(s) = x_3(s)/f_1(s)$, and $G_{14}(s) = x_4(s)/f_1(s)$; and will find the range of Δk for each transfer function over which CNMP zeros are eliminated using the sufficient condition **Result 5** (Eq.(4-34)). Note that even though we are using **Result 5** to inform the choice of stiffness Δk for each transfer function to be MP, we can also use **Result 5** to choose the sensor location for a given Δk and a given actuator location to guarantee that the transfer function is MP. The modal frequencies and mode shapes of the flexible system in terms of Δk are given below.

$$\omega_h = 0, \omega_c = \sqrt{600 + \Delta k - 100F(\Delta k)}, \omega_d = \sqrt{600}, \omega_e = \sqrt{600 + \Delta k + 100F(\Delta k)}$$

$$\phi_h = \begin{bmatrix} 1 \\ 1 \\ 1 \\ 1 \end{bmatrix}, \phi_c = \begin{bmatrix} -1 \\ \left(1 + F(\Delta k) - \frac{\Delta k}{100}\right) > 0 \\ \left(-1 - F(\Delta k) + \frac{\Delta k}{100}\right) < 0 \\ 1 \end{bmatrix}, \phi_d = \begin{bmatrix} 1 \\ -1 \\ -1 \\ 1 \end{bmatrix}, \phi_e = \begin{bmatrix} -1 \\ \left(1 - F(\Delta k) - \frac{\Delta k}{100}\right) < 0 \\ \left(-1 + F(\Delta k) + \frac{\Delta k}{100}\right) > 0 \\ 1 \end{bmatrix} \quad (4-50)$$

$$\text{where } F(\Delta k) = \frac{\sqrt{\Delta k^2 - 200\Delta k + 20000}}{100}$$

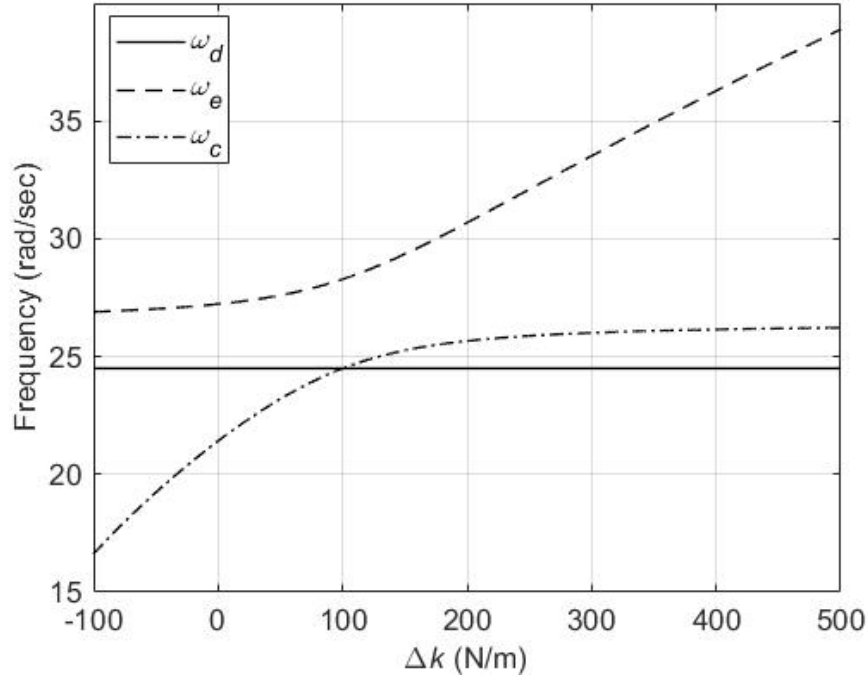


Fig 4-4 Modal frequencies of the Four DoF undamped flexible system as a function of Δk

To use Eq.(4-34), we must first ascertain the order in which the modal frequencies of the four DoF flexible system occur. The four modes of the flexible system namely mode h , mode c , mode d and mode e and their associated mode shapes are given by Eq.(4-50). Note that there are certain elements of mode shapes c and e that are functions of Δk . However, they have a fixed sign when $-100 < \Delta k < +\infty$ as shown in Eq.(4-50). Based on Eq.(4-50), $\omega_1 = \omega_h = 0$. Based on Fig 4-4, the order in which the remaining modal frequencies, ω_i occur and the construction of the mode shape matrix, $[\Psi]$ is shown below.

$$\begin{aligned} \Delta k < 100 N / m &\Rightarrow \omega_2 = \omega_c, \omega_3 = \omega_d, \omega_4 = \omega_e; [\Psi] = [\phi_h \ \phi_c \ \phi_d \ \phi_e] \\ \Delta k > 100 N / m &\Rightarrow \omega_2 = \omega_d, \omega_3 = \omega_c, \omega_4 = \omega_e; [\Psi] = [\phi_h \ \phi_d \ \phi_c \ \phi_e] \end{aligned} \quad (4-51)$$

For a lumped parameter flexible system, the modal decomposition of its transfer function is given by Eq.(4-52) [19].

$$G_{act-sens}(s) = \sum_{i=1}^n \frac{\alpha_i}{s^2 + \omega_i^2} \text{ where } \alpha_i = \frac{([\mathbf{D}][\boldsymbol{\Psi}]_i)([\boldsymbol{\Psi}]^T[\mathbf{B}]_i)}{m_i^{modal}} \quad (4-52)$$

The vectors $[\mathbf{B}]$ and $[\mathbf{D}]$ represent the actuator and sensor placement as described in Section 4.2. Since, the force is applied only at m_1 in Fig 4-3, $[\mathbf{B}] = [1 \ 0 \ 0 \ 0]^T$. For $G_{12}(s)$, the displacement of m_2 is being measured so $[\mathbf{D}] = [0 \ 1 \ 0 \ 0]$. Similarly, for $G_{13}(s)$ and $G_{14}(s)$, $[\mathbf{D}] = [0 \ 0 \ 1 \ 0]$ and $[\mathbf{D}] = [0 \ 0 \ 0 \ 1]$ respectively. m_i^{modal} represents the modal mass and is always positive. Based on Eqs.(4-50)-(4-52), we can find the sequence of modal residue signs for each transfer function as shown below.

		α_1	α_2	α_3	α_4
-100 N/m < Δk < 100 N/m	$G_{12}(s)$	+	-	-	+
	$G_{13}(s)$	+	+	-	-
	$G_{14}(s)$	+	-	+	-
$\Delta k > 100$ N/m	$G_{12}(s)$	+	-	-	+
	$G_{13}(s)$	+	-	+	-
	$G_{14}(s)$	+	+	-	-

Table 4-1 Modal residue sign sequence for transfer functions

Hoagg [35] provides the formula for the relative degree of transfer functions of collinear lumped parameter multi-DoF undamped flexible LTI systems. Based on that formula, the relative degree of $G_{12}(s)$, $G_{13}(s)$, and $G_{14}(s)$ is found to be 4 i.e. $2(n-m) = 4 \rightarrow m = 2$. Hoagg [35] also proved that these transfer functions do not have any zeros at the origin i.e. $q^* = 0$, and therefore $r = 1$ from Eq.(4-34). Therefore, the sufficient condition for the elimination of only CNMP zeros i.e. **Result 5** (Eq.(4-34)) requires that the number of modal residue sign changes is either 1 or 2. Thus, based on Table 4-1, the following inferences can be drawn.

1. The number of modal residue sign changes for $G_{12}(s)$ is 2 when $-100 \text{ N/m} < \Delta k < +\infty$. Therefore, $G_{12}(s)$ will not exhibit CNMP zeros over this range of Δk . This is independently validated by the zero locus of $G_{12}(s)$ shown below in Fig 4-5a.

2. The number of modal residue sign changes for $G_{13}(s)$ is 1 when $-100 \text{ N/m} < \Delta k < 100 \text{ N/m}$ and 3 when $\Delta k > 100 \text{ N/m}$. Therefore, $G_{13}(s)$ will not exhibit CNMP zeros when $-100 \text{ N/m} < \Delta k < 100 \text{ N/m}$. However, when $\Delta k > 100 \text{ N/m}$ $G_{13}(s)$ may or may not exhibit CNMP zeros because **Result 5** (Eq.(4-34)) is only a sufficient condition but not a necessary one to eliminate CNMP zeros. This inference is also independently validated by the zero locus of $G_{13}(s)$ in Fig 4-5b where CNMP zeros are shown not to occur when $-100 \text{ N/m} < \Delta k < 100 \text{ N/m}$ and $\Delta k > 367 \text{ N/m}$.

3. The number of modal residue sign changes for $G_{14}(s)$ is 3 when $-100 \text{ N/m} < \Delta k < 100 \text{ N/m}$ and 1 when $\Delta k > 100 \text{ N/m}$. Therefore, $G_{14}(s)$ may or may not exhibit CNMP zeros when $-100 \text{ N/m} < \Delta k < 100 \text{ N/m}$. However, when $\Delta k > 100 \text{ N/m}$ $G_{14}(s)$ will not exhibit CNMP zeros. This inference is independently validated by the zero locus of $G_{14}(s)$ in Fig 4-5c where CNMP zeros are shown not to occur when $-100 \text{ N/m} < \Delta k < -50 \text{ N/m}$ and $\Delta k > 100 \text{ N/m}$.

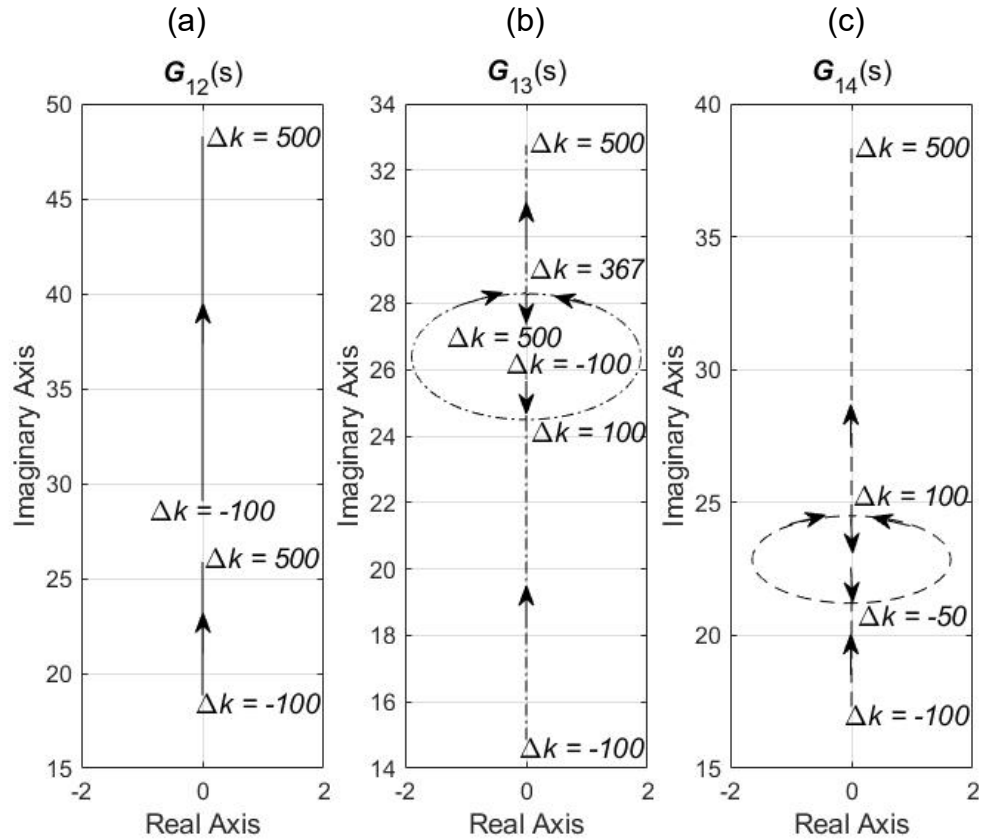


Fig 4-5 Zeros of transfer functions as a function of Δk (from $\Delta k = -100$ to $\Delta k = 500$)

In the example considered in this section, we had to make use of the equations of motion (EOMs) to derive the eigenvectors and eigenvalues in order to construct Table 4-1 and apply **Result 5**. However, **Result 5** becomes more useful and easy to apply if it can be satisfied via actuator-sensor placement. To accomplish this, an analytical model of the flexible system is not necessary. Once a rough estimate of the mode shapes are available via experimental modal analysis, then the design engineer can use them to tune the sequence of modal residue signs by varying the actuator [**B**] and/or sensor location [**D**] for the given mode shapes [ψ] (see Eq.(4-52)) to satisfy **Result 5**. **Result 5** provides all possible sequence of modal residue signs for the elimination of CNMP zeros and is not simply restricted to all modal residue signs being the same. This means that **Result 5** can

guarantee the elimination of CNMP zeros even for non-collocated actuator-sensor placement in multi-DoF undamped flexible LTI systems.

Note that, only a rough estimate of the mode shapes is enough to apply **Result 5**, since only the sign of modal residues is important and not their exact value. This also makes **Result 5** robust to parametric variations and modeling uncertainties. Once **Result 5** is satisfied, CNMP zeros are guaranteed to be absent as long as the modeling/parametric uncertainty is not large enough to alter the sequence of modal residue signs. However, if **Result 5** cannot be satisfied via actuator-sensor placement, then the design engineer will need to modify the mass-stiffness distribution to change the mode shapes directly in order to achieve the required sequence of modal residue signs. This process is more involved since it will require an analytical model of the flexible system to find the relationship between mass-stiffness distribution and the sign of modal residues.

4.5 Conclusion

This chapter provides a non-unique sufficient condition for the elimination of all NMP zeros in multi-DoF undamped flexible LTI systems in terms of the system parameters – modal residue and modal frequency without the narrow assumption of all modal residue signs being the same. In fact, the sufficient condition provided in this chapter subsumes the already known sufficient condition that ‘all modal residue signs are same’ as well as provide other possible sequences of modal residue signs to eliminate NMP zeros. Therefore, it opens up a wider design space in terms of actuator–sensor placement and mass–stiffness distribution in order to eliminate NMP zeros.

A sufficient condition for the elimination of only CNMP zeros was derived in Section 4.3.1 i.e. **Result 5**. If the undamped multi-DoF flexible LTI system is collinear lumped parameter as shown via an example in Section 4.4, then only **Result 5** needs to be satisfied to guarantee the elimination

of CNMP zeros since these systems never exhibit RNMP zeros. The sufficient condition for the elimination of all NMP zeros is derived in Section 4.3.2 i.e. **Result 6**. Note that in order for **Result 6** to be satisfied, **Result 5** must be satisfied first. Therefore, if **Result 6** is satisfied, it is implied that **Result 5** has also been satisfied thereby guaranteeing the elimination of all NMP zeros i.e. CNMP and RNMP zeros. For any general multi-DoF undamped flexible LTI system i.e. collinear or non-collinear lumped parameter, **Result 6** needs to be satisfied to guarantee the elimination of all NMP zeros.

When the sufficient condition for the elimination of NMP zeros is satisfied, the MP zeros in the multi-DoF undamped flexible LTI system lie purely on the imaginary axis i.e. MMP zeros. This is because RMP zeros always occur in pairs of RMP-RNMP zeros and CMP zeros always occur in quartets of CMP-CNMP zeros (Chapter 2). However, no practical flexible system is undamped. It has been recently demonstrated that depending on the damping strategy, the addition of damping can move the MMP zeros of undamped flexible systems to the right hand side of the imaginary axis leading to NMP zeros of their damped counterparts (Chapter 3). Therefore, in the presence of damping (even light damping), the sufficient condition derived in this chapter *may fail* to guarantee the elimination of NMP zeros. This motivates the need to identify atleast one damping strategy that preserve the MP behavior of the multi-DoF undamped flexible system by guaranteeing that the addition of damping moves the MMP zeros to the left hand side of the imaginary axis as shown below. This damping strategy is investigated in the subsequent chapter. In the presence of this damping strategy, when the flexible system is lightly damped, then the sufficient condition presented in this chapter will guarantee the elimination of NMP zeros. This will relax the strong assumption of ‘no damping’ made in this chapter.

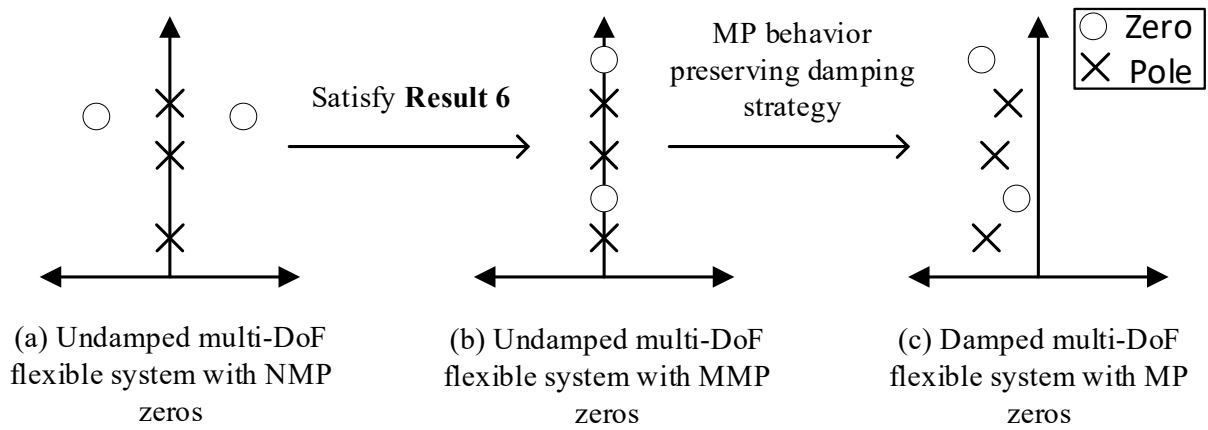


Fig 4-6 Damping strategy that preserves the MP behavior of multi-DoF undamped flexible systems

Chapter 5 Non-minimum Phase Zeros of Multi-DoF Damped Flexible Systems

This chapter investigates the non-minimum phase (NMP) zeros in the transfer function, between actuated load input and measured displacement output, of a multi-degree of freedom (DoF) flexible system in the presence of proportional viscous damping. NMP zeros have a negative impact on the dynamics and control of flexible systems and therefore are generally undesirable. Viscous damping is one potential means to eliminate NMP zeros. However, the impact of viscous damping on NMP zeros of multi-DoF flexible systems is not adequately studied or understood in the literature. In order to address this gap, a change of variable method is used to first establish a simple mathematical relationship between the zeros of a multi-DoF undamped flexible system and its proportionally damped counterpart. The “proportional” viscous damping model is used due to its practical amenability, conceptual simplicity and ease of application. This mathematical relationship (between zeros of an undamped system and its damped counterpart) is used to derive the necessary and sufficient condition for the elimination of NMP zeros in proportionally damped flexible systems. A graphical analysis of this necessary and sufficient condition is provided, which leads to the formulation of simple damping strategies. These informed damping strategies guarantee that the addition of proportional viscous damping to a multi-DoF undamped flexible system will convert all its zeros to minimum phase zeros.

5.1 Introduction and Background

The detrimental effects of non-minimum phase (NMP) zeros on the dynamic performance of flexible systems is well documented in the existing literature [14, 18, 40, 41, 82]. A zero is non-

minimum phase (NMP) if it has a positive real component, and minimum phase (MP) if it has a non-positive real component. Chen [82] mathematically demonstrated that a feedback controller's ability to reduce the tracking error is severely limited in the presence of NMP zeros in any plant dynamics including a flexible system. Freudenberg [14] and Middleton [18] mathematically demonstrated the tradeoff between disturbance rejection and stability robustness in the presence of NMP zeros. It was experimentally shown in two different investigations that poor stability robustness to modeling uncertainty due to the presence of NMP zeros leads to residual vibration in the end point positioning control of a cantilevered beam [40] and a pinned free beam [41]. These undesirable physical consequences of NMP zeros on the dynamic performance of flexible systems motivates the need to systematically and comprehensively investigate the relationship between NMP zeros and the system parameters. Such an understanding will inform the design of flexible systems in several applications, such as space structures [1, 2, 66], rotorcraft blades [5, 97], hard disk drives [3, 4], and flexure mechanisms [7, 131, 132], to intentionally eliminate NMP zeros.

In the preceding chapter, a non-unique sufficient condition was derived for the elimination of NMP zeros in the single input single output (SISO) transfer function of undamped multi-DoF flexible linear time invariant (LTI) systems. When this sufficient condition is satisfied, all the open loop zeros are guaranteed to lie on the imaginary axis along with the open loop poles, i.e. all the zeros are MMP. However, in practice, there is generally some, even if small, amount of energy dissipation, for example due to material hysteresis [133], or friction at joints/interfaces [134], or air damping [135]. In several situations, damping is intentionally added to a flexible system in order to reduce its residual vibrations in open loop [61] or to improve closed-loop robustness[136]. Irrespective of whether the damping is inherent or added externally, it moves the open loop poles of the flexible system to the left hand side (LHS) of the imaginary axis, which is generally

beneficial. However, the impact of damping on the open loop zeros is less straightforward and sparingly researched.

A detailed review of the existing literature on the effect of viscous damping on the zeros of flexible LTI systems is provided in Chapter 3. A brief summary of this review is provided here. Pang [108] demonstrated that the addition of viscous damping to an Euler-Bernoulli beam guarantees that all its zeros are MP. However, this study was limited to a collocated transfer function of a specific system and no inferences were provided on whether this result is applicable to the collocated transfer function of any general flexible system. Lin [60, 110] mathematically demonstrated that the zeros of a collocated transfer function of any general multi-DoF flexible system will be MP for any viscous damping. However, the zeros of non-collocated transfer function were not addressed. Section 3.3 in Chapter 3, under the assumption of classical viscous damping, mathematically proved that as long as all modal residue signs are the same, the zeros of collocated as well as non-collocated transfer function will be MP. A key gap in this existing literature is that it does not provide any inferences on how viscous damping can be used to eliminate NMP zeros in any general multi-DoF flexible system when all modal residue signs are not the same.

Chapter 3 investigated the effect of viscous damping on the zeros of three-DoF damped flexible systems when all modal residue signs are not the same and found that for some choice of damping values, viscous damping can convert the MMP zeros of the undamped flexible systems to NMP zeros of its damped counterpart. This is somewhat unexpected finding, i.e. that additional of damping can be detrimental to the dynamics of a flexible system. Although this detrimental effect of viscous damping on zeros was demonstrated for a three-DoF flexible system, it could be true for any multi-DoF flexible system. This means that even if the sufficient condition in the preceding

chapter is satisfied for an undamped multi-DoF flexible system and zeros are all MMP, the addition of viscous damping (either intentionally or unintentionally) can again shift the MMP zeros to the right hand side (RHS) of the imaginary axis leading to NMP zeros.

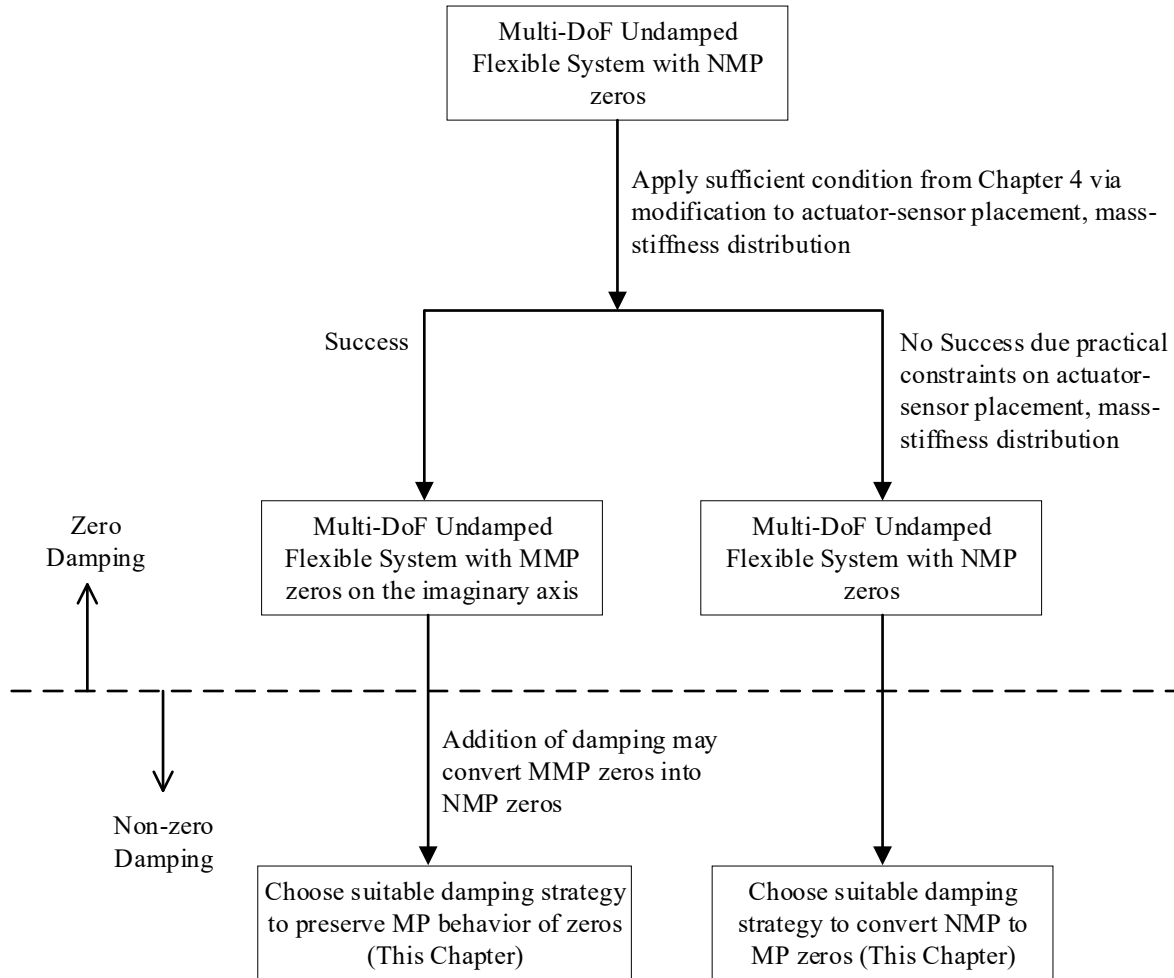


Fig 5-1 Flowchart of design strategies to eliminate NMP zeros

Fig 5-1 illustrates a design flowchart to eliminate NMP zeros in any general multi-DoF flexible system. First, an attempt is made to satisfy the sufficient condition developed in Chapter 4 via actuator-sensor placement and/or mass-stiffness distribution to guarantee the presence of only MMP zeros in the undamped flexible system, even when all modal residue signs are not the same. If this sufficient condition is satisfied, then there is a need to find at least one viscous damping

strategy that preserves this MP behavior by guaranteeing that the MMP zeros are moved to the LHS of the imaginary axis, and not to the RHS, upon addition of damping. This entire design strategy is depicted by the left arm of the flowchart in Fig 5-1. However, if the sufficient condition is not satisfied, could not be satisfied then there is a need for a viscous damping strategy that can directly convert the NMP zeros of the undamped flexible system into MP zeros of its damped counterpart. This design strategy is depicted by the right arm of the flowchart in Fig 5-1.

In order to find the suitable damping strategies described in Fig 5-1, Chapter 3 investigated the zero dynamics of three-DoF flexible systems under the assumption of “classical” viscous damping. Based on this investigation, a comprehensive set of all possible sufficient conditions were derived for the elimination of NMP zeros. This comprehensive set of all possible sufficient conditions is also the necessary condition for the elimination of NMP zeros. This necessary and sufficient condition provides the damping strategies that fulfill the requirements in Fig 5-1. However, this investigation is only practical for low DoF (e.g. 2 or 3 DoF) flexible systems because as the number of DoF (i.e. modes) increase, the parameter space also grows, making the investigation tedious and complicated.

Therefore, there remains a gap in the literature on damping strategies that meet the requirements of Fig 5-1 for any multi-DoF flexible system. In order to address this gap, we investigate the effect of proportional viscous damping on the zeros of SISO transfer functions of multi-DoF flexible LTI systems in this chapter. Proportional viscous damping is the most widely studied viscous damping model in the literature due to its conceptual simplicity and practical application in engineering practice [137-139]. In fact, proportional viscous damping is a subset of classical viscous damping [59] because it satisfies the Caughey and O’Kelly criterion, which defines classical viscous damping.

There are two novel contributions of this chapter: (1) Necessary and sufficient condition for the absence of NMP zeros in multi-DoF proportional viscous damped flexible systems (2) Case study to demonstrate the application of these proportional viscous damping strategies to guarantee the absence of NMP zeros. The rest of this chapter is organized as follows: In Section 5.2, a mathematical relationship between the zeros of a general multi-DoF undamped flexible system and its proportionally damped counterpart is formulated. In Section 5.3, the mathematical relationship derived in Section 5.2 is employed to derive the necessary and sufficient condition that guarantees that all the zeros of the multi-DoF undamped flexible system (i.e. MP and NMP zeros) are converted to MP zeros of the multi-DoF proportionally damped flexible system for a certain choice of damping. Furthermore, this necessary and sufficient condition is analytically and graphically investigated to formulate simple damping strategies to eliminate NMP zeros. Section 5.4 provides a case study of a four-DoF flexible system to demonstrate a proportional viscous damping strategy which guarantees that all the zeros of the undamped flexible system are converted into MP zeros of the resulting damped flexible system. Section 5.5 provides concluding remarks and briefly motivates the research direction in the subsequent chapters.

5.2 Proportional Damping and Modal Decomposition

Consider the equation of motion of a multi-DoF viscously damped flexible LTI system, given by:

$$\begin{aligned} [\mathbf{M}]_{n \times n} \ddot{w} + [\mathbf{C}]_{n \times n} \dot{w} + [\mathbf{K}]_{n \times n} w &= [\mathbf{B}]_{n \times 1} F \\ q &= [\mathbf{D}]_{1 \times n} w \end{aligned} \quad (5-1)$$

where $[\mathbf{M}]$, $[\mathbf{C}]$, and $[\mathbf{K}]$ denote the mass matrix, viscous damping matrix, and stiffness matrix respectively; F denotes the force acting on the flexible system through an input force vector $[\mathbf{B}]$

and q denotes the measured displacement and is a linear combination, captured by sensor vector $[\mathbf{D}]$, of the individual DoF displacements denoted by w . In this chapter we will analyze the zeros of the transfer function between applied force and measured displacement i.e. $q(s) / F(s)$.

For the flexible system to be proportionally damped, the damping matrix $[\mathbf{C}]$ should satisfy the equation below where c_M and c_K are the real valued proportional damping coefficients.

$$[\mathbf{C}] = 2c_M [\mathbf{M}] + 2c_K [\mathbf{K}] \quad (5-2)$$

Proportional damping is a special case of classical damping. Hence, the natural mode shapes of vibration (i.e. eigenvectors) of proportionally damped flexible systems are real valued and same as those of the associated undamped flexible systems [58]. Let $[\boldsymbol{\psi}]$ be a $n \times n$ vector whose columns denote the eigenvectors of the undamped multi-DoF flexible LTI system (i.e. Eq.(5-1) without the damping matrix $[\mathbf{C}]$). Since the eigenvectors of the undamped and proportionally damped multi-DoF flexible LTI system are the same, we use $[\boldsymbol{\psi}]$ to diagonalize $[\mathbf{M}]$, $[\mathbf{C}]$, and $[\mathbf{K}]$ matrices by following the steps shown in Eq.(5-3) and Eq.(5-4).

$$[\mathbf{M}]\ddot{w} + [\mathbf{C}]\dot{w} + [\mathbf{K}]w = [\mathbf{B}]F$$

$$\text{Change of variable: } w = [\boldsymbol{\psi}]w^*$$

$$\Rightarrow [\mathbf{M}][\boldsymbol{\psi}]w^{*\ddot{}} + [\mathbf{C}][\boldsymbol{\psi}]w^{*\dot{}} + [\mathbf{K}][\boldsymbol{\psi}]w^* = [\mathbf{B}]F \quad (5-3)$$

$$\text{Multiply LHS and RHS by } [\boldsymbol{\psi}]^T$$

$$\Rightarrow [\boldsymbol{\psi}]^T [\mathbf{M}][\boldsymbol{\psi}]w^{*\ddot{}} + [\boldsymbol{\psi}]^T [\mathbf{C}][\boldsymbol{\psi}]w^{*\dot{}} + [\boldsymbol{\psi}]^T [\mathbf{K}][\boldsymbol{\psi}]w^* = [\boldsymbol{\psi}]^T [\mathbf{B}]F$$

Assume that $[\boldsymbol{\psi}]$ has been normalized w.r.t $[\mathbf{M}]$

$$\Rightarrow [\boldsymbol{\psi}]^T [\mathbf{M}] [\boldsymbol{\psi}] = [\mathbf{I}]_{n \times n} \text{ where } [\mathbf{I}] \text{ is the identity matrix}$$

$$\Rightarrow [\boldsymbol{\psi}]^T [\mathbf{K}] [\boldsymbol{\psi}] = \text{diag}(\omega_1^2, \omega_2^2, \dots, \omega_n^2) \text{ where } \text{diag}(\)$$

represents a diagonal matrix (5-4)

Since $[\mathbf{C}] = 2c_M [\mathbf{M}] + 2c_K [\mathbf{K}]$

$$\Rightarrow [\boldsymbol{\psi}]^T [\mathbf{C}] [\boldsymbol{\psi}] = 2c_M [\boldsymbol{\psi}]^T [\mathbf{M}] [\boldsymbol{\psi}] + 2c_K [\boldsymbol{\psi}]^T [\mathbf{K}] [\boldsymbol{\psi}]$$

$$\Rightarrow [\boldsymbol{\psi}]^T [\mathbf{C}] [\boldsymbol{\psi}] = 2c_M [\mathbf{I}]_{n \times n} + 2c_K \text{diag}(\omega_1^2, \omega_2^2, \dots, \omega_n^2)$$

Substituting the diagonalized $[\mathbf{M}]$, $[\mathbf{C}]$, and $[\mathbf{K}]$ matrices from Eq.(5-4) into the equation of motion in Eq.(5-3) leads to a modified equation of motion in terms of the modal coordinates w^* as shown in Eq.(5-5).

$$[\mathbf{I}] \ddot{w}^* + (2c_M [\mathbf{I}] + 2c_K \text{diag}(\omega_1^2, \omega_2^2, \dots, \omega_n^2)) \dot{w}^* + \text{diag}(\omega_1^2, \omega_2^2, \dots, \omega_n^2) w^* = [\boldsymbol{\psi}]^T [\mathbf{B}] F \quad (5-5)$$

Since all the matrices on the LHS of Eq.(5-5) diagonal, the i^{th} element of w^* is given by Eq.(5-6).

$$\ddot{w}_i^* + (2c_M + 2c_K \omega_i^2) \dot{w}_i^* + \omega_i^2 w_i^* = ([\boldsymbol{\psi}]^T [\mathbf{B}])_i F$$

Taking the Laplace transform (5-6)

$$w_i^*(s) = \frac{([\boldsymbol{\psi}]^T [\mathbf{B}])_i}{s^2 + (2c_M + 2c_K \omega_i^2)s + \omega_i^2} F(s)$$

Making use of the relationship between w and w^* from Eq.(5-3) as well as w and q from Eq.(5-1), the modal decomposition of $q(s) / F(s)$ is given by Eq. (5-7). The transfer function $q(s) / F(s)$ will be denoted by $G_{pd}(s)$ where the subscript 'pd' stands for proportional damping.

Since $w = [\boldsymbol{\Psi}]w^*$ and $q = [\mathbf{D}]w$

$$\Rightarrow q = [\mathbf{D}][\boldsymbol{\Psi}]w^*$$

Taking Laplace transform

$$\Rightarrow \frac{q(s)}{F(s)} = \sum_{i=1}^n \frac{([\mathbf{D}][\boldsymbol{\Psi}]_i)([\boldsymbol{\Psi}]^T[\mathbf{B}]_i)}{s^2 + (2c_M + 2c_K\omega_i^2)s + \omega_i^2} \quad (5-7)$$

$$\Rightarrow G_{pd}(s) = \sum_{i=1}^n \frac{\alpha_i}{s^2 + (2c_M + 2c_K\omega_i^2)s + \omega_i^2}$$

$$\text{where } \alpha_i = ([\mathbf{D}][\boldsymbol{\Psi}]_i)([\boldsymbol{\Psi}]^T[\mathbf{B}]_i)$$

In this chapter, we will investigate a stable multi-DoF proportionally damped flexible system. Therefore, all the poles of the $G_{pd}(s)$ will lie on the left hand side of the imaginary axis. This implies the following:

$$c_M + c_K\omega_i^2 \geq 0 \text{ for all } \omega_i \text{ where } i \in [1, n]$$

$$\text{If } (c_M \geq 0 \text{ AND } c_K \geq 0) \Rightarrow c_M + c_K\omega_i^2 \geq 0 \text{ holds for any value of } c_M \text{ and } c_K$$

$$\text{If } (c_M > 0 \text{ AND } c_K < 0) \Rightarrow c_M + c_K\omega_i^2 \geq 0 \Leftrightarrow c_M + c_K\omega_n^2 \geq 0 \Leftrightarrow \sqrt{\frac{c_M}{-c_K}} \geq \omega_n \quad (5-8)$$

$$\text{If } (c_M < 0 \text{ AND } c_K > 0) \Rightarrow c_M + c_K\omega_i^2 \geq 0 \Leftrightarrow c_M + c_K\omega_1^2 \geq 0 \Leftrightarrow \sqrt{\frac{-c_M}{c_K}} \leq \omega_1$$

Now, we club the terms in the denominator of the second order modes and introduce a change of variable as shown in Eq.(5-9).

$$G_{pd}(s) = \frac{1}{(2c_Ks + 1)} \sum_{i=1}^n \frac{\alpha_i}{\frac{(s^2 + 2c_Ms)}{(2c_Ks + 1)} + \omega_i^2} \quad (5-9)$$

$$\text{Change of variable } \xi^2 = \frac{(s^2 + 2c_Ms)}{(2c_Ks + 1)}$$

The change of variable expresses the transfer function $G_{pd}(s)$ in terms of ξ as shown in Eq.(5-10)

$$G_{pd}(\xi) = \frac{1}{(2c_K Z(\xi) + 1)} \sum_{i=1}^n \frac{\alpha_i}{\xi^2 + \omega_i^2} \quad (5-10)$$

$$\text{where } s = Z_p(\xi) = -(c_M - c_K \xi^2) \pm \sqrt{(c_M - c_K \xi^2)^2 + \xi^2}$$

Next, we define another transfer function, $G_{ud}(\xi)$ as shown below.

$$G_{ud}(\xi) = \sum_{i=1}^n \frac{\alpha_i}{\xi^2 + \omega_i^2} \quad (5-11)$$

The subscript ‘*ud*’ stands for undamped. $G_{ud}(\xi)$ is the transfer function between the actuated load input, F and the measured displacement output, q in the absence of the proportional damping matrix $[C]$ in Eq.(5-1). This is due to the fact that the eigenvalues and the eigenvectors of the multi-DoF flexible LTI system, mathematically defined by Eq.(5-1), are independent of the proportional damping matrix $[C]$. Therefore, the modal residues (α_i) and modal frequencies (ω_i) of the undamped and proportionally damped flexible systems as shown in Eq.(5-11) and Eq.(5-7), respectively, will be the same. Hence, Eq.(5-10) can be re-written as shown below.

$$G_{pd}(s) = \frac{1}{(2c_K Z(\xi) + 1)} G_{ud}(\xi) \quad (5-12)$$

It is evident from Eq.(5-12) that the zeros of the proportionally damped flexible system, $G_{pd}(s)$ can be found by using the following method. First, find the zeros of the undamped flexible system, $G_{ud}(\xi)$ in terms of ξ by solving the equation below.

$$G_{ud}(\xi) = \sum_{i=1}^n \frac{\alpha_i}{\xi^2 + \omega_i^2} = 0 \quad (5-13)$$

Second, convert these zeros into the zeros of $G_{pd}(s)$ by using the mathematical function Z_p defined in Eq.(5-10). For example, if z_{ud} is a zero of $G_{ud}(\xi)$ which is found by solving Eq.(5-13),

then $Z_p(z_{ud})$ is the zero of $G_{pd}(s)$. Therefore, the function Z_p converts the zeros of the multi-DoF undamped flexible LTI system to the zeros of the multi-DoF proportionally damped flexible LTI system. If the relative degree of the transfer function of the undamped flexible system is greater than two, this means that some of its zeros are at infinity. When proportional viscous damping is added to the undamped flexible system, these zeros at infinity are converted to finite zeros given by Eq. (5-14). Therefore, a positive value of c_K must be used to convert the zeros of an undamped flexible system that lie at infinity to a RMP zero of the proportionally damped flexible system.

$$\xi^2 = \frac{(s^2 + 2c_M s)}{(2c_K s + 1)} \Rightarrow \text{If } \xi = \infty, \text{ then } s = -\frac{1}{2c_K} \quad (5-14)$$

5.3 Necessary and Sufficient Condition for the elimination of NMP Zeros

Non-minimum phase zeros are defined as zeros that lie strictly on the right hand side (RHS) of the imaginary axis. In this section, we present the necessary and sufficient condition for the elimination of NMP zeros in proportionally damped flexible system. It is given by:

$$\text{Re}(Z_p(\xi_{ud})) \leq 0 \quad (5-15)$$

ξ_{ud} is the zero of the undamped flexible system because it satisfies Eq.(5-11). Consider the Cartesian representation of ξ_{ud} i.e. $\xi_{ud} = x+jy$ and substitute it in the function $Z_p(\xi_{ud})$ given by Eq.(5-10). This leads to:

$$Z_p(x+jy) = -(c_M - c_K(x+jy)^2) \pm \sqrt{(c_M - c_K(x+jy)^2)^2 + (x+jy)^2} \quad (5-16)$$

Extracting the real part of $Z_p(x+jy)$ from Eq.(5-16) leads to:

$$\operatorname{Re}(Z_p(x + jy)) = f(x, y) \pm h(x, y)$$

where

$$f(x, y) \triangleq c_K(x^2 - y^2) - c_M$$

$$h(x, y) \triangleq \frac{\sqrt{\sqrt{h_1(x, y)^2 + h_2(x, y)^2} + h_1(x, y)}}{\sqrt{2}} \quad (5-17)$$

$$h_1(x, y) \triangleq (c_K(x^2 - y^2) - c_M)^2 - 4c_K^2 x^2 y^2 + x^2 - y^2$$

$$h_2(x, y) \triangleq 2xy(2c_K^2 x^2 - 2c_K^2 y^2 - 2c_M c_K + 1)$$

In order to find the necessary and sufficient condition for the elimination of NMP zeros, Eq.(5-15) must be satisfied. This leads to the following:

$$\operatorname{Re}(Z_p(x + jy)) \leq 0$$

$$\Rightarrow f(x, y) \pm h(x, y) \leq 0 \quad (5-18)$$

$$\Rightarrow f(x, y) - h(x, y) \leq 0 \text{ AND } f(x, y) + h(x, y) \leq 0$$

From Eq.(5-17), it can be inferred that $h(x, y)$ is a positive real valued function. However, $f(x, y)$ is real valued function that can take positive or negative values. Therefore, the following can be inferred:

$$f(x, y) + h(x, y) \leq 0$$

$$\Rightarrow f(x, y) - h(x, y) \leq -2h(x, y)$$

$$\text{Since } h(x, y) \geq 0 \quad (5-19)$$

$$\Rightarrow f(x, y) - h(x, y) \leq 0$$

$$\therefore f(x, y) \pm h(x, y) \leq 0 \Leftrightarrow f(x, y) + h(x, y) \leq 0$$

Therefore, based on Eq.(5-19), the necessary and sufficient condition for the elimination of NMP zeros is given by:

$$f(x, y) + h(x, y) \leq 0 \quad (5-20)$$

The zeros of a multi-DoF undamped flexible LTI system are symmetric about the real and imaginary axis (Chapter 2). The functions $f(x, y)$ and $h(x, y)$ are also symmetric about the real and imaginary axis i.e. the x and y axis in the Cartesian plane. Hence, given a multi-DoF undamped flexible LTI system, one can find its zeros and choose the proportional damping coefficients i.e. c_M and c_K such that Eq.(5-20) is satisfied for each undamped zero that lies in the first quadrant of the s -plane (or equivalently the Cartesian plane) including the positive real and imaginary axis (or equivalently the positive x and y axis). This will ensure that all the zeros of the proportionally damped multi-DoF flexible LTI system are minimum phase.

We will now provide the graphical depiction of Eq.(5-20) being satisfied in the x - y plane in order to attain design insights into the choice of proportional damping coefficients i.e. c_M and c_K . In order to graphically depict the region in the x - y plane where Eq.(5-20) is satisfied, we need to study the properties of the curve derived from Eq.(5-20). Since the curve derived from Eq.(5-20) does not represent any known conic section, we will refer to this curve as the envelope curve. It is mathematically defined in Eq.(5-21). The curve given by $f(x, y) = 0$ ($f(x, y)$ is defined in Eq.(5-17)) represents a standard hyperbola.

$$\begin{aligned} \text{Hyperbola: } f(x, y) &= 0 \\ \text{Envelope Curve: } f(x, y) + h(x, y) &= 0 \end{aligned} \quad (5-21)$$

The asymptote for this hyperbola is given by $x = y$ in the first quadrant of the Cartesian plane. The center of this hyperbola lies at the origin and its vertex lies either on the x axis or the y axis depending on the relative signs of c_M and c_K .

In order to find the region in the first quadrant of the Cartesian plane where Eq.(5-20) is satisfied, we need to plot the Envelope Curve in the Cartesian plane. Therefore, we find the intersection of the envelope curve with the x and y axis in **Result 1**. In **Result 2**, we find the bounds for the envelope curve. Based on **Result 1** and **Result 2**, we plot the envelope curve in the Cartesian plane as shown Fig 5-2. The envelope curve divides the Cartesian plane into two regions. In one region $f(x, y) + h(x, y) > 0$ and in another region $f(x, y) + h(x, y) < 0$. In **Result 3**, we ascertain which region of the Cartesian plane belongs to which inequality. This finally gives the region where Eq.(5-20) is satisfied. Note that in the sequence of this chapter, Fig 5-2 is repeatedly referenced during the discussion of **Results 1, 2** and **3** before it is actually presented. This is only done to demonstrate how the inferences from these results lead to the construction of Fig 5-2. All inferences about the zeros of the proportionally damped flexible system drawn from Fig 5-2 are provided after the presentation of the figure.

Result 1: The intersection of the hyperbola and the envelope curve with the x and y axis is summarized in below:

	Intersection with x axis	Intersection with y axis
	$c_M \geq 0$ AND $c_K \geq 0$	$x = \sqrt{\frac{c_M}{c_K}}$
		No intersection (except when $c_M = 0$)
Hyperbola	$c_M > 0$ AND $c_K < 0$	No intersection
		$y = \sqrt{-\frac{c_M}{c_K}}$
	$c_M < 0$ AND $c_K > 0$	No intersection
		$y = \sqrt{-\frac{c_M}{c_K}}$
	$c_M \geq 0$ AND $c_K \geq 0$	$x = 0$
		$y = 0$

			$y = 0$
Envelope	$c_M > 0$ AND $c_K < 0$	$x = 0$	$y = \sqrt{-\frac{c_M}{c_K}}$
Curve	$c_M < 0$ AND $c_K > 0$	No intersection	$y = \sqrt{-\frac{c_M}{c_K}}$

Table 5-1: Intersection of the hyperbola and envelope curve with the x and y axis.

Proof: As discussed before, the vertex of the hyperbola lies either on the x axis or on the y axis depending on the relative sign of c_M and c_K .

Vertex on the x axis: $y = 0$

$$f(x, 0) = 0$$

$$\Rightarrow c_K x^2 - c_M = 0 \quad (5-22)$$

$$\Rightarrow x = \pm \sqrt{\frac{c_M}{c_K}} \left(\text{Solution exists if } \frac{c_M}{c_K} \geq 0 \right)$$

Based on Eq.(5-22), it can be inferred that the vertex of the hyperbola lies on the x axis when $c_M \geq 0$ AND $c_K \geq 0$. Note that c_M and c_K cannot be negative simultaneously because it will lead to an unstable flexible system (refer to Eq.(5-7) and Eq.(5-8)). The hyperbola along with its asymptote is shown in Fig 5-2a and Fig 5-2c. Note that when $c_M > 0$ and $c_K = 0$, the hyperbola is said to lie at infinity because its vertex lies at infinity. Therefore, the hyperbola is not shown in Fig 5-2b.

Vertex on the y axis: $x = 0$

$$f(0, y) = 0$$

$$\Rightarrow -c_K y^2 - c_M = 0 \quad (5-23)$$

$$\Rightarrow y = \pm \sqrt{-\frac{c_M}{c_K}} \left(\text{Solution exists if } \frac{c_M}{c_K} < 0 \right)$$

Based on Eq.(5-23), it can be inferred that the vertex of the hyperbola lies on the y axis for two different combinations of signs of c_M and c_K : ($c_M > 0$ AND $c_K < 0$) and ($c_M < 0$ AND $c_K > 0$). The hyperbola along with its asymptote is shown in Fig 5-2d and Fig 5-2e.

For the envelope curve given by Eq.(5-21) and Eq.(5-17), the intersection with the x and y axis is given below:

$$\begin{aligned}
 &\text{Intersection with } x \text{ axis: } y = 0 \\
 &f(x, 0) + h(x, 0) = 0 \\
 &\Rightarrow (c_K x^2 - c_M) + \sqrt{(c_K x^2 - c_M)^2 + x^2} = 0 \\
 &\Rightarrow x = 0 \text{ (solution exists if } c_M > 0)
 \end{aligned} \tag{5-24}$$

Based on Eq.(5-24), the envelope curve intersects with the x axis at the origin for two different combinations of signs of c_M and c_K : ($c_M > 0$ AND $c_K > 0$) and ($c_M > 0$ AND $c_K < 0$).

$$\begin{aligned}
 &\text{Intersection with } y \text{ axis: } x = 0 \\
 &f(0, y) + h(0, y) = 0 \\
 &\Rightarrow -c_K y^2 - c_M + \sqrt{\frac{|h_1(0, y)| + h_1(0, y)}{2}} = 0 \\
 &\text{where } h_1(0, y) = (c_K y^2 + c_M)^2 - y^2
 \end{aligned} \tag{5-25}$$

$$\begin{aligned}
 &\text{If } h_1(0, y) > 0 \\
 &\Rightarrow -(c_K y^2 + c_M) + \sqrt{(c_K y^2 + c_M)^2 - y^2} = 0 \\
 &\Rightarrow y = 0 \text{ (solution exists if } c_M > 0 \Rightarrow h_1(0, 0) > 0)
 \end{aligned} \tag{5-26}$$

Eq.(5-26) leads to the same conclusion as Eq.(5-24) i.e. the envelope curve intersects with the x and y axis at the origin when ($c_M > 0$ AND $c_K > 0$) and ($c_M > 0$ AND $c_K < 0$).

$$\begin{aligned}
& \text{If } h_1(0, y) < 0 \\
& \Rightarrow -(c_K y^2 + c_M) = 0 \tag{5-27} \\
& \Rightarrow y = \sqrt{-\frac{c_M}{c_K}} \left(\text{solution exists if } \frac{c_M}{c_K} < 0 \Rightarrow h_1 \left(0, \sqrt{-\frac{c_M}{c_K}} \right) < 0 \right)
\end{aligned}$$

Based on Eq.(5-27), the envelope curve intersects with the y axis at non-zero values of y for two different combinations of signs of c_M and c_K : ($c_M > 0$ AND $c_K < 0$) and ($c_M < 0$ AND $c_K > 0$). The results from the above equations are summarized in Table 5-1.

Now, we will find the boundaries within which the envelope curve will lie in the Cartesian plane for different values of c_M and c_K . This is done because the envelope curve is a complicated curve and difficult to understand. Therefore, we seek to find simpler curves that bound the envelope curve. These simple curves derived in **Result 2** and graphically depicted in Fig 5-2 will help us better understand the properties of the envelope curve.

Result 2: The following statements provide the bounds for the envelope curve in the first quadrant of the Cartesian plane for different combination of signs of c_M and c_K :

Result 2.1: $(c_M \geq 0 \text{ AND } c_K > 0) \text{ AND } c_M c_K \leq 0.25$

\Rightarrow Envelope curve lies on the LHS of the curve: $x = y$

Result 2.2: $(c_M > 0 \text{ AND } c_K = 0)$

\Rightarrow Envelope curve lies on the LHS of the curve: $x = y$ AND on the LHS of the curve: $x = c_M$

Result 2.3: $(c_M > 0 \text{ AND } c_K > 0) \text{ AND } c_M c_K > 0.25$

\Rightarrow Envelope curve lies on the RHS of the curve: $x = y$ AND on the LHS of the hyperbola

Result 2.4: $(c_M > 0, c_K < 0)$

\Rightarrow Envelope curve lies inside the triangle whose edges are given by $x = y$, $y = \sqrt{-\frac{c_M}{c_K}}$,

and the y axis

Result 2.5: $(c_M < 0, c_K > 0)$

\Rightarrow Envelope curve lies on the LHS of the hyperbola

Proof: For $c_M \geq 0$ AND $c_K \geq 0$, **Result 1** showed that the vertex of the hyperbola (i.e. $f(x, y) = 0$) is on the x axis at $x = \sqrt{(c_M / c_K)}$. The hyperbola along with its asymptote $x = y$ is shown in Fig 5-2a and Fig 5-2c for the case $c_M \geq 0$ AND $c_K > 0$. For the special case $c_M > 0$ AND $c_K = 0$, the hyperbola lies at infinity and therefore not shown in Fig 5-2b. For $c_M \geq 0$ AND $c_K \geq 0$, **Result 1** showed that the envelope curve intersects the x and y axis only at the origin. Now we will prove that for $c_M \geq 0$ AND $c_K > 0$ the envelope curve always lies to the left hand side (LHS) of the hyperbola.

It can be observed from Fig 5-2a and Fig 5-2c that the hyperbola divides the first quadrant of the Cartesian plane (including the x and y axis) into two regions. In Fig 5-2b, since the hyperbola lies at infinity, the entire first quadrant of the Cartesian plane lies to the LHS of this hyperbola. In one region of the first quadrant of the Cartesian plane, $f(x, y) < 0$ and in another region $f(x, y) > 0$. The envelope curve whose equation is given by $f(x, y) + h(x, y) = 0$ can only exist in the region where

$f(x,y) < 0$ since $h(x,y) \geq 0$ (refer to Eq.(5-17)). Therefore, we need to ascertain which region of the first quadrant of the Cartesian plane belongs to $f(x,y) < 0$. It can be seen in Fig 5-2a and Fig 5-2c that the region on the left hand side (LHS) of the hyperbola consists of the entire y axis. Therefore, we evaluate the expression $f(x,y)$ on the y axis as shown below for the case when $c_M \geq 0$, $c_K \geq 0$:

$$f(0,y) = -c_K y^2 - c_M < 0 \quad (5-28)$$

Note that when $c_K = 0$, c_M has to be greater than 0 otherwise it will lead to an unstable flexible system (refer to Eq.(5-7) and Eq.(5-8)). Therefore, for the case $c_M > 0$ AND $c_K = 0$ the entire first quadrant of the Cartesian plan satisfies Eq.(5-28). Eq.(5-28) proves that the envelope curve exists in that region of the first quadrant of the Cartesian plane that consists of the y axis. Hence, the envelope curve always lies on the LHS of the hyperbola as shown in Fig 5-2a and Fig 5-2c when $c_M \geq 0$ AND $c_K > 0$. The envelope curve can lie anywhere in the first quadrant of the Cartesian plane when $c_M > 0$ AND $c_K = 0$.

Now, we will impose a stricter bound on envelope curve when $(c_M \geq 0$ AND $c_K > 0)$ AND $c_M c_K \leq 0.25$ i.e. the envelope curve will always lie on the LHS of the curve: $x = y$ as shown in Fig 5-2a.

The mathematical proof is as follows:

$$\begin{aligned} f(x,y) + h(x,y) &= 0 \\ \Rightarrow h(x,y)^2 &= f(x,y)^2 \\ \Rightarrow \sqrt{h_1(x,y)^2 + h_2(x,y)^2} + h_1(x,y) &= 2f(x,y)^2 \\ \Rightarrow h_1(x,y)^2 + h_1(x,y)^2 &= (2f(x,y)^2 - h_1(x,y))^2 \\ \Rightarrow x^2 y^2 (4c_K f(x,y) + 1) &= f(x,y)^2 (y^2 - x^2) \end{aligned} \quad (5-29)$$

Consider the following change of variable in terms of A and B as shown below and rewrite the last line of Eq.(5-29) by substituting $f(x,y)$ with A and B .

$$\begin{aligned}
A &\triangleq (y^2 - x^2), \quad B \triangleq xy \\
\Rightarrow B^2(-4c_K^2 A + 1 - 4c_K c_M) &= A(c_K A + c_M)^2 \\
\Rightarrow B^2(1 - 4c_K c_M) &= A[(c_K A + c_M)^2 + (2c_K B)^2]
\end{aligned} \tag{5-30}$$

So far in Eq.(5-29) and Eq.(5-30), we did not consider the sign of c_M and c_K . Consider the case when $c_M \geq 0$, $c_K \geq 0$. Based on Eq.(5-30), the following inference can be made:

$$\begin{aligned}
&\text{If } c_K c_M \leq 0.25 \\
&\Rightarrow B^2(1 - 4c_K c_M) \geq 0 \\
&\Rightarrow A[(c_K A + c_M)^2 + (2c_K B)^2] \geq 0 \\
&\Rightarrow A \geq 0 \Leftrightarrow y^2 \geq x^2
\end{aligned} \tag{5-31}$$

Eq.(5-31) shows that when ($c_M \geq 0$ AND $c_K > 0$) AND $c_K c_M \leq 0.25$, the envelope curve lies in that region of the first quadrant of the Cartesian plane where $y \geq x$. This completes the proof for **Result 2.1. Result 1** and **Result 2.1** are used together to plot the envelope curve in Fig 5-2a for the case when ($c_M \geq 0$ AND $c_K > 0$) AND $c_K c_M \leq 0.25$. Therefore, the envelope curve lies on the LHS of the curve: $y = x$ as shown in Fig 5-2a.

Now, we will consider the case when $c_M > 0$ AND $c_K = 0$. For this case as well Eq.(5-31) is true. Therefore, the envelope curve lies on the LHS of the curve: $y = x$ as shown in Fig 5-2b. Furthermore, we will show that for this case the envelope curve is also horizontally bounded by the line $x = c_M$.

$$\begin{aligned}
f(x, y) + h(x, y) &= 0 \\
\Rightarrow h(x, y) &= -f(x, y) \\
\text{Since } c_K &= 0 \\
\Rightarrow h(x, y) &= c_M \\
\text{Since } h(x, y) &\geq 0 \text{ and } c_M > 0 \\
\Rightarrow h(x, y)^2 &= c_M^2 \\
\Rightarrow \sqrt{h_1(x, y)^2 + h_2(x, y)^2} + h_1(x, y) &= 2c_M^2 \\
\Rightarrow \sqrt{(c_M^2 + x^2 - y^2)^2 + 4x^2y^2} &= (c_M^2 + y^2 - x^2) \\
\Rightarrow (c_M^2 + x^2 - y^2)^2 + 4x^2y^2 &= (c_M^2 + y^2 - x^2)^2 \\
\Rightarrow x^2y^2 + c_M^2x^2 &= c_M^2y^2 \\
\Rightarrow c_M^2x^2 &= y^2(c_M^2 - x^2)
\end{aligned} \tag{5-32}$$

Since the LHS of Eq.(5-32) is always a positive value, this implies that the RHS of Eq.(5-32) should also be a positive value. Therefore, the following inequality must hold:

$$x^2 < c_M^2 \tag{5-33}$$

Eq.(5-33) shows that when $c_M > 0$ AND $c_K = 0$, the envelope curve lies in that region of the first quadrant of the Cartesian plane where $x < c_M$. This completes the proof for **Result 2.2**. **Result 1** and **Result 2.2** are used together to plot the envelope curve in Fig 5-2b for the case when $c_M > 0$ AND $c_K = 0$. Therefore, the envelope curve lies on the LHS of the curves: $y = x$ and $x = c_M$ as shown in Fig 5-2b.

Now we consider the case when $(c_M > 0$ AND $c_K > 0)$ AND $c_K c_M > 0.25$. The following derivation is based on Eq.(5-30).

$$\begin{aligned}
& \text{If } c_K c_M > 0.25 \\
& \Rightarrow B^2 (1 - 4 c_K c_M) < 0 \\
& \Rightarrow A \left[(c_K A + c_M)^2 + (2c_K B)^2 \right] < 0 \\
& \Rightarrow A < 0 \Leftrightarrow y^2 < x^2
\end{aligned} \tag{5-34}$$

Eq.(5-34) shows that when $(c_M > 0 \text{ AND } c_K > 0) \text{ AND } c_K c_M > 0.25$, the envelope curve lies in that region of the first quadrant of the Cartesian plane where $y < x$. This concludes the proof for **Result 2.3. Result 1** and **Result 2.3** are used together to plot the envelope curve in Fig 5-2c for the case when $(c_M > 0 \text{ AND } c_K > 0) \text{ AND } c_K c_M > 0.25$. Therefore, the envelope curve lies on the RHS of the curve: $y = x$ and on the LHS of the hyperbola (as previously proven) as shown in Fig 5-2c.

Consider the case when $c_M > 0 \text{ AND } c_K < 0$. Based on Eq.(5-30), the following inference can be made:

$$\begin{aligned}
& \text{If } c_K c_M < 0 \\
& \Rightarrow B^2 (1 - 4 c_K c_M) > 0 \\
& \Rightarrow A \left[(c_K A + c_M)^2 + (2c_K B)^2 \right] > 0 \\
& \Rightarrow A > 0 \Leftrightarrow y^2 > x^2
\end{aligned} \tag{5-35}$$

Eq.(5-35) shows that when $c_M > 0 \text{ AND } c_K < 0$, the envelope curve lies in that region of the first quadrant of the Cartesian plane where $y > x$. Therefore, the envelope curve lies on the LHS of the curve: $y = x$ as shown in Fig 5-2d. Now we will prove that the envelope curve is also bounded vertically by the line $y = \sqrt{-(c_M / c_K)}$.

$$\begin{aligned}
& f(x, y) + h(x, y) = 0 \\
& \Leftrightarrow h(x, y)^2 - f(x, y)^2 = 0 \text{ AND } f(x, y) \leq 0
\end{aligned} \tag{5-36}$$

The function $h(x, y)^2 - f(x, y)^2 = 0$ is expanded based on Eq.(5-29) as shown below:

$$\begin{aligned}
& x^2 y^2 (4c_K f(x, y) + 1) - f(x, y)^2 (y^2 - x^2) = 0 \\
& \Rightarrow c_K^2 (x^2 + y^2)(x^4 - y^4) - 2c_K c_M (x^4 + y^4) \\
& \quad + c_M^2 (x^2 - y^2) + x^2 y^2 = 0 \\
& \Rightarrow a_1 x^6 + a_2 x^4 + a_3 x^2 + a_4 = 0
\end{aligned} \tag{5-37}$$

$$\begin{aligned}
& \text{where } a_1 = c_K^2, \quad a_2 = c_K^2 y^2 - 2c_K c_M \\
& a_3 = y^2 + c_M^2 - c_K^2 y^4, \quad a_4 = -c_K^2 y^6 - 2c_K c_M y^4 - c_M^2 y^2
\end{aligned}$$

$$\begin{aligned}
& \text{Let } g(w) = a_1 w^3 + a_2 w^2 + a_3 w + a_4 \\
& \Rightarrow g(x^2) = a_1 x^6 + a_2 x^4 + a_3 x^2 + a_4
\end{aligned} \tag{5-38}$$

Now, we will prove that when $c_M > 0$ AND $c_K < 0$, $f(x, y) \leq 0$ (from Eq.(5-36)) and $y > \sqrt{-(c_M/c_K)}$, it implies that $g(x^2) > 0$.

$$\begin{aligned}
& f(x, y) \leq 0 \text{ AND } \left(y^2 > -\frac{c_M}{c_K} \right) \\
& \Rightarrow x^2 \geq y^2 + \frac{c_M}{c_K} > 0
\end{aligned} \tag{5-39}$$

$$\text{Since } a_1 = c_K^2 > 0$$

$$\Rightarrow a_1 x^6 \geq a_1 \left(y^2 + \frac{c_M}{c_K} \right)^3$$

$$\text{Expand the expression: } a_2 \left(y^2 + \frac{c_M}{c_K} \right) + a_3$$

$$a_2 \left(y^2 + \frac{c_M}{c_K} \right) + a_3 = y^2 - c_M c_K \left(y^2 + \frac{c_M}{c_K} \right) > 0$$

$$\text{Since } x^2 \geq y^2 + \frac{c_M}{c_K} > 0$$

$$\Rightarrow a_2 x^2 + a_3 \geq a_2 \left(y^2 + \frac{c_M}{c_K} \right) + a_3 > 0$$

$$\begin{aligned} & \text{Multiple LHS by } x^2 \text{ and RHS by } \left(y^2 + \frac{c_M}{c_K} \right) \\ \Rightarrow a_2 x^4 + a_3 x^2 & \geq a_2 \left(y^2 + \frac{c_M}{c_K} \right)^2 + a_3 \left(y^2 + \frac{c_M}{c_K} \right) \end{aligned} \quad (5-40)$$

Adding the inequalities in Eq.(5-39) and Eq.(5-40) leads to the following:

$$\begin{aligned} g(x^2) & \geq g\left(y^2 + \frac{c_M}{c_K}\right) \\ \text{On expanding the expression: } g\left(y^2 + \frac{c_M}{c_K}\right) & \\ g\left(y^2 + \frac{c_M}{c_K}\right) & = y^2 \left(y^2 + \frac{c_M}{c_K} \right) > 0 \\ \Rightarrow g(x^2) & \geq g\left(y^2 + \frac{c_M}{c_K}\right) > 0 \end{aligned} \quad (5-41)$$

Eq.(5-41) shows that when $f(x, y) < 0$ and $y > \sqrt{-(c_M/c_K)}$, $h(x, y)^2 - f(x, y)^2 \neq 0$. Therefore, based on Eq.(5-36), we can conclude the following for the case when $c_M > 0$, $c_K < 0$.

$$f(x, y) + h(x, y) = 0 \Rightarrow y \leq \sqrt{-\frac{c_M}{c_K}} \quad (5-42)$$

Combining Eq.(5-35) and Eq.(5-42) leads to the triangular bound for the envelope curve.

$$f(x, y) + h(x, y) = 0 \Rightarrow x < y \leq \sqrt{-\frac{c_M}{c_K}} \quad (5-43)$$

Eq.(5-43) proves **Result 2.4**. **Result 1** and **Result 2.4** are used together to plot the envelope curve in Fig 5-2d for the case when ($c_M > 0$ AND $c_K > 0$). Therefore, Fig 5-2d shows when ($c_M > 0$ AND $c_K < 0$), the envelope curve lies inside the triangular region whose edges are given by $x = y$ and $y = \sqrt{-(c_M/c_K)}$ and the y axis.

For the case when ($c_M < 0$ AND $c_K > 0$), **Result 1** showed that the vertex of the hyperbola is on the y axis at $y = \sqrt{(-c_M/c_K)}$. The hyperbola along with its asymptote $x = y$ is shown in Fig 5-2e. For the case ($c_M < 0$ AND $c_K > 0$), **Result 1** showed that the envelope curve intersects only the y axis at $y = \sqrt{(-c_M/c_K)}$. Now we will prove that for ($c_M < 0$ AND $c_K > 0$) the envelope curve always lies to the left hand side (LHS) of the hyperbola. Since $h(x, y)$ is non-negative, the following inequality should hold true:

$$f(x, y) + h(x, y) = 0 \Rightarrow f(x, y) \leq 0 \quad (5-44)$$

It can be seen from Fig 5-2e that the hyperbola ($f(x, y) = 0$) divides the first quadrant of the Cartesian plane into two regions. In one region $f(x, y) > 0$ and in another region $f(x, y) < 0$. We need to ascertain which region belongs to which inequality. The region on the RHS of the hyperbola consists of the entire x axis. Therefore, we evaluate the sign of $f(x, y)$ on the x axis.

$$f(x, 0) = c_K x^2 - c_M > 0 \quad (5-45)$$

Eq.(5-45) shows that the region on the RHS of the hyperbola does not satisfy $f(x, y) < 0$. Hence, the region on the LHS of the hyperbola satisfies $f(x, y) < 0$. This completes the proof for **Result 2.5**. **Result 1** and **Result 2.5** are used together to plot the envelope curve in Fig 5-2e for the case when ($c_M < 0$ AND $c_K > 0$). Therefore, Fig 5-2e shows that when ($c_M < 0$ AND $c_K > 0$), the envelope curve lies on the LHS of the hyperbola.

So far we have only found the boundaries for the envelope curve in terms of simple curves for different values of c_M and c_K . We still have to find the region in the first quadrant of the Cartesian plane that satisfies the necessary and sufficient condition for the elimination of NMP zeros given by Eq.(5-20).

Result 3: For all combination of signs of c_M and c_K , the region in the first quadrant of the Cartesian plane (including the x and y axis) that satisfies Eq.(5-20) always lies on the LHS of the envelope curve.

Proof: In order to prove **Result 3**, we use the same mathematical technique that was used in **Result 2.1** and **Result 2.5**. It can be observed in Fig 5-2 that the envelope curve i.e. $f(x, y) + h(x, y) = 0$ divides the first quadrant of the Cartesian plane into two regions. One region lies on the LHS of the envelope curve and other region lies on its RHS. In one of the region, $f(x, y) + h(x, y) < 0$ and in the other region $f(x, y) + h(x, y) > 0$. The entire x axis resides in the RHS region for all combination of signs of c_M and c_K as observed in Fig 5-2. Therefore, we evaluate the function $f(x, y) + h(x, y)$ on the x axis to ascertain which inequality holds in the RHS region.

$$\begin{aligned}
 & f(x, 0) + h(x, 0) \\
 \Rightarrow & (c_K x^2 - c_M) + \sqrt{\frac{h_1(x, 0)^2 + h_2(x, 0)^2 + h_1(x, 0)}{2}} \\
 \text{Since } h_2(x, 0) = 0, & h_1(x, 0) = (c_K x^2 - c_M)^2 + x^2 \geq 0 \quad (5-46) \\
 \Rightarrow & (c_K x^2 - c_M) + \sqrt{(c_K x^2 - c_M)^2 + x^2} \geq 0 \\
 \Rightarrow & f(x, 0) + h(x, 0) \geq 0
 \end{aligned}$$

Based on Eq.(5-46), the region that lies on the RHS of the envelope curve does not satisfy $f(x, y) + h(x, y) < 0$. Hence, the region that lies on the LHS of the envelope curve will satisfy Eq.(5-20) for all combination of signs of c_M and c_K . This region is shaded in pink in Fig 5-2. Therefore, as long as all the zeros of the undamped multi-DoF flexible LTI system lie in the shaded region in Fig 5-2, the zeros of the proportionally damped multi-DoF flexible LTI system are guaranteed to be minimum phase.

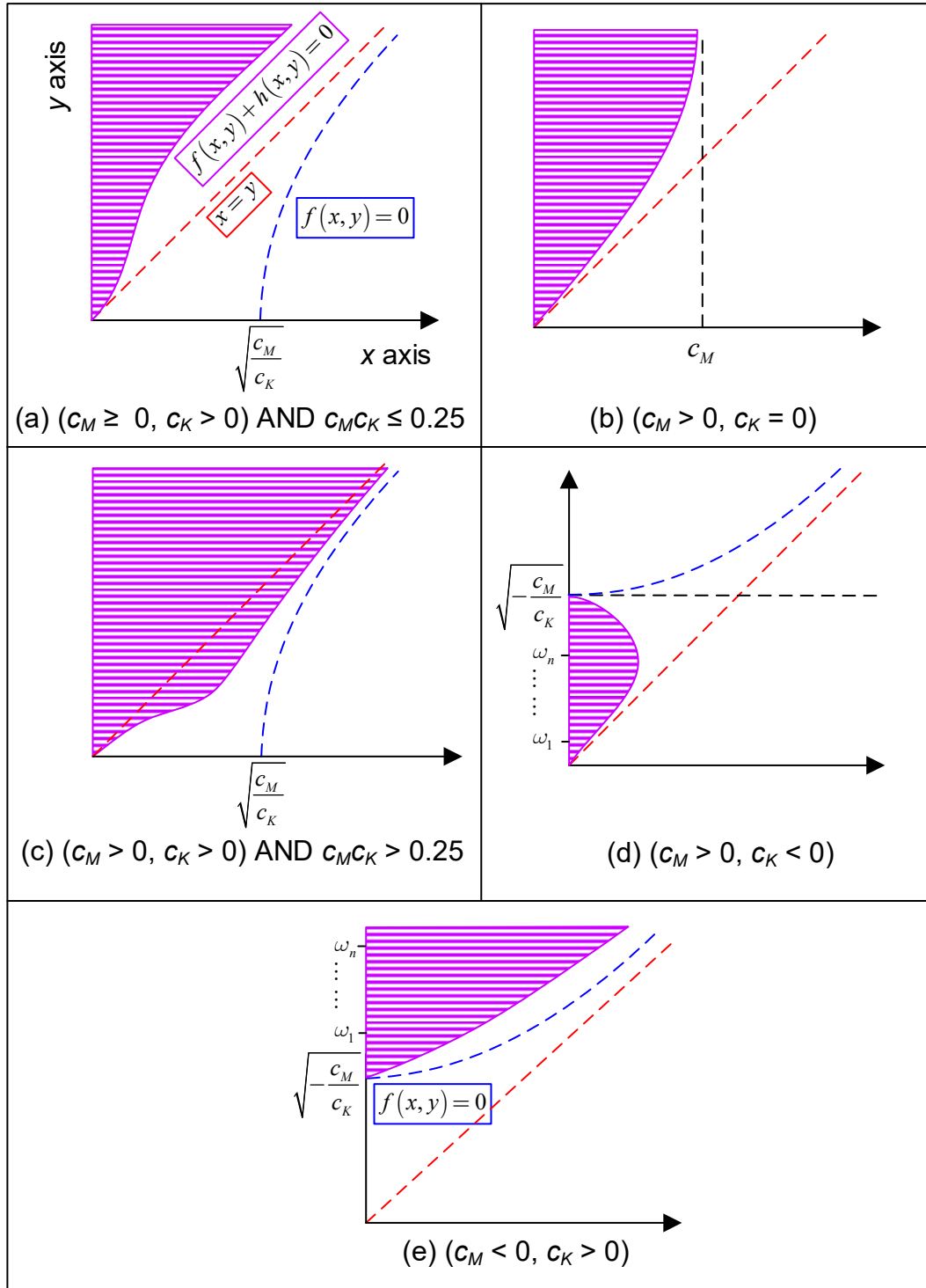


Fig 5-2 Pink shaded regions in the first quadrant of the Cartesian plane that satisfy Eq. (5-20)

The right edge of the shaded region is the envelope curve which is a rather complicated curve in terms of x and y . Therefore, Fig 5-2 also provides the boundaries within which the shaded region exists for a given set of damping coefficients c_M and c_K . These boundaries are in terms of relatively simpler curves such as a hyperbola and a straight line that can be easily visualized. It is a necessary but not a sufficient condition that the zeros of the undamped flexible system should lie inside these boundaries for the elimination of NMP zeros. For example, in Fig 5-2a, Fig 5-2b, Fig 5-2d, and Fig 5-2e the shaded region always lies on the LHS of the curve $x = y$. This means that if any NMP zero of the undamped flexible system lies outside this boundary i.e. to the RHS of the curve $x = y$, it can never be converted into a MP zero of the proportionally damped flexible system.

It can be clearly observed in Fig 5-2 that the entire positive real axis is never a part of the shaded region for any value of proportional damping coefficients c_M and c_K . Hence, a real non-minimum phase (RNMP) zero of a multi-DoF undamped flexible system cannot be converted to a minimum phase (MP) zero of the multi-DoF proportionally damped flexible system. However, for several practical applications with finite closed loop bandwidth requirement, it is not always necessary to eliminate a RNMP zero if it can be placed beyond the desired bandwidth. Given the desired closed loop bandwidth, desired reduction in the sensitivity function below the closed loop bandwidth, and the acceptable lower limit for the peak of the sensitivity function, the Poisson Sensitivity Integral theorem [14] will provide the desired position of the RNMP zero on the real axis, for example at z_d . If the RNMP zero of the undamped flexible system is at located at z_u , then Eq.(5-47) can be used to provide the values of the proportional damping coefficients c_M and c_K that converts the RNMP zero of the undamped flexible system at z_u to the RNMP zero of the proportionally damped flexible system at z_d . Achieving better dynamic performance in the presence of RNMP zeros as described above requires the RNMP zero to be moved further away from the imaginary axis i.e. z_d

$> z_u$. The next chapter will provide a proportional viscous damping strategy i.e. choice of c_M and c_K to move the RNMP zeros further away from the imaginary axis.

$$-(c_M - c_K z_u^2) + \sqrt{(c_M - c_K z_u^2)^2 + z_u^2} = z_d \quad (5-47)$$

Based on the graphical depiction of the necessary and sufficient condition provided in Fig 5-2, a few simple damping strategies can be formulated as shown below:

1. If all the zeros of the undamped flexible system lie purely on the imaginary axis, then any positive value of c_M and/or c_K , however small, will always guarantee that the ensuing zeros of the proportionally damped flexible system are strictly minimum phase i.e. lie to the LHS of the imaginary axis. This is because for this choice of c_M and c_K the entire y axis satisfies Eq.(5-20) as shown in Fig 5-2a – Fig 5-2c. Therefore, this damping strategy is particularly useful for application to infinite-DoF undamped flexible systems whose infinitely many zeros lie all over the imaginary axis. This damping strategy is robust to uncertainty and variation in the location of the zeros of the undamped flexible system on the imaginary axis.
2. If the complex non-minimum phase (CNMP) zeros of the undamped flexible system lies on the RHS of the curve $x = y$ i.e. the magnitude of its real part is larger than the magnitude of its imaginary part, then one must use values of c_M and c_K such that $c_M c_K > 0.25$ as shown in Fig 5-2c.
3. When either c_M or c_K are negative, only a portion of the imaginary axis is part of the shaded region as shown in Fig 5-2d and Fig 5-2e. The advantage of using negative c_M or c_K is that it leads to smaller damping values and fewer dashpots (i.e. viscous dampers) to fulfill the necessary and sufficient condition for the elimination of NMP zeros.

4. Therefore, if the imaginary part of the zeros of the undamped flexible system is lower than the modal frequency corresponding to the last mode i.e. ω_n as shown in Fig 5-2d, then one must consider using negative value of c_K and positive value of c_M .

5. Similarly, based on Fig 5-2e, if the imaginary part of the zeros of the undamped flexible system is higher than the modal frequency corresponding to the first mode i.e. ω_1 then one must consider using positive value of c_K and negative value of c_M .

5.4 Case Study: Four-DoF Flexible System

In this section, a proportional viscous damping strategy is provided to eliminate NMP zeros from the transfer functions of a four-DoF collinear lumped parameter flexible LTI system shown in Fig 5-3.

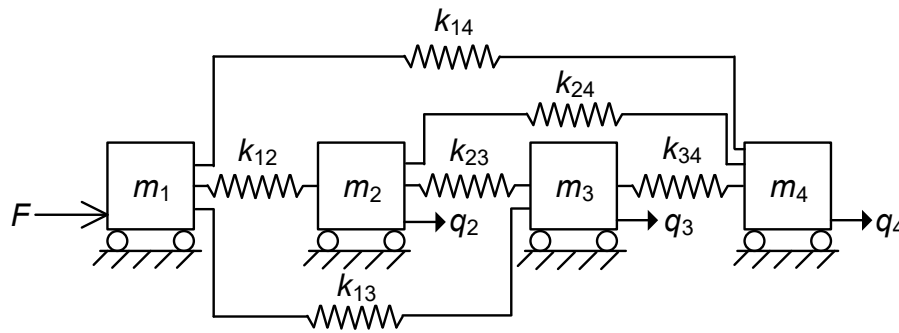


Fig 5-3 Undamped four-DoF flexible system

A collinear lumped parameter flexible system is any lumped parameter flexible system where each mass can only move in a single direction as shown in Fig 5-3 [35]. Hence, it represents a large class of flexible systems and its study is of great practical importance. A collinear lumped parameter flexible system does not exhibit RNMP zeros for any choice of physical parameters but it can exhibit CNMP zeros [35]. Therefore, it is possible to choose proportional damping coefficients c_M and c_K such that the necessary and sufficient condition for the elimination of NMP

zeros i.e. Eq.(5-20) is satisfied. In doing so, we will make use of a damping strategy formulated in Section 5.3 from the graphical depiction of Eq.(5-20) in Fig 5-2. Consider the four-DoF undamped flexible system shown in Fig 5-3. For this numerical example adopted from Section 4.4 of Chapter 4, $m_1 = m_2 = m_3 = m_4 = 1$, $k_{12} = k_{34} = 100$, $k_{13} = k_{14} = k_{24} = 200$, and $k_{23} = 100$. In this section, we will examine three transfer functions between force input and displacement output: $G_{12}(s) = q_2(s)/F(s)$, $G_{13}(s) = q_3(s)/F(s)$, and $G_{14}(s) = q_4(s)/F(s)$ and find the values of proportional damping coefficients c_M and c_K that guarantee that the zeros of all these transfer functions are minimum phase.

In order to do so, we first examine the zeros of these transfer function when the flexible system is undamped as shown in Fig 5-3. Based on the roots of their numerator, the zeros of the transfer functions is given by:

$$\begin{aligned}
 \text{Zeros of } G_{12,ud}(s) &: \pm 22.82j, \pm 31.29j \\
 \text{Zeros of } G_{13,ud}(s) &: \pm 19.53j, \pm 25.85j \\
 \text{Zeros of } G_{14,ud}(s) &: \pm 1.58 \pm 22.42j
 \end{aligned} \tag{5-48}$$

The zeros of the transfer function $G_{12,ud}(s)$ and $G_{13,ud}(s)$ lie purely on the y axis. One pair of zeros of the transfer function $G_{14,ud}(s)$ has positive real component i.e. it is CNMP zero pair. Since all the zeros in Eq.(5-48) and the envelope curve are symmetric about the x and y axis as discussed in Section 5.3, we will only consider the zeros that lie in the first quadrant of the Cartesian plane (including the x and y axis) in order to find the values of proportional damping coefficients c_M and c_K that satisfy Eq.(5-20). To do so, we set up an optimization problem that minimizes the amount of damping required to guarantee that all the zeros of the proportionally damped flexible system are minimum phase.

$$\begin{aligned}
& \min c_M^2 + c_K^2 \\
& \text{subject to } f(x_i, y_i) + h(x_i, y_i) \leq 0 \\
& \text{where } x_i + jy_i \text{ is the zero of the undamped flexible} \\
& \text{system that lies in the first quadrant}
\end{aligned} \tag{5-49}$$

Based on Eq.(5-48), there are 5 zeros of the undamped flexible system that lie in the first quadrant. Therefore, the optimization problem in Eq.(5-49) will have five constraints; i.e. one constraint corresponding to each zero. However, based on the damping strategies formulated at the end of Section 5.3 (see bullet point 1), we can reduce the number of constraints to be solved in Eq.(5-49). Four out of the five zeros in Eq.(5-48) lie purely on the y axis. Therefore, if we add the additional constraints that $(c_M \geq 0 \text{ AND } c_K \geq 0)$ to Eq.(5-49), we can remove the constraints corresponding to the purely imaginary zeros. This is because when $(c_M \geq 0 \text{ AND } c_K \geq 0)$, the entire y axis satisfies the Eq.(5-20) for any value of c_M and c_K as shown in Fig 5-2a, Fig 5-2b, and Fig 5-2c . Therefore, the optimization problem in Eq.(5-49) can be recast as follows:

$$\begin{aligned}
& \min c_M^2 + c_K^2 \\
& \text{subject to } f(1.58, 22.42) + h(1.58, 22.42) \leq 0 \\
& c_M \geq 0, c_K \geq 0
\end{aligned} \tag{5-50}$$

Since, we are assuming a proportional damping strategy i.e. $[\mathbf{C}] = 2c_M[\mathbf{M}] + 2c_K[\mathbf{K}]$, a non-zero value of c_M would physically mean that there are dashpot (i.e. viscous dampers) connections between the masses and the ground. The undamped flexible system considered in Fig 5-3 has no connections between any of the masses and the ground. Therefore, providing a proportional damping strategy with non-zero c_M may lead to loss of functionality for the flexible system. For example, the flexible system in Fig 5-3 may represent the lumped parameter model of a motion stage with transmission compliance that has infinite range of travel with respect to the ground and

placing a dashpot connecting the motion stage and the ground may limit its range of travel. Furthermore, it is logistically easier to reduce the number of dashpots required to accomplish the task of eliminating NMP zeros. Therefore, for the sake of practicality of the proposed proportional damping strategy, we assume that $c_M = 0$. Finally the optimization problem becomes the following:

$$\begin{aligned} \min \quad & c_K^2 \\ \text{subject to} \quad & f(1.58, 22.42) + h(1.58, 22.42) \leq 0, \quad c_K \geq 0 \end{aligned} \tag{5-51}$$

The optimization problem in Eq.(5-51) is solved in MATLAB using the fmincon routine. It leads to $c_K = 0.0032$. This is smallest value of c_K required to guarantee that all the zeros of the undamped flexible system are converted to minimum phase zeros of the proportionally damped flexible system. The envelope curve is graphically depicted below for three different values of c_K i.e. $c_K < 0.0032$, $c_K = 0.0032$, and $c_K > 0.0032$ along with the zeros of the undamped flexible system. The ensuing zeros of the proportionally damped flexible system are provided in the table below.

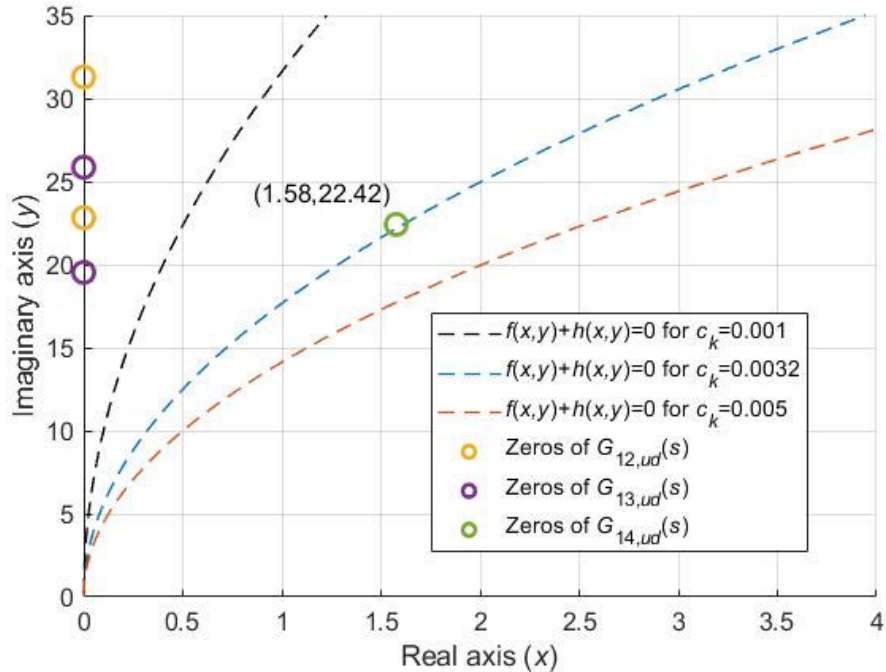


Fig 5-4 Position of the zeros of the undamped flexible system with respect to the envelope curve
for different c_K

	c_K		
	0.001	0.0032	0.005
$G_{12, pd}(s)$	$-0.52 \pm 22.81j$	$-1.66 \pm 22.76j$	$-2.60 \pm 22.67j$
	$-0.97 \pm 31.27j$	$-3.13 \pm 31.13j$	$-4.90 \pm 30.90j$
	-500.00	-156.25	-100.00
$G_{13, pd}(s)$	$-0.38 \pm 19.52j$	$-1.22 \pm 19.49j$	$-1.90 \pm 19.43j$
	$-0.66 \pm 25.84j$	$-2.14 \pm 25.77j$	$-3.34 \pm 25.64j$
	-500.00	-156.25	-100.00
$G_{14, pd}(s)$	$1.07 \pm 22.48j$	$-0.035 \pm 22.58j$	$-0.95 \pm 22.63j$
	$-2.07 \pm 22.34j$	$-3.16 \pm 22.13j$	$-4.04 \pm 21.92j$
	-500.00	-156.25	-100.00

Table 5-2 Zeros of the transfer functions of the proportionally damped four DoF flexible system

The following inferences are drawn from Fig 5-4 and Table 5-2:

1. If a value of $c_K < 0.0032$ is chosen, for example $c_K = 0.001$, then the CNMP zero of $G_{14, ud}(s)$ lies on the RHS of the envelope curve because the constraint in Eq.(5-51) is not satisfied. Hence, one zero pair of the $G_{14, pd}(s)$ will be NMP.
2. For $c_K = 0.0032$, the CNMP zero of $G_{14, ud}(s)$ lies on the LHS of the envelope curve but very close to the edge such that the equality constraint for $f(x,y)+h(x,y)$ in Eq.(5-51) is nearly satisfied. This means that the one of the zeros of $G_{14, pd}(s)$ will lie very close to imaginary axis.

3. However, if the CNMP zero of $G_{14, ud}(s)$ lies very close to the edge of the envelope curve, any uncertainty in the position of this zero can push it outside the envelope curve. Therefore, for practical purposes a larger value of c_K must be used i.e. $c_K > 0.0032$. For example, for $c_K = 0.005$, the CNMP zero of undamped $G_{14, ud}(s)$ lies well within the envelope curve. Therefore, all the zeros of $G_{14, pd}(s)$ will lie safely to the left hand side of the imaginary axis.
4. For any value of c_K , the zeros of $G_{12, ud}(s)$ and $G_{13, ud}(s)$ lie well within the envelope curve, hence the zeros of $G_{12, pd}(s)$ and $G_{13, pd}(s)$ will lie safely to the left hand side of the imaginary axis.
5. There is an additional real minimum phase (RMP) zero that appears in all the transfer functions of the proportionally damped flexible system. This additional RMP zero corresponds to the zero of the undamped flexible system that lied at infinity. The location of this additional zero is given by Eq.(5-14).

The proportional viscous damping strategy discussed above can be physically implemented as shown in Fig 5-5. Since $c_M = 0$ and c_k is a finite number, it means that there is a dashpot placed between two masses if there is a spring connecting them. The numerical value of the dashpots is given by Eq.(5-52).

$$c_{ij} = 2c_K k_{ij} \text{ where } c_K \geq 0.0032$$

$$\text{for any } i, j \in \{1, 2, 3, 4\} \text{ and } i \neq j$$
(5-52)

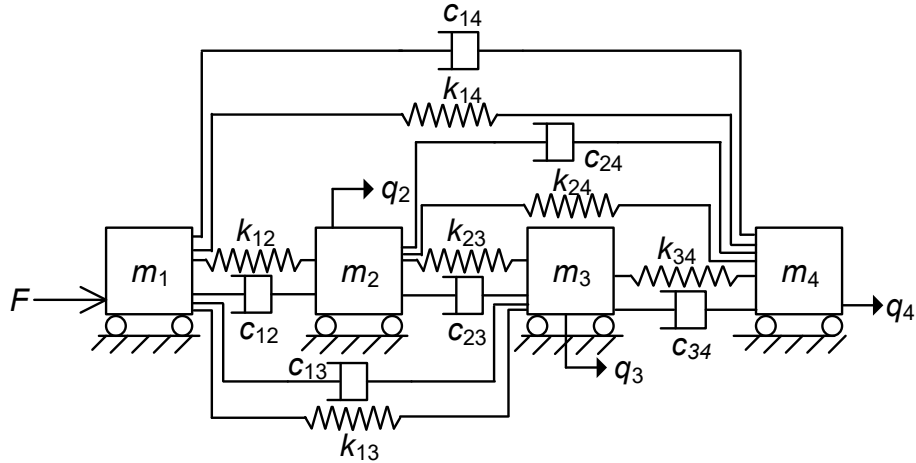


Fig 5-5 Dashpot placement in proportionally damped four-DoF flexible system

5.5 Conclusion

This chapter investigates the zeros of multi-DoF flexible LTI systems in the presence of proportional viscous damping and provides the necessary and sufficient condition for the elimination of NMP zeros. The motivation for this investigation came from the need to find a damping strategy that meets the requirements of Fig 5-1 in Section 5.1. The proportional viscous damping strategy discussed in Section 5.4 (via a case study) meets those requirements. The four-DoF undamped flexible system used in the case study in Section 5.4 was also used in the preceding Chapter 4. For the choice of stiffness values made in this chapter, $G_{12, ud}(s)$ and $G_{13, ud}(s)$ satisfy the sufficient condition for the elimination of NMP zeros in undamped flexible systems provided in Chapter 4 and therefore, they are MP. $G_{14, ud}(s)$ does not satisfy that sufficient condition and is found to be NMP. The proportional viscous damping strategy discussed in Section 5.4 preserves the MP behavior of $G_{12, ud}(s)$ and $G_{13, ud}(s)$ by guaranteeing that the zeros of $G_{12, pd}(s)$ and $G_{13, pd}(s)$ are MP and it also converts the NMP zeros of $G_{14, ud}(s)$ to the MP zeros of $G_{14, pd}(s)$. Therefore, it satisfies all the requirements of Fig 5-1.

The damping strategy discussed in this chapter is robust to parametric variations and modeling uncertainty in the actuator and sensor placement, given by $[\mathbf{B}]$ and $[\mathbf{D}]$ respectively. Variation in these vectors lead to variations in the position of the zeros of the undamped flexible system in the Cartesian plane. Therefore, a design engineer should choose the appropriate values of c_M and c_K to create a large enough envelope curve that accommodates all possible positions of the zeros of the undamped flexible system on its LHS. This will guarantee that the zeros of the proportionally damped flexible system are MP. The robustness of this damping strategy to variations in mass-stiffness distribution requires further investigation. Therefore it is a topic for future research which has not been covered in this thesis.

Chapter 6 Improving the Step Response Performance of Flexible Systems in the Presence of Real Non-minimum Phase Zeros

The presence of real non-minimum phase (RNMP) zeros places a severe tradeoff between the settling time and undershoot in the step response of flexible systems. This trade-off cannot be overcome by any combination of feedback and feedforward control. However, the severity of this tradeoff can be reduced by tuning the open-loop dynamics of the flexible system in order to push the RNMP zeros further away from the imaginary axis. In this chapter, RNMP zeros of flexible systems are investigated in the presence of proportional viscous damping. A proportional viscous damping strategy is proposed to push all the RNMP zeros further away from the imaginary axis. Finally, a step-by-step design strategy is proposed to apply this damping to a three link flexible manipulator in order to achieve simultaneous improvement in the settling time and undershoot in the step response of the flexible system.

6.1 Introduction and Background

Several flexible systems such as flexible link manipulators [41, 91, 140-143] and beams under different boundary conditions [31, 87, 89] exhibit real non-minimum phase (RNMP) zeros in their single input single output (SISO) transfer function when the actuator and sensor are non-collocated. A RNMP zero is a zero that lies on the positive real axis in the s -plane. The presence of these zeros makes the control of flexible systems a challenging problem to solve. Kamaldar [16] mathematically proved that the presence of RNMP zero guarantees undershoot in the step response

of any dynamic system including flexible systems. Furthermore, Middleton [18], Lau [17], and Kamaldar [16] independently proved that fast settling time and small undershoot, which are of practical relevance in several motion control applications, are incompatible requirements in the presence of an RNMP zero. This tradeoff between settling time and undershoot is algebraically expressed by the equation below.

$$\frac{1-\beta}{e^{xt_s}-1} \leq y_{us} \quad (6-1)$$

In Eq.(6-1), β is the settling window, t_s is the settling time for the given settling window β , x is the RNMP zero i.e. $x > 0$, y_{us} (> 0) is undershoot in the step response. Eq.(6-1) shows that for a fixed value of RNMP zero (x), if one tries to aggressively reduce the settling time (t_s), the lower limit for undershoot (y_{us}) will increase. This will eventually lead to a larger undershoot (y_{us}). Conversely, Eq.(6-1) also shows that smaller undershoot is achieved at the expense of larger settling time. This inference is true, even in the presence of any feedback or feedforward control strategy because they cannot change the location of the RNMP zeros of the plant. For example, Bayat [21] proposed a fractional order feedback controller to partially cancel the RNMP zeros of the plant. However, as a result of this, the settling time of the closed-loop system increased, demonstrating that the tradeoff between settling time and undershoot predicted by Eq.(6-1) was still active. As another example, Zhao [26] proposed a feedforward control strategy to guarantee the minimum possible settling time in accordance with Eq.(6-1) for a given undershoot and RNMP zero. Therefore, the only way to simultaneously achieve lower settling time and undershoot is to either eliminate RNMP zeros so that Eq.(6-1) is no longer valid or push the RNMP zeros further away from the imaginary axis to reduce the severity of the tradeoff imposed by Eq.(6-1). Both of

these objectives can only be accomplished by tuning the open loop dynamics of the flexible system via choice of actuator-sensor placement, mass-stiffness distribution and damping strategy.

A detailed review of RNMP zeros in flexible systems is provided in Chapter 1 and Chapter 2. A brief summary is provided here. Spector [31, 87] studied the effect of varying the sensor position in a pinned-free beam model and reported that as the separation between the actuator and sensor increases, the RNMP zeros move closer to the imaginary axis. Lee [89] reported the same observation for a free-free beam. However, no conclusions were drawn on how other physical parameters such as mass-stiffness distribution or damping can be varied to push RNMP zeros to higher frequencies, for a given actuator and sensor position. Vakil [91] investigated the effect of mass-stiffness distribution in order to push the RNMP zeros further away from the imaginary axis. However, these results were only applicable to a pinned-free beam. There are two key gaps in the existing literature. First, they are system-specific and do not provide any general design guideline for either eliminating or pushing the RNMP zeros further away from the imaginary axis, for any multi-DoF flexible system when the actuator and sensor are non-collocated. Second, they do not study the effect of damping on RNMP zeros. Among the various potential strategies for changing the location of RNMP zeros in flexible systems such as the addition of viscous damping, actuator-sensor placement and mass-stiffness distribution, the addition of viscous damping can prove to be the most desirable strategy. This is because it can be used to simultaneously shift the undamped poles of the flexible system to the left-hand side (LHS) of the imaginary axis and push the RNMP zeros further away from the imaginary axis, leading to better overall dynamic performance. However, while the impact of viscous damping on the poles is well characterized and is found to be beneficial [62, 102, 136], its impact on the zeros is less straightforward and sparingly researched as compared to the poles.

Chapter 3 provides a detailed review of the effect of viscous damping on the zeros of flexible systems. A brief summary of this review is provided here. Pang [108] investigated the effect of adding viscous damping to an Euler-Bernoulli beam model when the actuator and sensor are collocated and found that all zeros are minimum-phase (MP) i.e. the zeros have non-positive real component. However, this study did not comment on whether this result holds true for the collocated transfer function of any general flexible system. Lin [60, 110] showed that the zeros of a collocated transfer function of any general multi-DoF flexible system will be MP for any viscous damping. However, the zeros of non-collocated transfer function were not addressed. Section 3.3 in Chapter 3, under the assumption of classical viscous damping, showed that as long as all modal residue signs are the same, the zeros of collocated as well as non-collocated transfer function will be MP. A key gap in this existing literature is that it does not provide any inferences on how viscous damping can be used to either eliminate or push RNMP zeros further away from the imaginary axis, for any general multi-DoF flexible system when all modal residue signs are not the same.

In order to fill this gap, Section 3.4 and Section 3.5 in Chapter 3 investigated the effect of viscous damping on the zeros of two and three-DoF damped flexible systems when all modal residue signs are not the same and reported the necessary and sufficient conditions for the elimination of all NMP zeros including RNMP zeros. However, the methodology developed in these papers becomes increasingly complicated and tedious for higher DoF flexible systems. Therefore, there remains the need for a viscous damping strategy, applicable to any general multi-DoF flexible LTI system, that can either eliminate RNMP zeros or push them further away from the imaginary axis so that it is possible to simultaneously achieve fast settling time and small undershoot.

In order fill this gap, we investigate the effect of proportional viscous damping on the RNMP zeros of multi-DoF flexible LTI systems. Proportional viscous damping is the most widely studied viscous damping model in the literature due to its conceptual simplicity and practical application in engineering practice [137-139].

There are two novel contributions of this chapter: (1) Derivation of a proportional viscous damping strategy that moves all the RNMP zeros of any general multi-DoF flexible LTI system further away from the imaginary axis. This derivation is provided in Section 6.2 (2) A case study that demonstrates a step-by-step design strategy to apply this viscous damping to a multi-DoF flexible LTI system in order to simultaneously achieve fast settling time and small undershoot. This design strategy is provided in Section 6.3. Finally, Section 6.4 provides the conclusion and briefly discusses future research.

6.2 Proportional Viscous Damping Strategy

Consider the equation of motion of a multi-degree of freedom (DoF) viscously damped flexible LTI system, given by:

$$\begin{aligned} [\mathbf{M}]_{n \times n} \ddot{w} + [\mathbf{C}]_{n \times n} \dot{w} + [\mathbf{K}]_{n \times n} w &= [\mathbf{B}]_{n \times 1} F \\ q &= [\mathbf{D}]_{1 \times n} w \end{aligned} \tag{6-2}$$

where $[\mathbf{M}]$, $[\mathbf{C}]$ and $[\mathbf{K}]$ denote the mass, viscous damping, and stiffness matrices respectively; F denotes the force acting on the flexible system through an input vector $[\mathbf{B}]$; and q is the measured displacement and is a linear combination, captured by sensor vector $[\mathbf{D}]$, of the individual DoF displacements denoted by w . n is referred to as the number of DoFs of the flexible system. The transfer function of interest is between the applied force, F and measured displacement, q i.e. $q(s) / F(s)$.

If a flexible system is proportionally damped, then its damping matrix i.e. $[\mathbf{C}]$ should satisfy the following:

$$[\mathbf{C}] = 2c_M [\mathbf{M}] + 2c_K [\mathbf{K}] \quad (6-3)$$

c_K and c_M are real-valued constants referred to as the proportional damping coefficients. It was demonstrated in Section 5.2 of Chapter 5, that there exists a mathematical relationship between the zeros of the undamped flexible system (whose equations of motion are given by Eq.(6-2) without the damping matrix $[\mathbf{C}]$) and the zeros of its proportionally damped counterpart. This relationship is shown below.

$$z_{pd} = -(c_M - c_K z_{ud}^2) \pm \sqrt{(c_M - c_K z_{ud}^2)^2 + z_{ud}^2} \quad (6-4)$$

z_{pd} is the zero of the proportionally damped flexible system and z_{ud} is the zero of its undamped counterpart. In this chapter, we are interested in investigating the effect of proportional damping on real zeros. There are two types of real zeros: real minimum phase (RMP) zeros that lie on the negative real axis of the s -plane and real non-minimum phase (RNMP) zeros that lie on the positive real axis of the s -plane. The real zeros of any undamped flexible system occur in pairs of RMP – RNMP zeros. The RMP and RNMP zeros in each pair are equidistant from the imaginary axis as discussed in Chapter 2. Consider an RMP – RNMP zero pair of the undamped flexible system i.e. $z_{ud} = \pm x$ and substitute it in Eq.(6-4). This leads to:

$$z_{pd} = -(c_M - c_K x^2) \pm \sqrt{(c_M - c_K x^2)^2 + x^2} \quad (6-5)$$

Eq.(6-5) shows that the RMP – RNMP zero pair of the undamped flexible system is converted into two real zeros of its damped counterpart i.e. z_{pd} is real. However, it is yet to be determined if these real zeros are MP or NMP. Consider the first real zero from Eq.(6-5). It is referred to as $x_{pd,1}$.

$$x_{pd,1} = -(c_M - c_K x^2) - \sqrt{(c_M - c_K x^2)^2 + x^2}$$

Since $-(c_M - c_K x^2) \leq |(c_M - c_K x^2)| < \sqrt{(c_M - c_K x^2)^2 + x^2}$ (6-6)

$$\Rightarrow x_{pd,1} < 0$$

Based on the algebraic argument provided in Eq.(6-6), $x_{pd,1}$ is an RMP zero of the damped flexible system. Consider the second real zero from Eq.(6-5). It is referred to as $x_{pd,2}$.

$$x_{pd,2} = -(c_M - c_K x^2) + \sqrt{(c_M - c_K x^2)^2 + x^2}$$

Since $(c_M - c_K x^2) \leq |(c_M - c_K x^2)| < \sqrt{(c_M - c_K x^2)^2 + x^2}$ (6-7)

$$\Rightarrow x_{pd,2} > 0$$

It can be inferred from Eq.(6-7) that $x_{pd,2}$ is an RNMP zero of the damped flexible system. We will refer to the RMP and RNMP zeros of the undamped flexible system as $x_{RMP,ud}$ and $x_{RNMP,ud}$ respectively. Note that $x_{RMP,ud} = -x_{RNMP,ud}$. Similarly, we will refer to the RMP and RNMP zeros of the proportionally damped flexible system as $x_{RMP,pd}$ and $x_{RNMP,pd}$ respectively. Hence, we can infer from Eq.(6-6) and Eq.(6-7) that proportional damping converts $x_{RMP,ud}$ to $x_{RMP,pd}$ and $x_{RNMP,ud}$ to $x_{RNMP,pd}$. Therefore, it can be concluded that the addition of proportional damping to an undamped flexible system will preserve the RMP zeros as RMP, but the RNMP zeros will not be converted to an MP zero for any value of proportional damping coefficients c_M and c_K . Therefore, it is not possible to eliminate RNMP zeros via a proportional damping strategy. However, it may still be possible to move the RNMP zeros of the undamped flexible system further away from the imaginary axis via proportional damping. As discussed in Section 6.1, if the RNMP zeros are pushed further away from the imaginary axis, then the severity of the tradeoff between settling time and undershoot, implied by Eq.(6-1), is mitigated. Therefore, the problem at hand is to

determine the range of values of proportional damping coefficients c_M and c_K so that all the RNMP zeros of the damped system lie further away from the imaginary axis as compared to the all RNMP zeros of its undamped counterpart i.e. $x_{RNMP,pd,i} > x_{RNMP,ud,i}$. Eq.(6-7) can be generalized for the i^{th} RNMP zero as shown below:

$$x_{RNMP,pd,i} = -\left(c_M - c_K x_{RNMP,ud,i}^2\right) + \sqrt{\left(c_M - c_K x_{RNMP,ud,i}^2\right)^2 + x_{RNMP,ud,i}^2} \quad (6-8)$$

Given the complex mathematical relationship between $x_{RNMP,pd,i}$ and $x_{RNMP,ud,i}$ in Eq.(6-8), one can guess that there could be several ranges of c_M and c_K that lead to $x_{RNMP,pd,i} > x_{RNMP,ud,i}$ for all i RNMP zeros. In this chapter, we provide one such range of proportional damping coefficients c_M and c_K . Consider the case $c_M = 0$ and $c_K > 0$. For this case, Eq.(6-8) is simplified into Eq.(6-9) where the index i denotes the i^{th} RNMP zero and N is the total number of RNMP zeros of the system.

$$c_M = 0 \text{ and } c_K > 0$$

$$\text{For } i = 1, 2, \dots, N \quad (6-9)$$

$$x_{RNMP,pd,i} = c_K x_{RNMP,ud,i}^2 + x_{RNMP,ud,i} \sqrt{c_K^2 x_{RNMP,ud,i}^2 + 1}$$

As shown in Eq.(6-10) simple algebraic manipulation of Eq.(6-9) demonstrates that $x_{RNMP,pd,i} > x_{RNMP,ud,i}$ for all N RNMP zeros.

$$c_K > 0 \Rightarrow c_K x_{RNMP,ud,i}^2 > 0$$

$$\Rightarrow x_{RNMP,pd,i} > x_{RNMP,ud,i} \sqrt{c_K^2 x_{RNMP,ud,i}^2 + 1} \quad (6-10)$$

$$\Rightarrow x_{RNMP,pd,i} > x_{RNMP,ud,i}$$

Therefore, the simple proportional viscous damping strategy i.e. $c_M = 0$ and $c_K > 0$ guarantees that all the RNMP zeros of the damped flexible system are moved further away from the imaginary axis as compared to their undamped counterpart.

Next, consider the difference between the $x_{RNMP,ud,i}$ and $x_{RNMP,pd,i}$.

$$\begin{aligned}
 & \text{Let } \Delta x_{RNMP,pd-ud,i} \triangleq x_{RNMP,pd,i} - x_{RNMP,ud,i} \\
 \Rightarrow \Delta x_{RNMP,pd-ud,i} &= \left[c_K x_{RNMP,ud,i} + \left\{ \sqrt{c_K^2 x_{RNMP,ud,i}^2 + 1} - 1 \right\} \right] x_{RNMP,ud,i} \\
 & \text{Since } \left\{ \sqrt{c_K^2 x_{RNMP,ud,i}^2 + 1} - 1 \right\} > 0 \text{ and } c_K > 0 \\
 \Rightarrow \Delta x_{RNMP,pd-ud,i} &\propto x_{RNMP,ud,i}
 \end{aligned} \tag{6-11}$$

Eq.(6-11) implies that the distance $\Delta x_{RNMP,pd-ud,i}$ increases with $x_{RNMP,ud,i}$ indicating that the larger the RNMP zero of the undamped flexible system ($x_{RNMP,ud,i}$), the larger would be the distance ($\Delta x_{RNMP,pd-ud,i}$). Hence, for a constant value of c_K , the smallest RNMP zero is pushed the least while the largest RNMP zero is pushed the most towards the right-hand side (RHS) of the s -plane i.e. $\Delta x_{RNMP,pd-ud,1} < \Delta x_{RNMP,pd-ud,2} < \dots < \Delta x_{RNMP,pd-ud,N}$. Therefore, the smallest and largest RNMP zeros of the undamped flexible system respectively become the smallest and largest RNMP zeros of its damped counterpart. This result can be used to find the minimum values of c_K that move all the RNMP zeros further away from the imaginary axis beyond a certain point on the real axis in order to enable better dynamic performance of the flexible system.

Consider a scenario where it is required to move all the RNMP zeros beyond a certain value i.e. x_m on the positive real axis. This can be achieved by solving Eq.(6-9) to find the value of c_K , referred to as c_K^{\min} , which moves the smallest RNMP zero of the damped flexible system to x_m i.e. $x_{RNMP,pd,1} = x_m$. The inference from Eq.(6-11) guarantees that for this value of c_K , all the remaining zeros of the damped flexible system will also lie beyond x_m i.e. $x_{RNMP,pd,i} > x_m$ for all $2 \leq i \leq N$. The formula for c_K^{\min} is given by:

$$c_K^{\min} = \frac{x_m^2 - x_{RNMP,ud,1}^2}{2x_m x_{RNMP,ud,1}} \tag{6-12}$$

Furthermore, Eq.(6-6) demonstrated that the addition of proportional damping converts the RMP zeros ($x_{RMP,ud,i}$) of the undamped flexible system into RMP zeros ($x_{RMP,pd,i}$) of its damped counterpart for any value of c_K and c_M . The following equation provides the relationship between $x_{RMP,ud,i}$ and $x_{RMP,pd,i}$ for the case $c_M = 0$ and $c_K > 0$.

$$c_M = 0, c_K > 0$$

$$\text{For } i = 1, 2, \dots, N \quad (6-13)$$

$$x_{RMP,pd,i} = c_K x_{RMP,ud,i}^2 - |x_{RMP,ud,i}| \sqrt{c_K^2 x_{RMP,ud,i}^2 + 1}$$

As shown below, simple algebraic manipulation of Eq.(6-13) demonstrates that $x_{RMP,pd,i} > x_{RMP,ud,i}$ for all N RMP zeros.

$$\text{Since } x_{RMP,ud,i} < 0 \Rightarrow x_{RMP,ud,i} < x_{RMP,pd,i} \quad (6-14)$$

Therefore, the above equation implies that $x_{RMP,pd,i}$ moves closer to the imaginary axis as compared to $x_{RMP,ud,i}$ as c_K is increased. The RMP zeros ($x_{RMP,pd,i}$) of the damped flexible system tend to the origin as c_K tends to infinity but they never cross it to become RNMP zeros ($x_{RNMP,pd,i}$).

Consider an undamped flexible system with N RMP – RNMP zero pairs. Fig 6-1 visually illustrates how the proportional damping strategy with $c_M = 0$ and $c_K > 0$ affects all its N RMP and RNMP zeros. All the RNMP zeros of the damped flexible system are moved further away from the imaginary axis as compared to their undamped counterparts. The larger the undamped RNMP zero ($x_{RNMP,ud,i}$), the more its corresponding damped RNMP zero ($x_{RNMP,pd,i}$) gets pushed to the RHS of the imaginary axis. On the contrary, all the RMP zeros of the damped flexible system are moved closer to the imaginary axis as compared to their undamped counterparts.

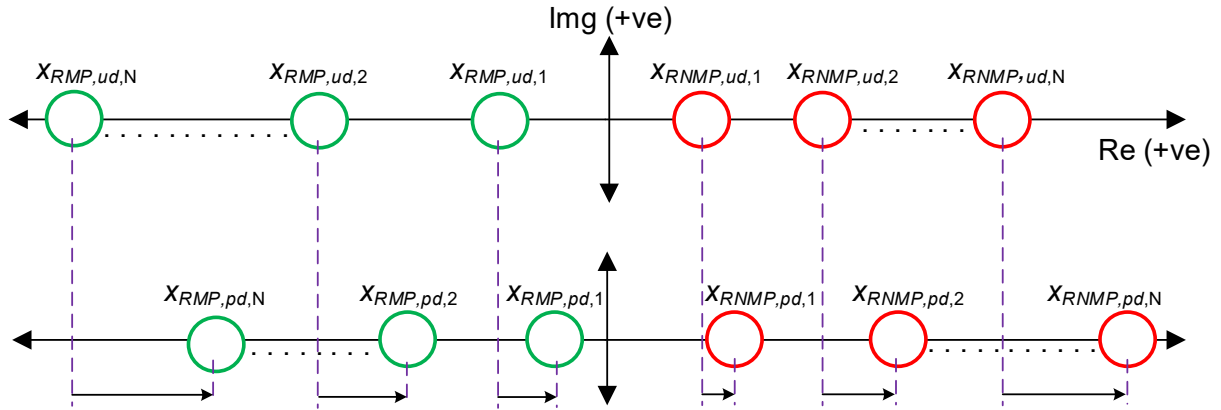


Fig 6-1 Effect of the proportional viscous damping strategy i.e. $c_M = 0$ and $c_K > 0$ on the real zeros of flexible systems

6.3 Three-link manipulator: Case Study

In this section, a plant-control co-design strategy is proposed for flexible systems in the presence of RNMP zeros. In this section, the term ‘plant-control co-design’ refers to tuning the plant and controller parameters in tandem to achieve better dynamic performance. This case study aims to demonstrate the application of the proportional damping strategy i.e. $c_M = 0$ and $c_K > 0$ to simultaneously achieve fast settling time and small undershoot in the step response of a flexible system. Therefore, only the damping parameter will be varied as part of plant parameter tuning.

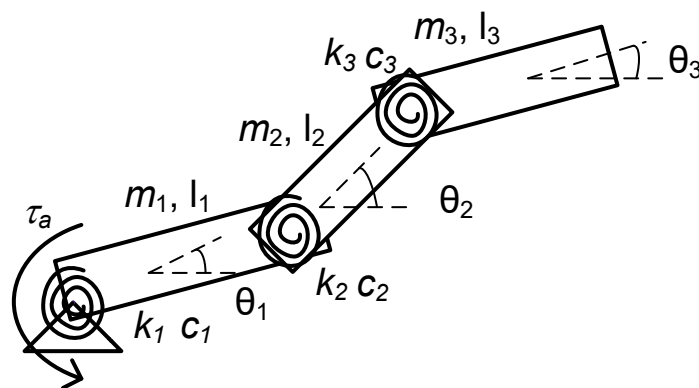


Fig 6-2 Schematic view of a three-link manipulator

A three-link flexible manipulator consisting of three rigid bars connected serially via springs and dampers is considered, as shown in Fig 6-2. Torque τ_a is applied at the connection of the 1st link with the ground and the rotational angle of the last rigid link, θ_3 is considered as the output. For the three-link manipulator, the linearized equations of motion were derived in [140] and simply stated below. It has been shown that the linearized transfer function (all rotation angles are linearized about zero radians) of such N link mechanisms from τ_a to θ_N (rotation angle of the last element) has $(N - 1)$ RNMP zeros [140, 141]. Therefore, the transfer function $G_3(s) = \theta_3/\tau_a$ will have 2 RNMP zeros. Accordingly, designing a controller to simultaneously achieve lower undershoot and settling time will be challenging due to the presence of these RNMP zeros.

$$[\mathbf{M}] = \begin{bmatrix} \left(\frac{m_1}{3} + m_2 + m_3\right)l_1^2 & \left(\frac{m_2}{2} + m_3\right)l_1l_2 & \frac{m_3}{2}l_1l_3 \\ \left(\frac{m_2}{2} + m_3\right)l_1l_2 & \left(\frac{m_2}{3} + m_3\right)l_2^2 & \frac{m_3}{2}l_2l_3 \\ \frac{m_3}{2}l_1l_3 & \frac{m_3}{2}l_2l_3 & \frac{m_3}{3}l_3^2 \end{bmatrix}, \quad [\mathbf{K}] = \begin{bmatrix} k_1 + k_2 & -k_2 & 0 \\ -k_2 & k_2 + k_3 & -k_3 \\ 0 & -k_3 & k_3 \end{bmatrix} \quad (6-15)$$

The following geometric properties are considered for the case study: $m_1=2$ kg, $m_2=3$ kg, $m_3=4$ kg, $l_1=2$ m, $l_2=1$ m, $l_3=1$ m, $k_1=7$ N-m/rad, $k_2=5$ N-m/rad, $k_3=6$ N-m/rad. Furthermore, the following performance objectives are considered for the step response of θ_3 : overshoot $< 2\%$, undershoot $< 2\%$ and settling time < 10 s. The step-by-step design strategy is as follows:

STEP I. Feedback controller design

In the first step, a full-state feedback controller of the form given below, is applied to the undamped version of the three-link flexible manipulator in Fig 6-2 i.e. $c_1 = c_2 = c_3 = 0$. The

controller is designed to relocate the poles of the closed-loop system to the LHS of the s -plane seeking the specified control objective.

$$F = -[\mathbf{K}_f]\theta \quad (6-16)$$

where K_f is 1 x 6 feedback gain vector and $\theta = [\theta_1 \ \theta_2 \ \theta_3 \ \dot{\theta}_1 \ \dot{\theta}_2 \ \dot{\theta}_3]^T$

Since the smallest (slowest) poles dominate the dynamics of the system, out of the six poles of the system, poles $p_3 - p_6$ are moved to some far away distance from the imaginary axis so that they have the least effect on the system dynamics. Now, the optimal location of the slowest pole pair $p_{1,2}$ is sought to achieve the performance objectives. Let $p_{1,2} = \text{Re}(p_1) \pm j \text{Im}(p_1)$. In the absence of a full-state feedback controller, $p_{1,2}$ lies on the imaginary axis, i.e. $\text{Re}(p_1) = 0$. The feedback gains in $[\mathbf{K}_f]$ are modified to slowly reduce $\text{Re}(p_1)$. Note that full-state feedback control allows arbitrary placement of all closed loop poles of the system. The step response of the system for three different values of $\text{Re}(p_1)$ is shown in Fig 6-3.

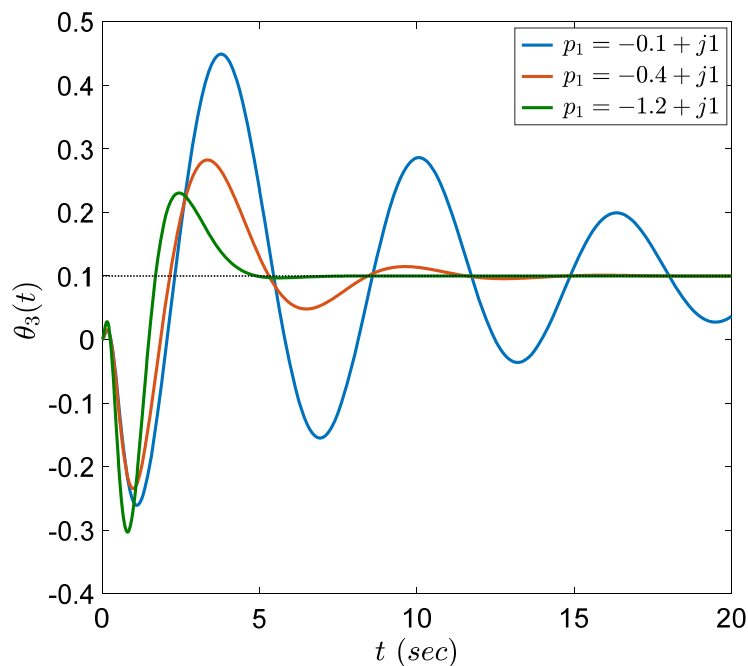


Fig 6-3 Step response of the system for various $\text{Re}(p_1)$

It can be observed from the figure that initially as $\text{Re}(p_1)$ is reduced from 0, the settling time, undershoot and overshoot decrease. However, after reaching a certain critical value of $\text{Re}(p_1)$, the undershoot starts increasing even though the settling time and overshoot continue to decrease. This critical value of $\text{Re}(p_1) = -0.4$. The observation made in Fig 6-3 agrees with Eq.(6-1). For a given position of RNMP zeros, an aggressive reduction in settling time eventually comes at the cost of an increase in undershoot.

Next, keeping $\text{Re}(p_1) = -0.4$, $\text{Im}(p_1)$ is reduced. It can be observed from Fig 6-4 that as $\text{Im}(p_1)$ is reduced, the settling time, undershoot and overshoot decrease. However, beyond a critical value of $\text{Im}(p_1)$, the settling time begins to increase even though undershoot and overshoot continue to decrease. This critical value of $\text{Im}(p_1) = 0.25$. Hence, the critical location of $p_{1,2} = -0.4 \pm j 0.25$. Note that for this case study, we have chosen a settling window of 5% of the steady state value as shown in Fig 6-4.

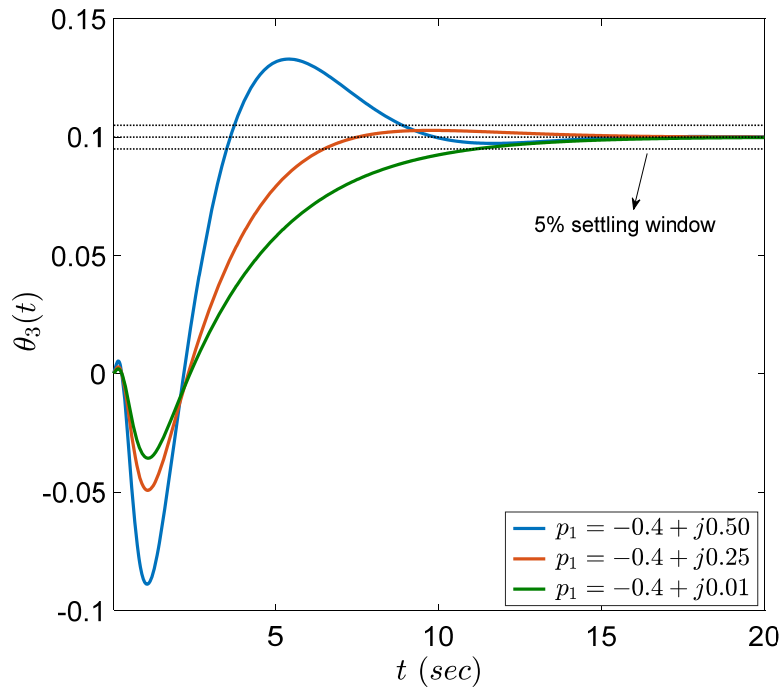


Fig 6-4 Step response of the system for various $\text{Im}(p_1)$

The observation made in Fig 6-4 again agrees with Eq.(6-1). For a given position of RNMP zeros, aggressive reduction in undershoot eventually comes at the cost of an increase in settling time. For the closed-loop pole location of $p_{1,2} = -0.4 \pm j 0.25$, the overshoot, undershoot and settling time are 0.89%, 44.37% and 7.68s respectively. Clearly, undershoot does not meet the specified performance objective which is $< 2\%$. Any further change in the location of $p_{1,2}$ beyond this critical point would lead to an increase in undershoot and/or settling time which is undesirable. Therefore, this can be regarded as the best achievable performance via full-state feedback control. Obviously, the control objective for undershoot cannot be achieved using only the control design. Note that in Step I above, the critical location of the slowest pole was ascertained by carefully varying the feedback gains in $[\mathbf{K}_f]$ and observing the resulting step response of the closed-loop system demonstrated in Fig 6-3 and Fig 6-4. This step can be time consuming but it was done in this manner to numerically demonstrate the tradeoff between settling time and undershoot. Interested researchers are encouraged to formulate Step I as an LQR problem with the right constraints and minimization function to get the answer faster.

STEP II. Addition of Proportional viscous damping

Due to the inability of full-state feedback control to decrease undershoot without increasing the settling time, the proportional viscous damping strategy derived in Section 6.2 is added to the flexible system to complement the controller performance. Physically, this means that $c_i = c_K k_i$ where $i = 1, 2, 3$ in Fig 6-2. Therefore, the damping matrix becomes:

$$[\mathbf{C}] = c_K [\mathbf{K}] \quad (6-17)$$

It was shown in Section 6.2 that the proportional viscous damping strategy, given by Eq.(6-17) pushes all the RNMP zeros further away from the imaginary axis. As a result, the value of x in Eq.(6-1) increases and therefore, the lower limit for undershoot (given by the LHS of Eq.(6-1))

decreases, leading to a smaller undershoot. To demonstrate this effect, the value of c_K is incrementally increased while keeping the location of the closed pole fixed. The step response of the system for different values of c_K is shown in Fig 6-5.

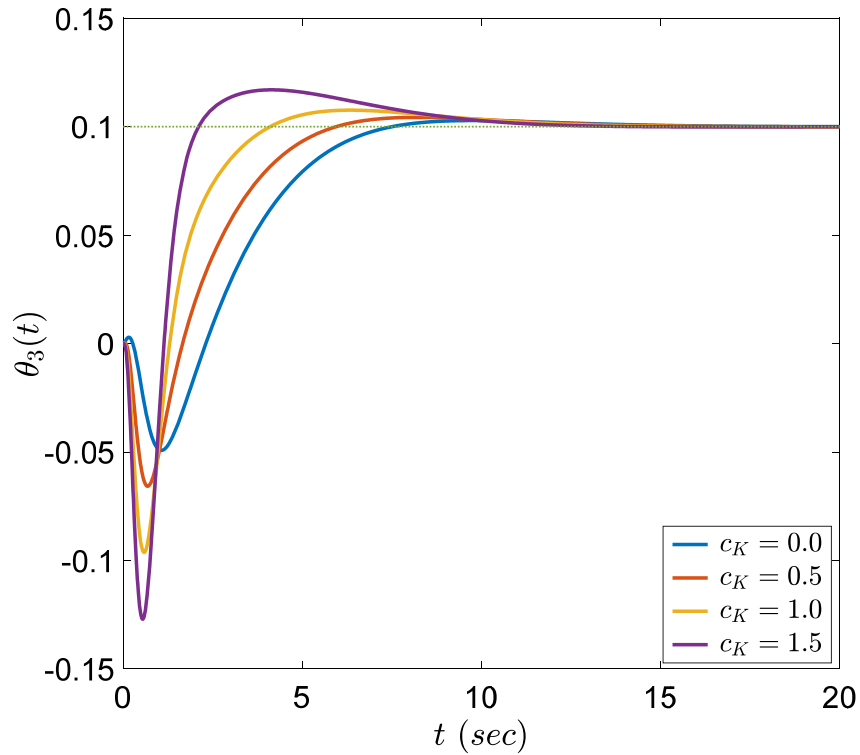


Fig 6-5 Step response of the system in the presence of feedback controller and proportional damping for various damping constants

The observation from Fig 6-5 is contrary to our expectation. As c_K increases, undershoot and overshoot increase rather than decrease. Meanwhile, the settling time remains roughly the same. This peculiar behavior is attributed to the RMP zeros moving closer to the imaginary axis as c_K is increased. Fig 6-1 demonstrated that the proportional damping strategy not only pushes the RNMP zeros away from the imaginary axis, but also pushes the RMP zeros closer to the imaginary axis (although they never cross it). It is not definitively understood why the movement of RMP zeros towards the imaginary axis should lead to an increase in undershoot and overshoot. To the best of

the authors' knowledge, an equivalent mathematical constraint such as Eq.(6-1) (applicable to RNMP zeros only) does not exist for RMP zeros so far.

It can be inferred from Fig 6-5 that although the placement of RNMP zeros to higher frequencies is supposed to reduce undershoot, this reduction is completely overshadowed by the RMP zeros which are also being pushed toward the imaginary axis by adding the proportional damping and therefore, produce additional undershoot and overshoot. Therefore, in the current plant-control configuration, simply increasing c_K cannot lead to any further improvement in the performance objectives.

STEP III. Relocating RMP zeros via feedforward controller

Since the RMP zeros are stable, i.e. they lie on the LHS of the imaginary axis, their position can be changed via a simple feedforward control strategy. As the RMP zeros are relocated to higher frequencies, i.e. further away from the imaginary axis, their undesirable effect on undershoot and overshoot is reduced. By keeping the RMP zeros fixed at higher frequencies, c_K can be increased as much as practically possible to push the RNMP zeros to higher frequencies and mitigate the tradeoff between settling time and undershoot. Note that in practice, while tuning the plant and control parameters, Step II and Step III go hand in hand because for every new c_K value, the position of the RMP zeros i.e. $x_{RMP,pd,1}$ and $x_{RMP,pd,2}$ will change. Therefore, the associated feedforward controller used to relocate these zeros to higher frequencies i.e. $x_{RMP,pd,1hf}$ and $x_{RMP,pd,2hf}$ must also change. The red curve in Fig 6-6 shows the step response of the flexible system after $c_K = 8.0$ is chosen and the RMP zeros are relocated to higher frequencies to meet the performance objectives.

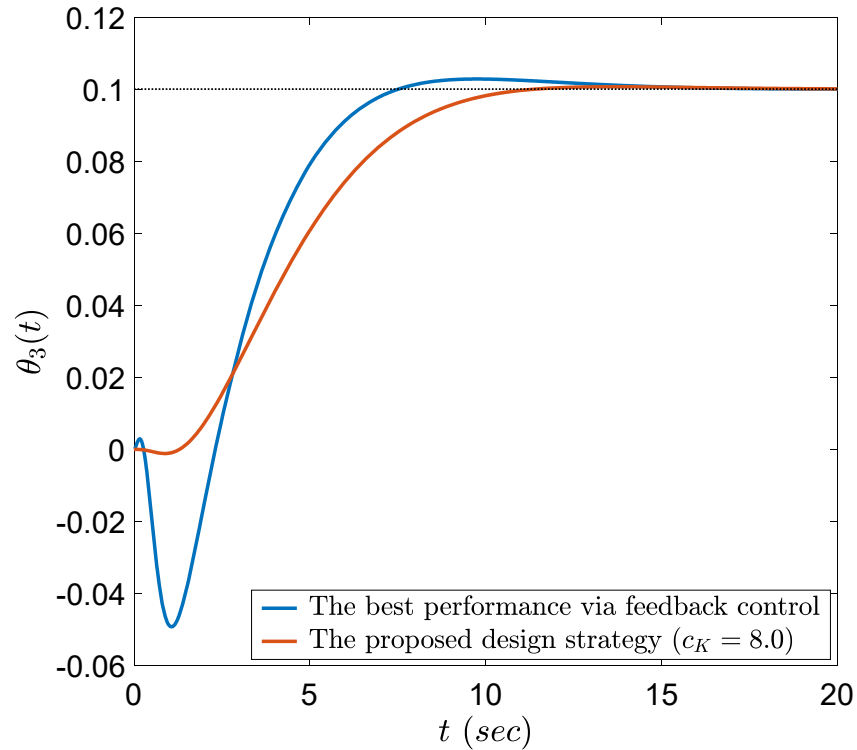


Fig 6-6 Final step response of the system vs. feedback controller best performance

Fig 6-6 illustrates a comparison between the final step response achieved at the end of Step III (red curve) and the step response achieved at the end of Step I (blue curve). This comparison yet again demonstrates that only tuning the controller parameters by themselves as shown in Step I cannot reduce undershoot beyond a certain point without increasing the settling time. However, the simultaneous tuning of plant and controller parameters as shown in Steps II and III can effectively reduce undershoot while maintaining/improving the other control objectives. The evolution of the numerical values of the control objectives through Step I – III are given in Table 6-1.

Parameter	Step I	Step II	Step III
Overshoot (%)	0.89	≥ 0.89	0.65
Undershoot (%)	44.37	≥ 44.37	1.14
Settling time (s)	7.68	≥ 7.68	8.83

Table 6-1 Step response characteristics during successive design steps

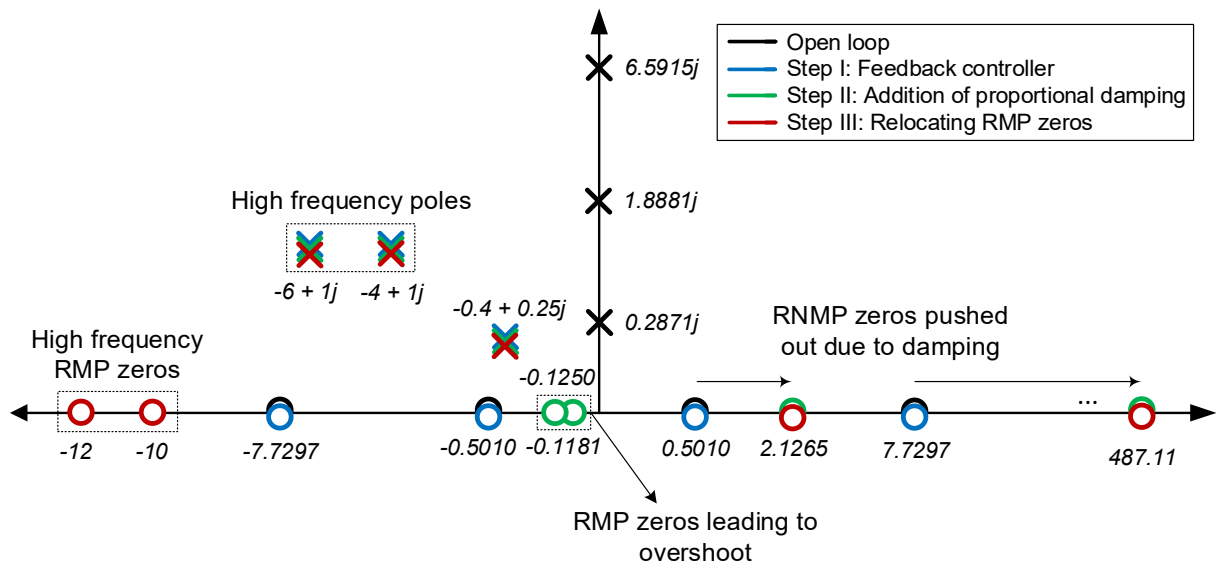


Fig 6-7 Pole-zero map of the system during the proposed design strategy steps

The pole-zero map in Fig 6-7 graphically illustrates how the location of poles and zeros change during the three steps of the proposed design strategy. In step I, all zeros are fixed and the pole locations are changed via full-state feedback control. Then, in step II, all poles are kept fixed and all the zero locations are changed by the addition of damping. Finally, in step III, only RMP zeros are relocated to high frequencies while all poles and RNMP zeros remain unchanged. The control block diagram of the proposed design strategy is shown in Fig 6-8.

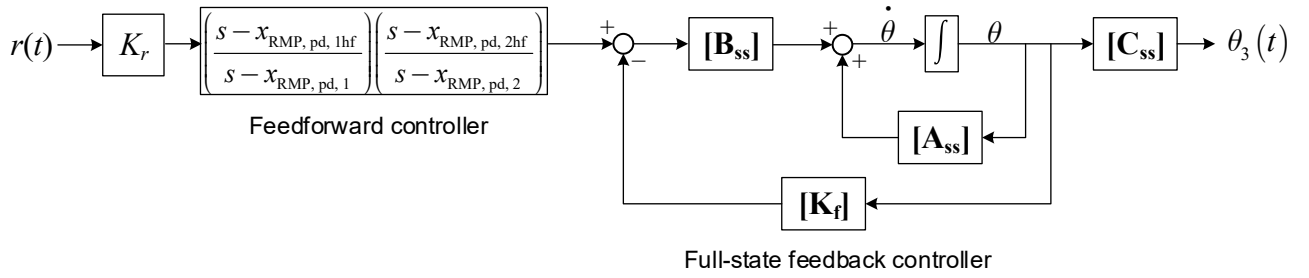


Fig 6-8 Control block diagram of the proposed design strategy

This block diagram demonstrates how this entire design strategy is implemented in practice. $[\mathbf{A}_{ss}]$, $[\mathbf{B}_{ss}]$ and $[\mathbf{C}_{ss}]$ are the state-space matrices of the open loop plant given by Eq.(6-18) ; $[\mathbf{K}_f]$ is a vector of feedback gains and K_r is the scalar feedforward controller gain required to tune the DC gain.

$$[\mathbf{A}_{ss}] = \begin{bmatrix} [0]_{3 \times 3} & [\mathbf{I}]_{3 \times 3} \\ -[\mathbf{M}]^{-1}[\mathbf{K}] & -[\mathbf{M}]^{-1}[\mathbf{C}] \end{bmatrix}, \quad [\mathbf{B}_{ss}] = \begin{bmatrix} [0]_{3 \times 1} \\ [\mathbf{M}]^{-1}[\mathbf{B}] \end{bmatrix} \quad (6-18)$$

$$[\mathbf{C}_{ss}] = \begin{bmatrix} [0]_{1 \times 2} & 1 & [0]_{1 \times 3} \end{bmatrix}$$

$[\mathbf{M}]$ and $[\mathbf{K}]$ are given by Eq.(6-15) and $[\mathbf{C}]$ is given by Eq.(6-17). In Step I of the proposed design strategy, $[\mathbf{K}_f]$ is varied to optimally place the closed-loop poles. In Step II, $[\mathbf{A}_{ss}]$ changes as a result of the addition of proportional damping, and $[\mathbf{K}_f]$ is also modified to keep the closed-loop pole position unchanged from Step I. In Step III, the RMP zeros, i.e. $x_{RMP,pd,1}$ and $x_{RMP,pd,2}$, are moved to higher frequencies, i.e. $x_{RMP,pd,1hf}$ and $x_{RMP,pd,2hf}$, respectively. The scalar feedforward gain, K_r is continually updated throughout Step I to III to ensure that the steady-state value of $\theta_3 = 0.1$.

6.4 Conclusion

This chapter provides a proportional viscous damping strategy that moves all the RNMP zeros of the damped flexible system further away from the imaginary axis as compared to its undamped counterpart. This reduces the severity of the tradeoff between settling time and undershoot, implied by Eq.(6-1). It must be noted that this damping cannot eliminate RNMP zeros. Therefore, even in its presence, the step response of the flexible system will demonstrate undershoot. However, the magnitude of this undershoot, for a given settling time, will be significantly smaller in the presence of this damping as compared to its absence. This is theoretically demonstrated via a step-by-step design strategy applied to a three-link flexible manipulator. The first step of this design strategy is the design of a full-state feedback controller, the second step is the application of proportional viscous damping, and the third step is the design of a feedforward controller. This design strategy leads to simultaneous improvement in overshoot, settling time and undershoot in the step response which could not be achieved through only feedback/feedforward controller design. Although shown for a specific flexible system in this chapter, this design strategy can be applied to any general multi-DoF flexible LTI system.

Chapter 7 Conclusion and Future Work

This thesis provided several new sufficient conditions for the absence of NMP zeros in multi-DoF flexible LTI systems with and without viscous damping when all modal residue signs are not the same. The most noteworthy sufficient condition derived in Chapter 4 clearly demonstrated that there exist other sequences of modal residue signs apart from ‘*all modal residue signs are same*’ that guarantee the absence of NMP zeros. Design strategies were provided in Chapter 4 to theoretically demonstrate how to choose physical parameters such as actuator-sensor placement and mass-stiffness distribution to achieve the required sequence of modal residue signs. However, this sufficient condition was derived under the assumption of ‘no damping’. Generally all flexible systems used in practical applications have non-zero amount of damping due to various energy dissipation mechanisms such air resistance, material hysteresis, joint friction etc. Therefore, the question arises: can the sequences of modal residue signs derived in this thesis (for undamped flexible systems) guarantee the absence of NMP zeros in lightly damped flexible systems as well? We will demonstrate the practical efficacy of this sufficient condition in the presence of light damping via the example of a flexure bearing based motion system shown in Fig 7-1.

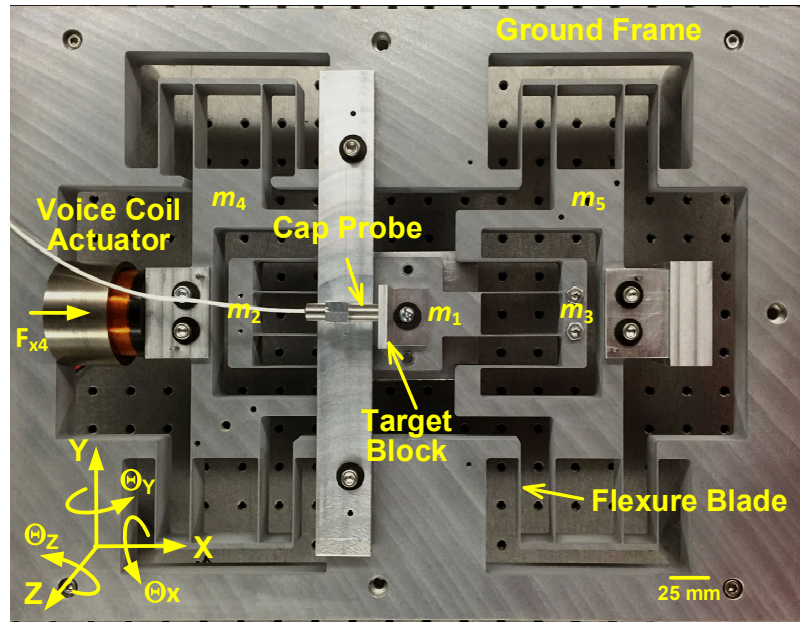


Fig 7-1 Flexure bearing based motion system

The flexure bearing based motion system shown in Fig 7-1 was designed by Cui [37]. A voice coil actuator applies force along the X direction i.e. F_{x4} which leads to the displacement of the motion stage (m_1) along the X direction via the bending deformation of the flexure blades. The X direction displacement of the motion stage (m_1) with respect to the ground is measured by the capacitance probe and target block. Under ideal bearing behavior [39], this flexure bearing based motion system should exhibit zero stiffness along its motion direction (MD) i.e. X direction and infinite stiffness along the other five directions referred to as the bearing directions (BD) i.e. Y, Z, Θ_X , Θ_Y , and Θ_Z directions. However, in reality, since the displacement of the motion stage (m_1) along the X direction happens via the bending deformation of flexure blades, the motion direction stiffness is small but non-zero. Similarly, due to the presence of parasitic compliance, the bearing direction stiffnesses are large but finite. Therefore, this flexure bearing based motion system is a multi-DoF flexible system with one low frequency flexible mode along the motion direction

referred to as the ‘rigid body’ mode and several high frequency flexible modes along the bearing directions.

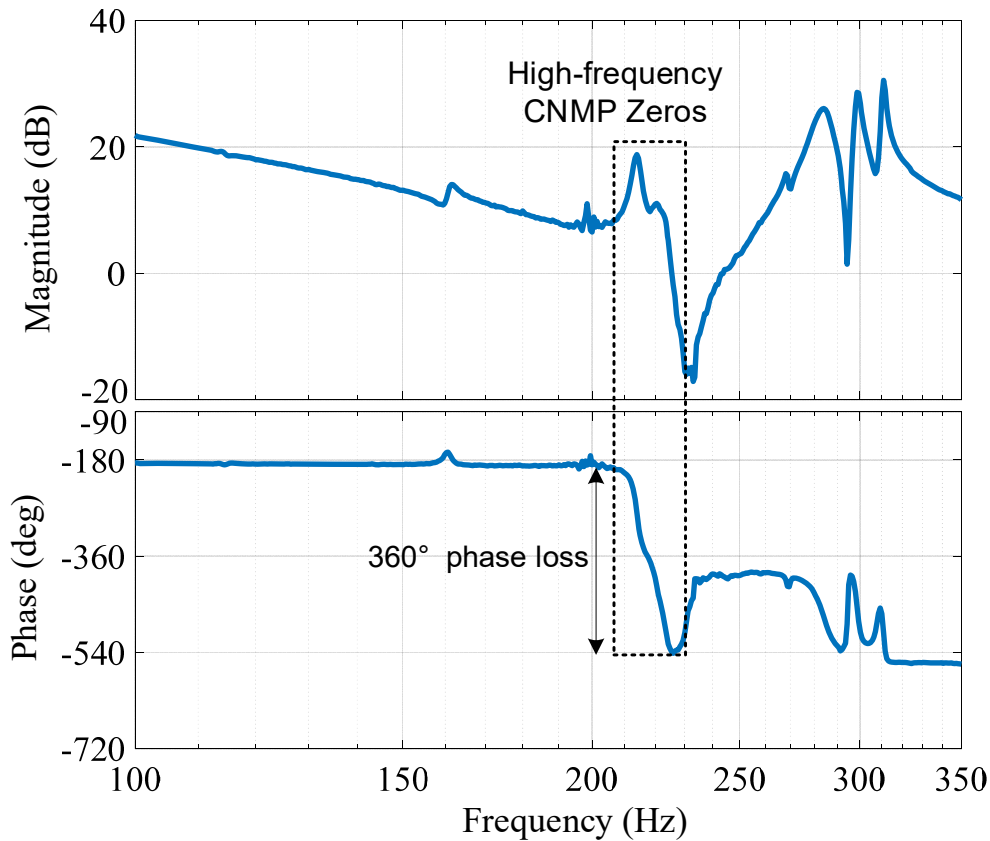


Fig 7-2 Frequency response function of the transfer function: $x_1(s)/F_{x4}(s)$

Fig 7-2 is the experimentally obtained frequency response function (FRF) of the transfer function between X direction displacement of the motion stage (m_1) i.e. x_1 and X direction force applied at m_4 i.e. F_{x4} . This FRF is shown in the frequency range between 100 Hz and 350 Hz to highlight the presence of two closely spaced modes at 210 Hz and 220 Hz and a quartet of CMP-CNMP zeros trapped between them. In order to apply the appropriate sufficient condition i.e. **Result 5** from Chapter 4 to guarantee the absence of these CNMP zeros, we make the following simplifying assumptions:

Assumption 1: The flexible system is undamped.

In reality, the flexible system is lightly damped ($\zeta \sim 0.005$). Even then, we will proceed to apply the sufficient condition derived in Chapter 4 (for undamped flexible systems) to demonstrate its efficacy even in the presence of light damping.

Assumption 2: Model the flexible system dynamics as a three-DoF system consisting of the rigid body mode, and the modes at 210 Hz and 220 Hz.

Note that the rigid body mode is a low frequency motion direction mode that occurs at roughly 30 Hz and therefore it is not visible in Fig 7-2. However, the fact that the phase is at -180 degrees at frequencies below the frequency of the closely spaced modes confirms that there is a low frequency rigid body mode in the FRF as expected. The assumption of three-DoF is made due to the fact that only one quartet of CMP-CNMP zeros exists between the two closely spaced modes in Fig 7-2. Chapter 2 proved that it takes at least three modes (one low frequency rigid body mode and two closely spaced high frequency modes) to explain the genesis of one quartet of CMP-CNMP zeros. Therefore, in reality, even though the flexible system has several flexible modes, we are choosing the simplest possible model consisting of three modes to apply the sufficient condition for the absence of CNMP zeros.

According to **Result 5** of Chapter 4, $n = 3$ (three pair of poles), $m = 2$ (one pair of CMP + one pair of CNMP zeros) for this flexure bearing based motion system. Therefore, $r = n - m - 1 = 0$. The sufficient condition for the absence of CNMP zeros (**Result 5** of Chapter 4) states that the number of modal residue sign change is either r or $r+1$. This means that the number of modal residue sign change must be either 0 or 1 to guarantee the absence of CNMP zeros. Therefore, the following sequences of the three modal residue signs guarantee the absence of the CNMP zero pair in the flexure bearing based motion system:

1. $\alpha_{RB} > 0, \alpha_{210\text{ Hz}} > 0, \alpha_{220\text{ Hz}} > 0$ (number of modal residue sign change = 0)

2. $\alpha_{RB} > 0, \alpha_{210\text{ Hz}} > 0, \alpha_{220\text{ Hz}} < 0$ (number of modal residue sign change = 1)
3. $\alpha_{RB} > 0, \alpha_{210\text{ Hz}} < 0, \alpha_{220\text{ Hz}} < 0$ (number of modal residue sign change = 1)

Since, it is the relative sign of the modal residues that matters, the sign of the modal residue corresponding to the rigid body mode i.e. α_{RB} can be assumed to be greater than zero without any loss of generality. Therefore, the three modal residue signs can be arranged to form four unique sequences (via permutation and combination), out of which three sequences guarantee the absence of CNMP zeros as shown above. This means that the fourth possible sequence given by: ($\alpha_{RB} > 0, \alpha_{210\text{ Hz}} < 0, \alpha_{220\text{ Hz}} > 0$) [number of modal residue sign change = 2] is necessary for the presence of CNMP zeros. Therefore, for the current configuration of the flexure bearing based motion system which leads to one quartet of CMP-CNMP zeros in Fig 7-2, the sequence of modal residue signs must be ($\alpha_{RB} > 0, \alpha_{210\text{ Hz}} < 0, \alpha_{220\text{ Hz}} > 0$). Now we will explain how the misalignment in actuator-sensor placement leads to this sequence of modal residue signs and therefore, cause CNMP zeros in the FRF in Fig 7-2.

The mathematical relationship between physical and system parameters provided in *Section 2* of Chapter 4 showed that the modal residue is the product of the values of the mode shape at the actuator and sensor locations. Since, $\alpha_{210\text{ Hz}} < 0$, this means that in the 210 Hz mode, the actuator and sensor location at mass m_4 and m_1 , respectively, move in opposite X directions. Since, $\alpha_{220\text{ Hz}} > 0$, the actuator and sensor location at mass m_4 and m_1 , respectively, move in the same X direction. Since, only the sign of the mode shapes at the actuator and sensor location is needed, a simple experimental modal analysis was conducted by placing accelerometers on m_4 and m_1 . It showed that these masses get excited in the Z direction at 210 Hz and 220 Hz when they are struck with a hammer in the Z direction. However, the 210 Hz and 220 Hz modes cannot be purely Z direction modes because a purely Z direction mode cannot be measured by the capacitance probe and target

block (shown in Fig 7-1). Therefore, in the 210 Hz and 220 Hz modes, the masses m_1 and m_4 must rotate about the Θ_Y direction as shown in Fig 7-3 so that these modes show up in the FRF in Fig 7-2.

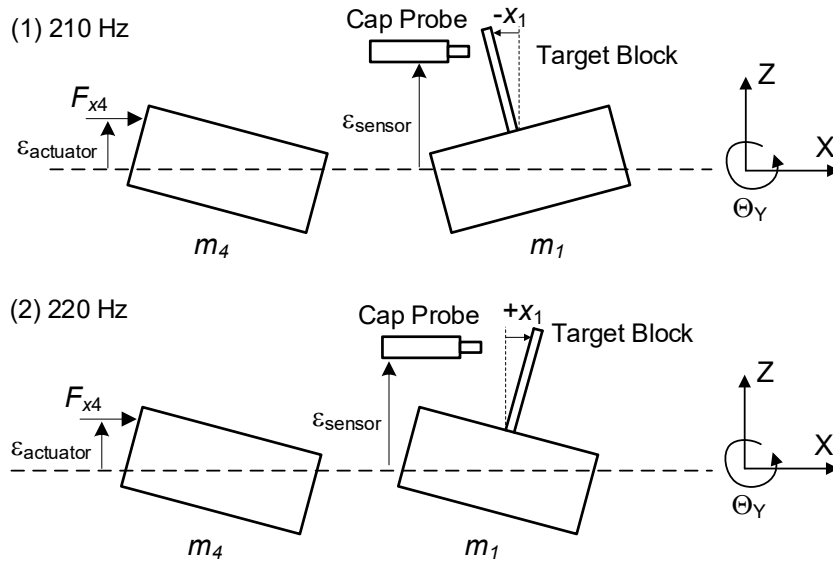


Fig 7-3 Mode shapes for 210 Hz and 220 Hz when $\epsilon_{actuator} > 0$ and $\epsilon_{sensor} > 0$ (only showing m_1 and m_4)

The most logical reason that these modes get excited is because of the misalignment in the actuator location ($\epsilon_{actuator}$). The center of stiffness of the flexure bearing lies on the dashed line in Fig 7-3. Since the flexure bearing is symmetric about the Z direction, this dashed line will be referred to as the ‘centerline’. If the actuator was placed exactly along this centerline, it would not excite these bearing direction modes. Similarly, if the capacitance probe and the target block measured the X displacement of m_1 exactly along the centerline, these modes will not be observed. However, in reality, owing to finite tolerances in manufacturing and assembly, there will always be some small but non-zero actuator misalignment ($\epsilon_{actuator}$) and sensor misalignment (ϵ_{sensor}) which leads to these two bearing direction modes showing up in the FRF in Fig 7-2. Small but

finite actuator and sensor misalignment lead to small but finite modal residues associated with these bearing direction modes i.e. $\alpha_{210 \text{ Hz}}$ and $\alpha_{220 \text{ Hz}}$ based on the mathematical relationship between physical and system parameters provided in *Section 2* of Chapter 4. Chapter 2 mathematically demonstrated that when the high frequency modes (210 Hz and 220 Hz modes in this case) are closely spaced, even small modal residues associated with these modes can lead to the presence of CNMP zeros. This is exactly what we observe in the FRF in Fig 7-2.

In the current configuration of the flexure based motion system, $\varepsilon_{\text{sensor}} > 0$ because the capacitance probe is placed above the centerline as shown in Fig 7-3. However, it is not practically possible to ascertain the sign of actuator misalignment because it is unintentional and therefore difficult to predict. So, we will assume $\varepsilon_{\text{actuator}} > 0$ i.e. actuator is misaligned above the centerline as shown in Fig 7-3. Later, we will show that the required sequence of modal residue signs is achieved irrespective of the sign of actuator misalignment because it is kept constant.

In the current configuration, the system exhibits CNMP zeros, therefore, as discussed earlier, its sequence of modal residue signs must be ($\alpha_{\text{RB}} > 0$, $\alpha_{210 \text{ Hz}} < 0$, $\alpha_{220 \text{ Hz}} > 0$). The modal residue sign corresponding to the rigid body mode can be assumed to be positive without any loss of generality i.e. $\alpha_{\text{RB}} > 0$. Fig 7-3 shows the order of mode shapes that satisfy this sequence of modal residue signs when $\varepsilon_{\text{actuator}} > 0$:

1. For the 210 Hz mode, the point of actuation moves in positive X direction but the target block moves in the negative X direction with respect to the capacitance probe. Therefore, $\alpha_{210 \text{ Hz}} < 0$.
2. For the 220 Hz mode, the point of actuation moves in positive X direction and the target block also moves in the positive X direction with respect to the capacitance probe. Therefore, $\alpha_{220 \text{ Hz}} > 0$.

If in reality the actuator was misaligned below the centerline i.e. $\varepsilon_{\text{actuator}} < 0$, the mode shapes for 210 Hz and 220 Hz shown in Fig 7-3 will get flipped to still maintain ($\alpha_{\text{RB}} > 0$, $\alpha_{210 \text{ Hz}} < 0$, $\alpha_{220 \text{ Hz}} > 0$) which is necessary for the presence of CNMP zeros in the FRF in Fig 7-2. Recall that the modal residue is the product of the values of the mode shape at the actuator and sensor locations. Therefore, we only need to change the sign of either the actuator ($\varepsilon_{\text{actuator}}$) or the sensor misalignment ($\varepsilon_{\text{sensor}}$) but not both to change the sequence of modal residue signs. Since, predicting and modifying the actuator misalignment ($\varepsilon_{\text{actuator}}$) is practically difficult, we will keep it constant and change the sign of sensor misalignment ($\varepsilon_{\text{sensor}}$) to the achieve one of the three sequences of modal residue signs that guarantee the absence of CNMP zeros.

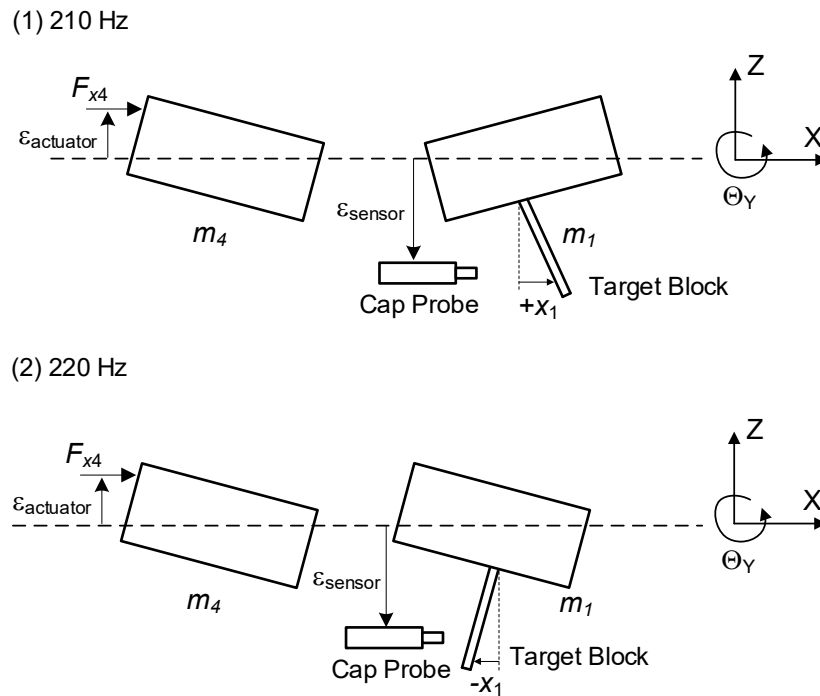


Fig 7-4 Mode shapes for 210 Hz and 220 Hz when $\varepsilon_{\text{actuator}} > 0$ and $\varepsilon_{\text{sensor}} < 0$ (only showing m_1 and m_4)

In Fig 7-4, the actuator misalignment remains the same i.e. $\varepsilon_{\text{actuator}} > 0$ but the capacitance probe and the target block are placed below the centerline i.e. $\varepsilon_{\text{sensor}} < 0$. Changing the sign of the sensor misalignment does not change the sign of the modal residue of the rigid body mode i.e. $\alpha_{\text{RB}} > 0$. However, the sign of the modal residues of the bearing direction modes (at 210 Hz and 220 Hz) undergo a change as shown in Fig 7-4:

1. For the 210 Hz mode, the point of actuation moves in positive X direction and the target block also moves in the positive X direction with respect to the capacitance probe. Therefore, $\alpha_{210 \text{ Hz}} > 0$.
2. For the 220 Hz mode, the point of actuation moves in positive X direction but the target block moves in the negative X direction with respect to the capacitance probe. Therefore, $\alpha_{220 \text{ Hz}} < 0$.

Therefore, the new sequence of modal residue signs is $(\alpha_{\text{RB}} > 0, \alpha_{210 \text{ Hz}} > 0, \alpha_{220 \text{ Hz}} < 0)$ [number of modal residue sign change = 1]. As discussed earlier, this sequence of modal residue signs guarantees the absence of CNMP zeros. Sure enough, this is exactly what is seen via actual experimental measurements, as demonstrated by the new FRF in Fig 7-5 obtained for $\varepsilon_{\text{sensor}} < 0$.

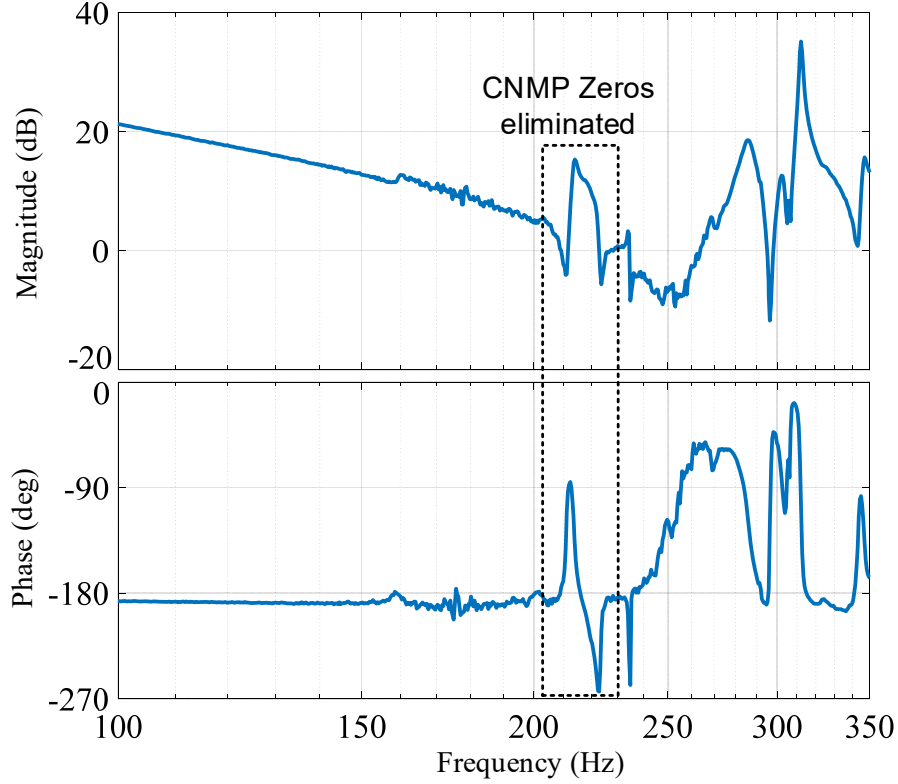


Fig 7-5 Frequency response function of the transfer function: $x_1(s)/F_{x4}(s)$ for $\varepsilon_{\text{sensor}} < 0$

Note that the absence of CNMP zeros obtained via sensor placement is independent of the actuator misalignment because it was kept constant/unchanged. If in reality $\varepsilon_{\text{actuator}} < 0$, changing the sign of sensor misalignment from $\varepsilon_{\text{sensor}} > 0$ to $\varepsilon_{\text{sensor}} < 0$ would still have changed the sequence of modal residue signs from $(\alpha_{\text{RB}} > 0, \alpha_{210 \text{ Hz}} < 0, \alpha_{220 \text{ Hz}} > 0)$ to $(\alpha_{\text{RB}} > 0, \alpha_{210 \text{ Hz}} > 0, \alpha_{220 \text{ Hz}} < 0)$, thereby still guaranteeing the absence of CNMP zeros.

Once the absence of CNMP zeros is guaranteed via the appropriate sequence of modal residue signs, Eq.(7-1) provides the mathematical condition for the absence of RNMP zeros as well (from **Result 6** of Chapter 4). As earlier, ‘MD’ stands for motion direction and ‘BD’ stands for bearing direction.

$$\left(\alpha_{\text{MD}} + \sum_{i=1}^n \alpha_{\text{BD}} \right) \left(\frac{\alpha_{\text{MD}}}{\omega_{\text{MD}}^2} + \sum_{i=1}^n \frac{\alpha_{\text{BD}}}{\omega_{\text{BD}}^2} \right) > 0 \quad (7-1)$$

For the flexure bearing based motion system with the modified sensor placement i.e. $\varepsilon_{\text{sensor}} < 0$, the inequality in Eq.(7-1) will be satisfied without any further physical design modifications. The reasoning for this is as follows: Small but finite misalignment of the actuator and sensor will lead to much smaller α_{BD} as compared to α_{MD} . This is because these bearing direction modes will not be strongly excited by the actuator or observed by the sensor if the misalignments are kept small. However, irrespective of the misalignment, the rigid body mode along the motion direction will always get excited. Therefore, the first bracketed term in the LHS of Eq.(7-1) i.e. sum of all modal residues will be greater than zero. Similarly, the frequencies of the flexible modes along the bearing directions will be much higher as compared to the rigid body mode along the motion direction i.e. $\omega_{\text{MD}} \ll \omega_{\text{BD}}$. Therefore, the second bracketed term in the LHS of Eq.(7-1) will also be greater than zero. Overall, the entire LHS of Eq.(7-1) will be greater than zero, and therefore the absence of RNMP zeros will also be guaranteed. This is evident in the FRF in Fig 7-5 where both CNMP and RNMP zeros are absent. Thus, the absence of all NMP zeros has been achieved in this flexure based motion stage via systematic and deterministic physical design choices even when all modal residue signs are not the same.

Based on this specific example, a few design guidelines or learnings are provided below that can be applied more generally to any motion system with finite bearing stiffness [3, 7, 39].

Design Guideline 1: In the absence of actuator-sensor collocation, which is very hard to achieve in any case, make an informed choice of actuator-sensor placement to achieve the desired sequence of modal residue signs (not necessarily ‘all modal residue signs are same’) in order to guarantee the absence of CNMP zeros.

Design Guideline 2: Choose appropriate values of physical parameters to push the bearing direction modes to higher frequencies without significantly increasing the frequency of the rigid

body mode along the motion direction. This leads to $\omega_{MD} \ll \omega_{BD}$ and therefore, aids in satisfying Eq.(7-1).

Design Guideline 3: Keep the actuator and sensor misalignments as small as possible to keep the modal residues associated with bearing direction modes as small as possible. This leads to $\alpha_{MD} \gg \alpha_{BD}$ and therefore, aids in satisfying Eq.(7-1).

Following **Design Guideline 1** leads to the absence of CNMP zeros. **Design Guideline 1** is generally practiced by designers and engineers but only to achieve the same sign of all modal residue via actuator-sensor collocation. However, this thesis demonstrates that it can be more widely applied to choose non-located actuator-sensor configurations and still guarantee the absence of CNMP zeros. Not only that, mass-stiffness distribution can also be modified to achieve the required sequence of modal residue signs as theoretically demonstrated via a case study in Chapter 4. However, as the example of the flexure bearing based motion system demonstrated here, it can be relatively easy to change the sensor location to alter the sequence of modal residue signs as compared to any other physical parameter. However, if the sensor or actuator position cannot be changed, then the design engineer must investigate the relationship between mode shapes and mass-stiffness distribution in order to achieve the required sequence of modal residue signs.

Once the required sequence of modal residue signs is achieved, following **Design Guidelines 2 and 3** means that Eq.(7-1) is satisfied and therefore, it leads to the absence of RNMP zeros. **Design Guidelines 2 and 3** are also generally practiced by designers and engineers to achieve good static performance such as large payload carrying capacity, low heat generation from actuators and small error motions along bearing directions. However, this thesis demonstrates (for the first time

to the best of the author's knowledge) how these design guidelines also affect and potentially improve the dynamic performance of motion systems by guaranteeing the absence of RNMP zeros.

In the above example, we have shown the practical utility of the sufficient condition for the absence of NMP zeros (derived for undamped flexible systems) in a lightly damped flexure bearing based motion system. Even though in this particular case of light damping, NMP zeros were found to be absent when the sufficient condition was satisfied, this may not always be the case. Chapter 3 and Chapter 5 proved that the addition of viscous damping is not always beneficial to the zeros of the flexible system. Therefore, even though satisfying the sufficient condition in Chapter 4 guarantees that all the zeros of the undamped flexible system are MMP, the addition of viscous damping can possibly push these MMP zeros to the RHS of the imaginary axis, making them NMP zeros. However, Chapter 5 showed that under the assumption of proportional viscous damping and for certain choices of proportional damping coefficients c_M and c_K , viscous damping will always have a beneficial effect on the zeros of flexible systems (i.e. will make the zeros MP). Therefore, once the sufficient condition in Chapter 4 has been satisfied, leading to all zeros lying purely on the imaginary axis i.e. MMP zeros, the addition of proportional viscous damping (for certain values of c_M and c_K) will guarantee that these MMP zeros always get pushed to the LHS of the imaginary axis, making either CMP or RMP zeros. This result from Chapter 5 is applicable to all levels of damping i.e. underdamped, critically and overdamped flexible systems.

So far in the existing literature, viscous damping has only been shown to push the poles of flexible systems to the LHS of the imaginary axis, leading to smaller residual vibration and overshoot. The effect of viscous damping on the zeros of flexible systems was less thoroughly investigated in the existing literature. This thesis not only investigated the effect of viscous damping on the zeros of flexible systems in detail but also provided several novel design strategies

to apply viscous damping to guarantee the absence of NMP zeros leading to better closed-loop bandwidth, stability robustness, smaller undershoot and faster settling time. Although, the theoretical contributions of this thesis on the effect of viscous damping on zeros is strong and novel, it does not demonstrate the practical application of viscous damping via experiments. These are the major bottlenecks in realizing the practical utility of viscous damping to guarantee the absence of NMP zeros:

1. This thesis assumes classical and proportional viscous damping to achieve no NMP zeros. However, in reality, the damping in flexible systems such as from material hysteresis, joint friction etc is neither classical nor proportional viscous damping. It may be possible that for small enough damping, certain damping mechanisms can be approximated as classical or proportional viscous damping. But no such approximations, along with suitable justifications, exist in the literature so far (including this thesis).
2. It is not always practically feasible to add viscous damping to flexible systems. For example, Varanasi [61] has experimentally demonstrated that foam based viscous dampers are effective in reducing the residual vibrations in flexure bearings. However, the foam material in these dampers may not be vacuum compatible and therefore cannot be used in flexure bearing based motions systems that need to operate in vacuum.

Therefore, this motivates the need to find practically feasible ways to apply viscous damping to flexible systems in a deterministic manner in order to satisfy the sufficient conditions derived in this thesis and therefore, guarantee the absence of NMP zeros. This task is left to future researchers who may find this problem interesting.

This thesis presented new mathematical frameworks to study the zeros of the SISO transfer functions of general flexible LTI systems. These mathematical frameworks were used to derive

new sufficient conditions for the absence of all NMP zeros, with and without viscous damping, when all modal residue signs are not the same. A brief summary of the various contributions of the thesis is provided below.

7.1 Conclusion

Chapter 2 investigated the zero dynamics of undamped two and three-DoF flexible systems using modal decomposition and zero locus techniques. This investigation led to the necessary and sufficient condition for the absence of CNMP and RNMP zeros in these flexible system. The most noteworthy sufficient condition for the elimination of CNMP zeros was the presence of non-alternating sequence of modal residue signs because the signs of modal residue is related to actuator-sensor placement and one can enforce this sufficient condition via informed choices of actuator and sensor position. This investigation motivated the need to find similar sufficient condition for undamped multi-DoF flexible system with any arbitrary number of modes and consider the effect of viscous damping on the behavior of zeros.

Chapter 3 investigated the zero dynamics of classically damped two-DoF and three-DoF flexible systems using modal decomposition and zero locus techniques. This investigation again led to the necessary and sufficient condition for the absence of CNMP and RNMP zeros in these flexible systems. More importantly, this investigation demonstrated the effect of viscous damping on the zeros of flexible system by drawing contrast between the zeros loci of the undamped flexible systems in Chapter 2 and their counterparts in Chapter 3. It revealed that unlike the beneficial effect of viscous damping on poles, zeros can be negatively impacted by adding damping to a flexible system. The addition of viscous damping can push MP zeros to become NMP zeros, thereby leading to worse dynamic performance in open as well as closed-loop. However, the necessary and sufficient conditions provided in this chapter for the absence of NMP zeros lead to

informed choice of viscous damping strategies that have an overall beneficial effect on the zeros of two- and three-DoF flexible systems, as shown via a case study.

Chapter 4 investigated the zero dynamics of multi-DoF undamped flexible systems with any arbitrary number of modes. It provides a new sufficient condition for the elimination of CNMP and RNMP zeros. Based on the existing literature, it was believed that only when all modal residue signs are the same, absence of NMP zeros was possible. However, Chapter 4 provides new sequences of modal residue signs that also guarantee the absence of NMP zeros. These sequences of modal residue signs can be enforced via either actuator-sensor placement or mass-stiffness distribution, as shown via a case study. However, the only drawback of this sufficient condition is that it is only applicable for undamped flexible systems (it has been empirically shown to guarantee the absence of NMP zeros in lightly damped flexible systems in the last chapter). Even when this sufficient condition is satisfied and therefore, all zeros are MMP, the addition of viscous damping can possibly convert these MMP zeros to NMP zeros. This motivated the need to find a viscous damping strategy that preserves the MP behavior of undamped multi-DoF flexible systems.

Chapter 5 investigated the zero dynamics of multi-DoF proportionally damped flexible systems with arbitrary number of modes. It provided the necessary and sufficient condition for the absence of NMP zeros by only making use of proportional viscous damping. It was shown that proportional viscous damping can only guarantee the absence of CNMP zeros; absence of RNMP zeros cannot be guaranteed via this choice of damping strategy. It was shown that for certain choices of damping parameters, the proportional damping strategy preserves the MP behavior of undamped multi-DoF flexible systems. This means that if the undamped flexible system already consists of only MP zeros then the informed choice of proportional damping parameters will ensure that these zeros remain MP. Furthermore, if the zeros of the undamped flexible system are CNMP then the

informed choice of proportional damping parameters will convert these CNMP zeros to MP zeros, as shown via a case study.

Chapter 6 investigated the effect of proportional viscous damping on the RNMP zeros of multi-DoF flexible systems with any arbitrary number of modes. Proportional viscous damping cannot guarantee the absence of RNMP zeros for any choice of damping parameters, as shown in Chapter 5. However, for some choices of damping parameters, all RNMP zeros can be pushed further away from the imaginary axis. The presence of RNMP zeros close to the imaginary axis makes it difficult to simultaneously achieve faster settling time and smaller undershoot. Therefore, pushing the RNMP zeros sufficiently away from the imaginary axis will lead to significant improvement in the dynamic performance of flexible systems. This is demonstrated in Chapter 6 via a case study where pushing all RNMP zeros further away from the imaginary axis via the application of proportional viscous damping led to faster settling time and smaller undershoot simultaneously.

7.2 Future Work

The following are the areas for future research in the field of zeros of flexible systems:

1. Zeros of multi-input multi-output (MIMO) flexible systems: Very little is known in terms of the necessary and/or sufficient conditions for the absence of NMP zeros that occur in MIMO systems. A few references on the zeros of MIMO systems are given in [144-146]. Unlike the zeros of a SISO system, there are several alternate ways to define the zeros of a MIMO system such as “Smith-McMillan” zeros, zeros using co-prime factorization of the transfer function, zeros from Rosenbrock system matrix, among others. The commonly used definition of zeros of MIMO systems is based on their transmission blocking property and these zeros can be calculated using the Rosenbrock system matrix (RSM). If $[A]$, $[B]$, $[C]$, and $[D]$ are the state space matrices of a system with ‘ n ’ states, ‘ p ’ inputs and ‘ q ’ outputs, then the RSM matrix is defined as shown below:

$$\text{RSM}(s) \triangleq \begin{bmatrix} s[\mathbf{I}]_{n \times n} - [\mathbf{A}]_{n \times n} & [\mathbf{B}]_{n \times p} \\ -[\mathbf{C}]_{q \times n} & [\mathbf{D}]_{q \times p} \end{bmatrix} \quad (7-2)$$

‘ z ’ is the transmission zero of the MIMO system if the determinant of the RSM matrix for $s = z$ is zero. In other words, the RSM matrix loses rank when $s = z$. This zero is referred to as the ‘transmission zero’ because when the MIMO system is excited at this frequency via the ‘ p ’ inputs, then the response of all ‘ q ’ outputs is zero. Therefore, this definition of zero blocks the transmission of signal from all the inputs to all the outputs. The zeros of the SISO system studied in this thesis also have this transmission blocking property. However, there is no existing literature that provides a mathematical relationship between the zeros of a MIMO system and the zeros of its constituent SISO systems. The derivation of such relationships will provide a better understanding of the zeros of MIMO systems as well as allow us to extend the necessary and sufficient conditions derived for the absence of NMP zeros in SISO systems to MIMO systems.

2. Experimental application of proportional viscous damping for absence of NMP zeros: Chapter 5 and Chapter 6 provide the theoretical results and design strategies to use proportional viscous damping for the absence of NMP zeros. However, realizing proportional viscous damping in practice is not always feasible. Damping that inherently occurs in flexible systems such as air damping, material hysteresis or damping due to joint friction in assembled machines are small but non-zero and they are not proportional in nature. Therefore, new and innovative techniques must be developed to add sufficient and deterministic proportional damping to flexible systems in order to guarantee the absence of NMP zeros and simultaneously push the poles to the LHS of the imaginary axis, leading to better overall dynamic performance.

3. Creating closely spaced MMP zeros for vibration isolation over a large range of frequency: MMP zeros lying purely on the imaginary axis are also referred to as antiresonant frequencies.

These antiresonant frequencies provide excellent vibration isolation, however only over a small band of frequency. Therefore, the idea is to design the flexible system in such a way that multiple MMP zeros lie close to each other on the imaginary axis (just like closely spaced modes discussed in Chapter 2). These closely spaced MMP zeros can provide excellent vibration isolation over a large range of frequency. Chapter 4 provides the sequence of modal residue signs that allows odd/even number of closely spaced MMP zeros without any poles in between. However, so far no example has been found in the existing literature where there are more than two closely spaced MMP zeros. Therefore, further research is needed to design flexible systems so that more than two closely spaced MMP zeros can be placed in the desired frequency range and achieve good vibration isolation.

4. Leveraging the large sensitivity of CNMP zeros to system parameters to design ultra-sensitive sensors: Chapter 2 demonstrated that in the presence of closely spaced modes and alternating sequence of modal residue signs, MMP zeros can very easily transition into CNMP zeros even for the slightest change in system parameters such as mass-stiffness distribution or actuator-sensor placement. Although this property of flexible systems makes it difficult to achieve good control performance but this sensitive dependence of the CNMP zeros on the system parameters can be exploited to improve the sensitivity of existing sensors such as accelerometers or mass sensors. Several researchers [147-149] have already exploited the phenomena of mode localization and curve veering to increase the sensitivity of these sensors. However, no one has reported the use of CNMP zeros and its sensitive dependence on system parameters to achieve the same goal. Therefore, further research is needed in this area to understand how the sensitivity of CNMP zeros can be leveraged to design ultra-sensitive sensors and what advantages it has over sensors built on the phenomena of mode localization.

Bibliography

1. Hu, Q., 2008, "Sliding mode maneuvering control and active vibration damping of three-axis stabilized flexible spacecraft with actuator dynamics," *Nonlinear Dynamics*, **52**(3), p. 227-248.
2. Gennaro, S.D., 2003, "Output stabilization of flexible spacecraft with active vibration suppression," *IEEE Transactions on Aerospace and Electronic Systems*, **39**(3), p. 747-759.
3. Chang, J.Y., 2007, "Hard disk drive seek-arrival vibration reduction with parametric damped flexible printed circuits," *Microsystem Technologies*, **13**(8), p. 1103-1106.
4. Feng, G., Fook Fah, Y., and Ying, Y., 2005, "Modeling of hard disk drives for vibration analysis using a flexible multibody dynamics formulation," *IEEE Transactions on Magnetics*, **41**(2), p. 744-749.
5. Friedmann, P.P. and Millott, T.A., 1995, "Vibration reduction in rotorcraft using active control - A comparison of various approaches," *Journal of Guidance, Control, and Dynamics*, **18**(4), p. 664-673.
6. Culpepper, M.L. and Anderson, G., 2004, "Design of a low-cost nano-manipulator which utilizes a monolithic, spatial compliant mechanism," *Precision engineering*, **28**(4), p. 469-482.
7. Roy, N.K. and Cullinan, M.A., 2018, "Design and characterization of a two-axis, flexure-based nanopositioning stage with 50 mm travel and reduced higher order modes," *Precision Engineering*, **53**, p. 236-247.
8. Chalhoub, N.G. and Ulsoy, A.G., 1986, "Dynamic Simulation of a Leadscrew Driven Flexible Robot Arm and Controller," *Journal of Dynamic Systems, Measurement, and Control*, **108**(2), p. 119-126.
9. Rattan, K. and Feliu, V., 1992, "Feedforward control of flexible manipulators," *Proceedings 1992 IEEE International Conference on Robotics and Automation*, p. 788,789,790,791,792,793.

10. Seifried, R., Held, A., and Dietmann, F., 2011, "Analysis of feed-forward control design approaches for flexible multibody systems," *Journal of System Design and Dynamics* **5**(3), p. 429-440.
11. Chen, S.-L., Li, X., Teo, C.S., and Tan, K.K., 2017, "Composite jerk feedforward and disturbance observer for robust tracking of flexible systems," *Automatica*, **80**, p. 253-260.
12. Chen, C.H. and Brussel, H.V., 1993, "Servo control of flexible beam with inverse-dynamics feedforward and disturbance observer," *ISIE '93 - Budapest: IEEE International Symposium on Industrial Electronics Conference Proceedings*, p. 702-707.
13. Hoagg, J.B. and Bernstein, D.S., 2007, "Nonminimum-phase zeros-much to do about nothing-classical control-revisited part II," *IEEE Control Systems Magazine*, **27**(3), p. 45-57.
14. Freudenberg, J. and Looze, D., 1985, "Right half plane poles and zeros and design tradeoffs in feedback systems," *IEEE Transactions on Automatic Control*, **30**(6), p. 555-565.
15. Marcopoli, V., Freudenberg, J., and Middleton, R., 2002, "Nonminimum phase zeros in the general feedback configuration," *Proceedings of the 2002 American Control Conference (IEEE Cat. No. CH37301)*, **2**, p. 1049-1054.
16. Kamaldar, M., Islam, S.A.U., Hoagg, J.B., and Bernstein, D.S., 2022, "Demystifying Enigmatic Undershoot in Setpoint Command Following [Focus on Education]," *IEEE Control Systems Magazine*, **42**(1), p. 103-125.
17. Lau, K., Middleton, R.H., and Braslavsky, J.H., 2003, "Undershoot and settling time tradeoffs for nonminimum phase systems," *IEEE Transactions on Automatic Control*, **48**(8), p. 1389-1393.
18. Middleton, R.H., 1991, "Trade-offs in linear control system design," *Automatica*, **27**(2), p. 281-292.
19. Cui, L., 2017, "On the Complex Non-Minimum Phase Zeros in Flexure Mechanism," Ph.D. dissertation, University of Michigan, Ann Arbor, MI.
20. Butterworth, J.A., Pao, L.Y., and Abramovitch, D.Y. *The effect of nonminimum-phase zero locations on the performance of feedforward model-inverse control techniques in discrete-time systems.* in *2008 American Control Conference*. 2008.

21. Merrikh-Bayat, F., 2013, "Fractional-order unstable pole-zero cancellation in linear feedback systems," *Journal of Process Control*, **23**(6), p. 817-825.
22. Torfs, D., De Schutter, J., and Swevers, J., 1992, "Extended Bandwidth Zero Phase Error Tracking Control of Nonminimal Phase Systems," *Journal of Dynamic Systems, Measurement, and Control*, **114**(3), p. 347-351.
23. Gross, E. and Tomizuka, M., 1994, "Experimental flexible beam tip tracking control with a truncated series approximation to uncancelable inverse dynamics," *IEEE Transactions on Control Systems Technology*, **2**(4), p. 382-391.
24. Ramani, K.S., Duan, M., Okwudire, C.E., and Galip Ulsoy, A., 2016, "Tracking Control of Linear Time-Invariant Nonminimum Phase Systems Using Filtered Basis Functions," *Journal of Dynamic Systems, Measurement, and Control*, **139**(1).
25. Wang, H., Kim, K., and Zou, Q., 2013, "B-spline-decomposition-based output tracking with preview for nonminimum-phase linear systems," *Automatica*, **49**(5), p. 1295-1303.
26. Zhao, S., Xue, W., and Gao, Z., 2013, "Achieving Minimum Settling Time Subject to Undershoot Constraint in Systems With One or Two Real Right Half Plane Zeros," *Journal of Dynamic Systems, Measurement, and Control*, **135**(3).
27. Sun, L., Li, D., Gao, Z., Yang, Z., and Zhao, S., 2016, "Combined feedforward and model-assisted active disturbance rejection control for non-minimum phase system," *ISA Transactions*, **64**, p. 24-33.
28. Miu, D.K., 1991, "Physical Interpretation of Transfer Function Zeros for Simple Control Systems With Mechanical Flexibilities," *Journal of Dynamic Systems, Measurement, and Control*, **113**(3), p. 419-424.
29. Van de Straete, H.J. and Youcef-Toumi, K., 1996, "Physical Meaning of Zeros and Transmission Zeros from Bond Graph Models," *IFAC Proceedings Volumes*, **29**(1), p. 4422-4427.
30. Calafiore, G.C., 1997, "A subsystems characterization of the zero modes for flexible mechanical structures," *Proceedings of the 36th IEEE Conference on Decision and Control*, **2**, p. 1375-1380.

31. Spector, V.A. and Flashner, H., 1990, "Modeling and Design Implications of Noncollocated Control in Flexible Systems," *Journal of Dynamic Systems, Measurement, and Control*, **112**(2), p. 186-193.
32. Bendiksen, O.O., 1987, "Mode localization phenomena in large space structures," *AIAA Journal*, **25**(9), p. 1241-1248.
33. Afolabi, D. and Alabi, B., 1992, "Catastrophe theory, curve veering and the vibration of bladed discs," *Proceedings of the Institution of Mechanical Engineers, Part C: Journal of Mechanical Engineering Science*, **206**(2), p. 143-144.
34. Castanier, M.P. and Pierre, C., 2006, "Modeling and analysis of mistuned bladed disk vibration: current status and emerging directions," *Journal of Propulsion and power* **22**(2), p. 384-396.
35. Hoagg, J.B., Chandrasekar, J., and Bernstein, D.S., 2006, "On the Zeros, Initial Undershoot, and Relative Degree of Collinear Lumped-Parameter Structures," *Journal of Dynamic Systems, Measurement, and Control*, **129**(4), p. 493-502.
36. Cui, L., Okwudire, C., and Awtar, S., 2017, "Modeling complex nonminimum phase zeros in flexure mechanisms," *Journal of Dynamic Systems, Measurement, and Control*, **139**(10), p. 101001.
37. Cui, L. and Awtar, S., 2019, "Experimental validation of complex non-minimum phase zeros in a flexure mechanism," *Precision Engineering*, **60**, p. 167-177.
38. Chandrasekar, J., Hoagg, J.B., and Bernstein, D.S., 2004, "On the zeros of asymptotically stable serially connected structures," 2004 43rd IEEE Conference on Decision and Control (CDC)(IEEE Cat. No. 04CH37601), **3**, p. 2638-2643.
39. Awtar, S. and Parmar, G., 2013, "Design of a Large Range XY Nanopositioning System," *Journal of Mechanisms and Robotics*, **5**(2), p. p.021008.
40. Loix, N., Kozanek, J., and Foltete, E., 1996, "On the complex zeros of non-located systems," *Journal of Structural Control*, **3**(1-2), p. 79-87.
41. Cannon, R.H. and Schmitz, E., 1984, "Initial Experiments on the End-Point Control of a Flexible One-Link Robot," *The International Journal of Robotics Research*, **3**(3), p. 62-75.

42. Awtar, S. and Craig, K.C., 2004, "Electromagnetic coupling in a dc motor and tachometer assembly," *Journal of Dynamic Systems, Measurement, and Control*, **126**(3), p. 684-691.
43. Martin, G.D., 1978, "On the control of flexible mechanical systems," Ph.D. dissertation, Stanford University, Stanford, CA.
44. Gevarter, W.B., 1970, "Basic relations for control of flexible vehicles," *AIAA Journal*, **8**(4), p. 666-672.
45. Williams, T., 1992, "Model order effects on the transmission zeros of flexible space structures," *Journal of guidance, control, and dynamics*, **15**(2), p. 540-543.
46. Williams, T. and Juang, J.N., 1992, "Sensitivity of the transmission zeros of flexible space structures," *Journal of guidance, control, and dynamics* **15**(2), p. 368-375.
47. Saad, M., Saydy, L., and Akhrif, O., 2000, "Noncollocated passive transfer functions for a flexible link robot," *CACSD. Conference Proceedings. IEEE International Symposium on Computer-Aided Control System Design (Cat. No.00TH8537)*, p. 971-975.
48. Liu, L.-Y. and Yuan, K., 2003, "Noncollocated passivity-based PD control of a single-link flexible manipulator," *Robotica*, **21**(2), p. 117-135.
49. Wang, D. and Vidyasagar, M., 1991, "Transfer Functions for a Single Flexible Link," *The International Journal of Robotics Research*, **10**(5), p. 540-549.
50. Damaren, C.J., 1999, "Passivity and Noncollocation in the Control of Flexible Multibody Systems," *Journal of Dynamic Systems, Measurement, and Control*, **122**(1), p. 11-17.
51. Caverly, R.J. and Forbes, J.R. *Linearly Combining Sensor Measurements Optimally to Enforce an SPR Transfer Matrix. in 2018 IEEE Conference on Control Technology and Applications (CCTA)*. 2018.
52. Damaren, C.J., 1995, "Passivity analysis for flexible multilink space manipulators," *Journal of Guidance, Control, and Dynamics* **18**(2), p. 272-279.

53. Damaren, C., 1996, "Approximate inverse dynamics and passive feedback for flexible manipulators with large payloads," *IEEE Transactions on Robotics and Automation* **12**(1), p. 131-138.
54. Christoforou, E.G. and Damaren, C.J. *Application of passivity-based techniques to the control of structurally flexible gantry robots.* in *2011 IEEE International Conference on Robotics and Automation.* 2011.
55. Christoforou, E.G. and Damaren, C.J. *A Passivity-Based Control Case Study of Flexible-Link Manipulators.* in *Proceedings of the 2005 IEEE International Conference on Robotics and Automation.* 2005.
56. Caverly, R.J. and Forbes, J.R., 2014, "Dynamic Modeling and Noncollocated Control of a Flexible Planar Cable-Driven Manipulator," *IEEE Transactions on Robotics*, **30**(6), p. 1386-1397.
57. Williams, T., 1989, "Transmission-zero bounds for large space structures, with applications," *Journal of Guidance, Control, and Dynamics*, **12**(1), p. 33-38.
58. Caughey, T.K., 1960, "Classical Normal Modes in Damped Linear Dynamic Systems," *Journal of Applied Mechanics*, **27**(2), p. 269-271.
59. Caughey, T.K. and O'Kelly, M.E.J., 1965, "Classical normal modes in damped linear dynamic systems," *Journal of Applied Mechanics*, **32**(3), p. 583-588.
60. Lin, J.L. and Juang, J.N., 1995, "Sufficient conditions for minimum-phase second-order linear systems," *Journal of Vibration Control*, **1**(2), p. 183-199.
61. Varanasi, K.K. and Nayfeh, S.A., 2006, "Damping of flexural vibration using low-density, low-wave-speed media," *Journal of Sound and Vibration*, **292**(1), p. 402-414.
62. Engelen, K., Ramon, H., Saeys, W., Franssens, W., and Anthonis, J., 2007, "Positioning and tuning of viscous damper on flexible structure," *Journal of Sound and Vibration*, **304**(3), p. 845-862.
63. Thompson, A.G., 1981, "Optimum tuning and damping of a dynamic vibration absorber applied to a force excited and damped primary system," *Journal of Sound and Vibration*, **77**(3), p. 403-415.

64. Stieber, M.E., Vukovich, G., and Petriu, E. *Stability aspects of vision-based control for space robots.* in *Proceedings of International Conference on Robotics and Automation.* 1997.
65. Book, W.J., 1993, "Structural flexibility of motion systems in the space environment," *IEEE Transactions on Robotics and Automation*, **9**(5), p. 524-530.
66. Hughes, P.C., 1974, "Dynamics of flexible space vehicles with active attitude control," *Celestial mechanics*, **9**(1), p. 21-39.
67. Dwivedy, S.K. and Eberhard, P., 2006, "Dynamic analysis of flexible manipulators, a literature review," *Mechanism and machine theory*, **41**(7), p. 749-777.
68. Zhu, G., Ge, S.S., and Lee, T.H., 1999, "Simulation studies of tip tracking control of a single-link flexible robot based on a lumped model," *Robotica*, **17**(1), p. 71-78.
69. Lozano, R. and Brogliato, B., 1992, "Adaptive control of robot manipulators with flexible joints," *IEEE Transactions on Automatic Control* **37**(2), p. 174-181.
70. de Queiroz, M.S., Donepudi, S., Burg, T., and Dawson, D.M., 1998, "Model-based control of rigid-link flexible-joint robots: an experimental evaluation," *Robotica*, **16**(1), p. 11-21.
71. Megahed, S.M. and Hamza, K., 2004, "Modeling and simulation of planar flexible link manipulators with rigid tip connections to revolute joints," *Robotica*, **22**(3), p. 285-300.
72. y Alvarado, P.V., Chin, S., Larson, W., Mazumdar, A., and Youcef-Toumi, K., 2010, "A soft body under-actuated approach to multi degree of freedom biomimetic robots: A stingray example," *2010 3rd IEEE RAS & EMBS International Conference on Biomedical Robotics and Biomechatronics*, p. 473-478.
73. Valdivia y Alvarado, P. and Youcef-Toumi, K., 2006, "Design of machines with compliant bodies for biomimetic locomotion in liquid environments."
74. La-orpacharapan, C. and Pao, L.Y., 2003, "Fast seek control for flexible disk drive systems with back EMF and inductance," *Proceedings of the 2003 American Control Conference*, **4**, p. 3077-3082.

75. Choi, K.B. and Lee, J.J., 2005, "Passive compliant wafer stage for single-step nano-imprint lithography," *Review of scientific instruments*, **76**(7), p. p.075106.
76. Roy, N., Yuksel, A., and Cullinan, M., 2016, "Design and modeling of a microscale selective laser sintering system," *International Manufacturing Science and Engineering Conference*, **49910**, p. V003T08A002.
77. Lee, C. and Salapaka, S.M., 2008, "Robust broadband nanopositioning: fundamental trade-offs, analysis, and design in a two-degree-of-freedom control framework," *Nanotechnology*, **20**(3), p. 035501.
78. Lee, C. and Salapaka, S., 2009, "Optimal-Control Methods for Design of Two-Degree-Freedom Systems for Nanopositioning," *Proceeding of the ASME 2009 Dynamic Systems and Control Conference*, **48937**, p. 589-596.
79. Kenton, B.J. and Leang, K.K., 2011, "Design and control of a three-axis serial-kinematic high-bandwidth nanopositioner," *IEEE/ASME Transactions on Mechatronics*, **17**(2), p. 356-369.
80. Devasia, S., Eleftheriou, E., and Moheimani, S.R., 2007, "A survey of control issues in nanopositioning," *IEEE Transactions on Control Systems Technology* **15**(5), p. 802-823.
81. Davison, D.E., Kabamba, P.T., and Meerkov, S.M., 1999, "Limitations of disturbance rejection in feedback systems with finite bandwidth," *IEEE transactions on automatic control*, **44**(6), p. 1132-1144.
82. Chen, J., Qiu, L., and Toker, O., 2000, "Limitations on maximal tracking accuracy," *IEEE Transactions on automatic control* **45**(2), p. 326-331.
83. Meirovitch, L., 1967, *Analytical methods in Vibration*, Vol. 19, The Macmillan Company, New York.
84. Miu, D.K., 2012, *Mechatronics: electromechanics and contromechanics*, Springer Science & Business Media.
85. Rankers, A.M., 1998, "Machine dynamics in mechatronic systems: An engineering approach," Ph.D. Thesis, Twente University, The Netherlands.

86. Coelingh, E., de Vries, T.J., and Koster, R., 2002, "Assessment of mechatronic system performance at an early design stage," *IEEE/ASME transactions on mechatronics*, **7**(3), p. 269-279.
87. Spector, V.A. and Flashner, H., 1989, "Sensitivity of Structural Models for Noncollocated Control Systems," *Journal of Dynamic Systems, Measurement, and Control*, **111**(4), p. 646-655.
88. Wie, B., 1981, "On the modeling and control of flexible space structures," Ph.D. Thesis, Stanford University, CA.
89. Lee, Y.J. and Speyer, J.L., 1993, "Zero locus of a beam with varying sensor and actuator locations," *Journal of guidance, control, and dynamics*, **16**(1), p. 21-25.
90. Aphale, S.S., Fleming, A.J., and Moheimani, S.R., 2007, "Integral resonant control of collocated smart structures," *Smart Materials and Structures* **16**(2), p. 439.
91. Vakil, M., Fotouhi, R., and Nikiforuk, P., 2010, "On the zeros of the transfer function of flexible link manipulators and their non-minimum phase behaviour," *Proceedings of the Institution of Mechanical Engineers, Part C: Journal of Mechanical Engineering Science*, **224**(10), p. 2083-2096.
92. Tohyama, M. and Lyon, R.H., 1989, "Zeros of a transfer function in a multi-degree-of-freedom vibrating system," *The Journal of the Acoustical Society of America*, **86**(5), p. 1854-1863.
93. Tohyama, M., 2008, "Room Transfer Function," *Handbook of Signal Processing in Acoustics*, p. 1381-1402.
94. Duffour, P. and Woodhouse, J., 2004, "Instability of systems with a frictional point contact. Part 1: basic modelling," *Journal of Sound and Vibration*, **271**(1-2), p. 365-390.
95. Enns, D.F., 1991, "Rocket stabilization as a structured singular value synthesis design example," *IEEE Control Systems Magazine* **11**(4), p. 67-73.
96. Preumont, A., 2018, *Vibration control of active structures: an introduction*, Vol. 246, Springer.

97. Uddin, M.M., Sarker, P., Theodore, C.R., and Chakravarty, U.K., 2018, "Active Vibration Control of a Helicopter Rotor Blade by Using a Linear Quadratic Regulator," ASME International Mechanical Engineering Congress and Exposition, **52002**, p. V001T03A014.
98. Varanasi, K.K. and Nayfeh, S.A., 2004, "The Dynamics of Lead-Screw Drives: Low-Order Modeling and Experiments," *Journal of Dynamic Systems, Measurement, and Control*, **126**(2), p. 388-396.
99. Mottershead, J.E., 2001, "COMPLEX AND DEFECTIVE ZEROS IN CROSS RECEPTANCES," *Journal of Sound and Vibration*, **246**(1), p. 190-197.
100. Mottershead, J., 2001, "Structural modification for the assignment of zeros using measured receptances," *J. Appl. Mech.*, **68**(5), p. 791-798.
101. Mottershead, J.E., Mares, C., and Friswell, M.I., 2001, "AN INVERSE METHOD FOR THE ASSIGNMENT OF VIBRATION NODES," *Mechanical Systems and Signal Processing*, **15**(1), p. 87-100.
102. Pierson, H., Brevick, J., and Hubbard, K., 2013, "The effect of discrete viscous damping on the transverse vibration of beams," *Journal of Sound and Vibration*, **332**(18), p. 4045-4053.
103. Main, J.A. and Krenk, S., 2005, "Efficiency and tuning of viscous dampers on discrete systems," *Journal of Sound and Vibration*, **286**(1), p. 97-122.
104. Banks, H.T. and Inman, D.J., 1991, "On Damping Mechanisms in Beams," *Journal of Applied Mechanics*, **58**(3), p. 716-723.
105. Morris, K.A. and Vidyasagar, M., 1990, "A Comparison of Different Models for Beam Vibrations From the Standpoint of Control Design," *Journal of Dynamic Systems, Measurement, and Control*, **112**(3), p. 349-356.
106. Hoffmann, N. and Gaul, L., 2003, "Effects of damping on mode-coupling instability in friction induced oscillations," *Journal of Applied Mathematics and Mechanics* **83**, p. 524-534.
107. Sun, C.T. and Bai, J.M., 1995, "Vibration of multi-degree-of-freedom systems with non-proportional viscous damping," *International Journal of Mechanical Sciences*, **37**(4), p. 441-455.

108. Pang, S.T., Tsao, T., and Bergman, L.A., 1993, "Active and Passive Damping of Euler-Bernoulli Beams and Their Interactions," *Journal of Dynamic Systems, Measurement, and Control*, **115**(3), p. 379-384.
109. Thomas, A.E., Dickerson, S.L., and Wayne, B.J., 1986, "On the Transfer Function Modeling of Flexible Structures with Distributed Damping," *ASME Winter Annual Meeting*, p. 23-30.
110. Lin, J.L., 1999, "On Transmission Zeros of Mass-Dashpot-Spring Systems," *Journal of Dynamic Systems, Measurement, and Control*, **121**(2), p. 179-183.
111. Roesset, J.M., Whitman, R.V., and Dobry, R., 1973, "Modal analysis for structures with foundation interaction," *Journal of the Structural Division*, **99**(3), p. 399-416.
112. Tsai, N.C., 1974, "Modal damping for soil-structure interaction," *Journal of the Engineering Mechanics Division*, **100**(2), p. 323-341.
113. Thomson, W.T., Calkins, T., and Caravani, P., 1974, "A numerical study of damping," *Earthquake Engineering and Structural Dynamics*, **3**(1), p. 97-103.
114. Rath, S., Cui, L., and Awtar, S., 2021, "On the Zeros of an Undamped Three-DOF Flexible System," *ASME Letters in Dynamic Systems and Control*, **1**(4), p. 041010.
115. Ramond, P., 2022, "The Abel–Ruffini Theorem: Complex but Not Complicated," *The American Mathematical Monthly*, **129**(3), p. 231-245.
116. Giurgiutiu, V., 2000, "Review of Smart-Materials Actuation Solutions for Aeroelastic and Vibration Control," *Journal of Intelligent Material Systems and Structures*, **11**(7), p. 525-544.
117. Roy, N.K. and Cullinan, M.A., 2018, "Fast Trajectory Tracking of a Flexure-Based, Multiaxis Nanopositioner With 50-mm Travel," *IEEE/ASME Transactions on Mechatronics*, **23**(6), p. 2805-2813.
118. Book, W.J., Maizza-Neto, O., and Whitney, D.E., 1975, "Feedback Control of Two Beam, Two Joint Systems With Distributed Flexibility," *Journal of Dynamic Systems, Measurement, and Control*, **97**(4), p. 424-431.

119. Torfs, D., Swevers, J., and Schutter, J.D. *Quasi-perfect tracking control of non-minimal phase systems.* in [1991] *Proceedings of the 30th IEEE Conference on Decision and Control.* 1991.
120. Hyung-Soon, P., Pyung, H.C., and Doo Yong, L. *Continuous zero phase error tracking controller with gain error compensation.* in *Proceedings of the 1999 American Control Conference.* 1999.
121. Rigney, B.P., Pao, L.Y., and Lawrence, D.A., 2009, "Nonminimum Phase Dynamic Inversion for Settle Time Applications," *IEEE Transactions on Control Systems Technology*, **17**(5), p. 989-1005.
122. Fleming, F.M., 1990, "The effect of structure, actuator, and sensor on the zeroes of controlled structures," Ph.D. dissertation, Massachusetts Institute of Technology, Cambridge, MA.
123. Cannon, R.H. and Rosenthal, D.E., 1984, "Experiments in control of flexible structures with noncolocated sensors and actuators," *Journal of Guidance, Control, and Dynamics*, **7**(5), p. 546-553.
124. Burke, S.E., Hubbard, J.E., and Meyer, J.E., 1993, "Distributed transducers and colocation," *Mechanical Systems and Signal Processing*, **7**(4), p. 349-361.
125. Wang, D. and Vidyasagar, M., 1990, "Passive control of a single flexible link," *Proceedings., IEEE International Conference on Robotics and Automation*, p. 1432-1437.
126. Yao, T.-F., Duenner, A., and Cullinan, M., 2017, "In-line metrology of nanoscale features in semiconductor manufacturing systems," *Precision Engineering*, **47**, p. 147-157.
127. Wu, W.H. and Chen, C.Y., 2001, "Simple lumped-parameter models of foundation using mass-spring-dashpot oscillators," *Journal of the Chinese Institute of Engineers*, **24**(6), p. 681-697.
128. Ritto, T., Aguiar, R., and Hbaieb, S., 2017, "Validation of a drill string dynamical model and torsional stability," *Meccanica*, **52**(11), p. 2959-2967.
129. Tang, X., Hu, X., Yang, W., and Yu, H., 2017, "Novel torsional vibration modeling and assessment of a power-split hybrid electric vehicle equipped with a dual-mass flywheel," *IEEE Transactions on Vehicular Technology*, **67**(3), p. 1990-2000.

130. Reichl, K.K. and Inman, D., 2017, "Lumped mass model of a 1D metastructure for vibration suppression with no additional mass," *Journal of Sound and Vibration* **403**, p. 75-89.
131. Xu, Q., 2013, "Design and development of a compact flexure-based XY precision positioning system with centimeter range," *IEEE Transactions on Industrial Electronics*, **61**(2), p. 893-903.
132. Yong, Y.K., Aphale, S.S., and Moheimani, S.R., 2008, "Design, identification, and control of a flexure-based XY stage for fast nanoscale positioning," *IEEE Transactions on Nanotechnology*, **8**(1), p. 46-54.
133. Goodman, L., 1976, *Material damping and slip damping*. Shock and vibration handbook, Vol. 36. 1-28.
134. Bowden, M. and Dugundji, J., 1990, "Joint damping and nonlinearity in dynamics of space structures," *AIAA journal*, **28**(4), p. 740-749.
135. Li, P. and Hu, R., 2007, "On the air damping of flexible microbeam in free space at the free-molecule regime," *Microfluidics and Nanofluidics*, **3**(6), p. 715-721.
136. Greene, M., 1987, "Robustness of active modal damping of large flexible structures," *International Journal of Control*, **46**(3), p. 1009-1018.
137. Trombetti, T. and Silvestri, S., 2004, "Added Viscous Dampers in Shear-type Structures: The Effectiveness of Mass Proportional Damping," *Journal of Earthquake Engineering*, **08**(02), p. 275-313.
138. Schwarz, B. and Richardson, M. *Proportional damping from experimental data*. in *Topics in Modal Analysis, Volume 7: Proceedings of the 31st IMAC, A Conference on Structural Dynamics, 2013*. 2014. Springer.
139. Adhikari, S., 2006, "Damping modelling using generalized proportional damping," *Journal of Sound and Vibration*, **293**(1), p. 156-170.
140. Isaacs, M.W., Hoagg, J.B., Morozov, A.V., and Bernstein, D.S. *A numerical study on controlling a nonlinear multilink arm using a retrospective cost model reference adaptive controller*. in *2011 50th IEEE Conference on Decision and Control and European Control Conference*. 2011. IEEE.

141. Morozov, A.V., Hoagg, J.B., and Bernstein, D.S., 2010, "Retrospective cost adaptive control of a planar multilink arm with nonminimum-phase zeros," 49th IEEE Conference on Decision and Control (CDC), p. 3706-3711.
142. Chen, B.-S. and Yang, T.-Y., 1993, "Robust Optimal Model Matching Control Design for Flexible Manipulators," *Journal of Dynamic Systems, Measurement, and Control*, **115**(1), p. 173-178.
143. Ming-Tzu, H. and Yi-Wei, T., 2005, "PID Controller Design for a Flexible-Link Manipulator," *Proceedings of the 44th IEEE Conference on Decision and Control*, p. 6841-6846.
144. Latawiec, K., Bańka, S., and Tokarzewski, J., 2000, "Control zeros and nonminimum phase LTI mimo systems," *Annual Reviews in Control*, **24**, p. 105-112.
145. Piron, D., Pathak, S., Deraemaeker, A., and Collette, C., 2022, "On the link between pole-zero distance and maximum reachable damping in MIMO systems," *Mechanical Systems and Signal Processing*, **181**, p. 109519.
146. Cavallo, A., Maria, G.D., Natale, C., and Pirozzi, S. *H ∞ Strongly Stabilizing Bandpass Controllers for Flexible Systems*. in *Proceedings of the 45th IEEE Conference on Decision and Control*. 2006.
147. Zhao, C., Montaseri, M.H., Wood, G.S., Pu, S.H., Seshia, A.A., and Kraft, M., 2016, "A review on coupled MEMS resonators for sensing applications utilizing mode localization," *Sensors and Actuators A: Physical*, **249**, p. 93-111.
148. Humbert, C., Walter, V., Kacem, N., and Leblois, T., 2020, "Towards an Ultra Sensitive Hybrid Mass Sensor Based on Mode Localization without Resonance Tracking," **20**(18), p. 5295.
149. Zhang, H., Li, B., Yuan, W., Kraft, M., and Chang, H., 2016, "An Acceleration Sensing Method Based on the Mode Localization of Weakly Coupled Resonators," *Journal of Microelectromechanical Systems*, **25**(2), p. 286-296.